Universidad del País Vasco
Euskal Herriko Unibertsitatea

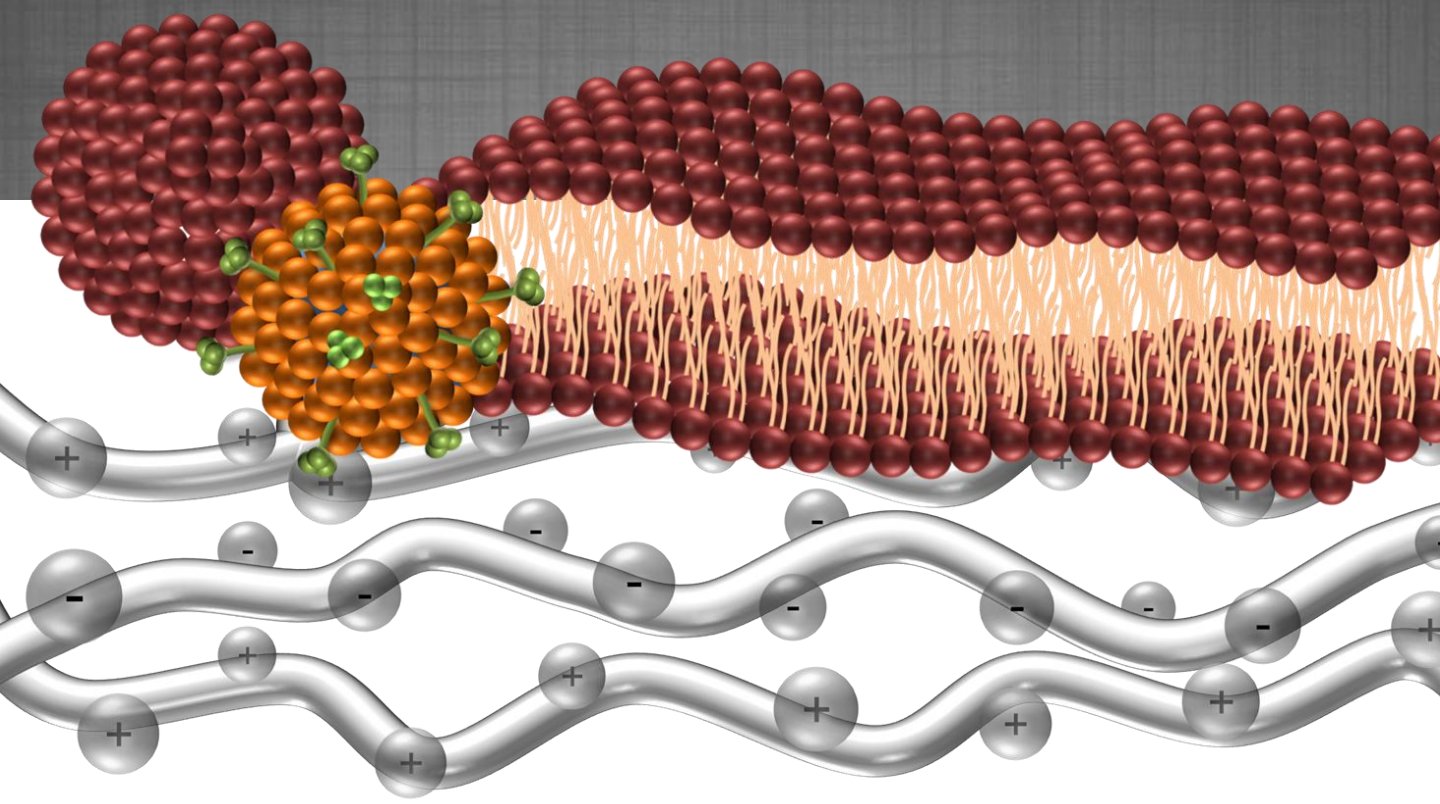

Eleftheria Diamanti

Engineered Interfaces with Polyelectrolyte Multilayers, Lipid Bilayer Membranes and Virosomes for Biomedical Applications

Donostia – San Sebastian, Spain, 2016

Engineered Interfaces with Polyelectrolyte Multilayers, Lipid Bilayer Membranes and Virosomes for Biomedical Applications

Dissertation presented to the

Department of Science and Technology of Polymers

University of the Basque Country (UPV/EHU), Donostia-San Sebastian

For the degree of Doctor in Applied Chemistry and Polymeric Materials

Presented by

Eleftheria Diamanti

Thesis Supervisor: Dr. Sergio E. Moya

University Tutor: Professor Antxon Santamaria

Donostia – San Sebastian, 2016

The PhD-Thesis has been carried out at:

CIC biomaGUNE
Soft Matter Nanotechnology Group
Donostia – San Sebastian, Spain

Zhejiang University
Department of Polymer Science and Engineering
Hangzhou, China

Universidad Nacional de La Plata
Instituto de Investigaciones Fisicoquímicas Teóricas y Aplicadas
Consejo Nacional de Investigaciones Científicas y Técnicas
La Plata, Argentina

UNIVERSITÄT LEIPZIG

Leipzig University

Institute for Medical Physics and Biophysics

Leipzig, Germany

Surflay Nanotec GmbH
Berlin, Germany

Yerevan State University
Department of Molecular Physics
Yerevan, Armenia

Acknowledgements

While this thesis is coming to an end, I would like to say thank you to all the people that shared with me one of the most significant periods of my life.

First I would like to thank Sergio, my supervisor, for supporting me and giving me the opportunity to work in a variety of projects that enriched me with knowledge and experiences. Besides, I would really like to thank him for his support in personal matters and for giving me the opportunity to travel in places where I could never imagine I would be, meeting great people, eating delicious food in unforgettable landscapes.

I am also thankful to my tutor Professor Antxon Santamaria from the department of Applied Chemistry for the great help.

Working in a laboratory full of music, laughs and voices was always a pleasure. So I would like to thank all my “labmates”, present and former, for showing me that science is not nice only when you get good results but also if you are surrounded with people full of positive energy.

I would like to thank even more the people who have been more than “labmates” to me. So thank you from the heart to my Tonti, Jodiba, Patito, La Croata, Richie, Angelito, La Txata and Martita for the good moments we have spent together either working, having fun or when facing a bad day trying to cheer each other up.

A big thank you goes also to the CIC biomaGUNE people; the platform managers for being really helpful and for being always there when needed, also the ones that I really enjoyed sharing a small talk in the corridors of biomaGUNE or long ones in the streets of San Sebastian. My deep gratitude goes also to David Casado for being always a great and cheerful help.

I am also thankful to all the people I met during my visits in China, Argentina, Germany and Armenia that contributed to make my stays easier and enjoyable. The financial support from the Marie Currie projects, TrasNade, Viroma and HYMADE is also greatly appreciated.

Επίσης θα ήθελα να ευχαριστήσω την οικογένεια μου, που είναι πάντα δίπλα μου όσα χιλιόμετρα κι αν μας χωρίζουν και με στηρίζουν με την αγάπη τους. Τέλος θα ήθελα να ευχαριστήσω το *αγόρι* μου που με μια του αγκαλιά με γεμίζει με ενέργεια και όρεξη να συνεχίσω να γεμίζω την ζωή μου με αξέχαστες εμπειρίες σαν κι αυτή.

Contents

List of Figures

Chapter 1

List of Tables

Abbreviations

^{1}H NMR	*Proton nuclear magnetic resonance spectroscopy*
AFM	*Atomic force microscopy*
AFS	*Atomic force spectroscopy*
Alg	*Alginic acid sodium salt*
BLMs	*Black lipid membranes*
BPFs	*Bilayer phospholipid fragments*
BSA	*Bovine serum albumin*
CA	*Contact angle*
Chol.	*Cholesterol*
CIP	*Citric acid-sodium phosphate buffer*
CLSM	*Confocal laser scanning microscopy*
CryoTEM	*Cryogenic transmission electron microscopy*
DLS	*Dynamic light scattering*
DOPC	*1,2-dioleoyl-sn-glycero-3-phosphocholine or phosphatidylcholine*
DOPS	*1,2-dioleoyl-sn-glycero-3-phospho-L-serine or phosphatidylserine*
EDC	*N-(3-Dimethylaminopropyl)-N´-ethylcarbodiimide hydro-chloride*
EIS	*Electrochemical impedance spectroscopy*
FITC	*Fluorescein isothiocyanate*
FRAP	*Fluorescence recovery after photobleaching*
FSC	*Forward scatter channel*
GUVs	*Giant unilamellar vesicles*

HA	*Hemagglutinin*
Hepes	*(4-(2-hydroxyethyl)-1-piperazineethanesulfonic acid*
IRIVs	*Immunostimulating reconstituted influenza virosomes*
L-B	*Langmuir-Blodgett*
LbL	*Layer by Layer*
L-S	*Langmuir–Schäfer*
LUVs	*large unilamellar vesicles*
MES	*2-(N-morpholino)ethanesulfonic acid*
MLVs	*Multilamellar vesicles*
MPS	*Sodium 3-mercapto-1-propanesulfonate*
NA	*Neuraminidase*
PAA	*Polyacrylic acid*
PAH	*Polyallylamine hydrochloride*
PBS	*Phosphate buffered saline*
PDADMAC	*Polydiallyldimethylammonium chloride*
PE	*Polyelectrolyte*
PEM	*Polyelectrolyte multilayer/membrane*
PLL	*Poly-L-lysine*
POPC	*1-palmitoyl-2-oleoyl-sn-glycero-3-phosphocholine*
POPS	*1-plamitoyl-2-oleoylsn- glycero-3-phosphor-L-serine*
PSS	*Polystyrene sulfonate sodium salt*
QCM-D	*Quartz crystal microbalance with dissipation*
R18	*Rhodamin B-octadecylester-perchlorate*
Rhd	*Rhodamine B isothiocyanate*
SAMs	*self assembled monolayers*

sBLM	*supported lipid bilayer membranes*
SHE	*Standard hydrogen electrode*
SSC	*Side scatter channel*
SUVs	*Small unilamellar vesicles*
tBLMs	*Tethered lipid bilayer membranes*
TEM	*Transmission electron microscopy*
Tris	*Tris(hidroximetil)aminometano*
UV	*Ultra-Violet*
XPS	*X-ray photoelectron spectroscopy*

Summary

This thesis presents different approaches for the surface engineering by means of polyelectrolyte multilayers (PEMs), alone or in combination with lipid bilayers and influenza virosomes for biomedical applications.

In chapter 1, PEMs of poly-L-lysine (PLL) and alginic acid sodium salt (Alg) are fabricated applying the layer by layer (LbL) technique and annealed at constant temperatures; 37, 50 and 80 °C, for 72 hours. Atomic force microscopy (AFM) reveals changes in the topography of the PEM, which is changing from a fibrillar to a smooth surface after annealing. Advancing contact angle in water varies from 36° before annealing to around 93°, 77° and 95° after annealing at 37, 50 and 80 °C respectively. Changes in surface energy after annealing were calculated from advancing and receding contact angle measurements performed with water and with organic solvents. Changes in the physical properties of the PEMs are interpreted as a result of the reorganization of the polyelectrolytes in the PEMs from a layered structure into complexes where the interaction of polycations and polyanions is enhanced. PEMs from biological origin have many potential applications in tissue engineering and regenerative medicine. However, the softness of biocompatible PEMs results in limited cell adhesion. Thermal annealing is suggested as a novel strategy for the enhancement of cellular

adhesion on PEMs. The impact of thermal annealing at 37 °C, on the adhesion of human lung cancer A549 and myoblast C2C12 cell lines is studied. Cell adhesion, measured by the projected average cells spreading and focal contact is remarkably improved for the annealed PEMs. Quartz crystal microbalance with dissipation (QCM-D), contact angle and fluorescence spectroscopy measurements show a significant decrease in the adsorption of the bovine serum albumin protein to the PEMs after annealing. Our results provide a simple method to tune the wettability of bio-PEMs, improve cellular adhesion and endow them with antifouling characteristics.

In chapter 2, the self-assembly of small unilamellar vesicles (SUVs) of mixed lipids zwitterionic phosphatidylcholine (DOPC, PC) and anionic phosphatidylserine (DOPS, PS) phospholipids on top of PEMs of poly(allylamine hydrochloride) (PAH), as a polycation, and poly(sodium 4-styrenesulfonate) (PSS), as a polyanion, is investigated as a function of the composition of the assembled vesicles by means of QCM-D, cryo-transmission electron microscopy (CryoTEM), AFM and atomic force spectroscopy (AFS). Vesicles with molar percentages of PS between 50 % and 70 % result in the formation of a lipid bilayer on top of the PEMs. AFS studies performed with a PAH-modified cantilever approaching and retracting from the lipid assemblies reveal that the main interaction between PAH and the lipids takes place through hydrogen bonding between the amine groups of PAH and the carboxylate and phosphate groups of PS and with the phosphate groups of PC.

The influence of the surface chemistry of PEMs on the formation of lipid bilayers is also studied for PEMs with poly(diallyldimethylammonium chloride) (PDADMAC) as

polycation and top layer, and PSS as polyanion. SUVs composed of DOPC and DOPS at 50:50 molar ratio are deposited on top of PEM films and studied via QCM-D and fluorescence recovery after photobleaching (FRAP). SUVs deposition on PDADMAC/PSS results in vesicles adsorption while on PAH/PSS under the same conditions a bilayer is formed. FRAP measurements confirm that SUVs are not ruptured on top of PDADMAC/PSS. The role of phosphate ions, in solution, on the formation of lipid bilayers is also analysed. X-ray photoelectron spectroscopy (XPS) shows the complexation of phosphate salts to the primary amines of PAH and no interaction with the quaternary amines of PDADMAC. ζ – potential measurements show a potential close to 0 mV for the PAH/PSS multilayers in PBS while PDADMAC/PSS display a potential of 38 mV. A model is presented for the formation of lipid bilayers on PAH/PSS PEMs taking into account the role of phosphate ions in decreasing electrostatic interactions between SUVs and PEMs and the formation of hydrogen bonding between the phospholipids and the primary amines of PAH.

QCM-D and FRAP experiments show that when vesicles with a lipid composition of 50:50 DOPC:DOPS are adsorbed on PEMs where PSS is replaced by Alg or poly(acrylic acid) (PAA) the vesicle deposition does not result in a bilayer formation but in bilayer patches together with adsorbed intact vesicles. Therefore, the fusion of the lipid bilayer is not only affected by the last deposited layer that mainly interacts with the lipids but also by the overall composition of the PEM film.

In chapter 3, SUVs prepared by a mixture of 30:70 DOPC:DOPS are assembled on top of a PEM cushion of PAH/PSS and the electrical properties of the bilayer are studied by

electrochemical impedance spectroscopy (EIS). The bilayer supported on the PEMs shows a high resistance, in the order of 10^7 Ω cm^2 which is indicative of a continuous, dense bilayer. Such resistance is comparable with the resistance of black lipid membranes, being the first time that these values are obtained for lipid bilayers supported on PEMs. The assembly of polyelectrolytes on top of a lipid bilayer decreases the resistance of the bilayer up to 2 orders of magnitude. Thus the assembly of the polyelectrolytes on the lipid bilayer induces defects or pores in the bilayer followed by a subsequent decrease in resistance.

Finally, this thesis addresses, in Chapter 4, the fusion of immunostimulating reconstituted influenza virosomes (IRIVs) with the functional viral envelope glycoprotein, hemagglutinin (HA), to artificial supported lipid membranes assembled on PAH/PSS PEMs on both colloidal particles and planar substrates. R18 assay is used to prove the IRIVs fusion in dependence of pH, temperature and HA concentration. IRIVs display a pH-dependent fusion mechanism, fusing at low pH in analogy to the influenza virus. The pH dependent behaviour is confirmed by QCM-D. AFM imaging shows that at low pH virosomes are integrated in the supported membrane displaying flatered features and a reduced vertical thickness. IRIVs fusion offers a new strategy for transferring biological functions on artificial supported membranes with potential applications in targeted delivery and sensing.

Resumen

Esta tesis presenta diferentes enfoques para la ingeniería de superficies mediante el uso de multicapas de polielectrolitos (PEMs) solas o en combinación con bicapas lipídicas y virosomas formados a partir del virus de la influenza para aplicaciones biomédicas.

En el capítulo 1, PEMs de poli-L-lisina (PLL) y alginato (Alg) se prepararon empleando la técnica de capa a capa del inglés ´´Layer by layer´´ (LbL). Las multicapas fueron sometidas a curado a temperaturas constantes de 37, 50 y 80 °C, durante 72 horas. La microscopía de fuerza atómica (AFM) revela cambios en la topografía de los PEMs, que se reorganizan a partir de una estructura fibrilar en una superficie homogénea y poco rugosa. El ángulo de contacto en agua varía de 36° antes del curado a 93°, 77° y 95° después de curar a 37, 50 y 80 °C, respectivamente. Los cambios de energía superficia después del curado, se calcularon a partir de medidas del ángulo de contacto en diferentes disolventes orgánicos. Los cambios en las propiedades físicas de la multicapa se interpretan como un resultado de la reorganización de los polielectrolitos en la multicapa; que pasa de una estructura laminar a una estructura formada por complejos donde se ve favorecida la interacción entre policationes y polianiones. Las multicapas de polielectrolitos biológicos tienen múltiples aplicaciones posibles en

medicina regenerativa e Ingeniería del tejido. Sin embargo, el modulo elástico bajo de las PEMs biocompatibles resulta en una adhesión celular limitada. El curado térmico se presenta como una nueva estrategia para la mejora de la adhesión celular de las PEMs. De esta manera se estudia el impacto del curado a 37 °C de PLL/Alg sobre la adhesión de líneas celulares de células humanas de cáncer de pulmón A549 y mioblastos C2C12. La adhesión celular, medida por el promedio del área de las células que se extienden sobre la superficie estableciendo contacto focal con las superficies se ha mejorado notablemente para las PEMs después del curado. Se muestra mediante la microbalanza de cuarzo con disipación (QCM-D), medidas de ángulo de contacto y de fluorescencia que la adsorción de proteína albúmina de suero bovino (BSA) disminuye notablemente sobre las PEMs después del curado. Este trabajo propone un método sencillo para modificar el mojado superficial de las bio-PEMs, mejorar la adhesión celular y darles características de antiicrustante.

En el capítulo 2, el autoensamblado de vesículas de una mezcla de lípidos de fosfatidilcolina, un lípido zwitteriónico (DOPC, PC) y los fosfolípidos aniónicos de fosfatidilserina (DOPS, PS) sobre PEMs de hidrocloruro de poli(alilamina) (PAH), como policatión y sulfonato de poliestireno (PSS), como polianión, se investigó en función de la composición de vesículas mediante la QCM-D, microscopía electrónica de crio-transmisión (CryoTEM), AFM y espectroscopia de fuerza atómica (AFS). Vesículas con porcentajes molares de PS entre 50% y 70% resultan en la formación de una bicapa lipídica sobre las PEMs. Estudios de AFS con un cantilever modificado con PAH que se acerca y se retrae a los ensamblados de los lípidos, indican que la interacción principal

entre PAH y los lípidos se lleva a cabo a través de enlace de hidrógeno entre los grupos aminos de PAH y los grupos de carboxilato y fosfato de la PS y con los grupos de fosfato de la PC. La influencia de la química superficial de la PEM en la formación de bicapas de lípidos se ha estudiado también con PEMs de cloruro de polidialildimetilamonio (PDADMAC) como capa superior policatiónica y PSS como polyanión. Vesiculas compuestas por DOPC y DOPS en relación molar de 50:50 se depositaron sobre PEMs de PDADMAC/PSS y se caracterizaron mediante QCM-D y fluorescencia recuperada después de fotoblanquear (FRAP). La deposición de vesículas sobre PDADMAC/PSS resulta en la adsorción de vesículas, mientras que sobre PAH/PSS en las mismas condiciones se forma una bicapa lipídica. Las medidas de FRAP confirman que las vesículas no se fusionan quedando adsorbidas sobre la superficie de la multicapa de PDADMAC/PSS. También se analiza la influencia de los iones de fosfato en solución, en la formación de una bicapa. Mediante la espectroscopia de fotoelectrones de rayos-X (XPS) se muestra la formación de complejos de sales de fosfato con las aminas primarias de PAH pero ninguna interacción con las aminas cuaternarias de PDADMAC. Medidas del potencial zeta muestran un potencial cerca a 0 mV para las multicapas de PAH/PSS en PBS mientras que para PDADMAC/PSS se observa un potencial de 38 mV. Se presenta un modelo para la formación de bicapas lipídicas soportadas en PAH/PSS teniendo en cuenta la influencia de los iones de fosfato que reducen las interacciones electrostáticas entre las SUVs y las PEMs y la formación de enlace de hidrógeno entre los fosfolípidos y las aminas primarias del PAH.

Se realizaron experimentos de QCM-D y FRAP para demostrar la adsorción de vesículas de 50:50 PC:PS en cuando el PSS es reemplazada por Alg ó por poly(acido acrilico) (PAA). Se observó en estos casos la formación de parches de bicapas junto con vesículas adsorbidas sobre las PEMs. Por lo tanto, la formación de la bicapa lipídica no depende solamente de las características de la última capa de polielectrolito depositada, que interactúa principalmente con los lípidos, sino de la composición de la multicapa definida por el polianión en conjunto con el policatión.

En el capítulo 3, vesiculas formadas por una mezcla de 30:70 DOPC:DOPS fueron depositadas sobre una multicapa de PAH/PSS formando una bicapa y se estudiaron las propiedades eléctricas de la bicapa por medio de la espectroscopia de impedancia electroquímica (EIS). La bicapa en la PEM muestra una alta resistencia, en el orden de 10^7 cm^2 Ω que es indicativo de una bicapa continua y densa. Tal resistencia es comparable con la resistencia de las membranas lipídicas negras, siendo la primera vez que estos valores se obtienen para bicapas de lípidos ensambladas en PEMs. El ensamblado de polielectrolitos encima de la bicapa de lípidos disminuye la resistencia de la bicapa hasta 2 órdenes de magnitud. El ensamblado sobre la bicapa lipídica induce defectos o poros en la bicapa, seguida por una posterior disminución en la resistencia.

Por último, en el capítulo 4, se presenta la fusión de virosomas inmunoestimulados reconstituidos a partir del virus de la gripe (IRIVs) conteniendo la glicoproteína de

envoltura viral funcional, hemaglutinina (HA), a bicapas lipídicas artificiales ensambladas sobre multicapas de PAH/PSS soportadas en partículas coloidales y sustratos planos. El ensayo de R18 se utiliza para probar la fusión de los IRIVs en dependencia del pH, la temperatura y la concentración de HA. Los IRIVs muestran un mecanismo de fusión dependiente del pH, ya que se fusionan a pH bajo similar al virus de la gripe. El comportamiento dependiente del pH se confirma por medio de la QCM-D. Las imágenes obtenidas por AFM muestran que a pH bajo los virosomas están integrados en la membrana soportada exhibiendo las características de una estructura aplanada y un espesor vertical reducido. La fusión de los virosomas ofrece una nueva estrategia para la transferencia de funciones biológicas a membranas artificiales soportadas con aplicaciones potenciales en la liberación dirigida de medicamentos y en sensores biológicos.

General Introduction

Self-Assembly

Molecular self-assembly describes the autonomous organization of multiple molecular components into patterns or structures without external intervention[1]. It can be observed at different sizes and scales varying from macro- to nanoscale structures with a precise control over size and shape[1]. Self-assembly is usually taking place through non-covalent interactions like hydrogen-bonding, van der Waals bonds, hydrophobic and electrostatic interactions among other molecular interactions. Hydrogen bond is an attractive electrostatic interaction between a hydrogen atom covalently bound to an electronegative element like nitrogen, oxygen or fluorine and another electronegative atom or a group of atoms in the same or a different molecule[2]. Hydrogen bonding interactions are highly directional and their strength depends mainly on the nature of the atom to which the hydrogen is connected, as well as by the solvent[3]. The energies associated with hydrogen bonding are between 1 and 5 kcal mol^{-1}, which makes it stronger than Van der Waals but weaker than covalent or ionic bonding.

Over the years materials' scientists have exploited the principles of self-assembly, inspired by nature, for the generation of artificial materials with organized structures and tailored properties. Cell membranes represent one of the most relevant examples of self-assembly in nature. The main structure of cell membranes is based on a lipid bilayer that is composed of phospholipids. Phospholipids are amphiphilic molecules

bearing a hydrophobic tail and a hydrophilic head. In lipid bilayers other molecules are assembled such as cholesterol, proteins, glycol proteins, etc. (**Figure 1a**). Nucleic acids and viruses are also some examples of self-assembled systems that play a key role in life. The double-stranded DNA, is a major component of all eukaryotic genomes; formed from nucleotides (building blocks of DNA) and shaped like a double helix through hydrogen bonding between nucleotides located in different strands[4] (**Figure 1b**). Another example of molecular self-assembly in biology can be found in viruses. From a material´s science point of view viruses are self-assembled biopolymer nanoparticles. They generally display an icosahedral or helical structure resulting in a spherical or rod-shape particle[5].

All these examples show a precise organization at the nanometric scale, which is derived from specific interactions at molecular level[6]. Molecular self-assembly is of great importance in chemistry and biochemistry[4,7]. In chemistry, applies non-covalent interactions which are often weaker than covalent bonds and are reversible[8].

The development of supramolecular chemistry, the last two decades, led to the designed molecular self-assembly of a wide variety of synthetic molecules[9,10]. It offers a simple and robust way to construct discrete supramolecular nanostructures of various sizes and shapes which can be applied in nanotechnology and biotechnology[11–13].

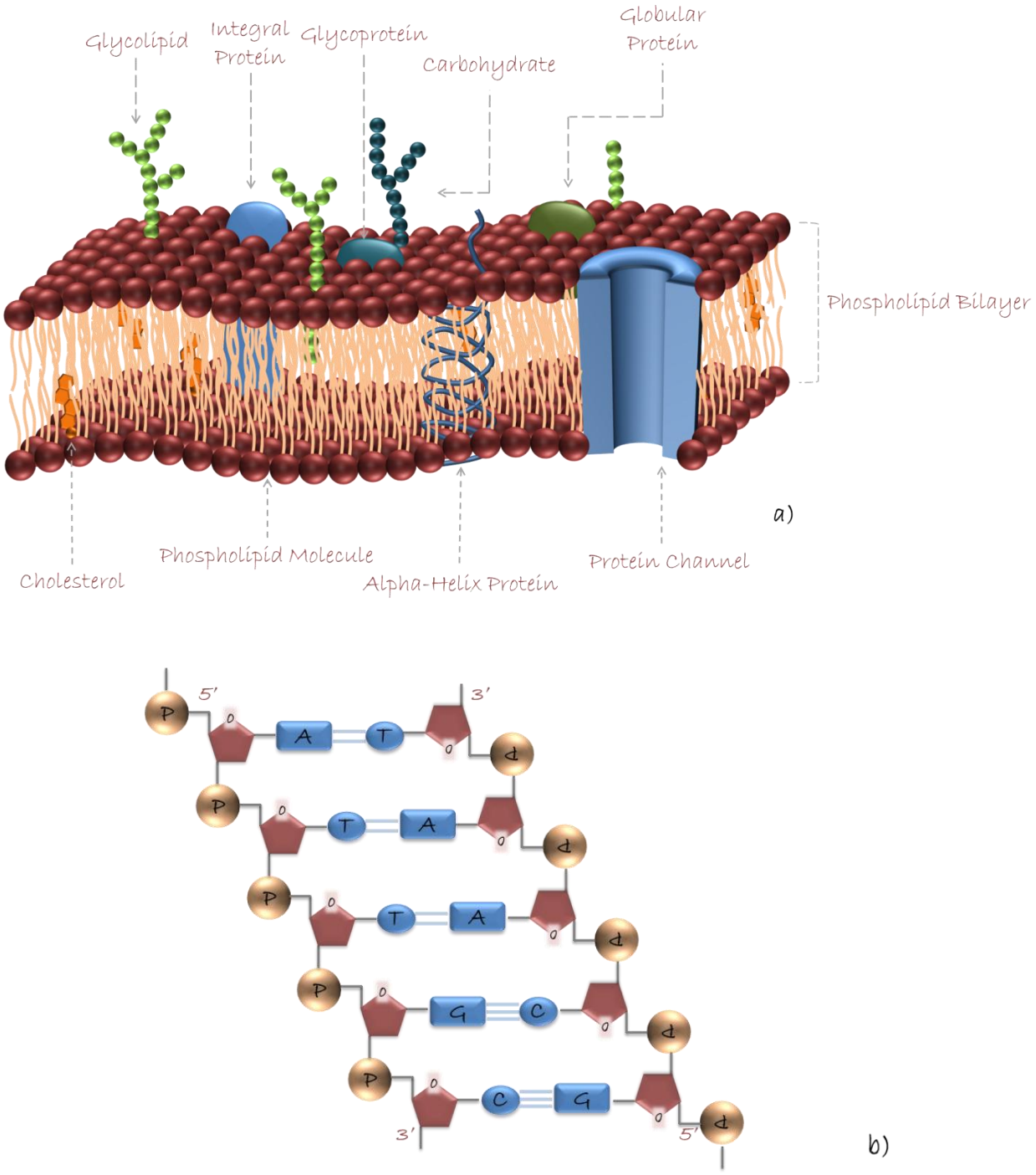

Figure 1 Examples of self-assembly in nature; schematic illustration of a) the structure of a plasma membrane and b) a DNA- helix molecule model.

Applying self-assembly concepts, synthetic and biological building blocks i,e nanoparticles, polymers, virus, proteins etc are combined to obtain functional materials

for different applications in medicine, sensing, electronics, coatings, etc. In biomedicine supramolecular assemblies of polymers, surfactants, viruses, nucleic acids, lipids, peptides and others have found applications as carriers for drug or gene delivery[14,15] and therapeutics[16], diagnostics (biosensing)[17,18] or in tissue engineering[19].Self-assembled organic films with nm precision have been successfully used for biological applications, for the development of sensors or drug delivery systems and for the engineering of devices and surfaces to provide biocompatibility, biological functions or recognition[20,21]. Some examples of organic self-assembled films applied for biomedical applications are Langmuir – Blodgett monolayer films (LB)[22], self-assembled monolayers (SAMs)[23], polyelectrolyte multilayer films (PEMs)[24], supported lipid bilayer membranes (sBLM)[25].

Polyelectrolyte Multilayers (PEMs)

Polyelectrolytes (PEs) are polymers with ionizable repeating units[26]. When PEs are dissolved in water their ionizable groups dissociate resulting in a charged polymer backbone and free counterions. PEs can be classified as strong or weak PEs depending on the influence of the bulk pH on their charge. Strong PEs are those that retain their charged state in solution regardless the pH changes (e.g. poly(sodium 4-styrene sulfonate), PSS), while the charge of a weak PE strongly depends on the changes in pH (e.g. poly(acrylic acid), PAA) (**Figure 2**).

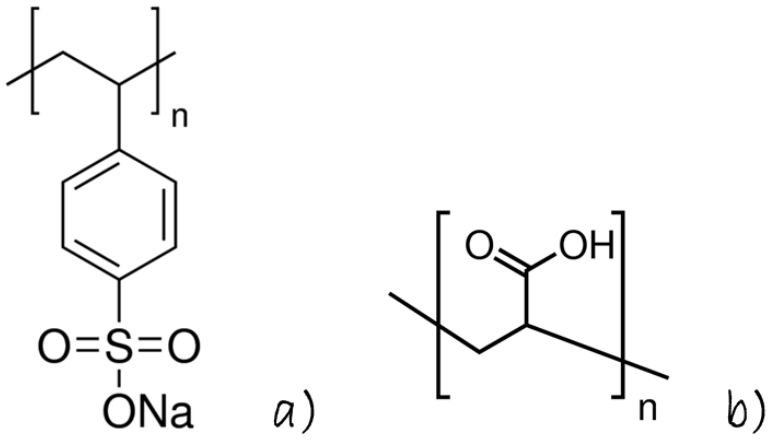

Figure 2 Chemical structure of a **a)** strong polyelectrolyte; poly(sodium 4-styrene sulfonate) and **b)** weak polyelectrolyte; poly(acrylic acid).

Langmuir and Blodget introduced the transfer of insoluble monolayers from an aqueous solution onto solid supports based on molecular interactions between certain functional groups of the monolayer and the solid surface[27]. The Langmuir-Blodgett (L-B) technique was the simplest for the design of molecular interfaces with nm precision for surface modification. Nevertheless L-B monolayers are based on weak molecular interactions and show limited stability under ambient and physiological conditions. Decher et. al[24] showed in 1992 the build-up of multilayer films of polyelectrolytes using the layer by layer technique (LbL). This technique is based on the alternating deposition of oppositely charged PEs on top of charged surfaces[24,28,29] (**Figure 3**). The assembly is driven by attractive electrostatic interactions and entropy considerations[30,31]. The LbL technique is a powerful strategy for non-covalent modification of charged surfaces. It is an easy and reliable method for surface engineering and has many potential applications in diverse areas such as optoelectronics, nanofiltration, tissue engineering or devices such as carriers for drug delivery[28,29,32–37].

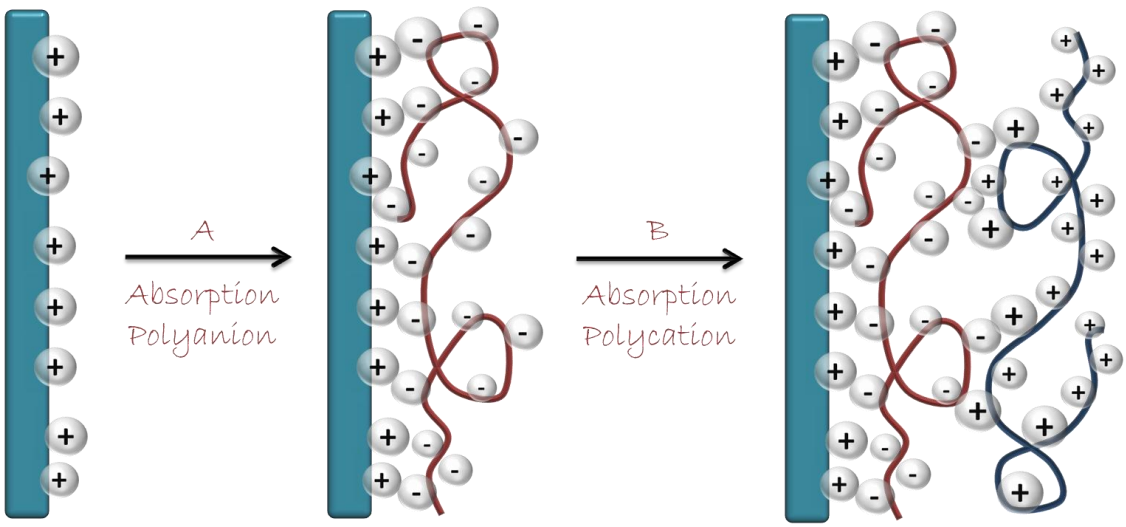

Figure 3 Schematic illustration of the assembly of multilayers by cyclic repetition of steps A) adsorption of anionic polyelectrolytes and B) of cationic polyelectrolytes.

Since 1992 until today significant research has been conducted using the LbL technique to produce PEM films combing a diversity of components. Synthetic PEs, biopolymers such as proteins, polypeptides, polysaccharides and nucleic acids, lipids, and inorganic particles have been introduced in the fabrication of multilayer films[38–40]. In 1998 Decher et al. showed the incorporation of enzymes in LbL films for either biosensing or multistep biocatalysis[28]. Möhwald et al. extended the deposition of thin films of PEMs, besides on planar surfaces, on top of colloidal particles[41]. Following the assembly on colloidal particles, the choice of sacrificial templates allowed for the fabrication of empty capsules retaining the size and the shape of the colloidal template. Capsules were used for controlled release and targeting[42].

PEMs assembled by the LbL process can be also considered as a special case of polycation/polyanion complex formation. The layered structure of the film is a

consequence of the step-wise assembly of polycations and polyanions. However, the layers are not fully stratified, as there is a certain degree of interdigitation among them. One layer in PEMs can be sensed up to 4 layers below[43]. Interdigitation is partially a consequence of the presence of free space within the film, which is filled by the following depositing layers[44].

An important characteristic of PEMs is that despite there is no chemical functionalization or covalent bonding they are very stable. They are not easily removed unless at least one of the PE is weak and loses charges by changing the pH, or there is a specific ion or surfactant interacting with the polymers that can weaken the electrostatic attraction between oppositely charged PEs[45,46]. Only at very high ionic strength the films can be partially removed[47]. Despite PEM stability, the layered arrangement of the PE is not always energetically optimal. From an intuitive point of view the best arrangement of the oppositely charged PEs would not be as separated layers but as complexes, where there is a maximal compensation of the negative and positive charges. In a complex state the oppositely charged polyelectrolytes will be closer. However, a reorganization of the PEMs into complexes, with the disappearance of the characteristic stratified structure could compromise the stability of the PEM itself. Exposing the PEMs to heat for a defined period of time, gives the polyelectrolyte molecules the energy to rearrange in the films and find more convenient conformations. It has been shown that annealing to capsules of poly(diallyldimethylammonium chloride) (PDADMAC)/PSS lead to the rearrangement of the polymers with a consequent loss of internal volume and increased layer thickness. This phenomenon occured only when PDADMAC is the last layer[48–51]. Glinel et al. showed the impact of

annealing on the responsive behaviour of PE films in relation with changes on the architecture of the multilayers[52].

Biopolyelectrolyte PEMs for Biological Applications

Over the years PEMs have attracted attention in bioengineering as they offer a facile route for the fabrication of biocompatible coatings when polysaccharides, proteins or polypeptides are used as layer constituents[53,54]. Biopolyelectrolyte multilayer films display appealing properties for tissue engineering[29].

A major issue in tissue engineering and regenerative medicine is the development of novel materials and surface coatings[55–57] with mechanical and biological characteristics that enhance cell adhesion and promote long-term tissue regeneration[58]. Cellular adhesion strongly depends on the mechanical properties of the substrate. Material properties such as surface topography, roughness, stiffness, chemical composition, the distribution and availability of ligands, surface charge and hydrophobicity are fundamental in determining cell adhesion at different scales[55,59]. For a proper cell adhesion it is necessary to balance the adequate substrate stiffness with the forces from the intracellular tension generated by the stress fibers[60]. It is also important to control the surface chemistry based on biocompatible elements so that they will not have negative impact on proliferation. Furthermore, the material should provide capability to adsorb a certain amount of proteins from the cell media, as the adhered cells do not interact directly with the surface of the material but with the adsorbed proteins that are coming from the biological fluids[61].

Several different materials have been employed to mimic the aspects of the interactions between cells and their environment and therefore to increase cell adhesion ranging from protein-coated poly(acrylamide) or poly(dimethylsiloxane) polymeric substrates with tunable stiffness[62], hydrogels that can be biochemically and mechanically altered by chemical functionalization or by varying cross-linking density[63]. Furthermore, microgels have been employed to fabricate thin film substrates combined with polyelectrolytes in PEMs[64]. PEMs have gained particular interest as coatings for implantable materials. They can mimic the complex extracellular matrix as they display a soft fibril structure. Thus due to their tunable nature, is possible to tailor their surface topography, chemical composition and mechanical properties.

Strategies to Tune PEMs Behavior for Biological Approaches

The properties of PEMs in regards to cell adhesion can be tuned by changing the assembling conditions of the PEs, i.e., ionic strength, pH or the even layer composition[65]. Since PEMs made upon biopolymers are soft, cross-linking agents can be used in order to increase their elastic modulus and favour cell adhesion. The use of cross-linking agents can be a drawback as the biocompatibility of the PEMs may be affected[21,66–69]. Their use provides stiffness to the PEMs, to a degree that is correlated with the amount of the cross-linker agent employed, leading ultimately to better cell adhesion. PEM stiffness has been also increased by the addition of particles into the PEM structure[21,70] or by capping soft multilayers with a varying number of synthetic PE layers[68,71]. Synthetic polymers such as PSS increase significantly the elastic modulus of a multilayer due to their glassy nature. Poly(acrylamide hydrochloride), (PAH)/PSS

PEMs for example display elasticity modulus of the order of 600 MPa. On the other hand the use of synthetic polyelectrolytes that result in stiffer films, in comparison to biopolymers, has the same drawbacks as the cross-linking, since their biocompatibility is limited. Thus their potential use for biomedical applications is questionable. However Moya et. al[65] showed an interesting approach to improve cellular adhesion by depositing 2 blocks of PEs; Poly-L-lysine (PLL)/PSS and PLL/Alginic acid sodium salt (Alg) multilayers combining by that way the mechanical properties and the biocompatibility of both synthetic and natural PEs, respectively.

Besides the use of PEMs for applications that require biocompatibility they have also recently attracted the attention as antifouling coatings. Some natural polymers like chitosan are known to have antifouling properties that can be enhanced or tuned in the LbL film combined with other polymers or with nanoparticles. Several interesting strategies have been followed i.e. the use of perfluorinated poly(ethylene glycol) copolymers as layer constituents, the control of the surface charge density or the use of a sacrificial top layer that can be removed together with the foulant and later reassembled[72–77].

Biological Membranes

Biological membranes play a fundamental role in life as they define the cell wall and they control the transport of substances and energy enabling cellular functions and ultimately life[78]. So in addition to their function as barriers biological membranes mediate the signal transduction and communications between the inner and outer spaces[79]. All membranes have a common structure (**Figure 1**) that consists of a phospholipid bilayer with sugars and integral proteins embedded in it[80]. Proteins carry out most of the specific functions of biological membranes and their amount and types vary for each type of cell. The most common proteins are the transmembrane proteins (extend across the membrane), anchored or integral proteins and peripheral proteins. Among them integral proteins are known as channel proteins as their main function is to transport ions, sugars and amino acids across phospholipid membranes. Essentially, channel proteins are water-filled pores that mediate the diffusion of inorganic ions through the membrane[81].

Membrane Lipids

Lipids can be defined as amphiphilic substances that are insoluble in water but soluble in organic solvents such as chloroform, acetone, ethanol and ethoxyethane. There are three major types of lipids found in biological membranes: phospholipids, glycolipids and cholesterol.

The most common lipids are phospholipids, which are found in basically mammalian cells. Phospholipids have a phosphate polar headgroup connected either to a sphingosine bonded to a fatty acid, or to a glycerol backbone (glycerophospholipids)

which is bonded to two fatty acid chains (**Figure 4a**). Depending on the head group, phospholipids can be negatively (e.g. 1,2-dioleoyl-sn-glycero-3-phospho-L-serine, DOPS), positively charged (e.g. 1,2-dioleoyl-3-trimethylammonium-propane) or zwitterionic (e.g. 1,2-dioleoyl-sn-glycero-3-phosphocholine, DOPC). Phospholipids display a hydrophilic headgroup and a hydrophobic tail so when they are in contact with an aqueous environment lipids self-assembly leading to a double layered structure, with the headgroups towards the aqueous phase and the tails towards the interior. When the phospholipids are hydrated they simultaneously assembled into structures called vesicles (liposomes) of different size.

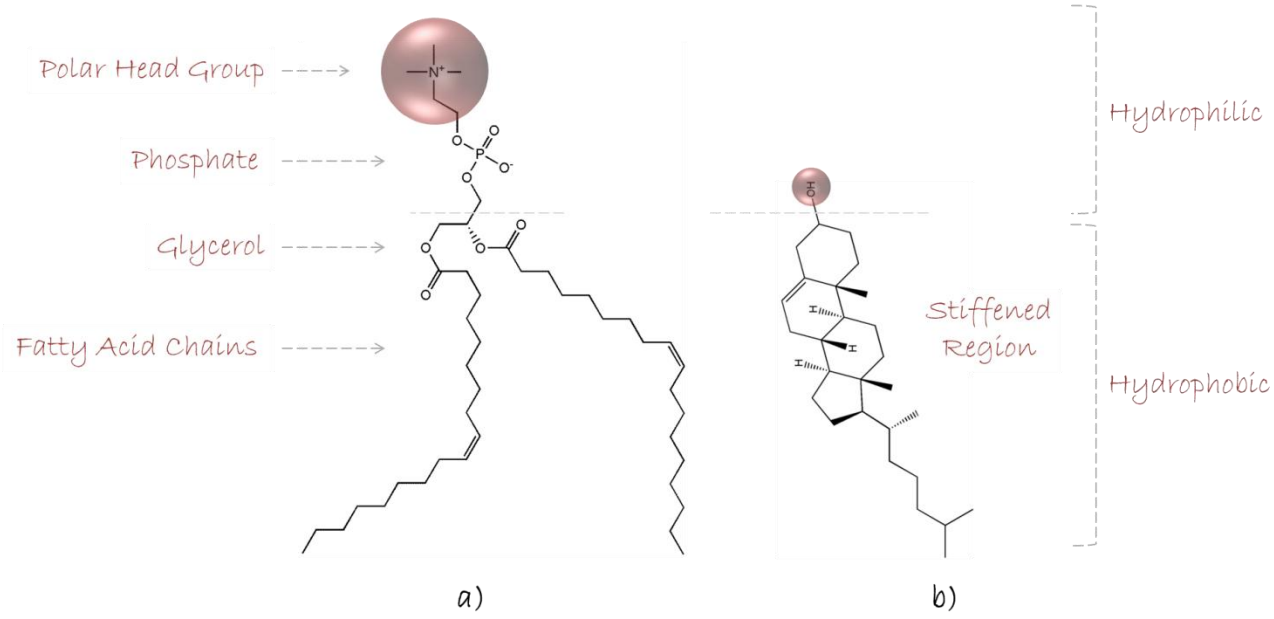

Figure 4 Chemical structure and characteristic parts of a) the phospholipid, 1,2-dioleoyl-*sn*-glycero-3-phosphocholine and b) cholesterol.

Multilamellar vesicles (MLVs) display sizes ranging between 500-10000 nm; they form spontaneously upon hydration of phospholipid films and they are composed of several lipid bilayers. MLVs can be formulated into small unilamellar vesicles (SUVs) with a size

less than 100 nm or into large and giant unilamellar vesicles (LUVs & GUVs) with sizes larger than 100 and 1000 nm respectively (**Figure 5**). Unilamellar vesicles are composed of just one bilayer[82,83].

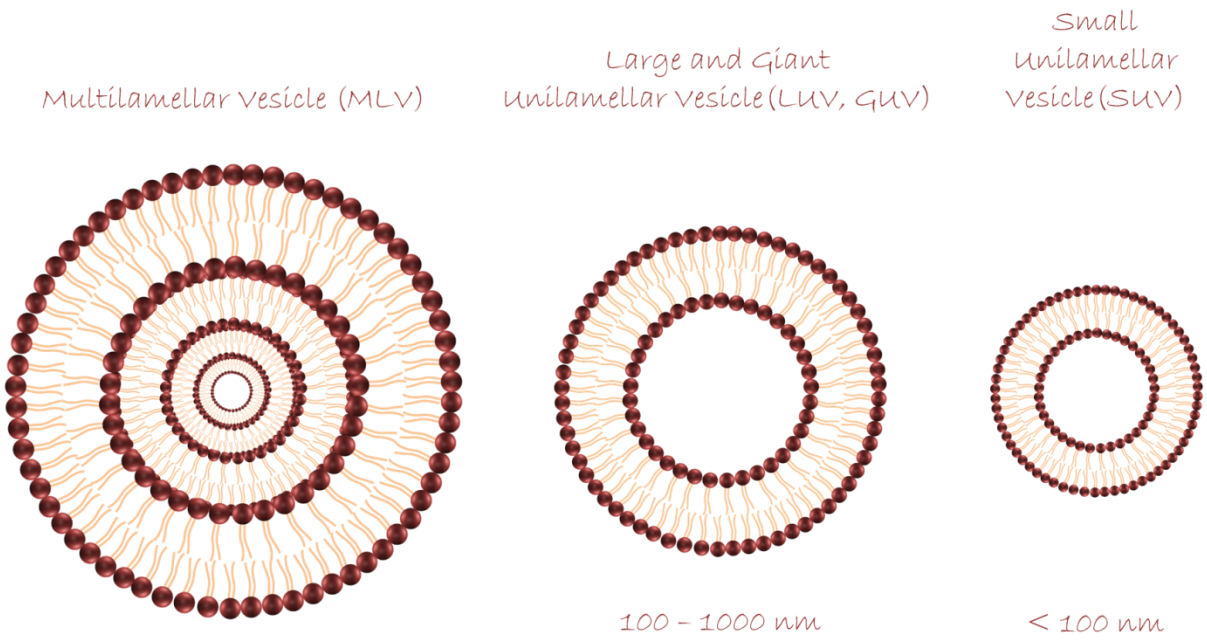

Figure 5 Schematic illustrations of liposomes of different sizes and types of lamellarity.

MLVs can be converted into SUVs or LUVs by mechanical means, generating an intermediate state called bilayer phospholipid fragments (BPFs)[84]. Due to the thermodynamic instability produced at the edge of the BPFs they bend and self-close into vesicles. The mechanical force needed in order to achieve the formation of BPFs and subsequently of SUVs or LUVs can be achieved by extrusion, sonication or freeze-thaw by which is also possible to control the size of the resulting vesicles[85–89].

Cholesterol is a type of membrane lipid. Cholesterol belongs to the family of steroids, contains a four-ring steroid structure with a short hydrocarbon side-chain and a hydroxyl

group and it is hydrophobic (**Figure 4b**). It is found in mammalian membranes and mycoplasmas[90]. Numerous structural investigations have been conducted focusing on the incorporation of cholesterol into lipid bilayers in order to regulate membrane properties[43,91–94]. Cholesterol is mainly used to change the fluidity and reduce permeability of the membranes. The more cholesterol present in the membrane the less fluid is the membrane, resulting in an increase in bending stiffness.

Artificial Membranes

Artificial membranes have been studied as a model of cellular membranes for biochemical reactions, to study transport pathways and surface interactions. Over the years artificial membranes have been studied as free standing, supported, tethered or as cushioned membranes (**Figure 6**). Initially cellular membrane properties were investigated using artificial black lipid membranes (BLMs)[95]. BLMs have been produced across the aperture in a typically teflon film or a small polymer cup forming a freestanding bilayer film surrounded by aqueous solution (**Figure 6a**). They were used as model systems to study the properties of cell membranes[96–100]. BLMs had a short life time of a few hours due to their fragility and thus there was a need of improving their stability for more accurate and long term studies.

Membranes supported on solid hydrophilic materials (**Figure 6b**) presented enhanced stability and they offered the possibility of the development of model systems for the detailed and multiscale investigation of cell membranes[101,102]. Supported membranes have been deposited on several different surfaces and studied in terms of spatial arrangement of lipids, stability of the assembled lipid bilayer membrane, transport

properties etc. Significant research has been conducted on membranes supported on planar and hard substrates such as glass, titania (TiO_2), mica, silicon oxide (SiO_2) and various metals such as gold (Au)[101,103–106]. They are typically used as models for biophysical studies of cell membranes[107–109] and as a mean of surface modification for biocompatibility[110,111]; to anchor proteins or receptors to surfaces or devices profiting from the biological resemblance of the lipid environment in cells[112,113]. Thus sBLMs were studied incorporating channels or non-natural molecules[114–116] for sensor development[117,118].

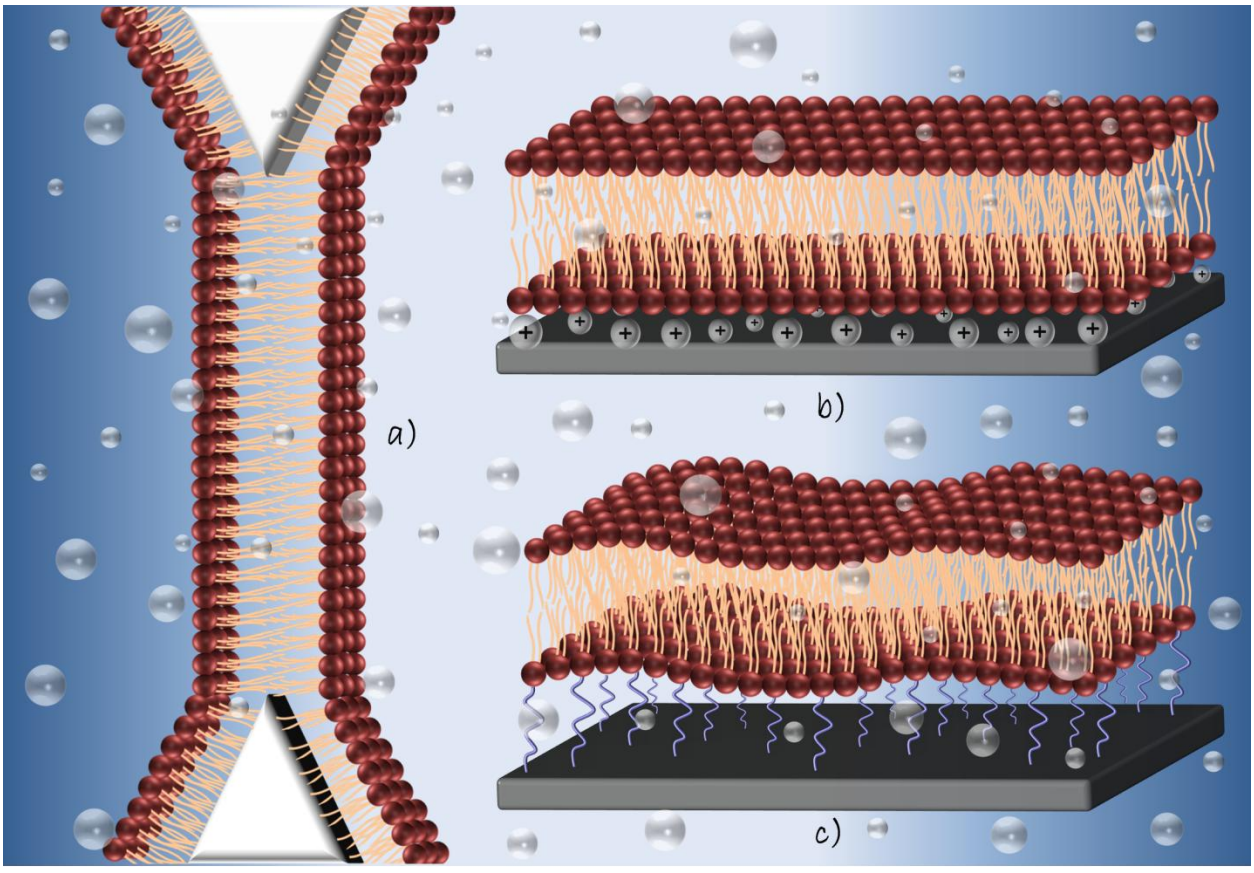

Figure 6 Schematic description of **a)** a freestanding black lipid membrane (BLM), **b)** a supported bilayer membrane (sBLM) and **c)** a tethered lipid bilayer membrane with a spacer that covalently anchors the inner leaflet to the substrate.

Biological membranes are supported on top of a cushion of biopolymers, the glycocalix or the cell wall[119] so solid supported membranes display limitations which can be overcome by creating a spacer with controlled thickness between the solid support and the lipid bilayer. Soft cushioned bilayer membranes mimic better the natural membranes on the extracellular matrix. In order to produce more realistic model membranes the so called tethered lipid bilayer membranes (tBLMs)[119–121] were produced (**Figure 6c**). Here the membrane is covalently linked to a solid support through a variety of linkers. Cornell et al.[122] bound the inner leaflet of the bilayer to a gold support via polar linkers and sulphur–gold bonds creating a short spacer group between the membrane and the support. Generally thiol anchors (e.g. mercapto anchoring groups) were used to graft the bilayer onto a surface, which is in most of the cases a gold electrode, allowing for electrical characterization of the membrane. Furthermore by the incorporation of various membrane proteins in such a system it was possible to create a functional biosensor[123–125].

Polymer-supported membranes have been studied with the aim to fabricate model membranes with characteristics that resemble the cell membrane. Additionally they offer the possibility to reduce contact of transmembrane proteins (incorporated in the membrane) and the surface preventing their denaturalization[126], if the surface is an electrode and to fabricate more functional biomimetic interfaces in devices.

Lipid membranes have been assembled as well on top of PEM cushions[127]. Möhwald et al. assembled lipid layers on top of PEMs of PAH/PSS by vesicles' fusion and by deposition from monolayers by the Langmuir–Schäfer (LB/LS) technique in order to study the homogeneity, electrical resistivity and lateral diffusion of the membranes[128].

Their studies confirmed the possibility of fusing lipids into a bilayer in order to develop a continuous film where the lipids exhibit long-range lateral diffusion. The authors suggested that the polymer support participates in the formation of conducting defects while they acknowledge that many questions regarding their nature remain open[128]. Further studies were conducted by the same group in later years exploiting the diffusion properties of the lipid layers on top of PEMs[129]. Some additional research has been done using PAH/PSS multilayers as a soft cushion for the support of BLMs by Knoll et al. exploring the electrostatic interaction strength between the lipid bilayer and the supporting polyelectrolyte cushion[130]. PEMs have been additionally fabricated on top of colloidal particles and capsules[107,108,117,131]. In all cases lipid layers have been assembled on PEMs by exposing them to lipid vesicles.

In 2008 Donath et al[132] showed the conditions for the assembly of sBLMs on top of PEMs and showed that this assembly requires a balance between zwitterionic and charged lipids, which is achieved when the proportion of charged lipids is more than a 50 % of the total lipid content. To this regard is interesting to understand which are the interactions under which these proportions of lipids result in a bilayer on top of the PAH/PSS films. Besides electrostatic interactions that are most likely taking place between PAH and phospholipids the amines of PAH could form hydrogen bonds with the phosphate and carboxylic groups of phospholipids. Most of the work conducted on the assembly of lipid bilayers on top of PEMs has been done using the combination of PAH and PSS PEs. This combination of PEs results in a rigid film with mechanical properties of the range of GPa which could be also a determining parameter for the rupture and fusion of the vesicles to a lipid bilayer. Further studies on the assembly of

lipids on top of different combination of PEs; strong, weak, synthetic, natural etc., would reveal more information about the interactions between lipid head groups and PEs.

The coating of PE capsules with lipids is very interesting as the lipid layer can be used to reduce capsule permeability, blocking the passage of small and medium size molecules through the capsule walls[133,134]. Moreover, lipid layers on top of capsules display a capacitive behaviour and restricted ionic conductivity[135–137]. Besides that, the lipid layers were also used as a platform for the addition of biological functions provided by biomolecules assembled in the lipid layers such as receptors or polypeptides that can be used for targeted delivery[138,139]. In summary, the coating of capsules with lipids results in a supported membrane in the colloidal domain with a structural resemblance to the plasma membrane of a cell.

PEM supported lipid bilayers can be also used for the preparation of electrochemical sensors. In that case the stability, continuity and fluidity of the bilayer are crucial for the potential integration of proteins, ligands or receptors. Electrochemical studies have been conducted by Knoll et. al[130] and Mohwald et. al[128] in membranes deposited on top of PAH/PSS films. A lipid bilayer that displays high resistance is indicative of a stable and continuous (with no pores) bilayer, nevertheless in the works conducted until now including the works of Knoll and Mohwald the lipid layers showed much lower resistivity and capacitance values[128,130,140]. Mohwald et al. suggested that the low resistivity obtained values, are due to the polymer support that participates in the formation of conducting defects. In any case, these values show that the conditions for the assembly of lipids on top of PEMs, used in these studies, did not result in a complete and dense

bilayer. Therefore it would be appealing to obtain a bilayer assembled on PEMs with resistance and capacitance similar to that of a black lipid membrane.

Immunostimulating Reconstituted Influenza Virosomes (IRIVs)

Immunostimulating reconstituted influenza virosomes (IRIVs) are virus like nanoparticles similar to influenza virus envelopes lacking viral genetic material[141]. The first reconstituted viral membranes were prepared derived from the Sendai virus[142] while the term virosomes was introduced in 1975 by Almeida et al. who reconstituted influenza virus membranes[143]. Virosomes have been prepared from various enveloped viruses including, sendai virus[144,145], influenza virus[146–148] and several others[149–152].

IRIVs are essentially spherical, unilamellar vesicles with a mean diameter of less than 200 nm[153–156]. Their base is a liposome comprised of DOPC, phosphatidylethanolamine and lipids derived from the influenza virus[156]. In contrast to liposomes, virosomes contain functional viral envelope glycoproteins: influenza virus hemagglutinin (HA) and neuraminidase (NA) intercalated in the phospholipid bilayer as illustrated in **Figure 7**. HA is a spike protein (~135 Å) and is involved in receptor binding and membrane fusion. HA is synthesized as a single polypeptide, HA0, and contain a stipe region at the base of the protein and a globular head at the end. Due to the presence of both proteins reconstituted influenza virosomes retain the receptor binding and membrane fusion activity of influenza virus[142].

Virosomes have demonstrated to be a versatile and efficient carrier system for a variety of antigens, for example proteins, peptides, nucleic acids and carbohydrates[154,157]. They have been mainly developed as prospective adjuvants to potentiate an immune response, since antigens alone are often poor immunogens. While most adjuvants, including IRIVs, induce humoral immune response;

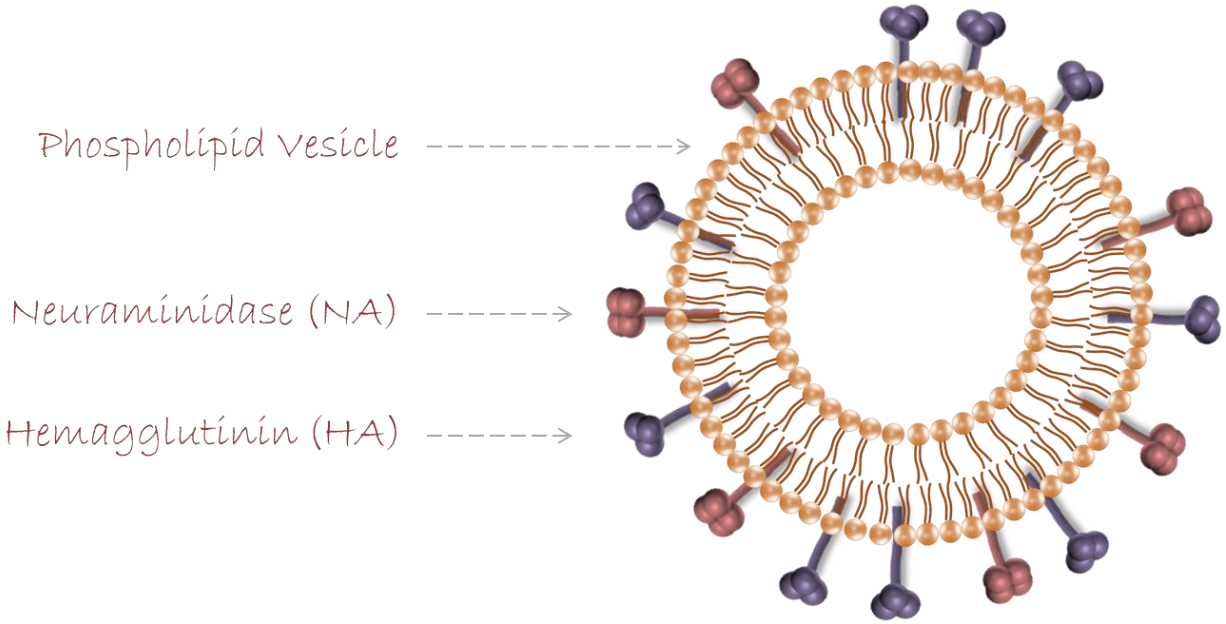

Figure 7 Illustration of an immunostimulating reconstituted influenza virosome with its functional glycoproteins; influenza virus hemagglutinin and neuraminidase.

Furthermore, virosomes have potential applications as drug carriers, like liposomes, with the advantage that the viral glycoprotein HA promotes the fusion of the virosome within the cell membrane, which can in turn lead to the release of the virosome cargo directly in the cytoplasm of the cell[158].

Since virosomes retain fusion properties of virus they could also be fused on artificial lipid membranes bringing the functionalities carried on their membranes to the supported lipids. Colloidal particles engineered with virosomes could have interesting applications in drug delivery beside their obvious importance for vaccine development. Virosome engineered particles could find applications as adjuvants, as influenza virus proteins will be present on the surface of the colloidal particles[159–161].

Additionally other proteins like antibodies or specific ligands can be integrated into the virosome or attached to the surface of the virosomes employing a lipid anchor[162,163].

These biomolecules would be then transferred to the supported membranes[164–166]. This represents an alternative to the direct functionalization of supported membranes, which is not always possible once the membrane is formed. Also the use of lipid vesicles entailing proteins and other biomolecules does not always result in the formation of a bilayer as they can affect the assembly, rupture and fusion process of liposomes. For the colloidal particles the presence of proteins in liposomes can also lead to major particle aggregation if the biomolecule prevents charge compensation during an electrostatically driven assembly. Therefore, virosomes could act as transfer agents of biological functionalities to supported membranes in a sequential way through a fusion mechanism without jeopardizing membrane formation and reducing particle aggregation in case of colloids. Fusion of virosomes has been extensively studied in cell cultures[162,167] while the fusion mechanism and the state of virosomes and glycoproteins after fusion have not been studied in detail.

References

(1) Evans, D. F.; Wennerström, H. *The Colloidal Domain : Where Physics, Chemistry, Biology, and Technology Meet*; Wiley-VCH, 1999.

(2) Arunan, E.; Desiraju, G. R.; Klein, R. a.; Sadlej, J.; Scheiner, S.; Alkorta, I.; Clary, D. C.; Crabtree, R. H.; Dannenberg, J. J.; Hobza, P.; et al. Definition of the Hydrogen Bond (IUPAC Recommendations 2011). *Pure Appl. Chem.* **2011**, *83* (8), 1637–1641.

(3) Mendes, A. C.; Baran, E. T.; Reis, R. L.; Azevedo, H. S. Self-Assembly in Nature: Using the Principles of Nature to Create Complex Nanobiomaterials. *Wiley Interdiscip. Rev. Nanomedicine Nanobiotechnology* **2013**, *5* (6), 582–612.

(4) Whitesides, G. M.; Mathias, J. P.; Seto, C. T. Molecular Self-Assembly and Nanochemistry: A Chemical Strategy for the Synthesis of Nanostructures. *Science* **1991**, *254* (5036), 1312–1319.

(5) Liu, Z.; Qiao, J.; Niu, Z.; Wang, Q. Natural Supramolecular Building Blocks: From Virus Coat Proteins to Viral Nanoparticles. *Chem. Soc. Rev.* **2012**, *41* (18), 6178–6194.

(6) Kushner, D. J. Self-Assembly of Biological Structures. *Bacteriol. Rev.* **1969**, *33* (2), 302–345.

(7) Zhang, S.; Yan, L.; Altman, M.; Lässle, M.; Nugent, H.; Frankel, F.; Lauffenburger, D. A.; Whitesides, G. M.; Rich, A. Biological Surface Engineering: A Simple System for Cell Pattern Formation. *Biomaterials* **1999**, *20* (13), 1213–1220.

(8) Gokel, G. W. Self-Assembly in Supramolecular Systems. In *Ciba Found Symp*; 1991; Vol. 158, pp 23–28, 39–41.

(9) Phlip, D. Supramolecular Chemistry: Concepts and Perspectives. By J.-M. Lehn, VCH, Weinheim 1995, X, 271 Pp., Softcover, DM 58.00, ISBN 3-527-2931 1-6. *Adv. Mater.* **1996**, *8* (10), 866–868.

(10) Gerhart, J.; Kirschner, M. *Cells, Embryos and Evolution*; 1997.

(11) Whitesides, G.; Kriebel, J.; Mayers, B. Self-Assembly and Nanostructured Materials. In *Nanoscale Assembly*; 2005; pp 217–239.

(12) Bishop, K. J. M.; Campbell, C. J.; Mahmud, G.; Grzybowski, B. A. Chapter 2 Biomimetic Design of Dynamic Self-Assembling Systems. *Stud. Multidiscip.* **2008**, *5* (7), 21–48.

(13) Kitamoto, D.; Morita, T.; Fukuoka, T.; Konishi, M. a.; Imura, T. Self-Assembling Properties of Glycolipid Biosurfactants and Their Potential Applications. *Curr. Opin. Colloid Interface Sci.* **2009**, *14* (5), 315–328.

(14) Praetorius, N. P.; Mandal, T. K. Engineered Nanoparticles in Cancer Therapy. *Recent Pat. Drug Deliv. Formul.* **2007**, *1* (1), 37–51.

(15) Subedi, R. K.; Kang, K. W.; Choi, H.-K. Preparation and Characterization of Solid Lipid Nanoparticles Loaded with Doxorubicin. *Eur. J. Pharm. Sci.* **2009**, *37* (3–4), 508–513.

(16) Pinheiro, A. V; Han, D.; Shih, W. M.; Yan, H. Challenges and Opportunities for Structural DNA Nanotechnology. *Nat. Nanotechnol.* **2011**, *6* (12), 763–772.

(17) Krishnan, Y.; Simmel, F. C. Nucleic Acid Based Molecular Devices. *Angew. Chemie - Int. Ed.* **2011**, *50* (14), 3124–3156.

(18) Gattuso, G.; Menzer, S.; Nepogodiev, S. A.; Stoddart, J. F.; Williams, D. J. Carbohydrate Nanotubes. *Angew. Chemie-International Ed. English* **1997**, *36* (13–14), 1451–1454.

(19) Jayawarna, V.; Ali, M.; Jowitt, T. A.; Miller, A. F.; Saiani, A.; Gough, J. E.; Ulijn, R. V. Nanostructured Hydrogels for Three-Dimensional Cell Culture through Self-Assembly of Fluorenylmethoxycarbonyl-Dipeptides. *Adv. Mater.* **2006**, *18* (5), 611–614.

(20) Elbert, D. L.; Herbert, C. B.; Hubbell, J. A. Thin Polymer Layers Formed by Polyelectrolyte Multilayer Techniques on Biological Surfaces. *Langmuir* **1999**, *15* (16), 5355–5362.

(21) Costa, R. R.; Mano, J. F. Polyelectrolyte Multilayered Assemblies in Biomedical Technologies. *Chem. Soc. Rev.* **2014**, *43* (10), 3453–3479.

(22) Whang, D.; Jin, S.; Wu, Y.; Lieber, C. M. Large-Scale Hierarchical Organization of Nanowire Arrays for Integrated Nanosystems. *Nano Lett.* **2003**, *3* (9), 1255–1259.

(23) Aizenberg, J.; Black, a J.; Whitesides, G. M. Control of Crystal Nucleation by Patterned Self-Assembled Monolayers. *Nature* **1999**, *398* (6727), 495–498.

(24) Decher, G.; Hong, J. D.; Schmitt, J. Buildup of Ultrathin Multilayer Films by a Self-Assembly Process: III. Consecutively Alternating Adsorption of Anionic and Cationic Polyelectrolytes on Charged Surfaces. *Thin Solid Films* **1992**, *210–211*, 831–835.

(25) Keller, C. A.; Glasmästar, K.; Zhdanov, V. P.; Kasemo, B. Formation of Supported Membranes from Vesicles. *Phys. Rev. Lett.* **2000**, *84* (23), 5443–5446.

(26) Hara, M. *Polyelectrolytes: Science and Technology*; 1992.

(27) Blodgett, K. B.; Langmuir, I. Built-Up Films of Barium Stearate and Their Optical Properties. *Phys. Rev.* **1937**, *51* (11), 964–982.

(28) Decher, G.; Eckle, M.; Schmitt, J.; Struth, B. Layer-by-Layer Assembled Multicomposite Films. *Curr. Opin. Colloid Interface Sci.* **1998**, *3* (1), 32–39.

(29) Detzel, C. J.; Larkin, A. L.; Rajagopalan, P.; Detzel, C. J.; Larkin, A. L.; Rajagopalan, P. Multilayers in Tissue Engineering. *Tissue Eng. Part B. Rev.* **2011**, *17* (2), 101–113.

(30) Farhat, T. R.; Schlenoff, J. B. Ion Transport and Equilibria in Polyelectrolyte Multilayers. *Langmuir* **2001**, *17* (4), 1184–1192.

(31) Schlenoff, J. B.; Ly, H.; Li, M. Charge and Mass Balance in Polyelectrolyte Multilayers. *J. Am. Chem. Soc.* **1998**, *120* (30), 7626–7634.

(32) Wu, A.; Yoo, D.; Lee, J. K.; Rubner, M. F. Solid-State Light-Emitting Devices Based on the Tris-Chelated ruthenium(II) Complex: 3. High Efficiency Devices via a Layer-by-Layer Molecular-Level Blending Approach. *J. Am. Chem. Soc.* **1999**, *121*, 4883–4891.

(33) Ouyang, L.; Malaisamy, R.; Bruening, M. L. Multilayer Polyelectrolyte Films as Nanofiltration Membranes for Separating Monovalent and Divalent Cations. *J. Memb. Sci.* **2008**, *310* (1–2), 76–84.

(34) Onitsuka, O.; Fou, a C.; Ferreira, M.; Hsieh, B. R.; Rubner, M. F. Enhancement of Light Emitting Diodes Based on Self-Assembled Heterostructures of Poly(p-Phenylene Vinylene). *J. Appl. Phys.* **1996**, *80* (7), 4067–4071.

(35) Patel, I. F.; Kiryukhin, M. V.; Yakovlev, N. L.; Gupta, H. S.; Sukhorukov, G. B. Naturally Inspired Polyelectrolyte Multilayer Composite Films Synthesised through Layer-by-Layer Assembly and Chemically Infiltrated with $CaCO_3$. *J. Mater. Chem. B* **2015**, *3* (24), 4821–4830.

(36) Holmes, C.; Daoud, J.; Bagnaninchi, P. O.; Tabrizian, M. Polyelectrolyte Multilayer Coating of 3D Scaffolds Enhances Tissue Growth and Gene Delivery: Non-Invasive and Label-Free Assessment. *Adv. Healthc. Mater.* **2014**, *3* (4), 572–580.

(37) C. Gao, E. Donath, S.Moya, V. Dudnik, H. M. Elasticity of Hollow Polyelectrolyte Capsules Prepared by the Layer-by-Layer Technique. *Eur. Phys. J. E* **2001**, *5*, 21–27.

(38) Lvov, Y.; Ariga, K.; Ichinose, I.; Kunitake, T. Assembly of Multicomponent Protein Films by Means of Electrostatic Layer-by-Layer Adsorption. *J. Am. Chem. Soc.* **1995**, *117*, 6117–6123.

(39) Decher, G.; Lehr, B.; Lowack, K.; Lvov, Y.; Schmitt, J. New Nanocomposite Films for Biosensors: Layer-by-Layer Adsorbed Films of Polyelectrolytes, Proteins or DNA. *Biosens. Bioelectron.* **1994**, *9* (9–10), 677–684.

(40) Laurent, D.; Schlenoff, J. B. Multilayer Assemblies of Redox Polyelectrolytes. *Langmuir* **1997**, *7463* (25), 1552–1557.

(41) Sukhorukov, G. B.; Donath, E.; Lichtenfeld, H.; Knippel, E.; Knippel, M.; Budde, A.; Mohwald, H. Layer-by-Layer Self Assembly of Polyelectrolytes on Colloidal Particles. *Colloids Surfaces a-Physicochemical Eng. Asp.* **1998**, *137* (1–3), 253–266.

(42) Donath, E.; Sukhorukov, G. B.; Caruso, F.; Davis, S. a; Möhwald, H. Novel Hollow Polymer Shells by Colloid- Templated Assembly of Polyelectrolytes. *Angew Chem Int Ed Engl* **1998**, *37* (16), 2201–2205.

(43) Georgieva, R.; Moya, S. E.; Bäumler, H.; Möhwald, H.; Donath, E. Controlling Ionic Conductivity in Lipid Polyelectrolyte Composite Capsules by Cholesterol. *J. Phys. Chem. B* **2005**, *109* (38), 18025–18030.

(44) Krebs, T.; Tan, H. L.; Andersson, G.; Morgner, H.; Gregory Van Patten, P. Increased Layer Interdiffusion in Polyelectrolyte Films upon Annealing in Water and Aqueous Salt Solutions. *Phys. Chem. Chem. Phys.* **2006**, *8*, 5462–5468.

(45) Shiratori, S. S.; Rubner, M. F. pH-Dependent Thickness Behavior of Sequentially Adsorbed Layers of Weak Polyelectrolytes. *Macromolecules* **2000**, *33* (11), 4213–4219.

(46) Gregurec, D.; Olszyna, M.; Politakos, N.; Yate, L.; Dahne, L.; Moya, S. E. Stability of Polyelectrolyte Multilayers in Oxidizing Media: A Critical Issue for the Development of Multilayer Based Membranes for Nanofiltration. *Colloid Polym. Sci.* **2014**, *293* (2), 381–388.

(47) Decher, G.; Schmitt, J. Fine-Tuning of the Film Thickness of Ultrathin Multilayer Films Composed of Consecutively Alternating Layers of Anionic and Cationic Polyelectrolytes.

Prog. Colloid Polym. Sci. **1992**, *89*, 160–164.

(48) Köhler, K.; Shchukin, D. G.; Möhwald, H.; Sukhorukov, G. B. Thermal Behavior of Polyelectrolyte Multilayer Microcapsules. 1. The Effect of Odd and Even Layer Number. *J. Phys. Chem. B* **2005**, *109* (39), 18250–18259.

(49) Gao, C.; Leporatti, S.; Moya, S.; Donath, E.; Möhwald, H. Swelling and Shrinking of Polyelectrolyte Microcapsules in Response to Changes in Temperature and Ionic Strength. *Chem. - A Eur. J.* **2003**, *9* (4), 915–920.

(50) Köhler, K.; Shchukin, D. G.; Sukhorukov, G. B.; Möhwald, H. Drastic Morphological Modification of Polyelectrolyte Microcapsules Induced by High Temperature. *Macromolecules* **2004**, *37* (25), 9546–9550.

(51) Leporatti, S.; Gao, C.; Voigt, a; Donath, E.; Möhwald, H. Shrinking of Ultrathin Polyelectrolyte Multilayer Capsules upon Annealing: A Confocal Laser Scanning Microscopy and Scanning Force Microscopy Study. *Eur. Phys. J. E* **2001**, *5* (1), 13–20.

(52) Glinel, K.; Déjugnat, C.; Prevot, M.; Schöler, B.; Schönhoff, M.; Klitzing, R. V. Responsive Polyelectrolyte Multilayers. *Colloids Surfaces A Physicochem. Eng. Asp.* **2007**, *303* (1–2), 3–13.

(53) Picart, C.; Lavalle, P.; Hubert, P.; Cuisinier, F. J. G.; Decher, G.; Schaaf, P.; Voegel, J.-C. Buildup Mechanism for Poly(L -lysine)/Hyaluronic Acid Films onto a Solid Surface. *Langmuir* **2001**, *17* (17), 7414–7424.

(54) Gribova, V.; Auzely-Velty, R.; Picart, C. Polyelectrolyte Multilayer Assemblies on Materials Surfaces: From Cell Adhesion to Tissue Engineering. *Chem. Mater.* **2012**, *24* (5), 854–869.

(55) Ventre, M.; Netti, P. A. Engineering Cell Instructive Materials To Control Cell Fate and Functions through Material Cues and Surface Patterning. *ACS Appl. Mater. Interfaces* **2016**, acsami.5b08658.

(56) Murphy, N. P.; Lampe, K. J.; Murphy, N. P. Mimicking Biological Phenomena in Hydrogel-Based Biomaterials to Promote Dynamic Cellular Responses. *J. Mater. Chem. B* **2015**, *3*, 7867–7880.

(57) Sicari, B. M.; Londono, R.; Badylak, S. F. Strategies for Skeletal Muscle Tissue Engineering: Seed vs. Soil. *J. Mater. Chem. B* **2015**, *3* (40), 7881–7895.

(58) Bačáková, L.; Filová, E.; Rypáček, F.; Švorčík, V.; Starý, V. Cell Adhesion on Artificial Materials for Tissue Engineering. *Physiol. Res.* **2004**, *53* (SUPPL. 1).

(59) Biela, S. A.; Su, Y.; Spatz, J. P.; Kemkemer, R. Different Sensitivity of Human Endothelial Cells, Smooth Muscle Cells and Fibroblasts to Topography in the Nano-Micro Range. *Acta Biomater.* **2009**, *5* (7), 2460–2466.

(60) Mih, J. D.; Marinkovic, A.; Liu, F.; Sharif, A. S.; Tschumperlin, D. J. Matrix Stiffness Reverses the Effect of Actomyosin Tension on Cell Proliferation. *J. Cell Sci.* **2012**, *125* (Pt 24), 5974–5983.

(61) Bacakova, L.; Filova, E.; Parizek, M.; Ruml, T.; Svorcik, V. Modulation of Cell Adhesion, Proliferation and Differentiation on Materials Designed for Body Implants. *Biotechnol.*

Adv. **2011**, *29* (6), 739–767.

(62) Engler, A.; Sheehan, M.; Sweeney, H. L.; Discher, D. E. Substrate Compliance vs Ligand Density in Cell on Gel Responses. *Eur. Cells Mater.* **2003**, *6* (SUPPL. 1), 7–8.

(63) Kharkar, P. M.; Kiick, K. L.; Kloxin, A. M. Designing Degradable Hydrogels for Orthogonal Control of Cell Microenvironments. *Chem. Soc. Rev.* **2013**, *42* (17), 7335–7372.

(64) Saxena, S.; Spears, M. W.; Yoshida, H.; Gaulding, J. C.; García, A. J.; Lyon, L. A. Microgel Film Dynamics Modulate Cell Adhesion Behavior. *Soft Matter* **2014**, *10* (9), 1356–1364.

(65) Muzzio, N. E.; Pasquale, M. A.; Gregurec, D.; Diamanti, E.; Kosutic, M.; Azzaroni, O.; Moya, S. E. Polyelectrolytes Multilayers to Modulate Cell Adhesion: A Study of the Influence of Film Composition and Polyelectrolyte Interdigitation on the Adhesion of the A549 Cell Line. *Macromol. Biosci.* **2016**, *16* (4), 482–495.

(66) Chang, H.; Zhang, H.; Hu, M.; Chen, X.; Ren, K.; Wang, J.; Ji, J. Surface Modulation of Complex Stiffness via Layer-by-Layer Assembly as a Facile Strategy for Selective Cell Adhesion. *Biomater. Sci.* **2015**, *3* (2), 352–360.

(67) Chaubaroux, C.; Vrana, E.; Debry, C.; Schaaf, P.; Senger, B.; Voegel, J. C.; Haikel, Y.; Ringwald, C.; Hemmerl??, J.; Lavalle, P.; et al. Collagen-Based Fibrillar Multilayer Films Cross-Linked by a Natural Agent. *Biomacromolecules* **2012**, *13* (7), 2128–2135.

(68) Kocgozlu, L.; Lavalle, P.; Koenig, G.; Senger, B.; Haikel, Y.; Schaaf, P.; Voegel, J.-C.; Tenenbaum, H.; Vautier, D. Selective and Uncoupled Role of Substrate Elasticity in the Regulation of Replication and Transcription in Epithelial Cells. *J. Cell Sci.* **2010**, *123* (Pt 1), 29–39.

(69) Schneider, A.; Richert, L.; Francius, G.; Voegel, J.-C.; Picart, C. Elasticity, Biodegradability and Cell Adhesive Properties of Chitosan/hyaluronan Multilayer Films. *Biomed. Mater.* **2007**, *2* (1), S45-51.

(70) Schmidt, S.; Madaboosi, N.; Uhlig, K.; Köhler, D.; Skirtach, A.; Duschl, C.; Möhwald, H.; Volodkin, D. V. Control of Cell Adhesion by Mechanical Reinforcement of Soft Polyelectrolyte Films with Nanoparticles. *Langmuir* **2012**, *28* (18), 7249–7257.

(71) Francius, G.; Hemmerl??, J.; Ball, V.; Lavalle, P.; Picart, C.; Voegel, J. C.; Schaaf, P.; Senger, B. Stiffening of Soft Polyelectrolyte Architectures by Multilayer Capping Evidenced by Viscoelastic Analysis of AFM Indentation Measurements. *J. Phys. Chem. C* **2007**, *111* (23), 8299–8306.

(72) Zhu, X.; Jańczewski, D.; Lee, S. S. C.; Teo, S. L. M.; Vancso, G. J. Cross-Linked Polyelectrolyte Multilayers for Marine Antifouling Applications. *ACS Appl. Mater. Interfaces* **2013**, *5* (13), 5961–5968.

(73) Zhu, X.; Guo, S.; Jańczewski, D.; Parra Velandia, F. J.; Teo, S. L.-M. M.; Vancso, G. J. Multilayers of Fluorinated Amphiphilic Polyions for Marine Fouling Prevention. *Langmuir* **2013**, *30*, 288–296.

(74) Zhu, X.; Jańczewski, D.; Guo, S.; Lee, S. S. C.; Parra Velandia, F. J.; Teo, S. L.; He, T.; Puniredd, S. R.; Vancso, G. J. Polyion Multilayers with Precise Surface Charge Control

for Antifouling. *ACS Appl. Mater. Interfaces* **2015**, *7*, 852–861.

(75) Irigoyen, J.; Politakos, N.; Murray, R.; Moya, S. E. Design and Fabrication of Regenerable Polyelectrolyte Multilayers for Applications in Foulant Removal. *Macromol. Chem. Phys.* **2014**, *215* (16), 1543–1550.

(76) Guo, S.; Jańczewski, D.; Zhu, X.; Quintana, R.; He, T.; Neoh, K. G. Surface Charge Control for Zwitterionic Polymer Brushes: Tailoring Surface Properties to Antifouling Applications. *J. Colloid Interface Sci.* **2015**, *452*, 43–53.

(77) Zhou, J.; Romero, G.; Rojas, E.; Ma, L.; Moya, S.; Gao, C. Layer by Layer Chitosan/alginate Coatings on Poly(lactide-Co-Glycolide) Nanoparticles for Antifouling Protection and Folic Acid Binding to Achieve Selective Cell Targeting. *J. Colloid Interface Sci.* **2010**, *345* (2), 241–247.

(78) Edidin, M. Lipids on the Frontier: A Century of Cell-Membrane Bilayers. *Nat. Rev. Mol. Cell Biol.* **2003**, *4* (5), 414–418.

(79) Vinet, L.; Zhedanov, A. *A "missing" family of Classical Orthogonal Polynomials*; 2010; Vol. 7.

(80) Singer, S. J.; Nicolson, G. L. The Fluid Mosaic Model of the Structure of Cell Membranes. *Science (80-.).* **1972**, *175* (4023), 720–731.

(81) Current Topics in Biophysics 2001 Vol.25(1). **2001**.

(82) Gregoriadis, G. Liposome Technology: Liposome Preparation and Related Techniques https://books.google.com/books?id=7tIvMH9Cp8UC&pgis=1 (accessed Apr 3, 2016).

(83) Jesorka, A.; Orwar, O. Liposomes: Technologies and Analytical Applications. *Annu. Rev. Anal. Chem. (Palo Alto. Calif).* **2008**, *1*, 801–832.

(84) Lasic, D. D.; Martin, F. J. On the Mechanism of Vesicle Formation. *J. Memb. Sci.* **1990**, *50* (2), 215–222.

(85) Huang, C. Studies on Phosphatidylcholine Vesicles. Formation and Physical Characteristics. *Biochemistry* **1969**, *8* (1), 344–352.

(86) Hope, M.; Nayar, R.; Mayer, L. Reduction of Liposome Size and Preparation of Unilamellar Vesicles by Extrusion Techniques. *Liposome Technol.* **1993**, *I*, 123–139.

(87) Berger, N.; Sachse, A.; Bender, J.; Schubert, R.; Brandl, M. Filter Extrusion of Liposomes Using Different Devices: Comparison of Liposome Size, Encapsulation Efficiency, and Process Characteristics. *Int. J. Pharm.* **2001**, *223* (1–2), 55–68.

(88) MacDonald, R. C.; MacDonald, R. I.; Menco, B. P. M.; Takeshita, K.; Subbarao, N. K.; Hu, L. R. Small-Volume Extrusion Apparatus for Preparation of Large, Unilamellar Vesicles. *Biochim. Biophys. Acta - Biomembr.* **1991**, *1061* (2), 297–303.

(89) MacDonald, R. C.; Jones, F. D.; Qui, R. Fragmentation into Small Vesicles of Dioleoylphosphatidylcholine Bilayers during Freezing and Thawing. *BBA - Biomembr.* **1994**, *1191* (2), 362–370.

(90) Haberland, M. E.; Reynolds, J. a. Self-Association of Cholesterol in Aqueous Solution.

Proc. Natl. Acad. Sci. U. S. A. **1973**, *70* (8), 2313–2316.

(91) Fleischer, S.; Brierley, G. Solubilization of Cholesterol in Phospholipid Micelles in Water. *Biochem. Biophys. Res. Commun.* **1961**, *5* (5), 367–372.

(92) Naumowicz, M.; Figaszewski, Z. A. Pore Formation in Lipid Bilayer Membranes Made of Phosphatidylcholine and Cholesterol Followed by Means of Constant Current. *Cell Biochem. Biophys.* **2013**, *66* (1), 109–119.

(93) Karolis, C.; Coster, H. G.; Chilcott, T. C.; Barrow, K. D. Differential Effects of Cholesterol and Oxidised-Cholesterol in Egg Lecithin Bilayers. *Biochim. Biophys. Acta* **1998**, *1368* (2), 247–255.

(94) Naumowicz, M.; Figaszewski, Z. a. Impedance Analysis of Lipid Domains in Phosphatidylcholine Bilayer Membranes Containing Ergosterol. *Biophys. J.* **2005**, *89* (5), 3174–3182.

(95) Bi, Z. C.; Tien, H. T.; Ottova, A. L. The Lipid Bilayer Concept and Its Experimental Realization. *Prog. Biochem. Biophys.* **2001**, *28* (4), 447–454.

(96) Hladky, S. B.; Haydon, D. A. Ion Transfer across Lipid Membranes in the Presence of Gramicidin A. I. Studies of the Unit Conductance Channel. *BBA - Biomembr.* **1972**, *274* (2), 294–312.

(97) Mueller, P.; Rudin, D. O. Action Potentials Induced in Biomolecular Lipid Membranes. *Nature* **1968**, *217*, 713–719.

(98) Tombola, F.; Carlesso, C.; Szabò, I.; de Bernard, M.; Reyrat, J. M.; Telford, J. L.; Rappuoli, R.; Montecucco, C.; Papini, E.; Zoratti, M. Helicobacter Pylori Vacuolating Toxin Forms Anion-Selective Channels in Planar Lipid Bilayers: Possible Implications for the Mechanism of Cellular Vacuolation. *Biophys. J.* **1999**, *76* (3), 1401–1409.

(99) Ren, D.; Navarro, B.; Xu, H.; Yue, L.; Shi, Q.; Clapham, D. E. A Prokaryotic Voltage-Gated Sodium Channel. *Science (80-.).* **2001**, *294* (5550), 2372–2375.

(100) Lundbæk, J. A. Regulation of Membrane Protein Function by Lipid Bilayer Elasticity-a Single Molecule Technology to Measure the Bilayer Properties Experienced by an Embedded Protein. *J. Phys. Condens. Matter* **2006**, *18* (28), S1305-44.

(101) Keller, C. A.; Kasemo, B. Surface Specific Kinetics of Lipid Vesicle Adsorption Measured with a Quartz Crystal Microbalance. *Biophys. J.* **1998**, *75* (September), 1397–1402.

(102) Reimhult, E.; Höök, F.; Kasemo, B. Vesicle Adsorption on SiO2 and TiO2: Dependence on Vesicle Size. *J. Chem. Phys.* **2002**, *117* (16), 7401–7404.

(103) Rossetti, F. F.; Textor, M.; Reviakine, I. Asymmetric Distribution of Phosphatidyl Serine in Supported Phospholipid Bilayers on Titanium Dioxide. *Langmuir* **2006**, *22* (8), 3467–3473.

(104) Richter, R. P.; Escarpit, R. R.; Cedex, P. In V Ited Feature Article Formation of Solid-Supported Lipid Bilayers : An Integrated View. *Langmuir* **2006**, *22* (8), 3497–3505.

(105) Reviakine, I.; Brisson, A. Formation of Supported Phospholipid Bilayers from Unilamellar Vesicles Investigated by Atomic Force Microscopy. *Langmuir* **2000**, *16* (4), 1806–1815.

(106) Richter, R. P.; Maury, N.; Brisson, A. R.; Bordeaux, I.; Escarpit, R. R.; Cedex, P. On the Effect of the Solid Support on the Interleaflet Distribution of Lipids in Supported Lipid Bilayers. *Langmuir* **2005**, *21*, 299–304.

(107) Reimhult, E.; Zäch, M.; Höök, F.; Kasemo, B. A Multitechnique Study of Liposome Adsorption on Au and Lipid Bilayer Formation on SiO2. *Langmuir* **2006**, *22* (7), 3313–3319.

(108) Cremer, P. S.; Boxer, S. G. Formation and Spreading of Lipid Bilayers on Planar Glass Supports. *J. Phys. Chem. B* **1999**, *103*, 2554–2559.

(109) Spinke, J.; Yang, J.; Wolf, H.; Liley, M.; Ringsdorf, H.; Knoll, W. Polymer-Supported Bilayer on a Solid Substrate. *Biophys. J.* **1992**, *63* (6), 1667–1671.

(110) Gabriela Romero, David José Sanz a, Yuan Qiu a, Dahai Yu b, Zhengwei Mao b, Changyou Gao b, and S. E. M. Lipid Layer Engineering of Poly(lactide-Co-Glycolide) Nanoparticles to Control Their Uptake and Intracellular Co-Localization . **2013**, *35*, 1–3.

(111) McConnell, H. M.; Watts, T. H.; Weis, R. M.; Brian, A. A. Supported Planar Membranes in Studies of Cell-Cell Recognition in the Immune System. *BBA - Rev. Biomembr.* **1986**, *864* (1), 95–106.

(112) Kalb, E.; Frey, S.; Tamm, L. K. Formation of Supported Planar Bilayers by Fusion of Vesicles to Supported Phospholipid Monolayers. *Biochimica et Biophysica Acta (BBA) - Biomembranes*, 1992, *1103*, 307–316.

(113) Thid, D.; Holm, K.; Eriksson, P. S.; Ekeroth, J.; Kasemo, B.; Gold, J. Supported Phospholipid Bilayers as a Platform for Neural Progenitor Cell Culture. *J. Biomed. Mater. Res. A* **2008**, *84* (4), 940–953.

(114) Vallejo, A. E.; Gervasi, C. A. Chapter 10 On the Use of Impedance Spectroscopy for Studying Bilayer Lipid Membranes. In *Advances in Planar Lipid Bilayers and Liposomes*; 2006; Vol. 3, pp 331–353.

(115) Naumowicz, M.; Figaszewski, Z. Impedance Analysis of Phosphatidylcholine Membranes Modified with Gramicidin D. *Bioelectrochemistry* **2003**, *61* (1–2), 21–27.

(116) Terrettaz, S.; Mayer, M.; Vogel, H. Highly Electrically Insulating Tethered Lipid Bilayers for Probing the Function of Ion Channel Proteins. *Langmuir* **2003**, *19* (14), 5567–5569.

(117) Reimhult, E.; Kasemo, B.; Höök, F. Rupture Pathway of Phosphatidylcholine Liposomes on Silicon Dioxide. *Int. J. Mol. Sci.* **2009**, *10* (4), 1683–1696.

(118) Edvardsson, M.; Svedhem, S.; Wang, G.; Richter, R.; Rodahl, M.; Kasemo, B. QCM-D and Reflectometry Instrument: Applications to Supported Lipid Structures and Their Biomolecular Interactions. *Anal. Chem.* **2009**, *81* (1), 349–361.

(119) Jackman, J.; Knoll, W.; Cho, N.-J. Biotechnology Applications of Tethered Lipid Bilayer Membranes. *Materials (Basel).* **2012**, *5* (12), 2637–2657.

(120) Mayer, M.; Terrettaz, S.; Stora, T.; Vogel, H.; Al, E. T. Chapter 8 Functional Analysis of Ion Channels : Planar Patch Clamp and Impedance Spectroscopy of Tethered Lipid Membranes. 153–184.

(121) Naumann, R.; Schiller, S. M.; Giess, F.; Grohe, B.; Hartman, K. B.; Kärcher, I.; Köper, I.; Lübben, J.; Vasilev, K.; Knoll, W. Tethered Lipid Bilayers on Ultraflat Gold Surfaces. *Langmuir* **2003**, *19* (13), 5435–5443.

(122) Cornell, B. a; Braach-Maksvytis, V. L. B.; King, L. G.; Osman, P. D. J.; Raguse, B.; Wieczorek, L.; Pace, R. J. Abiosensor That Uses Ion-Channel Switches. *Nature* **1997**, *387* (6633), 580–583.

(123) Naumann, R.; Schmidt, E. K.; Jonczyk, A.; Fendler, K.; Kadenbach, B.; Liebermann, T.; Offenhausser, A.; Knoll, W. The Peptide-Tethered Lipid Membrane as a Biomimetic System to Incorporate Cytochrome c Oxidase in a Funnctionallu Active Form. *Biosens. Bioelectron.* **1999**, *14*, 651–662.

(124) Keizer, H. M.; Dorvel, B. R.; Andersson, M.; Fine, D.; Price, R. B.; Long, J. R.; Dodabalapur, A.; K??per, I.; Knoll, W.; Anderson, P. A. V; et al. Functional Ion Channels in Tethered Bilayer Membranes - Implications for Biosensors. *ChemBioChem* **2007**, *8* (11), 1246–1250.

(125) Andersson, M.; Okeyo, G.; Wilson, D.; Keizer, H.; Moe, P.; Blount, P.; Fine, D.; Dodabalapur, A.; Duran, R. S. Voltage-Induced Gating of the Mechanosensitive MscL Ion Channel Reconstituted in a Tethered Lipid Bilayer Membrane. *Biosens. Bioelectron.* **2008**, *23* (6), 919–923.

(126) Tanaka, M.; Sackmann, E. Polymer-Supported Membranes as Models of the Cell Surface. *Nature* **2005**, *437* (7059), 656–663.

(127) Michel, M.; Arntz, Y.; Fleith, G.; Toquant, J.; Haikel, Y.; Voegel, J.-C.; Schaaf, P.; Ball, V. Layer-by-Layer Self-Assembled Polyelectrolyte Multilayers with Embedded Liposomes: Immobilized Submicronic Reactors for Mineralization. *Langmuir* **2006**, *22* (5), 2358–2364.

(128) Cassier, T.; Sinner, A.; Offenhäuser, A.; Möhwald, H. Homogeneity, Electrical Resistivity and Lateral Diffusion of Lipid Bilayers Coupled to Polyelectrolyte Multilayers. *Colloids Surfaces B Biointerfaces* **1999**, *15* (3–4), 215–225.

(129) Wang, L.; Schönhoff, M.; Möhwald, H.; Scho, M. Lipids Coupled to Polyelectrolyte Multilayers: Ultraslow Diffusion and the Dynamics of Electrostatic Interactions. *J. Phys. Chem. B* **2002**, *106*, 9135–9142.

(130) Kügler, R.; Knoll, W. Polyelectrolyte-Supported Lipid Membranes. *Bioelectrochemistry* **2002**, *56* (1–2), 175–178.

(131) Georgieva, R.; Moya, S.; Donath, E.; Bäumler, H. Permeability and Conductivity of Red Blood Cell Templated Polyelectrolyte Capsules Coated with Supplementary Layers. *Langmuir* **2004**, *20* (5), 1895–1900.

(132) Fischlechner, M.; Zaulig, M.; Meyer, S.; Estrela-Lopis, I.; Cuéllar, L.; Irigoyen, J.; Pescador, P.; Brumen, M.; Messner, P.; Moya, S.; et al. Lipid Layers on Polyelectrolyte Multilayer Supports. *Soft Matter* **2008**, *4* (11), 2245–2258.

(133) Moya, S. E.; Georgieva, R.; Bäumler, H.; Richter, W.; Donath, E. Composite Lipid Polyelectrolyte Capsules Templated on Red Blood Cells: Fabrication and Structural Characterisation. *Med. Biol. Eng. Comput.* **2003**, *41* (4), 504–508.

(134) Moya, S.; Donath, E.; Sukhorukov, G. B.; Auch, M.; Ba, H.; Lichtenfeld, H.; Mo, H. Lipid Coating on Polyelectrolyte Surface Modified Colloidal Particles and Polyelectrolyte Capsules. *Macromolecules* **2000**, *33*, 4538–4544.

(135) Georgieva, R.; Moya, S.; Leporatti, S.; Neu, B.; Ba, H.; Reichle, C.; Donath, E.; Mo, H. Conductance and Capacitance of Polyelectrolyte and Lipid-Polyelectrolyte Composite Capsules As Measured by Electrorotation. *Langmuir* **2000**, *16* (17), 7075–7081.

(136) Montal, M.; Mueller, P. Formation of Bimolecular Membranes from Lipid Monolayers and a Study of Their Electrical Properties. *Proc. Natl. Acad. Sci. U. S. A.* **1972**, *69* (12), 3561–3566.

(137) Lundgren, A.; Hedlund, J.; Andersson, O.; Brändén, M.; Kunze, A.; Elwing, H.; Höök, F. Resonance-Mode Electrochemical Impedance Measurements of Silicon Dioxide Supported Lipid Bilayer Formation and Ion Channel Mediated Charge Transport. *Anal. Chem.* **2011**, *83* (20), 7800–7806.

(138) Zhou, J.; Wang, Q. X.; Zhang, C. Y. Liposome-Quantum Dot Complexes Enable Multiplexed Detection of Attomolar DNAs without Target Amplification. *J. Am. Chem. Soc.* **2013**, *135* (6), 2056–2059.

(139) Lin, J.; Szymanski, J.; Searson, P. C.; Hristova, K.; Chsearson, P.; Hristova, K. Effect of a Polymer Cushion on the Electrical Properties and Stability of Surface-Supported Lipid Bilayers. *Langmuir* **2009**, *26* (5), 3544–3548.

(140) Singh, S.; Junghans, A.; Tian, J.; Dubey, M.; Gnanakaran, S.; Chlistunoff, J.; Majewski, J. Polyelectrolyte Multilayers as a Platform for pH-Responsive Lipid Bilayers. *Soft Matter* **2013**, *9* (37), 8938.

(141) Kammer, A. R.; Amacker, M.; Rasi, S.; Westerfeld, N.; Gremion, C.; Neuhaus, D.; Zurbriggen, R. A New and Versatile Virosomal Antigen Delivery System to Induce Cellular and Humoral Immune Responses. *Vaccine* **2007**, *25* (41), 7065–7074.

(142) Shimizu, K.; Hosaka, Y.; Shimizu, Y. K. Solubilization of Envelopes of HVJ (Sendai Virus) with Alkali-Emasol Treatment and Reassembly of Envelope Particles with Removal of the Detergent. *J. Virol.* **1972**, *9* (5), 842–850.

(143) Almeida, J.; Edwards, D. C.; Brand, C.; Heath, T. Formation of Virosomes From Influenza Subunits and Liposomes. *Lancet* **1975**, *306* (7941), 899–901.

(144) Bagai, S.; Puri, A.; Blumenthal, R.; Sarkar, D. P. Hemagglutinin-Neuraminidase Enhances F Protein-Mediated Membrane Fusion of Reconstituted Sendai Virus Envelopes with Cells. *J. Virol.* **1993**, *67* (6), 3312–3318.

(145) Kaneda, Y.; Yamamoto, S.; Nakajima, T. Development of HVJ Envelope Vector and Its Application to Gene Therapy. *Adv. Genet.* **2005**, *53* (5), 307–332.

(146) Mair, C. Membrane Fusion Mediated by the Influenza Virus Hemagglutinin – The pH Dependence of Conformational Change and Its Relevance for Host Adaptation, 2014.

(147) Stegmann, T.; Morselt, H. W. M.; Booy, F. P.; van Breemen, J. F.; Scherphof, G.; Wilschut, J.; Booy ', F. P.; Van Breemen ', J. F. L.; Scherphof, G.; Wilschut, J.; et al. Functional Reconstitution of Influenza Virus Envelopes. *EMBO J.* **1987**, *6* (9), 2651–

2659.

(148) Glück, R. Immunopotentiating Reconstituted Influenza Virosomes (IRIVs) and Other Adjuvants for Improved Presentation of Small Antigens. *Vaccine* **1992**, *10* (13), 915–919.

(149) Metsikkö, K.; van Meer, G.; Simons, K. Reconstitution of the Fusogenic Activity of Vesicular Stomatitis Virus. *EMBO J.* **1986**, *5* (13), 3429–3435.

(150) Scheule, R. K. Novel Preparation of Functional Sindbis Virosomes. *Biochem.* **1986**, *25* (1983), 4223–4232.

(151) Grimaldi, S.; Giuliani, A.; Giuliani, A.; Ferroni, L.; Lisi, A.; Santoro, N.; Pozzi, D. Engineered Liposomes and Virosomes for Delivery of Macromolecules. *Res. Virol.* **1995**, *146* (4), 289–293.

(152) Cobaleda, C.; Muñoz-Barroso, I.; Sagrera, A.; Villar, E. Fusogenic Activity of Reconstituted Newcastle Disease Virus Envelopes: A Role for the Hemagglutinin-Neuraminidase Protein in the Fusion Process. *Int. J. Biochem. Cell Biol.* **2002**, *34* (4), 403–413.

(153) Glück, R.; Metcalfe, I. C. Novel Approaches in the Development of Immunopotentiating Reconstituted Influenza Virosomes as Efficient Antigen Carrier Systems. *Vaccine* **2003**, *21* (7–8), 611–615.

(154) Amacker, M.; Engler, O.; Kammer, A. R.; Vadrucci, S.; Oberholzer, D.; Cerny, A.; Zurbriggen, R. Peptide-Loaded Chimeric Influenza Virosomes for Efficient in Vivo Induction of Cytotoxic T Cells. *Int. Immunol.* **2005**, *17* (6), 695–704.

(155) *Delivery Technologies for Biopharmaceuticals*; Jorgensen, L., Nielsen, H. M., Eds.; John Wiley & Sons, Ltd: Chichester, UK, 2009.

(156) Moser, C.; Müller, M.; Kaeser, M. D.; Weydemann, U.; Amacker, M. Influenza Virosomes as Vaccine Adjuvant and Carrier System. *Expert Rev. Vaccines* **2014**.

(157) Felnerova, D.; Viret, J. F.; Glück, R.; Moser, C. Liposomes and Virosomes as Delivery Systems for Antigens, Nucleic Acids and Drugs. *Curr. Opin. Biotechnol.* **2004**, *15* (6), 518–529.

(158) Harrison, S. C. Viral Membrane Fusion. *Nat. Struct. Mol. Biol.* **2008**, *15* (7), 690–698.

(159) de Bruijn, I. A.; Nauta, J.; Gerez, L.; Palache, A. M. The Virosomal Influenza Vaccine Invivac: Immunogenicity and Tolerability Compared to an Adjuvanted Influenza Vaccine (Fluad in Elderly Subjects. *Vaccine* **2006**, *24* (44–46), 6629–6631.

(160) Douglas, T. Viruses: Making Friends with Old Foes. *Science (80-.).* **2006**, *312* (5775), 873–875.

(161) Moser, C.; Amacker, M.; Zurbriggen, R. Influenza Virosomes as a Vaccine Adjuvant and Carrier System. *Expert Rev. Vaccines* **2011**, *10* (7), 437–446.

(162) Bungener, L.; Serre, K.; Bijl, L.; Leserman, L.; Wilschut, J.; Daemen, T.; Machy, P. Virosome-Mediated Delivery of Protein Antigens to Dendritic Cells. *Vaccine* **2002**, *20* (17–18), 2287–2295.

(163) Lee, L. A.; Niu, Z.; Wang, Q. Viruses and Virus-like Protein Assemblies-Chemically Programmable Nanoscale Building Blocks. *Nano Res.* **2009**, *2* (5), 349–364.

(164) Fischlechner, M.; Zschörnig, O.; Hofmann, J.; Donath, E. Engineering Virus Functionalities on Colloidal Polyelectrolyte Lipid Composites. *Angew. Chemie Int. Ed.* **2005**, *44* (19), 2892–2895.

(165) Fischlechner, M.; Donath, E. Viruses as Building Blocks for Materials and Devices. *Angew. Chemie - Int. Ed.* **2007**, *46* (18), 3184–3193.

(166) Toellner, L.; Fischlechner, M.; Ferko, B.; Grabherr, R. M.; Donath, E. Virus-Coated Layer-by-Layer Colloids as a Multiplex Suspension Array for the Detection and Quantification of Virus-Specific Antibodies. *Clin. Chem.* **2006**, *52* (8), 1575–1583.

(167) Johnson, D. C.; Spear, P. G. Monensin Inhibits the Processing of Herpes Simplex Virus Glycoproteins, Their Transport to the Cell Surface, and the Egress of Virions from Infected Cells. *J. Virol.* **1982**, *43* (3), 1102–1112.

Objectives and Aims of the Thesis

This PhD thesis aims to develop PEMs alone or in combination with lipid layers with potential biomedical applications in tissue engineering, antifouling applications, targeting drug delivery or for the fabrication of multifunctional sensor devices. The work focuses on a nanofabrication and characterization aspect. The main objectives and aims of this thesis are the following:

Objective 1

Apply ***thermal annealing*** on biopolymer PEM films as an alternative method to cross-linking in order to tune the physicochemical and mechanical properties of the films to subsequently promote cellular adhesion for applications in tissue engineering. We aim to understand how the thermal annealing affects the physicochemical properties of PEMs, i.e. surface topography, hydrophilicity, surface charge and energy. The enhancement in cell adhesion after annealing will be interpreted on the basis of the changes in the physicochemical properties of the PEMs. Besides, our goal is to study as well, the impact of thermal annealing on the adsorption of proteins for the use of the annealed films in antifouling applications.

Objective 2

To study the conditions for the ***assembly of a lipid bilayer from negatively charged vesicles on top of polyelectrolyte cushions*** with different polymer composition. We aim to understand how the composition of PEMs and vesicles determine either the formation of a bilayer, or the assembly of intact vesicles. The influence of the composition of the lipid vesicles, in terms of percentage of charged and zwitterionic lipids will be first studied. The nature of the interaction between lipids and polyelectrolytes and the role of surface chemistry of the PEM on the bilayer formation will be analyzed. The assembly of vesicles will be performed onto PEMs with a top layer that bears primary amines and a top layer that bears quaternary amines. The role of the polyanions behind the top layer will be considered as well. It will be shown that phosphate ions displayed in PBS play a fundamental role in the formation of lipid bilayers onto PEMs.

Objective 3

To generate a supported lipid bilayer on top of PEMs with a ***resistivity*** that is comparable with that of black lipid membranes, for potential applications in ***electrochemical sensors***. Electrochemical impedance spectroscopy will be applied to characterize the electrical properties of the supported bilayers onto PEMs. We will show that assembling the vesicles in the conditions required for bilayer formation a resistivity of 1.89 10^7 Ω cm^2 will be obtained for the supported bilayer. This value is significantly

higher than the obtained values, reported in literature, hinting the potential use of supported bilayers on PEMs as part of sensors or in bioelectrochemistry.

Objective 4

To study the ***fusion of virosomes on PEM supported lipid membranes*** as a mean to engineer colloidal particles. We aim to get insigth in the conditions and mechanism for virosome fusion on supported membranes taking into consideration the influence of pH, temperature and hemagglutinin content. Virosome fusion offers a new strategy for transferring biological functions on artificial supported membranes with potential applications in targeted delivery and sensing.

The work performed during this PhD-thesis will be presented in the four following chapters.

Chapter 1 deals with the thermal annealing of PEMs to increase cell adhesion and antifouling properties. PEMs of PLL and Alg are fabricated applying the LbL technique and annealed at constant temperature; 37, 50 and 80 °C, for 72 hours. Atomic force microscopy (AFM) is used to reveal changes in the topography of the PEM, from a fibrillar to a smooth surface. Advancing contact angle in water varies from 36° before annealing to 93°, 77° and 95° after annealing at 37, 50 and 80 °C, respectively. Surface energy changes after annealing will be calculated from contact angle measurements performed with organic solvents. Quartz crystal microbalance with dissipation (QCM-D),

contact angle and fluorescence spectroscopy measurements will show a significant decrease in the adsorption of the bovine serum albumin protein to the PEMs after annealing. Cellular adhesion is evaluated by studying the adhesion of human lung cancer A549 and myoblast C2C12 cell lines. It will be shown that cellular adhesion measured by the projected average cell spreading and focal contact is promoted after annealing at 37 °C. Changes in the physical properties of the PEMs are interpreted as a result of the reorganization of the polyelectrolytes in the PEMs from a layered structure into complexes where the interaction of polycations and polyanions is enhanced. This chapter proposes a simple method to endow bio-PEMs with antifouling characteristics and tune their wettability.

Chapter 2 is focused on the mechanism of the assembly of a lipid bilayer on top of PEMs. The self-assembly of mixed vesicles of zwitterionic DOPC and anionic DOPS phospholipids on top of PEMs is investigated as a function of the vesicle composition, PE combination and the solution used for lipids hydration. We showed via QCM-D and fluorescence recovery after photobleaching (FRAP) measurements that vesicles with molar percentages of DOPS between 50 to 70 % resulted in the formation of lipid bilayers on top of PAH/PSS films. Vesicles with over 50 % of DOPC or over 80 % of DOPS did not assembly into bilayers. Atomic force spectroscopy (AFS) studies performed with a PAH modified cantilever approaching and retracting from the lipid assemblies revealed that the main interaction between PAH and lipids is through hydrogen bonding between the amine groups of PAH and the carboxylate and phosphate groups of DOPS and with the phosphate groups of DOPC. The interaction of

PAH with DOPS is much stronger than with DOPC. QCM-D and FRAP experiments also showed that vesicles with a lipid composition of 50 % DOPS and 50 % DOPC did not form complete bilayers neither when PAH is replaced by PDADMAC and nor when PSS is replaced by Alg or PAA. The impact of the mechanical properties of the film to the lipid vesicles rupture and fusion were also considered. The role of the buffer conditions was studied as well and we showed that the use of PBS for the hydration of the lipid film is fundamental for the formation of a bilayer on top of PEMs. X-ray photoelectron spectroscopy (XPS) and ζ – potential measurements revealed that PBS interacted with the primary amine groups of PAH, but not with the quaternary amine groups of PDADMAC, leaving phosphate groups on the surface of the film that subsequently interacted with the lipids.

Chapter 3 is focused on the study of the electrochemical properties of supported membranes on top of PEMs by impedance spectroscopy. The electrical properties of lipid bilayers of 30:70 molar ratio of DOPC:DOPS vesicles supported on 11 layers of PAH/PSS films were studied by electrochemical impedance spectroscopy (EIS). The bilayer supported on the PEMs showed a high resistance, in the order of 10^7 Ω cm^2 which is indicative of a continuous and dense bilayer. Such resistance is comparable with the resistance of black lipid membranes, being the first time that these values are obtained for lipid bilayers supported on PEMs. Furthermore electrochemical impedance studies are also conducted on DOPC:DOPS 30:70 vesicles with the incorporation of 30 % of cholesterol assembled on top of the PEMs. Finally was shown that the assembly of PEs on top of a lipid bilayer decreased the resistance of the bilayer up to 2 orders of

magnitude. The assembly of the PEs on the lipids induced defects or pores in the bilayer, responsible for the decrease in resistance.

Chapter 4 deals with the use of virosomes for engineering colloidal particles and basic studies of virosome fusion on supported membranes. The fusion mechanism of IRIVs to artificial supported lipid membranes were assembled onto PEMs on both colloidal particles and planar substrates. R18 assay was used to prove the IRIVs fusion in dependence of pH, temperature and HA concentration. IRIVs displayed a pH-dependent fusion mechanism, fusing at low pH in analogy to the influenza virus. The pH dependence was confirmed by the QCM-D technique. AFM imaging showed that at low pH virosomes are integrated in the supported membrane displaying flattered features and a reduced vertical thickness.

Materials and Methods

Materials

The following reagents and solvents were employed during this thesis: poly-L-lysine solution 0.1% (w/v) in water (PLL, Mw 150 – 300 kDa), bovine serum albumin hydrolyzed powder, pH 7, ≥ 98 % (BSA, Mw ~ 66 kDa), polyallylamine hydrochloride, (PAH, Mw 15 kDa), poly(styrene sulfonate) sodium salt (PSS, Mw 70 kDa), polyacrylic acid solution in water 35 wt % (PAA, Mw 100 kDa), poly(diallyldimethylammonium chloride) (PDADMAC, Mw 200-350 kDa), cholesterol (Mw 386,65 g/mol), sodium 3-mercapto-1-propanesulfonate (MPS, Mw 178,21 g/mol), rhodamine B octadecyl ester perchlorate, sodium chloride (NaCl), potassium chloride (KCl, 99,99%), phosphate buffer saline (PBS), sodium bicarbonate ($NaHCO_3$), sodium phosphate dibasic (Na_2HPO_4), sodium hydroxide (NaOH), citric acid (CA), (4-(2-hydroxyethyl)-1-piperazineethanesulfonic acid) (Hepes) dimethyl sulfoxide (DMSO) solvent, ethylene glycol (EG), chloroform anhydrous (>99%), anti-mouse IgG-FITC antibody, triton X-100 and tween-20 were obtained from Sigma-Aldrich. Ethanol absolute (99.9% HPLC) was obtained from Scharlau S.A. Alginic acid sodium salt (Alg, Mw 10 – 600 kDa). PAH (Mw 15 kDa) labeled with Rhodamine B isothiocyanate (Rhd) and were kindly offered from Surflay Nanotec GmbH. Fluorescent label ATTO 488 NHS-ester (1 mg) was purchased from ATTO – TEC – Fluorescent Labels and Dyes.

Actin cytoskeleton and focal adhesion staining kit and antifade mounting solution were obtained from Millipore. RPMI 1640 with L-glutamine was purchased from Lonza and fetal bovine serum (FBS) from Fisher.

The phospholipids 1,2-dioleoyl-sn-glycero-3-phosphocholine (DOPC, 10 mg mL^{-1} in chloroform), 1,2-dioleoyl-sn-glycero-3-phospho-L-serine (DOPS, sodium salt, 10 mg mL^{-1} in chloroform), 1-plamitoyl-2-oleoylsn- glycero-3-phosphor-L-serine (POPS, sodium salt, 10 mg mL^{-1} in chloroform), 1-palmitoyl-2-oleoyl-sn-glycero-3-phosphocholine (POPC, 10 mg mL^{-1} in chloroform), chain-labeled 18:1-12:0 NBDPC and 18:1-12:0 NBDPS and polycarbonate membrane filter (50 nm) were purchased from Avanti Polar Lipids, Inc.

The immunostimulating reconstituted influenza virosomes (IRIVs) (7 mg mL^{-1}, lipid DOPC: 1-oleoyl-2-palmitoyl-phosphatidyl ethanolamine (OPPE) in a mass ratio 4:1) were prepared with 1.3 mg mL^{-1} hemagglutinin of the influenza strain A/Sing/6/86 H1N1.

Materials: Disposable PD – 10 desalting columns filled with Sephadex® G-25 gel filtration medium were purchased from GE Healthcare Life Sciences. SiO_2 particles with a diameter of 3 µm and 200 nm were purchased from Attenbio. Gold-coated cantilevers were obtained from Veeco (model NPG-10).

Methods

Quartz Crystal Microbalance with Dissipation (QCM-D)

A quartz crystal is an easy to process, piezoelectric material that generates an electric field when a stress is applied. Crystals used in QCM are in discs shape with overlapping metal electrodes on its two faces, like a parallel plate (**Figure 8a**) and when an alternating electric field is applied to the crystal it resonates at the frequency of the applied field due to the converse piezoelectric effect. The frequency of such oscillation (**Figure 8b**) is determined by the thickness of the crystal and the speed of the shear waves in quartz. Furthermore oscillation decays with the time after the applied voltage is stopped, and dissipation describes the time needed for the amplitude to decay.

Sauerbrey showcased the extremely sensitive nature of these piezoelectric materials towards mass changes at the surface of the quartz crystals and related the mass change per unit area at the QCM crystal to the observed change in oscillation frequency of the crystal by the so called Sauerbrey equation (**Equation 1**)[1].

$$\Delta f = -C_f \times \Delta m \qquad \text{(Eq. 1)}$$

Where Δf, is the observed frequency change (Hz), Δm, is the change in mass per unit area (g/cm^2) and C_f is the sensitivity factor for the crystal used, which for sensors with a resonance frequency of 4.95 ± 0.02 MHz is C_f = 18.06 ± 0.15 ng·cm^{-2} Hz^{-1}.

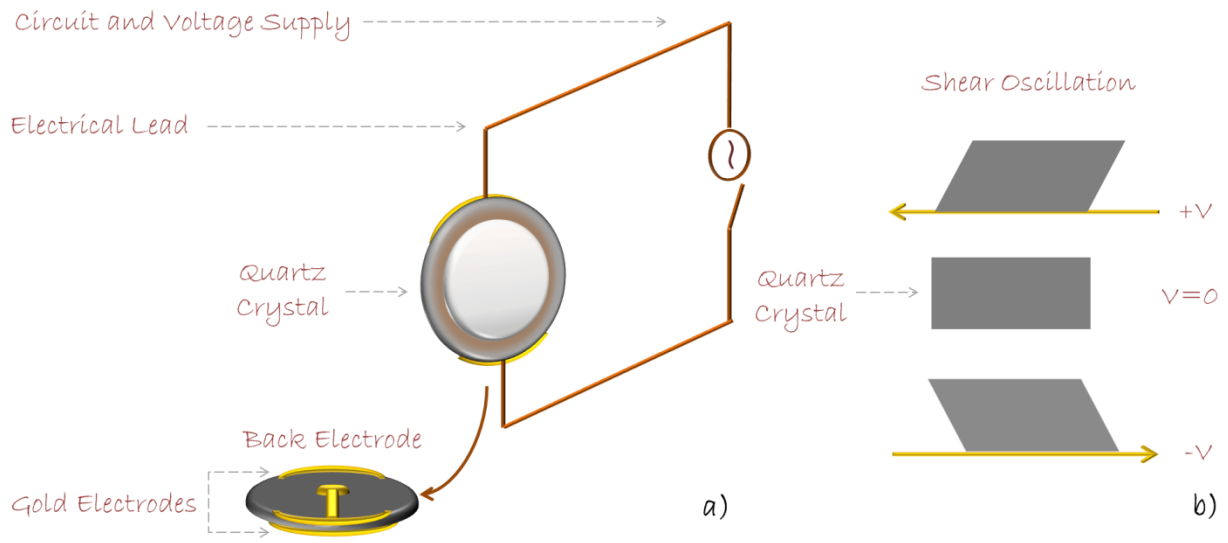

Figure 8 Scheme of a) an electric field applied onto a quartz crystal representation of its components and b) a transverse shear mode of oscillation.

For homogeneous thin films that do not dissipate energy, the relationship between resonance frequency, f_n and the area mass density of the adsorbed film, Δm is linear:

$$\Delta f_n = -{}^{n\Delta m}/_{C} \qquad \text{(Eq. 2)}$$

Where n, is the overtone number. However when it comes to soft or viscoelastic films that do not fully couple to the oscillating crystal the Sauerbrey relationship is not applicable anymore[2]. In these cases the correlation of frequency and mass is more complicated and therefore more complicated data interpretation is required[3,4].

Contact Angle Goniometer

Contact angle goniometer measurements are essential for understanding the wetting characteristics of an analysed surface. The contact angle (*CA*) is defined as the angle made by a sessile drop of liquid (l) in contact with a solid (s) surface and is measured

according the young's equation (**Equation 3**)[5] from the side of the liquid as seen in **Figure 9**.

$$\sigma_{lg} \cos \vartheta = \sigma_{sg} - \sigma_{sl} \quad \text{(Eq. 3)}$$

Analysing the *CA* when a drop of water is placed on a surface we can conclude about the degree of hydrophobicity or hydrophilicity of almost any kind of surfaces[6].

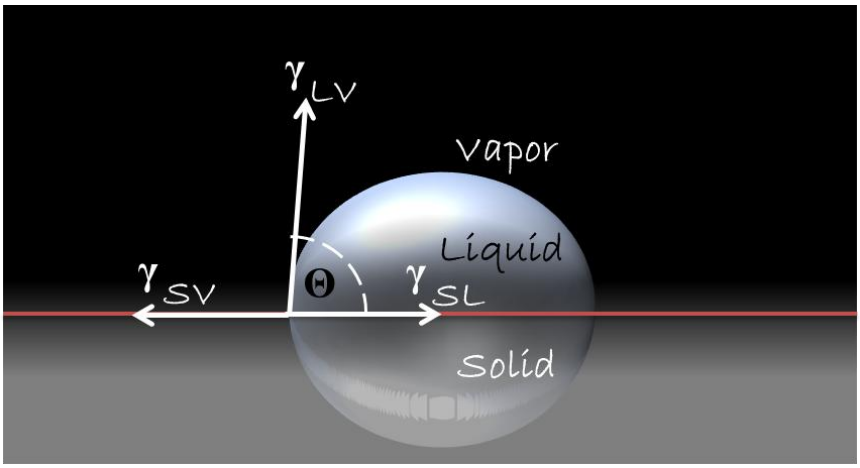

Figure 9 Vector representations of Young's equation on a sessile drop for measuring Young's contact angle.

One of the most common techniques used to measure *CA* is by goniometry, where basically the *CA* is measured by an image of the drop adsorbed on the specimen's surface. After imaging, a tangent is drawn along the solid-liquid interface and the *CA* is measured from the drop profile. Young's model is applied only to systems with smooth and homogeneous surfaces. For rough and heterogeneous surfaces have been established modifications to the Young's model.

The Wilhelmy plate technique developed by Neumann is widely used to determine the advancing and receding contact angles and therefore the surface free energy of analysing surfaces.

Dynamic Light Scattering (DLS)

Dynamic light scattering (DLS) is a powerful technique for probing soft matter particles mainly at the sub-micron region. DLS is based on the time-resolved measurement of the scattered intensity, I(t) produced by particles suspended in a liquid undergoing the Brownian motion. The Brownian motion is correlated with the scattered light therefore the larger the particle, the slower the Brownian motion will be; the diffusion due to Brownian motion of the particles is obtained by recording the rate at of fluctuation of the intensity of the scattered light. Subsequently small particles display more rapid scattered light intensity fluctuation in contrast with large particles. Further information about the random fluctuations in a time-resolved manner is provided by the autocorrelation function (**Equation 4**).

$$g\,(t) = \frac{\langle I(t + t_0) \times I(t_0) \rangle}{\langle I \rangle^2} \qquad \text{(Eq. 4)}$$

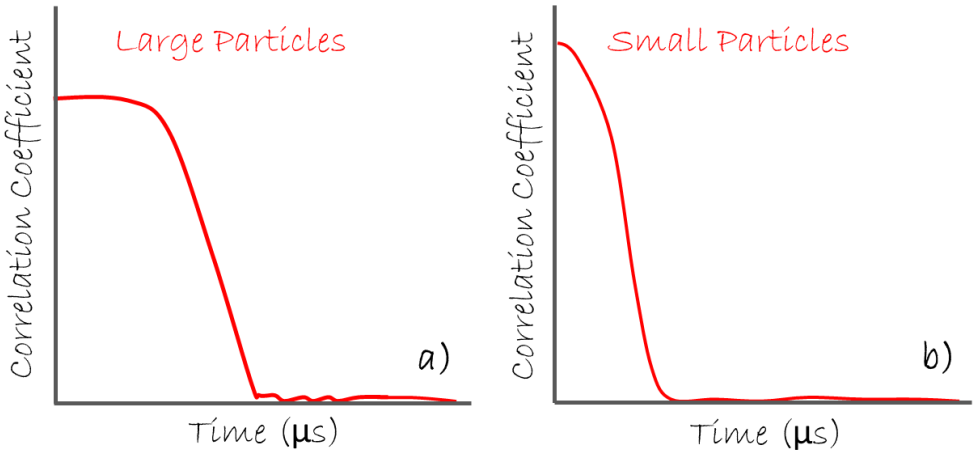

Figure 10 Correlation function obtained from a sample containing a) large particles and b) small particles.

Form the plotted data one can obtain more specific information related to the size of the particles (**Figure 10**). For large particles the correlation of the signal takes more time to decay while for small particles the correlation decreases rapidly as a consequence of the movement of the particles.

According to Stokes-Einstein equation (**Equation 5**) the particle size is given in terms of hydrodynamic radius which is defined by the diameter of a sphere that has the same translational diffusion coefficient as the particle[8].

$$D = \frac{k_B T}{6\pi\eta R_H} \quad \text{(Eq. 5)}$$

Where D is the diffusion coefficient, k_B is Boltzmann's constant, T is the temperature, η is the viscosity of the medium and R_H is the hydrodynamic radius of the analysed particle.

DLS is offering also the possibility to measure the ζ-potential of a particle by measuring the electrophoretic mobility, which is the velocity of the motion of the particles in the solvent under the influence of an electric field. A potential exists between the analysed particle surface and the dispersing liquid which varies according to the distance from the particle surface. By Henry's equation (**Equation 6**) it is possible to correlate the electrophoretic mobility and ζ-potential.

$$\mu_e = \frac{\varepsilon\zeta}{6\pi\eta} f(ka) \quad \text{(Eq. 6)}$$

where ε is the dielectric constant of the media, η is the viscosity, ζ is the ζ-potential and $f(ka)$ is Henry´s factor. $f(ka)$ depends on the ratio between the particle radius (a) and the thickness of the double layer ($1/k$) (**Figure 11**). Therefore when the particle is

smaller than the double layer then fits to the Hückel's limit; $f(ka) = 1$ and when particle is bigger than the double layer then fits to Smoluchowsky's limit; $f(ka) = 1.5$.

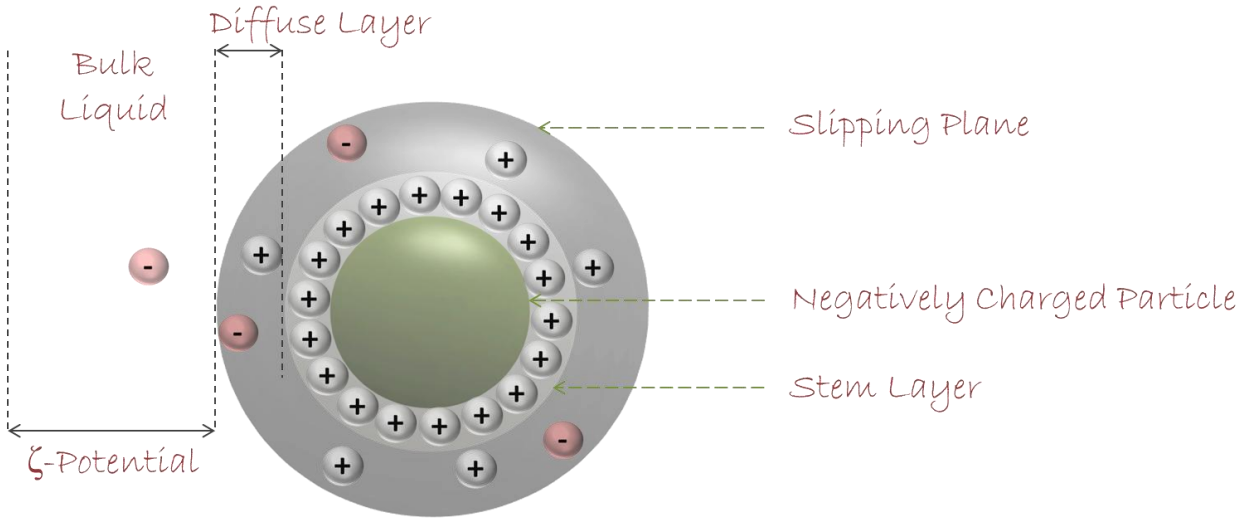

Figure 11 Representation of a charged particle dispersed in a solvent.

X – ray Photoelectron Spectroscopy (XPS)

X-ray Photoelectron Spectroscopy (XPS) is a surface analysis technique based in a very simple process that uses x-rays in an ultra-high vacuum environment to obtain information about a sample surface related to the chemical compounds, composition and chemical states. The basic principle of the photoelectric effect was enunciated by Einstein in 1905[9].

$$E = h\nu \qquad \text{(Eq. 7)}$$

Briefly in XPS the photoelectric effect is used to investigate the binding energy (BE) of the electrons on a sample surface. The molecules of the analysed sample are exposed

to X-rays with a defined energy, $h\nu$. A high enough energy will emit electrons from the sample and the number of emitted electrons will be detected as well as their kinetic energy (KE) (**Figure 12**). The BE can be calculated (**Equation 8**) as the difference between the photon energy $h\nu$,E and Φ the work function.

$$BE = h\nu - KE - \Phi \quad \text{(Eq. 8)}$$

The binding energies of the electrons are unique for every element for its electronic surrounding. Therefore XPS can be used to investigate quantitatively the elemental composition and its chemical environment.

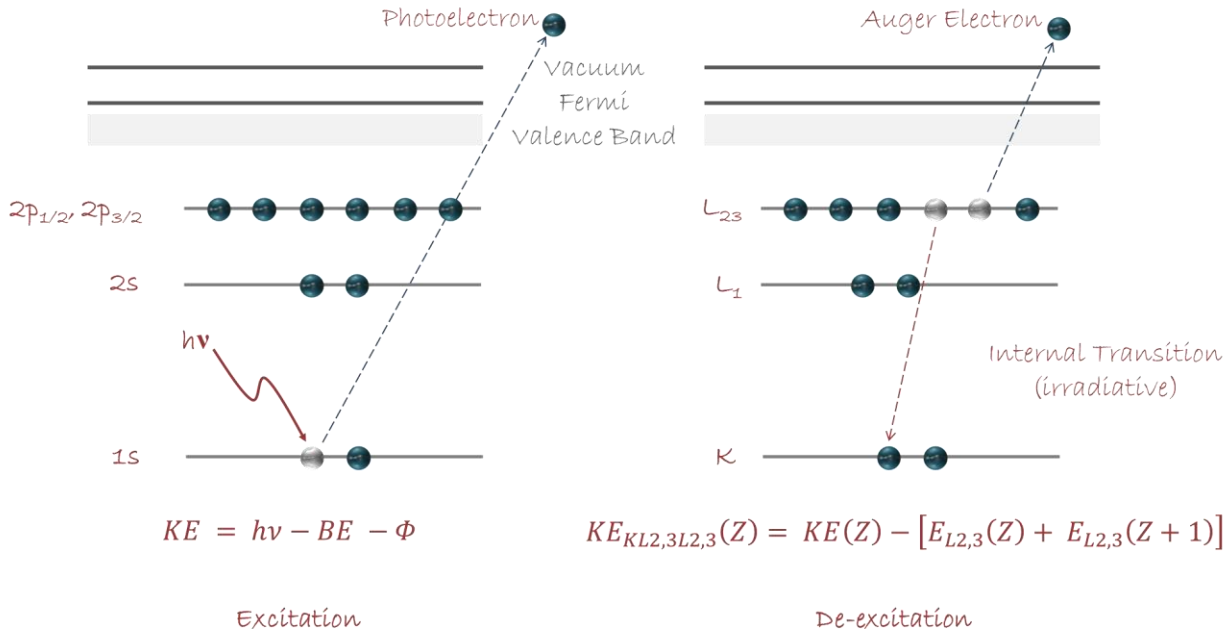

Figure 12 Schematic representation of XPS-basic principle.

Electrochemical Impedance Spectroscopy (EIS)

Electrochemical impedance spectroscopy (EIS) is a valuable tool for studying electrochemical reactions at interfaces the ion transport properties of materials. As a generic approach EIS is based on the application of a current to a material and the

measure of the resulting current or voltage. Electrical impedance is a complex concept of the electrical resistance which according to Ohm's law is the ability of a circuit element to resist the flow of electrical current. **Equation 9** defines resistance in terms of the ratio between electric voltage, E, and current, I.

$$R \equiv \frac{E}{I} \quad \text{(Eq. 9)}$$

However a resistor described with Ohm's law concludes several simplifications which in reality are not applicable in the real world which contains circuit elements with more complex behaviour. Such simplifications are that Ohm's law is applicable at all current and voltage levels, the resistance is independent of the frequency while alternating circuit current and voltage signals of a resistor are in phase with each other. Impedance on the other hand describes a more general circuit and is described as the ability of a circuit to resist the flow of electrical current, but unlike resistance, it is not limited by the simplifying properties. There are several approaches to measure electrical impedance[10] in this thesis the approach that is used is based on the sinusoidal stimulus. According to sinusoidal stimulus approach a multi-frequency current is applied to the material and the resulting frequency-dependent voltage is measured. The response is measured in the frequency range of interest in terms of either phase shift or amplitude or real and imaginary parts.

Impedance represented in terms of a magnitude, Z_0, and a phase shift, φ and as a complex number as seen in **Equation 10**.

$$Z(\omega) = \frac{E}{I} = Z_0 \exp(j\varphi) = Z_0 \left(cos\varphi + jsin\varphi\right) \quad \text{(Eq. 10)}$$

$Z(\omega)$ is composed of a real and an imaginary part. When we plot the real part on the X-axis and the imaginary part on the Y-axis we get a Nyquist Plot (**Figure 13a**). In the Nyquist Plot the impedance is represented as a vector of length $|Z|$ and the angle between this vector and the X-axis is called phase angle. Another possible representation of the data is with the Bode plot, where the impedance is plotted with log frequency on the X-axis and both the absolute values of the impedance ($|Z| = Z_0$) and the phase-shift on the Y-axis (**Figure 13b**).

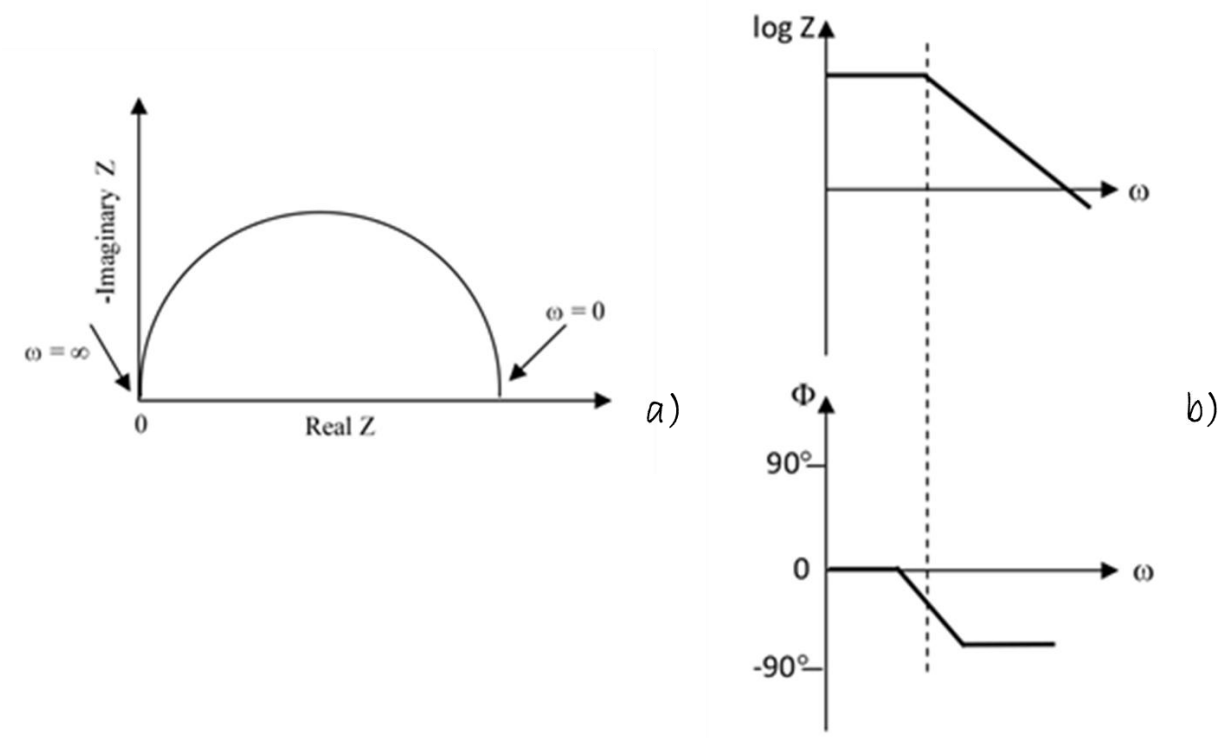

Figure 13 a) Nyquist plot showing the real vs imaginary part of impedance and b) Bode plots showing the variation of impedance (log Z) and phase angle (Φ) with respect to change in frequency[11].

Fluorescence Spectroscopy

Fluorescence spectroscopy is based on the excitation and emission in molecules. Any molecule can absorb the light and its electronic state changes from the low energy state

to one of the various vibrational states in the excited electronic state. Absorbance is related with the transition from a ground state to an excited state. A limited number of molecules display the phenomenon of fluorescence which involves the relaxation from excited to ground state. The Jablonski diagram illustrates the mechanism of the excitation/relaxation in a molecule (**Figure 14**). Dynamic properties of excited molecules offer the possibility to study via florescence spectroscopy ultrafast processes, such as electron transfer, proton transfer, energy transfer and others.

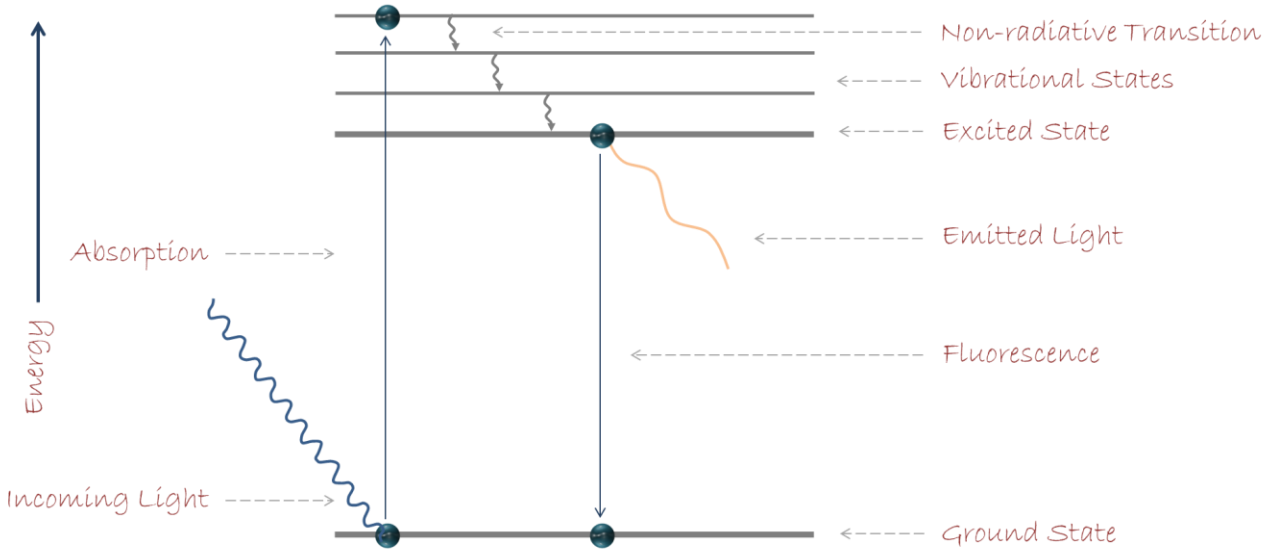

Figure 14 Illustration of the Jablonski diagram of the mechanism of excitation/relaxation in a molecule.

Flow Cytometry

Cytometry is used to analyse quantitatively via fluorescence and scattering a population of cells, organelles, or other particles of similar size. Cytometry is mainly used in biological/haematological laboratories for cells analysis and sorting[12]. Additionally, over the years flow cytometry has been used to measure the properties of individual particles[13–15]. When a sample in solution is injected into a flow cytometer, the particles

are randomly distributed in three-dimensional space. The sample is ordered into a stream of single particles by hydrodynamic focusing and then each particle or cell is flown individually in front of the laser source. The light that is scattered in the forward direction, typically up to 20^{o} offset from the axis of the laser beam, and collected by a lens, is called forward scatter channel (FSC). FSC intensity is associated with the size of the particles and is commonly used to distinguish between living and dead cells. The rest of the scattered light, measured approximately at a 90^{o} angle to the excitation beam, is called side scatter channel (SSC). SSC provides information about the complexity of cells or particles, i.e their state of aggregation. The emitted fluorescent light is detected by separate fluorescence channels. Detectors depending on the machine are either silicon photodiodes or photomultiplier tubes (PMTs) and their number varies according the manufacturer. PMTs are used for scatter and fluorescence readings and silicon photodiodes are used to measure the forward scattered signal[16].

Confocal Laser Scanning Microscopy (CLSM)

Confocal laser scanning microscopy (CLSM) is a technique widely used for three dimensional optical imaging with high resolution[17]. CLSM is based on the scanning of the specimen point by point by focusing the light coming from it onto a spatial pinhole while eliminating the out of focus light. In this way it is possible to obtain images with high resolution and contrast in the direction of optical axis[18]. Additionally with CLSM is possible to obtain high resolution fluorescent images using a laser as light source. The illuminating light coming from the specimen under study is focused by an objective onto the target surface and then the reflected and scattered light from the surface is focused

again onto a pinhole to collect afterwards the light coming from the pinhole to a photo detector (**Figure 15**).

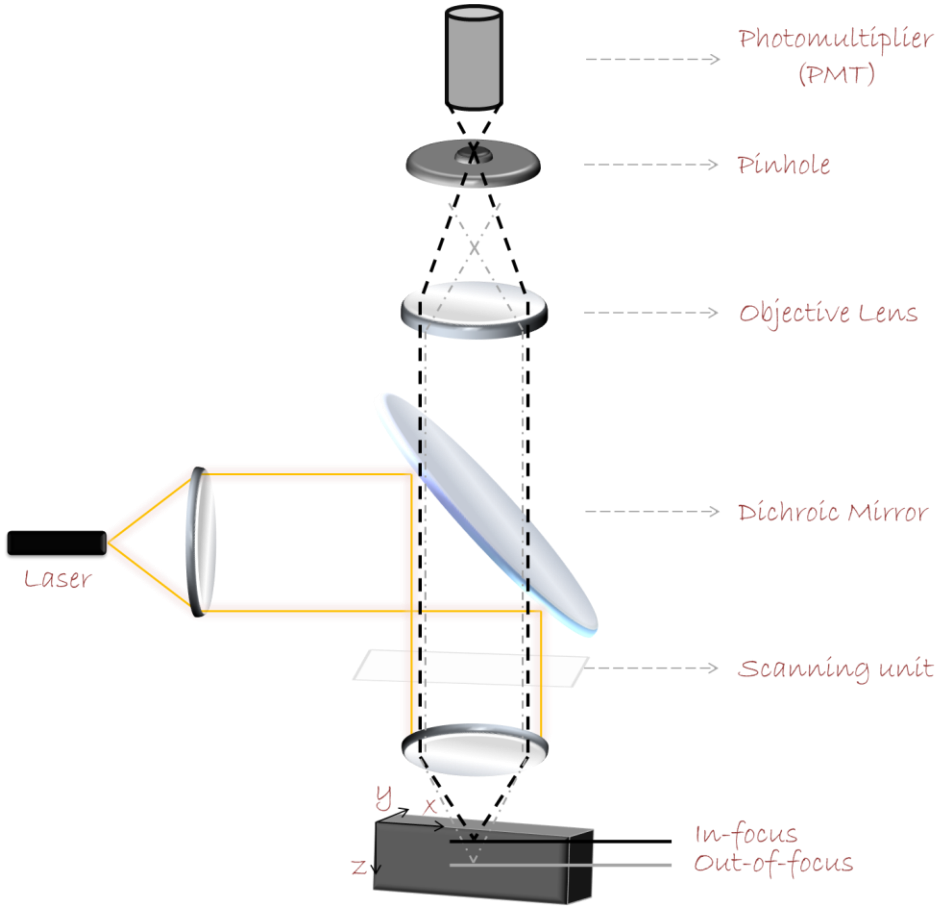

Figure 15 Scheme of a typical configuration of a confocal laser scanning microscope.

Fluorescence Recovery after Photobleaching (FRAP)

FRAP is basically used to measure the transport (lateral diffusion) of fluorescent molecules in small systems such as individual living cells. In CLSM is possible to perform this technique by a simple way; a defined region of a surface that contains mobile fluorescent molecules is exposed to a brief intense pulse of light or laser causing irreversible photochemical bleaching of the fluorophore in that region. The unbleached fluorophore of lateral regions is transported into the bleached region in order to recover

the fluorescence intensity thereby transport coefficients like the diffusion coefficients are determined[19].

Axelrod et al.[19] and Soumpasis et al.[20] developed a simple method based on theoretical and practical guidelines for the performance of FRAP measurements and the analysis of the obtained data in order to extract the mobile fractions and diffusion coefficients. For the experimental configuration a round spot of a 22 μm diameter is photobleached while at the same time a non – bleached spot of the same size is taken into account as a reference. The fluorescence recovery is defined as

$$f(t) = \frac{F(t) - F(0)}{F(i) - F(0)} \quad \text{(Eq. 11)}$$

Where $F(t)$, is the fluorescence recovery in the bleached area after photobleaching at time t . $F(0)$, is the fluorescence intensity in the bleached area at $t = 0$ after photobleaching and $F(i)$is the normalized fluorescence intensity in the non-bleached spot. By applying this equation the fluorescence intensity drift of the whole sample due to the photobleaching during the scanning process is normalized. For the calculation of D a fitting of $f(t)$ is required;

$$f(t) = exp\left(-2\frac{\tau_D}{t}\right)\left[I_0\left(2\frac{\tau_D}{t}\right) - I_1\left(2\frac{\tau_D}{t}\right)\right] \quad \text{(Eq. 12)}$$

I_0 and $I_1$are modified Bessel functions, τ_D is the characteristic diffusion time calculated from

$$\tau_D = \frac{\omega^2}{4D} \quad \text{(Eq. 13)}$$

Where D, is the diffusion coefficient and ω is the radius of the bleached area at zero time. Finally the mobile fraction is calculated using **Equation 14**.

$$\boldsymbol{M = \frac{[F(\infty) - F(0)]}{[F(i) - F(0)]}} \quad \text{(Eq. 14)}$$

Atomic Force Microscopy (AFM)

This technique is based on using a sharp probe (tip) to explore the properties such as topography, stiffness, module of elasticity of a sample by obtaining a map of a certain area of the surface of the sample. The mapping of the specimen surface is obtained by scanning in a controlled way the probe, which is mounted on the end of a cantilever (**Figure 16**). The topography of a surface of a material is determined by the deflection of a soft cantilever with a sharp probe. AFM can be conducted by three operation modes; contact or static mode, noncontact or dynamic mode and finally the tapping mode. In the contact mode the tip is in full contact with the surface and the topography is measured by the static deflection of the cantilever.

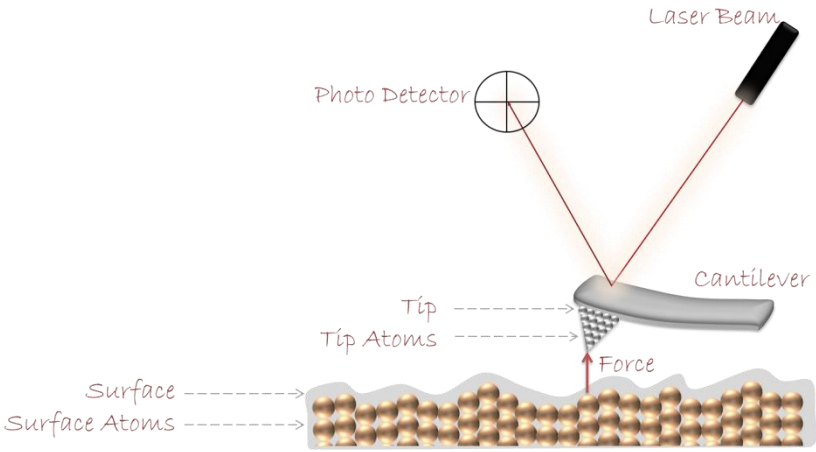

Figure 16 Schematic representation of the working principle of the atomic force spectroscopy.

From this technique we can obtain topographic information at atomic scale resolution. In the case of dynamic mode the cantilever is driven almost to its resonant frequency and the interaction force modulates the frequency of vibration, amplitude and phase. The surface topography can be determined by the oscillator modulation. Finally, the tapping mode combines both the static and dynamic modes and because of the very short contact time between the tip and the surface is considered as a noncontact mode. The oscillating tip gets in contact with the surface at the maximum deflection of the cantilever[21].

Cryogenic Transmission Electron Microscopy (CryoTEM)

CryoTEM is complementary technique to transmission electron microscopy (TEM) which permits to image soft matter probes at high resolution nanometer scale containing atomic data. Observing hydrated biological specimens by TEM is difficult due to the extreme conditions of exposure at high vacuum and intense electron beams while the thickness of the sample is also crucial as it has to be thin enough in order to be electron transparent. In cryoTEM, the specimen suspended in aqueous solution is rapidly frozen in liquid ethane cooled to liquid nitrogen temperature resulting in a frozen-hydrated specimen embedded in a thin film of vitreous (glass-like) state. This specimen can be explored close to their natural, hydrated state.

Electrons in TEM have low wavelength offering the possibility to get resolution of thousand times better than with a light microscope and observe objects of the size of a few angstrom. When electrons are emitted from the electron gun, they travel over a vacuum column and pass through condenser lenses that focus the electrons into a very

thin beam towards the specimen. The objective lenses and the projector lenses magnify the transmitted beam and project it onto a fluorescent viewing screen. Electrons excite the screen and produce a visible magnified image of the sample which is recorded with a CCD camera.

In the case of cryoTEM the principle is the same but the specimen is vitrified and therefore during imaging the sample is kept in liquid nitrogen atmosphere to preserve it vitrified as long as possible.

References

(1) Sauerbrey, G. *The Use of Quartz Oscillators for Weighing Thin Layers and for Microweighing*; 1959; Vol. 155.

(2) Buttry, D. A. Application of the Quartz Crystal Microbalance to Electrochemistry. In *A Series of Advances in Electroanalytical Chemistry*; 1991; pp 23–33.

(3) Bahrami Samani, M.; Whitten, P.; Spinks, G.; Cook, C. Viscoelastic Study of Conducting Polymers Using Quartz Crystal Microbalance. *Proc. SPIE* **2006**, *6168*, 616827–616827.

(4) Standford Research Systems. Quartz Crystal Microbalance Theory and Calibration The QCM Oscillator. **2004**, *408*, 744–9040.

(5) Young, T. An Essay on the Cohesion of Fluids. *Philos. Trans. R. Soc. London* **1805**, *95*, 65–87.

(6) de Gennes, P. G. Wetting: Statics and Dynamics. *Rev. Mod. Phys.* **1985**, *57* (3), 827–863.

(7) Adamson, A. W. *Physical Chemistry of Surfaces*; 1990.

(8) Russel, W. B.; Saville, D. A.; Schowalter, W. R. *Colloidal Dispersions*; Cambridge University Press, 1989.

(9) A. Einstein. On a Heuristic Point of View Concerning the Production and Transformation of Light. *Ann. Phys.* **1905**, *17*, 132–148.

(10) Macdonald, J. R. Impedance Spectroscopy. *Ann. Biomed. Eng.* **1992**, *20* (3), 289–305.

(11) Dhawan, G. R. and S. K. *Modern Electrochemical Methods in Nano, Surface and Corrosion Science*; Aliofkhazraei, M., Ed.; InTech, 2014.

(12) Shen, C.; Assche, G. V; Colpaert, S.; Maerten, P.; Geboes, K.; Rutgeerts, P.; Ceuppens, J. L. Adalimumab Induces Apoptosis of Human Monocytes: A Comparative Study with Infliximab and Etanercept. *Alimentary pharmacology & therapeutics*. February 1, 2005, pp 251–258.

(13) Qiu, Y.; Palankar, R.; Echeverría, M.; Medvedev, N.; Moya, S. E.; Delcea, M. Design of Hybrid Multimodal Poly(lactic-Co-Glycolic Acid) Polymer Nanoparticles for Neutrophil Labeling, Imaging and Tracking. *Nanoscale* **2013**, *5*, 12624–12632.

(14) Yoo, H. S.; Lee, K. H.; Oh, J. E.; Park, T. G. In Vitro and in Vivo Anti-Tumor Activities of Nanoparticles Based on Doxorubicin-PLGA Conjugates. *J. Control. Release* **2000**, *68* (3), 419–431.

(15) Romero, G.; Sanz, D. J.; Qiu, Y.; Yu, D.; Mao, Z.; Gao, C.; Moya, S. E. Lipid Layer Engineering of Poly(lactide-Co-Glycolide) Nanoparticles to Control Their Uptake and Intracellular Co-Localisation. *J. Mater. Chem. B* **2013**, *1*, 2252–2259.

(16) Weaver, J. L. *Introduction to Flow Cytometry.*; 2000; Vol. 21.

(17) Wilson, T. Principles of Three-Dimensional Imaging in Confocal Microscopes. *J. Microsc.* **1999**, *193* (1), 91–92.

(18) Paddock, S. W. Principles and Practices of Laser Scanning Confocal Microscopy. *Mol. Biotechnol.* **2000**, *16* (2), 127–149.

(19) Axelrod, D.; Koppel, D. E.; Schlessinger, J.; Elson, E.; Webb, W. W. Mobility Measurement by Analysis of Fluorescence Photobleaching Recovery Kinetics. *Biophys. J.* **1976**, *16* (9), 1055–1069.

(20) Soumpasis, D. M. Theoretical Analysis of Fluorescence Photobleaching Recovery Experiments. *Biophys. J.* **1983**, *41* (1), 95–97.

(21) Geisse, N. A. AFM and Combined Optical Techniques. *Mater. Today* **2009**, *12* (7–8), 40–45.

Chapter 1

Impact of Thermal Annealing on Wettability, Antifouling and Cell Adhesion Characteristics of Alginate Poly–L–lysine Polyelectrolyte Multilayer Films

1.1 Motivation

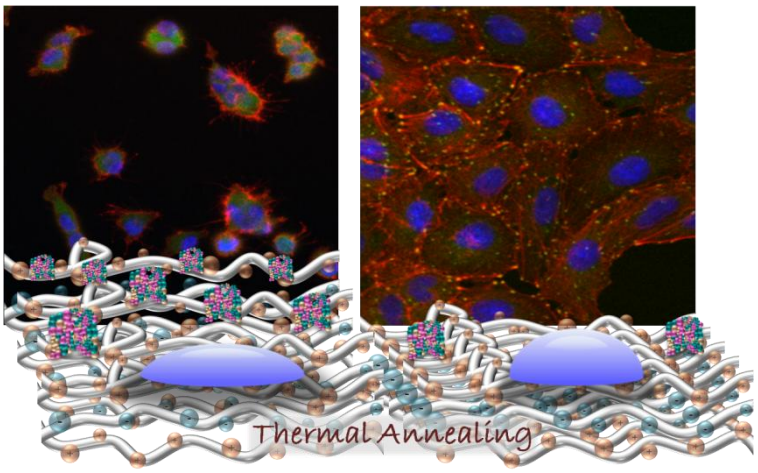

The development of novel materials and surface coatings with mechanical and biological characteristics that enhance cell adhesion has been studied extensively over the years. A major issue in these applications is the production of surface coatings suitable for cells adhesion prior to tissue regeneration. Proper cell adhesion presupposes cell spreading, migration, proliferation and differentiation which strongly depends on the surface topography, roughness, material stiffness, chemical composition, the distribution and availability of ligands, surface charge and hydrophobicity[1,2].

In recent years different materials mimicking aspects of the interactions between cells and their environment, has been employed to increase cell adhesion[3]: natural and

synthetic PEMs, protein-coated poly(acrylamide) or poly(dimethylsiloxane) polymeric substrates with tunable stiffness[4], hydrogels that can be biochemically and mechanically altered by chemical functionalization or by varying cross-linking density, respectively[5]. Microgels have been used as such to fabricate thin film substrates or combined with polyelectrolytes in PEMs[6]. The LbL technique provides a simple method for the non-covalent modification of surfaces and implants with biocompatible polymers and the engineering of scaffolds[7,8].

PEMs have been also used on the basis of biopolymer electrolytes forming a biocompatible cushion on which proteins, peptide sequences and other biomolecules can be covalently bound or assembled, impacting on cell functionalities[9–11]. As mentioned the magnitude and strength of cell adhesion, proliferation and differentiation, depend on the physical and chemical properties of the biomaterial surface. PEMs fabricated on the basis of polysaccharides such as chitosan, alginate, hyaluronan or polypeptides such as PLL are non-toxic surfaces thus highly biocompatible. However these films display low elastic modulus and surface topography that are not favourable for cellular migration[4,11,12]. Chemical cross-linking has been often applied to tune the mechanical properties of these films, resulting in films with enhanced stiffness and a more fibril surface topograpgy[13]. Although cross-linking has been effective to improve cellular adhesion and migration to biopolymer PEMs the biocompatibility of the cross-linking agents is limited. Alternatives to cross-linking have been proposed such as the use of synthetic PEs that resulted in stiffer films nevertheless, their biocompatibility is also limited.

In this chapter thermal annealing is used as an alternative method to trigger the physicochemical and mechanical properties of a PEM film made upon biopolyelectrolytes. Exposing the PEMs to heat for a defined period of time, leads to enhanced cell adhesion. Previous works on annealing of polyelectrolytes have shown that thermal annealing gives the polyelectrolyte molecules the energy to rearrange and find more convenient conformations which define the final properties of the film[14–18].

In addition, PEMs have also attracted attention as antifouling coatings, as they can be easily assembled on almost any charged surface. The stepwise assembly of polyelectrolytes allows for a precise control of composition of the multilayers in the vertical plane, combining different polyelectrolytes and nanomaterials, with synergic antifouling effects. We will show that thermal annealing can be applied, as well, to biopolymer PEMs to enhance antifouling behaviour of the film.

This chapter represents a study of the effect of thermal annealing on PEMs constructed upon the positively charged PLL and the negatively charged Alg, two biopolymers that have been extensively used for biomedical applications as they provide enhanced surface biocompatibility[9,19–22]. We will demonstrate that by applying annealing at 37, 50 and 80 °C on these films their wetting properties will dramatically change with variations in the contact angle in water from highly hydrophilic to hydrophobic. Changes in surface energy due to thermal annealing will be evaluated, as well, by receding and advancing contact angle measurements in water, ethylene glycol (EG) and dimethylsulfoxide (DMSO). Variations in the physical properties of the PEMs are interpreted as a result of the reorganization of the polyelectrolytes in the PEMs from a layered structure into complexes where the interaction of polycations and polyanions is enhanced which could

be visualized by AFM[23,24]. The deposition of PEMs as well as the adsorption of BSA before and after annealing will be evaluated via QCM-D. In addition to QCM-D, fluorescence spectroscopy measurements will be conducted to verify the protein adsorption.

The impact of the thermal annealing at 37 °C of PEMs on cellular adhesion will be studied in human lung cancer A549 and myoblast C2C12 cell lines. Evaluation of the cellular adhesion will be done via projected average cell spreading and focal contact formation studies in CLSM.

This chapter proposes a friendly method without additional chemical treatment to tune PLL/Alg PEMs wettability, cell adhesion and a method to endow bio-PEMs with antifouling characteristics.

1.2 Experimental Section

1.2.1 Annealing Process

The annealing of the samples was conducted during 3 days in a Memmert UNE 200–300 oven with a range of temperature 5 – 250, under atmosphere conditions for three different temperatures; 37, 50 and 80 °C. Prior to annealing all samples were left to dry in air.

1.2.2 AFM Measurements

Structural details of the PLL/Alg films were investigated using a Nanowizard II AFM (JPK, Berlin, Germany). Images were acquired on dry samples; PE films were washed with nanopure water and left to dry at room temperature. TESP-V2 cantilever (Brucker, AFM Probes) with a nominal spring constant of 40 N m^{-1} was used for imaging in intermittent mode. The resonant frequency was in the range of 280 to 320 kHz. The root mean square (RMS) roughness is calculated as the average of RMS line profiles across vertical and horizontal direction of the AFM images using the Gwyddion software.

1.2.3 Contact Angle Measurements

The wetting properties of the PEM film were characterized before and after annealing in a DSA 100 contact angle measuring system with a DSA 100 control from the Krüss company at room temperature (23 °C) and ambient atmospheric conditions. During the measurement, the liquid drops remained attached to the steel tip with outer diameter, d = 0.5 mm. Images of a 3 µL drop with 500 µL min^{-1} velocity were captured after the liquid volume was slowly inflated or deflated until the contact line moved gradually

outward or inward, respectively. Drop profiles were recorded and fitted with the included software package (DSA 3). Apparent contact angles of the drops for 5 repetitions of each sample were obtained with a standard deviation, SD = 1.9.

Contact angle measurements were performed using different test liquids to characterize the surface energy of PEMs before and after annealing. Water, EG, and DMSO were chosen as test liquids to determine the dispersion component γ_s^D and the polar component γ_s^p, as well as the total interfacial free energy of the bare substrate, γ_s . For each test liquid, we measure the static advancing contact angle, θ_a, and the static receding contact angle, θ_a.

1.2.4 XPS Measurements

Surface analysis by XPS was performed in a SPECS SAGE HR 100 system spectrometer. The X-ray source employed for this analysis was a Mg Kα (1253.6 eV) which operated at 12.5 kV and 250 W. The take-off angle was fixed at 90º and the analysis was conducted at a pressure of ~10^{-6} Pa. Detailed spectra were acquired for C 1s and N 1s regions with pass energy of 15 eV.

Spectra were analyzed with the CasaXPS 2.3.15dev87 software. The analysis consisted of satellite removal, Shirley background subtraction, calibration of the binding energies related to the C 1s C-C peak at 285 eV, and peak fitting with Gaussian-Lorentizan line shapes to determine the atomic percentages and chemical states of elements present on the surface.

1.2.5 Polyelectrolyte Assembly on Colloids

For ζ – potential measurements PEMs were assembled on top of SiO_2 particles (3 μm). For LbL assembly SiO_2 particles were first suspended in Hepes 10 mM / NaCl 150 mM (pH 7,4) buffer at 1 mg mL^{-1}. Subsequently the particles were incubated at the polyelectrolyte solution (1 mg mL^{-1}) for 15 min. The procedure was repeated for every layer deposition for the construction of 15 layers. In between polyelectrolyte depositions three washing steps were performed via centrifugation.

1.2.6 ζ -potential Measurements

Changes on the surface charge of the PEM coated colloids were recorded using a Zetasizer (Malvern, of the UK). ζ – potential measurements were conducted in a disposable folded capillary cell at 25 °C and they were performed at a cell drive voltage of 30 V, using a monomodal analysis model. Five repetitions were conducted for each sample. Samples were diluted in Hepes 10 mM / NaCl 150 mM (pH 7.4) buffer at a final concentration 0.1 mg mL^{-1}.

1.2.7 Cell Culture

A549 epithelial cell line from a human lung carcinoma, and C2C12, a mouse myoblast cell line, were grown in RPMI medium supplemented with 10% FBS (and antibiotics) and incubated at 37 °C in a 5 % CO_2 and 97% humidified atmosphere.

For adhesion assays, all PEMs were deposited on top of glass slides and placed into petri dishes with 35 mm diameter (Falcon) and UV-sterilized for 1 h. Then, 5 x 10^4 cells in 3 mL culture medium were seeded. Phase-contrast images were taken at 1 and 2

days employing a Nikon T100 inverted microscope with a CFI flat field ADL 10X objective.

1.2.8 Cell Immunostaining

Vinculin, actin and cell nucleus were fluorescently stained in order to study cell adhesion. Fixed cells were permeabilized at room temperature with 0.1% Triton X-100 in PBS for 5 min. After washing with PBS cells were incubated during 30 min with a blocking solution, 1% BSA in PBS. Anti-vinculin antibody was diluted in the blocking solution and incubated for 1 h. After three washing steps with PBS the anti-mouse IgG-FITC conjugated antibody was diluted together with the TRITC-conjugated phalloidin in PBS and incubated simultaneously for 45 min for double labelling. Finally cells were incubated for 3 min with DAPI diluted in PBS for nucleus staining. The samples were washed and mounted on a slide using fluoromount aqueous mounting medium and observed by CLSM (Zeiss LSM510).

1.2.9 QCM-D Measurements

The assembly of the PLL/Alg PEM and the deposition of BSA protein before and after annealing were monitored via the QCM–D, Q–Sense E4 system. The coating of the PEM film was conducted on SiO_2 (50 nm) coated quartz crystals (5 MHz, Q-Sense). PE solutions were injected in the 4-sensor chamber with the help of a peristaltic pump and left under incubation for 10 min. After stabilization of the frequency another 10 min rinsing with Hepes 10 mM / NaCl 150 mM buffer (pH 7.4) was followed. Experiments

were conducted at 23 °C. For the deposition of the protein, BSA was dissolved at 1 mg mL^{-1} concentration in Hepes 10 mM / NaCl 150 mM buffer.

1.2.10 Fluorescence Spectroscopy Measurements

The adsorption of labelled BSA on PEMs was quantified using a Fluorolog® – HORIBA JOBIN YVON fluorescence spectrometer. Protein labelling was performed using amine reactive ATTO 488 – Labels (NHS-Esters). The protocol used for the labelling of the BSA was obtained from ATTO-TEC. Measurements were done at the emission spectral acquisition configuration; excitation was set at a wavelength of 488 nm (1 nm slit width) and the emission wavelength range was set between 510 – 700 nm (1 nm slit width). For fluorescence measurements the PLL/Alg PEM film was deposited, following the procedure previously described, on top of quartz microscope slides (25 mm x 25 mm x 1 mm) from UQG Optics. The ATTO 488 labelled BSA with a 1mg mL^{-1} concentration was deposited onto the PEM films before and after annealing.

1.3 Results & Discussion

1.3.1 Effect of Annealing on PLL/Alg PEMs

The assembly of the PLL/Alg PEM was first followed by means of QCM-D to demonstrate the growth of the PEM upon each PE layer deposition (**Figure 1.1**). The continuous stepwise decrease in frequency (Δf = 524 Hz) proves the deposition of the 15 polyelectrolyte layers. Once the multilayer was build up the films were annealed at 37, 50 and 80 °C for 72 h as described in the experimental section.

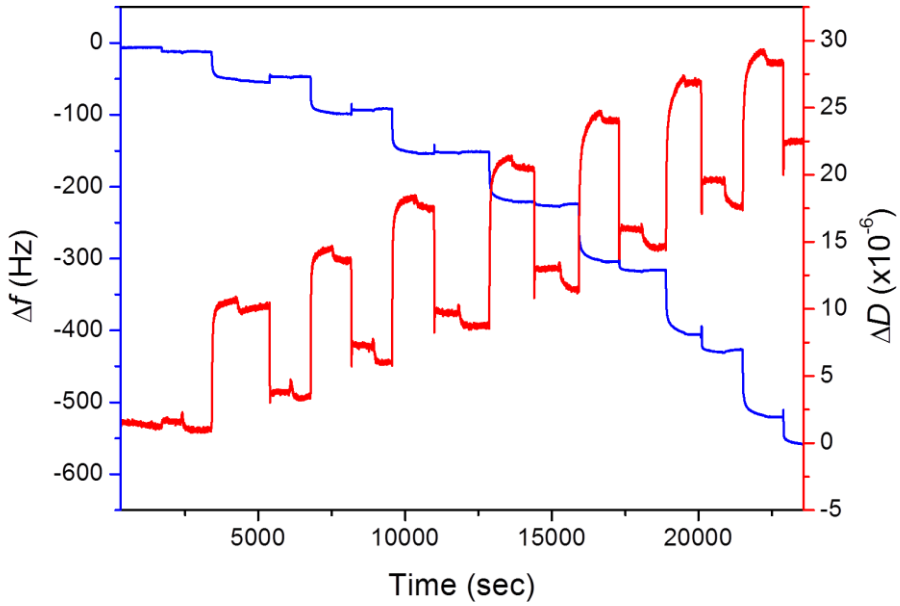

Figure 1.1 QCM-D curves representing changes in frequency (in red) and dissipation (in blue) during the assembly of 15 layers of PLL/Alg.

AFM imaging was performed on the PEMs to visualize the impact of the annealing on the surface morphology. The topography and roughness of the film, without thermal annealing is displayed in **Figure 1.2a**. The PLL/Alg PEMs shows a non-homogeneous porous morphology consisted of a fibrillar network. The highest features of the network

display a height up to ~150 nm as seen from the roughness profile, with free space between the polymer fibres of 1 to 2 µm on average.

It is worth noting that below the top fibrillar structures there is more polymeric material, assembled into fibrillar networks as well. This can be seen in the last 5 µm of the roughness profile (*bottom panel of* **Figure 1.2a**). The substrate cannot be visualized between the highest peaks, although there are observed peaks of lower heights, reaching up to 40 nm. PEMs roughness (RMS) of 38.2 ± 8.3 nm was calculated from the AFM images. The glass substrate underneath the PEM displays a smoother profile. For glass the roughness is in the range of 0.5 – 2 nm [25]. The influence of the temperature on the structural reorganization of the PEMs is shown in **Figure 1.2b**. The PEM has been annealed at 37 °C and displays a smoother topography. The morphology does not show any more a complete network-like organization. Instead, we observe the presence of grains across the surface, with heights of 5 to 10 nm. In the bottom panel of **Figure 1.2b**, in the roughness profile, we can observe two peaks with heights of ~35 nm. These peaks correspond to the features from the upper image in lighter colours, corresponding to higher values in the colour scale. These are appearing as isolated networks when compared to the ones in **Figure 1.2a** where a network covers the whole surface. RMS decreases significantly to 4.9 ± 1.7 nm. When the PEM is annealed at 80 °C, the AFM imaging shown in **Figure 1.2c**, reveals that the surface displays a less rough morphology than at 37 °C, with fewer grain-like structures where the polymer network is no longer observed. RMS, however, increases to 8.7 ± 5.8 nm for the PEM annealed at 80 °C, this value is slightly higher than for the PEM annealed at 37 °C but still smaller than for the non-annealed samples.

AFM clearly shows that the PE chains reorganize when they are annealed at 37 °C and higher temperatures. The fact that the surface becomes smoother implies that the chains are rearranging in a more compact structure and hints that the layered structure of the PLL/Alg PEM is changing, as the fibres observed in the non-annealed PEM disappear progressively with the increase of temperature.

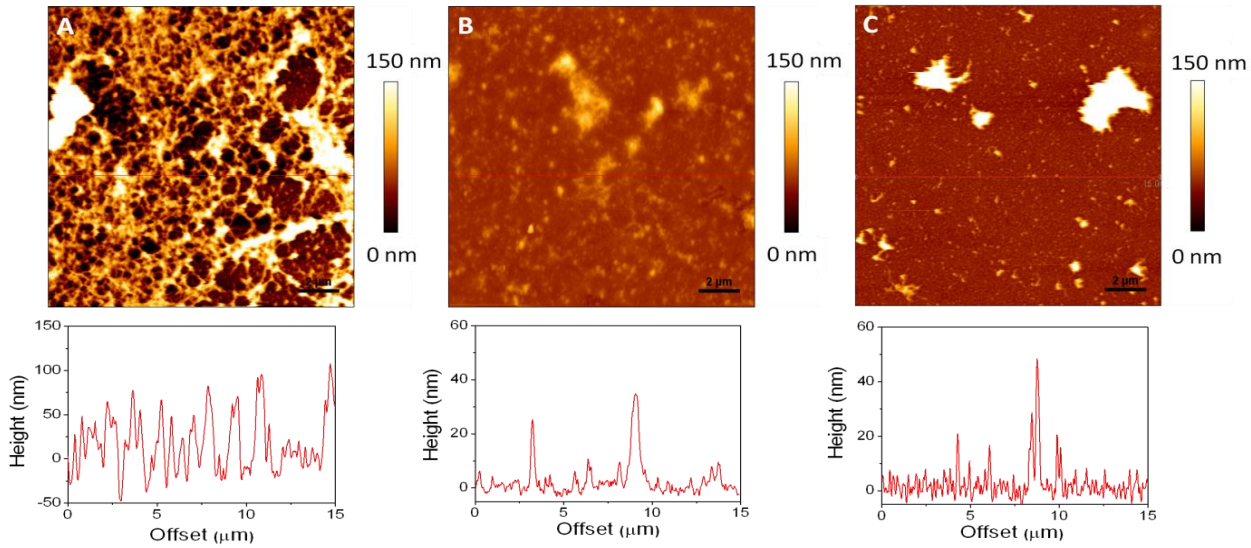

Figure 1.2 AFM images (15 x 15 μm) acquired on dry $(PLL/Alg)_{7.5}$ multilayers a) before annealing, b) after annealing at 37 °C and c) after annealing at 80 °C. Bottom panels display roughness profiles taken as cross-sections of the above images.

Contact angle experiments were conducted at room temperature, 23 °C, to determine the wettability of multilayers before and after annealing. The mean advancing water contact angle for $(PLL/Alg)_{7.5}$ before annealing was 36° ± 2.8 (**Figure 1.3**). This value corresponds to a hydrophilic surface. Both Alg and PLL are charged and considering the hydrophilic amine groups of the last PLL layer the contact angle values are reasonable. When the PEM was annealed during 72 h at 37 °C the wetting properties of the film changed drastically, giving contact angle values of 93° ± 4.6. After annealing at 50 and 80 °C the contact angle changed indeed in both cases from hydrophilic to

hydrophobic giving values of 77° and 95°, respectively. Surprisingly the annealing at 50 °C caused a decrease in the contact angle in 16° but higher temperatures resulted again in an increase of the contact angle. These variations are indicative of a restructuring of the PEM with the temperature as the contact angle will be affected by the density of charges on the surface and the exposure of the organic backbone of the polymer chains in the PEM surface.

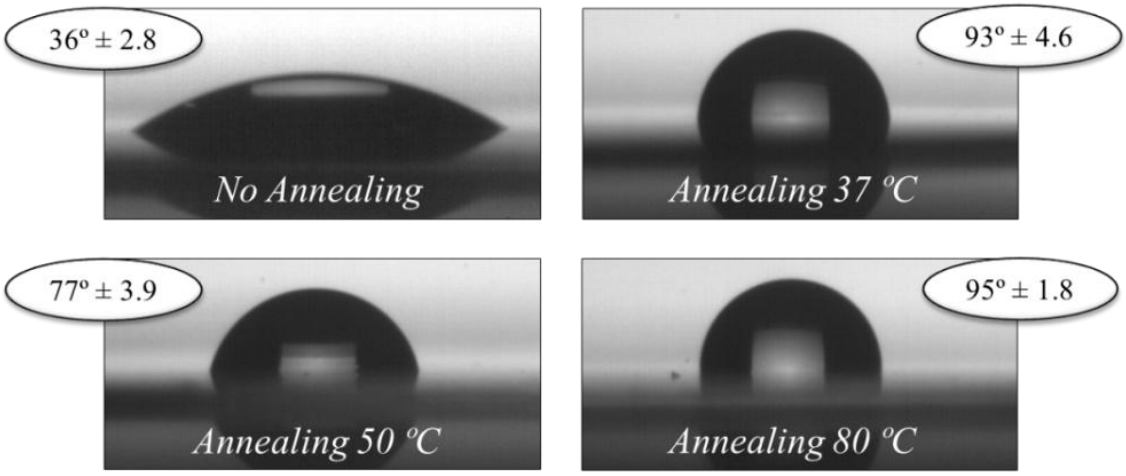

Figure 1.3 Advancing water contact angle values for the $(PLL/Alg)_{7.5}$ films before annealing and for different annealing temperatures.

Table 1.1 Advancing and receding contact angle values for the $(PLL/Alg)_{7.5}$ films before annealing and after annealing at 37, 50 and 80 °C. Contact angle values were measured with water, DMSO and EG. θα: Static advancing contact angle, θr; Static receding contact angle.

Solvents	No Annealing $T = 20°C$		Annealing at $T = 37°C$		Annealing at $T = 50°C$		Annealing at $T = 80°C$	
	θ_α	θ_r	θ_α	θ_r	θ_α	θ_r	θ_α	θ_r
DMSO	7.3° ± 0.7	-	20.6° ± 1.1	17.6° ± 0.9	20.9° ± 1.8	19.9° ± 2.3	26.9° ± 2.1	22.6° ± 1.5
EG	27.1° ± 2.0	-	36.1° ± 1.4	28.5° ± 1.2	33.6° ± 1.7	29.5° ± 1.5	42.0° ± 3.6	39.4° ± 2.7
Water	36.0° ± 2.8	22.7° ± 1.3	93.0° ± 4.6	57.6° ± 2.9	77.0° ± 3.9	53.0° ± 2.0	95.0° ± 1.8	55.3° ± 2.4

Table 1.1 provides the values of the advancing and receding contact angle for different solvents; water, EG and DMSO for the PEMs before and after annealing. The lowest

contact angle was measured in DMSO, being around 7° (advancing) for the non-annealed sample and displaying values between 20° and 30° in the case of the annealed PEMs. For EG the contact angle was 27° for non-annealed samples and increased to values between 28° and 42° for the annealed ones. Receding contact angle could not be measured for the non-annealed samples with DMSO and EG as the droplet partially absorbs on the polymer surface. There was a small hysteresis between advancing and receding contact angle values for DMSO and EG for the annealed samples. In the case of water the hysteresis was more pronounced; approximately 10° for the non-annealed samples, and increased up to 40° for the sample annealed at 80 °C. Contact angle hysteresis on inert and rigid solids can be explained from the presence of microscopic chemical and/or topographic surface heterogeneities[26]. Both types of heterogeneities can act as pinning centres to the free liquid interface and create a dense spectrum of meta-stable interfacial configurations. Even in the limit of small interfacial velocities, these energy barriers contribute to the irreversible work necessary to displace the three phase contact line between the liquid phase, ambient air and the solid. On the macroscopic scale of a wetting drop, this dissipation manifests in form of a history dependent static contact angle. Hence, changes of the contact angle hysteresis interval $[\theta_r, \theta_a]$ after surface treatment can also hint to a changing degree of chemical and topographic heterogeneity of a polymer surface. Despite AFM imaging of non-annealed PEMs showed a more irregular surface it is likely that the annealed PEM displayed a higher heterogeneity at subnano scale, mainly related to the charged groups which would explain the large hysteresis in water and not in the organic liquids. Contact angle hysteresis on a PEM could also be an effect of the slow equilibration

kinetics between the wetting liquid and polymer surface[26]. The high contact angle hysteresis of the PEM with water, in particular for the non-annealed samples can be due to slow reorientations of certain moieties of the polymer chains in contact to water. Other kinetic effects are linked to a slow migration of water molecules (swelling) into the polymer network.

The advancing and receding contact angle values for the different liquids were used to calculate the interfacial tension γ_l of the test liquids for non-annealed and annealed PEMs along with the corresponding dispersive component, γ_l^D, and polar component, γ_s^p. Both components of the interfacial energy are determined from the Owens-Wendt method[27]. Particular values of the interfacial tension and the surface energy components are taken from the book of Van Oss[28]. Following the approach of Owens and Wendt, the free energy per area γ_{ls}, of an interface between a liquid (l) and a substrate (s) is related to their respective interfacial tensions γ_l and γ_s by:

$$\gamma_{ls} = \gamma_l + \gamma_s - 2\left(\gamma_s^p \gamma_l^p\right)^{\frac{1}{2}} - 2(\gamma_s^D \gamma_l^D)^{\frac{1}{2}} \quad \textbf{Eqn. 1.1}$$

Where, the interfacial tension of the material (i) is the sum $\gamma_i = \gamma_i{}^D + \gamma_i^p$ of both components. Employing the contact angle θ in thermodynamic equilibrium and Young's relation $\gamma_l \cos\theta = \gamma_s - \gamma_{ls}$, we arrive at

$$\gamma_l(1+\cos\theta)/2(\gamma_l^D) = (\gamma_s^p)^{1/2}\,(\gamma_l^p/\gamma_l^D)^{1/2} + (\gamma_s^D)^{1/2} \quad \textbf{Eqn. 1.2}$$

being of the form $y = mx + n$ in the variable $x = \left(\gamma_l^p/\gamma_l^D\right)$ with a slope $m = \left(\gamma_s^p\right)^{1/2}$ and intercept $y_0 = \left(\gamma_s^p\right)^{1/2}$ with the ordinate. **Eqn. 1.2** allows us to determine the dispersive and the polar component of the substrate free energy by fitting the experimental data with linear relation. Experimentally, only the apparent contact angles θ_a and θ_r are

available from measurements, and we have to make a further assumption to estimate the contact angle θ in the thermodynamic minimum (i.e the material or Young's contact angle). In principle, it is impossible to infer the irreversible part of the work to enlarge or diminish the substrate area in contact to the wetting liquid from measurement of only θ_a, θ_r, and γ_l. However, fundamental thermodynamic considerations demand that Young's contact angle θ must satisfy the inequality $\theta_r < \theta < \theta_a$. To estimate the surface energy from the measured contact angles data we fit the advancing and receding contact angles data with **Eqn. 1.1** separately. Water is excluded because the difference between the cosines of the advancing and receding contact angles are much larger than for DMSO and EG. Here, we considered the receding contact angle of DMSO and EG on the non-annealed PEMs to be zero.

Figure 1.4 displays an Owen-Wendt plot of the experimental data according to **Eqn. 1.2** for the PEMs without annealing and for the annealed PEMs at temperatures 37, 50 and 80 °C. The upper and lower extremities of the error bars correspond to the data of advancing contact angles, θ_a, and receding contact angles, θ_r, respectively. The magnitude of the dispersion component, γ_s^D, and the polar component, γ_s^p, of the surface energy are determined from the slope and intercept, respectively, of the contact angle data for DMSO and EG. As the contact angle hysteresis of water on the PEMs is much larger than for DMSO and EG, we excluded water for quantitative analysis.

The results of the linear interpolation, the surface energy and the respective components are summarized in **Table 1.2**. In total, the surface energy γ_s diminishes as the annealing temperature increases, from a value of 44.6 mJ m^{-2} for the non-annealed PEM to 38 mJ m^{-2} after annealing at 80 °C. The surface energies after annealing at 37 and 50 °C were very similar and close to 40 mJ m^{-2}.

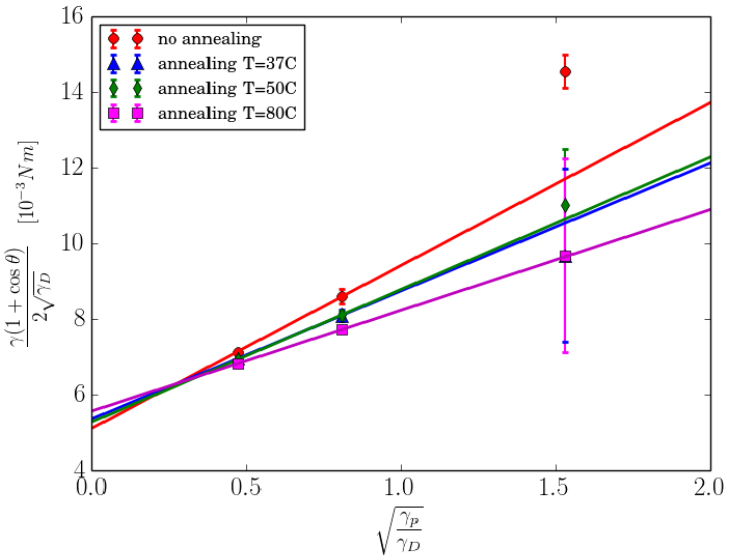

Figure 1.4 Owens-Wendt plot to determine the polar and dispersive component of the surface energy for the multilayer coated substrates after annealing at different temperatures.

Table 1.2 Surface energies of $(PLL/Alg)_{5.5}$ substrate.

Surface energy [mJ/m^2]		No annealing	Annealing at $T = 37°C$	Annealing at $T = 50°C$	Annealing at $T = 80°C$
Dispersion	γ_s^D	26.5 ± 1.5	28.7 ± 1.5	27.8 ± 1.3	30.9 ± 0.5
Polar	γ_s^p	18.6 ± 4.5	11.5 ± 2.5	12.3 ± 1.9	7.11 ± 0.8
Total	γ_s	45.1 ± 6.0	40.2 ± 4.0	40.1 ± 3.2	38.0 ± 1.3

It is interesting to look at the magnitude of the surface energy components γ_s^d and γ_s^p separately. In comparison to the non-annealed sample, the polar component γ_s^p decreases almost to the half value after annealing at 37 °C. However, the polar component does not differ from samples annealed at 37 and 50 °C. Only in the case of

annealing at the highest temperature, 80 °C, the magnitude of γ_s^p showed a further decrease. On the other hand, the dispersion component γ_s^D increases gradually between annealing at 37, 50 and 80 °C by roughly 15%.

The significant decrease of γ_s^p between 37 and 80 °C is indicative of the further compensation of the charges of PLL and Alg and would hint that the polyelectrolyte layers are reorganizing to find themselves in an energetically more favourable arrangement, where the interaction between positive and negative charges is maximized. The increase in γ_s^D in parallel is indicative of the surface becoming more hydrophobic and with a lower charge density, which is also coherent with the charge compensation. The annealing seems to induce a rearrangement of the layers into a more complex-like structure where the oppositely charged PLL and Alg are close enough to induce charge compensation. Results obtained from annealing at 50 °C are more surprising. It seems that after annealing for 72 h at this temperature the arrangement of the chains on the surface was such that the PEMs become more hydrophilic. Probably the annealing at this temperature induces a restructuring of the layers that results in a higher density of Alg on the surface.

The possibility that the annealing could induce changes in the chemistry of the PEMs was also analysed. Amide bonds could be forming between the carboxylate of alginates and primary amines of PLL during the annealing. XPS measurements were performed for the PEMs before and after the annealing at all three considered temperatures. High resolution spectra of N 1s region are shown in **Figure 1.5**. Two peaks are assigned to N-CO/C-NH_2 and C-NH_3 bonds at ~400 eV and ~401.5 eV, respectively[29]. No changes in the XPS spectra regarding the binding energies of the two species could be observed

between the reference spectra of non-annealed PEMs (**Figure 1.5a**) and PEMs annealed at 37, 50 and 80 °C (**Figure 1.5b**, **c** and **d**).

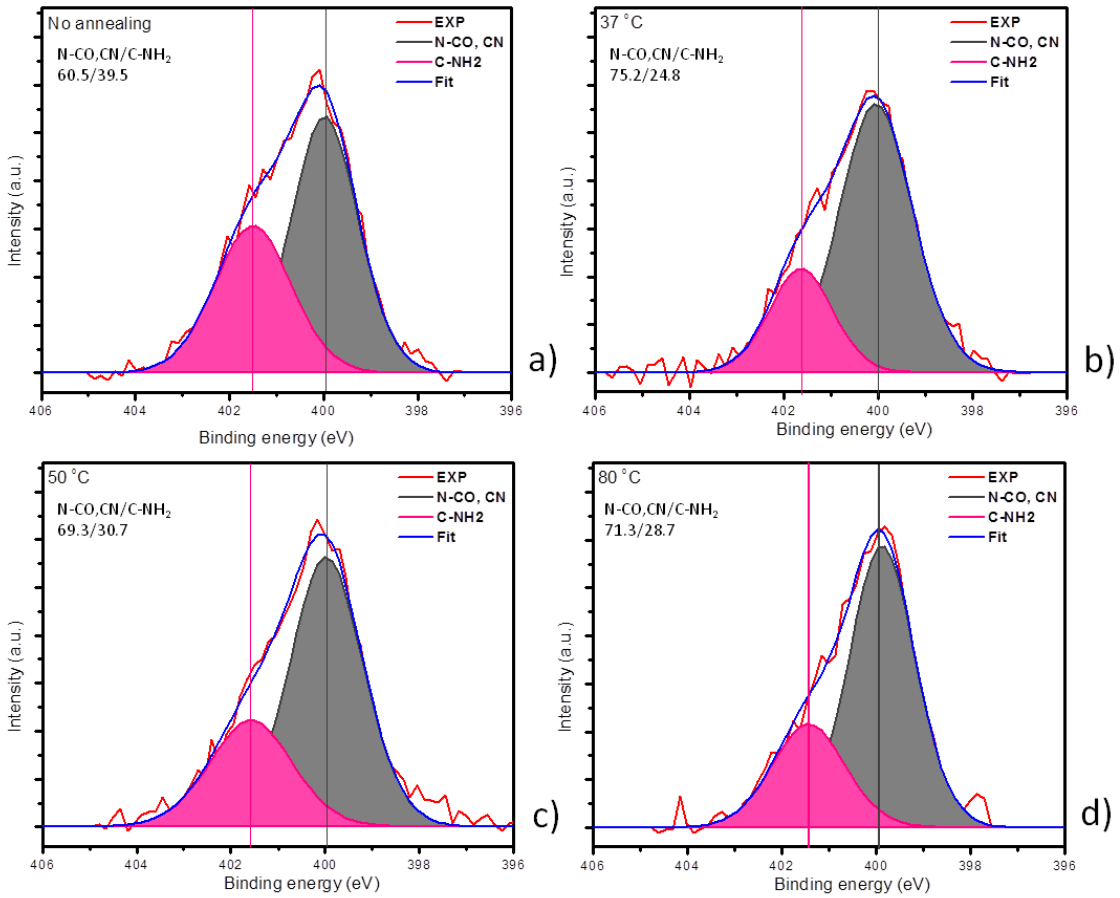

Figure 1.5 XPS analysis for the $(PLL/Alg)_{7.5}$ films a) before annealing and after annealing at b) 37, c) 50 and d) 80 °C.

If there is cross-linking between the amines of PLL and the carboxylates of alginate an amide bound should be formed but this is already present in PLL and consequently there would not appear new signals. However, the ratio of the intensity of the bands of $N\text{-}CO/C\text{-}NH_2$ and $C\text{-}NH_3$ changes with the annealing. The band of $N\text{-}CO/C\text{-}NH_2$ increases in relation with the $C\text{-}NH_3$. This could be meaning that more N-CO is being formed after the annealing, which would be the result of the crosslinking of the amines

of PLL with the carboxylate groups of Alg. But at the same time the relative increase of the bands at 400 eV to the one at 401.5 eV could mean that the NH_3 groups are deprotonating with annealing and the relative amount of NH_2 increases. This would be a consequence of the dehydration of the pendant groups of PLL.

Table 1.3 Surface chemical compositions calculated from XPS experiments, expressed as relative atomic percentage (at.%) for non-annealed and annealed PEMs at 37, 50 and 80 °C.

PLL-Alg	C (at. %)	O (at. %)	N (at.%)
No annealing	58.52	31.72	9.76
37 °C	60.37	30.11	9.52
50 °C	59.20	32.40	8.40
80 °C	59.53	31.40	9.07

When we compare the surface chemical composition of the samples, the molar percentages of C, O and N (**Table 1.3**), we do not observe any significant changes between non-annealed and annealed samples. The cross-linking of the PEM should result in a decrease in the O content as during the formation of an amide bond a OH group from the alginate is lost. Therefore, the absence of changes in the molar percentage of C, N, and O in the film after annealing, hint that there is no cross-linking taking place. Also, if cross-linking would take place one would expect that the PEMs would be more stable nevertheless in the case of annealing at 80 °C we observe that the film has been partially erased (**Figure 1.7**). Therefore, despite we cannot fully disregard the possibility of cross-linking we strongly believe that the changes observed in contact angle must be associated with the electrostatic compensation of the charges of polycations and polyanions due to PE rearrangement.

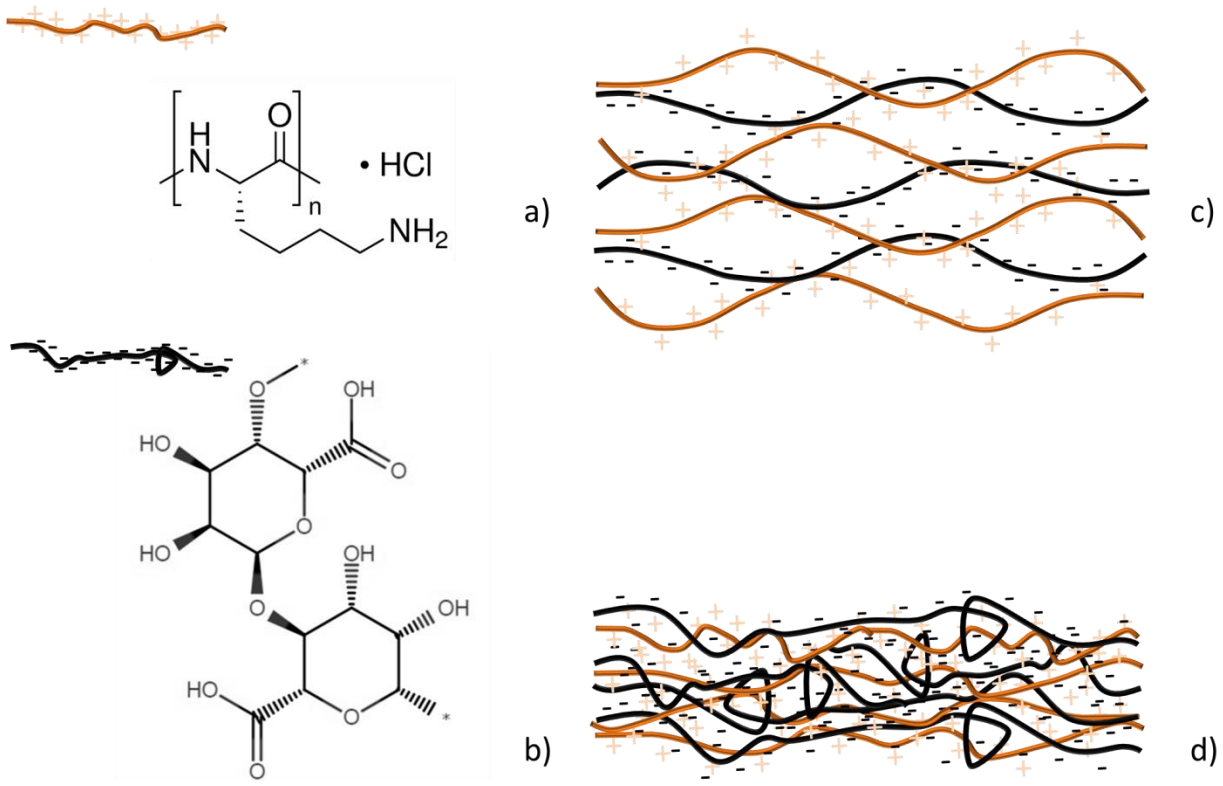

Figure 1.6 Representation of the chemical structures of a) poly-L-lysine hydrochloride and b) alginic acid sodium salt. Scheme of the structure of the PLL/Alg polyelectrolyte multilayer c) before and d) after annealing.

We further investigated changes in charge density in the PEMs after annealing by ζ – potential measurements. $(PLL/Alg)_{7.5}$ were assembled on colloidal particles and annealed afterwards. The annealing of the colloidal particles was also conducted in dry state. The particles were placed in the oven during 72h for each annealing temperature. Finally, the annealed particles were suspended in the Hepes/NaCl solution to measure the ζ – potential. Before annealing the ζ-potential of the PEM was -1.3 mV and after annealing at 37 °C changed to -14.1 mV (**Table 1.4**). By further increase of the temperature at 80 °C, the ζ – potential showed a more pronounced decrease to – 27 mV. The negative potential of the non-annealed PEMs which is very close to zero is

indicative either of the Alg chains protruding from the PEM or of the interdigitation of the PLL and Alg layers.

Table 1.4 ζ – potential values of the $(PLL/Alg)_{7.5}$ coated colloids before and after annealing at 37 and 80 °C.

Sample	$(PLL/Alg)_{7.5}$		
Comments	No Annealing	Annealing at 37 °C	Annealing at 80 °C
Zp (mV)	-1.3	-14.1	-27.0

From QCM-D measurements we know that the film grows progressively and the last layer of PLL is deposited on top of the PEM. There may also be slight differences in the layer characteristics when going from the planar PEM surfaces to a colloidal one as the assembly processes involves steps that are not included on the planar assembly in QCM-D. Nevertheless, despite the slightly negative value it is interesting to follow the evolution of the surface charge with the annealing. As the annealing temperature increased the charge became more negative. This means that either the last PLL layer is removed or most likely there is rearrangement of the Alg and PLL molecules leaving the Alg chain more exposed to the surface and probably surrounding the PLL molecules which are trapped in the Alg. The fact that the maximum molecular weight of Alginate is 600 kDa, while for PLL, is only 300 kDa could also explain the observed excess of negative charges. As the complexes between PLL and Alg molecules are formed there is a compensation of the charges and the charge of the longer chains prevails.

The annealing process allows the polyelectrolyte to restate and reorganize to a molecular arrangement where the interaction of the oppositely charged polyelectrolytes is maximized. The ζ – potential measurements hint to a situation where after annealing Alg charges are more presented on the surface resulting to a higher density of negative

surface charge than before the annealing. However, this does not mean that the density of hydrophilic groups is higher than before annealing, since the top layer was PLL with positively charged amines. A lower density of hydrophilic groups is hinted by the changes in the polar component of the surface energy, which decreases significantly with the annealing at 80 °C. It is important to take into account that the annealing takes place in dry conditions, thus a possible driving force for the process would be the decrease in the PEM surface/air interfacial energy, thus an enhanced amount of hydrophobic groups are expected to be found at the interface, as it has been reported[30]. This would cause a decrease in the density of hydrophilic groups on the surface. AFM shows clearly the reorganization of the surface for the annealing process. The surface roughness of the PEM gets smoother as the annealing temperature increases. This probably indicates that the grains intermix as complexes are being formed.

A scheme of the proposed rearrangement of the PEM after annealing is shown in **Figure.1.6**. In the scheme we have sketched the layered structure of the PEMs and the disappearance of this structure after heating, resulting in the formation of complexes of Alg and PLL chains.

1.3.2 Interaction of PEMs with Proteins

In several situations the interactions of PEMs with proteins is of critical importance. Charged proteins normally interact with PEMs electrostatically so their deposition depends on the charge of both PEM and proteins. We studied the interaction of the BSA protein, and the film before and after annealing. QCM-D experiments were conducted to monitor the adsorption of the BSA on the PEM. PEMs deposited on the quartz crystals

were annealed with the same procedure used for the films assembled on glass substrates, placed back in the QCM-D chamber and rehydrated with the buffer prior to exposure to the protein.

Figure 1.7a shows the frequency and dissipation changes upon adsorption of BSA on a non-annealed PEM. In this case immediately after the assembly the PEM was exposed to the BSA solution. The frequency decreased meaning that there is adsorption of protein on top of the PEM. The frequency shift after deposition of the BSA was Δf = 186.5 Hz. After rinsing with buffer the frequency increased with a total frequency shift of 102 Hz, proving the adsorption of the protein.

When BSA was deposited on the 37 °C annealed PEM the adsorption of the protein decreased to a half compared with the non-annealed PEM (Δf = 45.5 Hz) (**Figure 1.7b**).

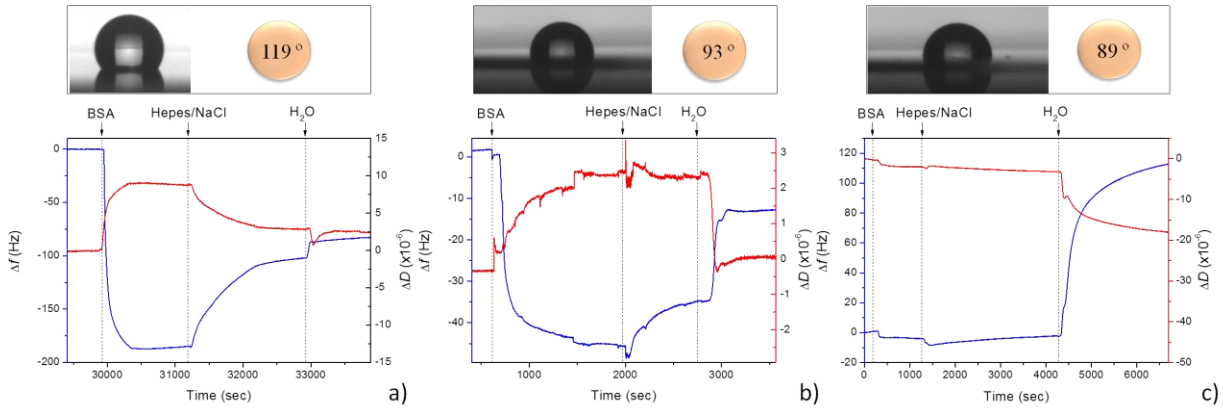

Figure 1.7 Changes in frequency and dissipation after adsorption of BSA protein on top of $(PLL/Alg)_{7.5}$ coated SiO_2 QCM-D crystals and their corresponding contact angle data for the cases of a) non-annealed surface, b) annealed surface at 37 °C and c) annealed surface at 80 °C.

When the film is rinsed with the buffer there is a removal of non-bounded protein as the frequency increases and the final frequency shift is Δf = 35 Hz. In the case of annealing at 80 °C there is no apparent adsorption of protein (**Figure 1.7c**). The total frequency

shift after the BSA deposition was Δf = 3.5 Hz. When the film is rinsed with buffer there is almost no change in frequency or dissipation indicating that there is no protein adsorption or deposition on the film annealed at 80 °C.

Advancing contact angle measurements on the films after deposition of the protein revealed a certain degree of hydrophobicity for all the cases. Nevertheless, for the case of adsorption of the BSA on non-annealed PEMs we obtained the highest values 119° (**Figure 1.7a**) while for the annealed samples at 37 and 80 °C the contact angle values were 93° and 89° respectively, which are close to the contact angle values before annealing (**Figure 1.7b** and **c**). This hints of a limited deposition of the BSA on the annealed PEMs.

In order to have additional information on the changes in protein adsorption to the film, fluorescently labelled BSA has been deposited on top of the PLL/Alg film and its fluorescence was quantified (**Figure 1.8**). Results were in agreement with QCM-D measurements. There is a significant decrease in fluorescence from the non-annealed to the annealed PEMs, meaning a lower amount of protein adsorbed. Normalizing the intensity curves to the non-annealed PEM the intensity of the maxima of the curves for the annealed PEMs at 37 and 80 °C were 0.34 and 0.13 a.u. respectively, 1/3 and 1/10 of the values for the non-annealed PEM.

QCM-D, contact angle, and fluorescence measurements show that thermal annealing has an impact on the interaction of BSA with the PEM. The change of the hydrophilicity of the PEM with the annealing and the exposure of the Alg chains to the surface with compensated charges brings an antifouling character to the PEM.

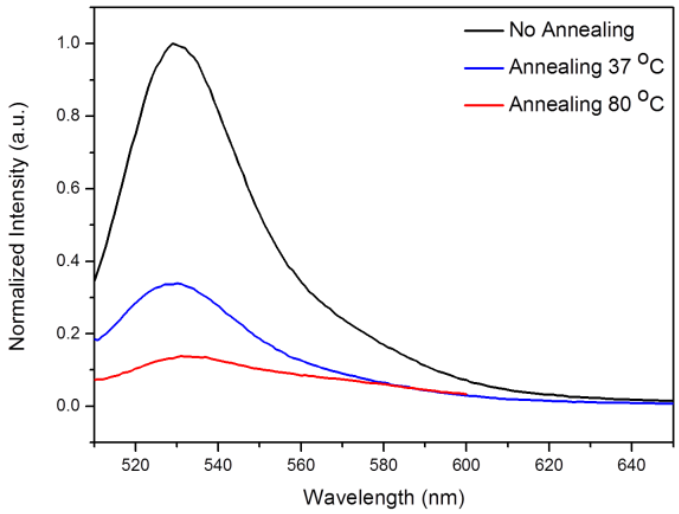

Figure 1.8 Fluorescence spectra after adsorption of labelled BSA onto the $(PLL/Alg)_{7.5}$ films before and after annealing at 37 and 80 °C.

The decrease of protein adsorption with increasing temperature may be indicative of a more significant presence of Alg chains with compensated charges on the surface. It is known that Alg has an antifouling character that probably is increased if the charges of the alginate are partially neutralized[23,31]. The presence of a negative charge on the surface could also be responsible for the decrease on protein deposition as BSA preferentially adsorb on positively charged surfaces[27]. The loss of mass in the PEMs annealed at 80 °C after treatment with BSA may imply that the interaction among the complexes in the film is weak and it is weaker by the interaction with the protein. Further experiments on the study of the rearrangement of polyelectrolyte and the interaction with proteins are being performed.

1.3.3 Evaluation of Cell Adhesion

Cell adhesion was studied before and after annealing using the A549 and C2C12 cell lines. The changes in the average spreading area, aspect ratio and roundness of the adhered cells were studied by transmission imaging of the cells. Before annealing both cell lines showed poor cell adhesion on $(PLL/Alg)_{7.5}$ PEMs (**Figure 1.9** and **1.10**) with average cell spreading areas close to 370 and 400 μm^2 (**Figure 1.9d** and **1.10d**), respectively.

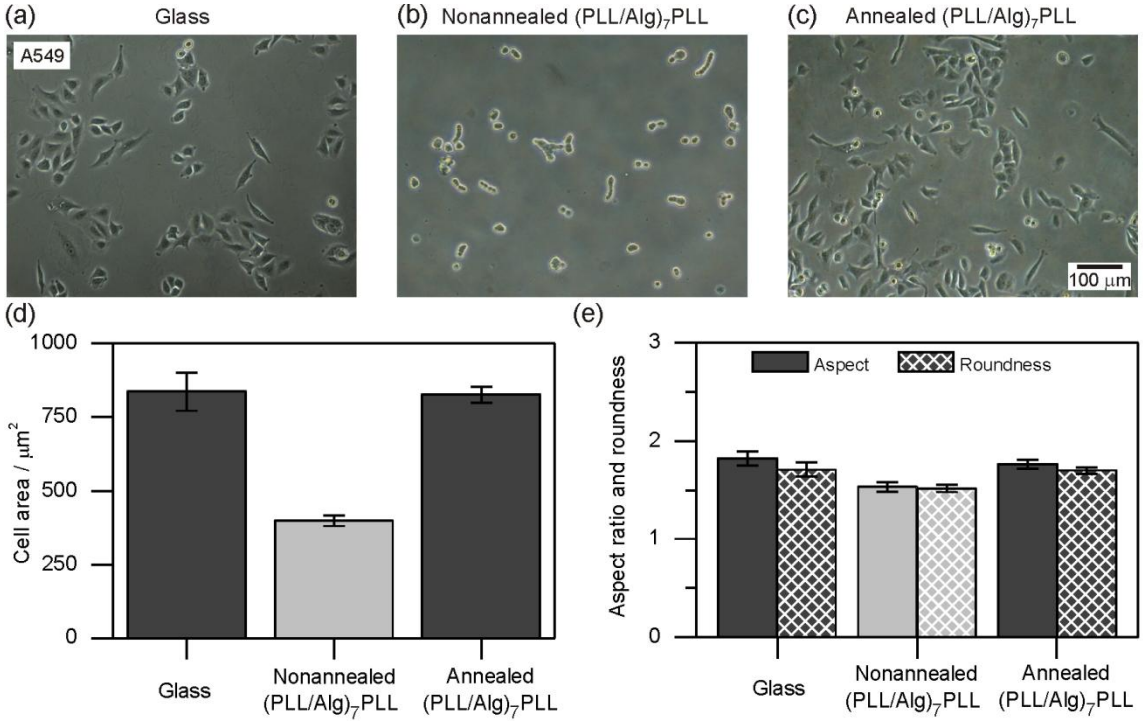

Figure 1.9 Images of A549 cells spreading characteristics seeded on a) glass, b) non-annealed and c) annealed $(PLL/Alg)_{7.5}$ PEMs. d) Average cell spreading area and e) average aspect ratio and roundness quantified from the corresponding images.

The areas obtained from the images were significantly smaller than those obtained on glass, i.e. 870 μm^2 for A549 and 920 μm^2 for C2C12 cells. After thermal annealing at 37 ºC, both the cell spreading area and the evaluated morphological parameters attained

similar values to those obtained on glass (**Figure 1.9e** and **1.9e**), except for the average roundness of C2C12 myoblasts that was significantly larger than on glass (2.70 ± 0.09 for $(PLL/Alg)_{7.5}$ PEM and 2.43 ± 0.09 for glass).

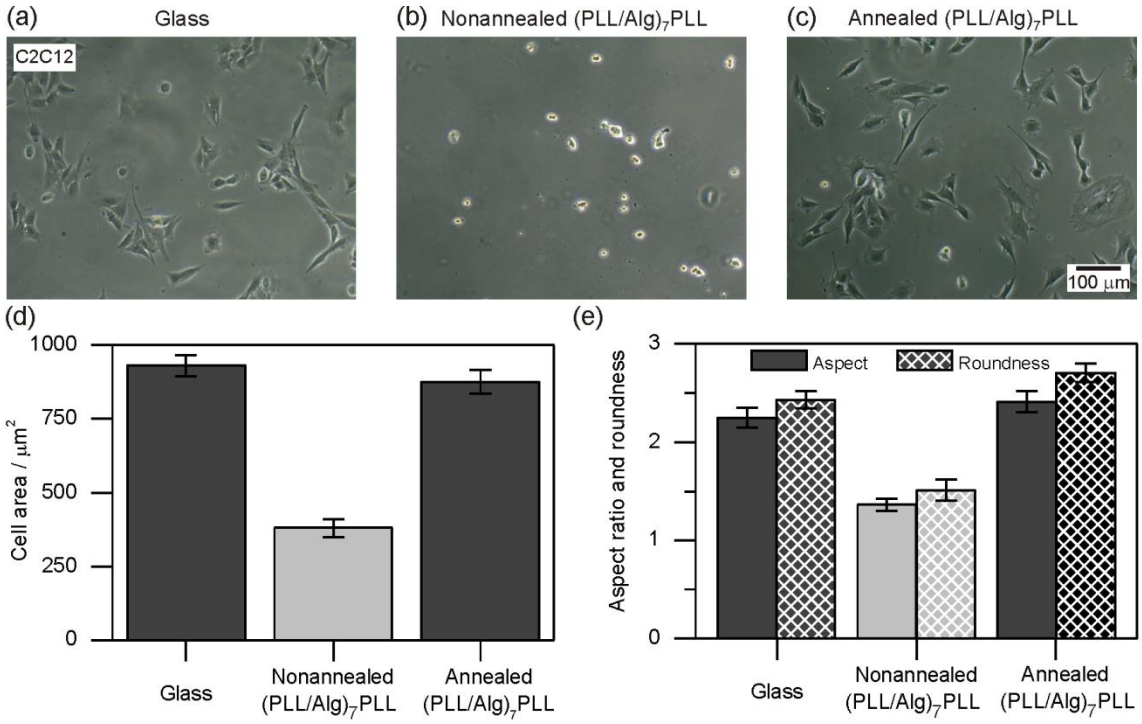

Figure 1.10 Images of C2C12 cells spreading characteristics seeded on a) glass, b) non-annealed and c) annealed $(PLL/Alg)_{7.5}$ PEMs. d) Average cell spreading area and e) average aspect ratio and roundness quantified from the corresponding images.

In focal adhesion experiments, A549 and C2C12 cells on non-annealed $(PLL/Alg)_{7.5}$ PEMs exhibited a diffuse actin cytoskeleton mostly localized at the cell periphery. Spread cells on glass and on annealed films showed well-ordered stress fibers that extended over the cytoplasm (**Figure 1.11** and **1.12**). Adhered cells spread on the substrates and interact via deposited protein from the culture medium forming well-defined focal contacts. Vinculin is an intracellular protein connecting stress fibres with the membrane at the sites of cell anchorage.

Cell adhesion was assessed by measuring the total area of vinculin-stained focal contacts per cell. For A549 cells adhered on $(PLL/Alg)_{7.5}$ films, the adhesion area changed from 5.2 ± 0.1 μm^2 for the non-annealed PEM to 23.2 ± 0.1 μm^2 after thermal annealing, a value similar to that obtained for glass, 27.7 ± 0.1 μm^2.

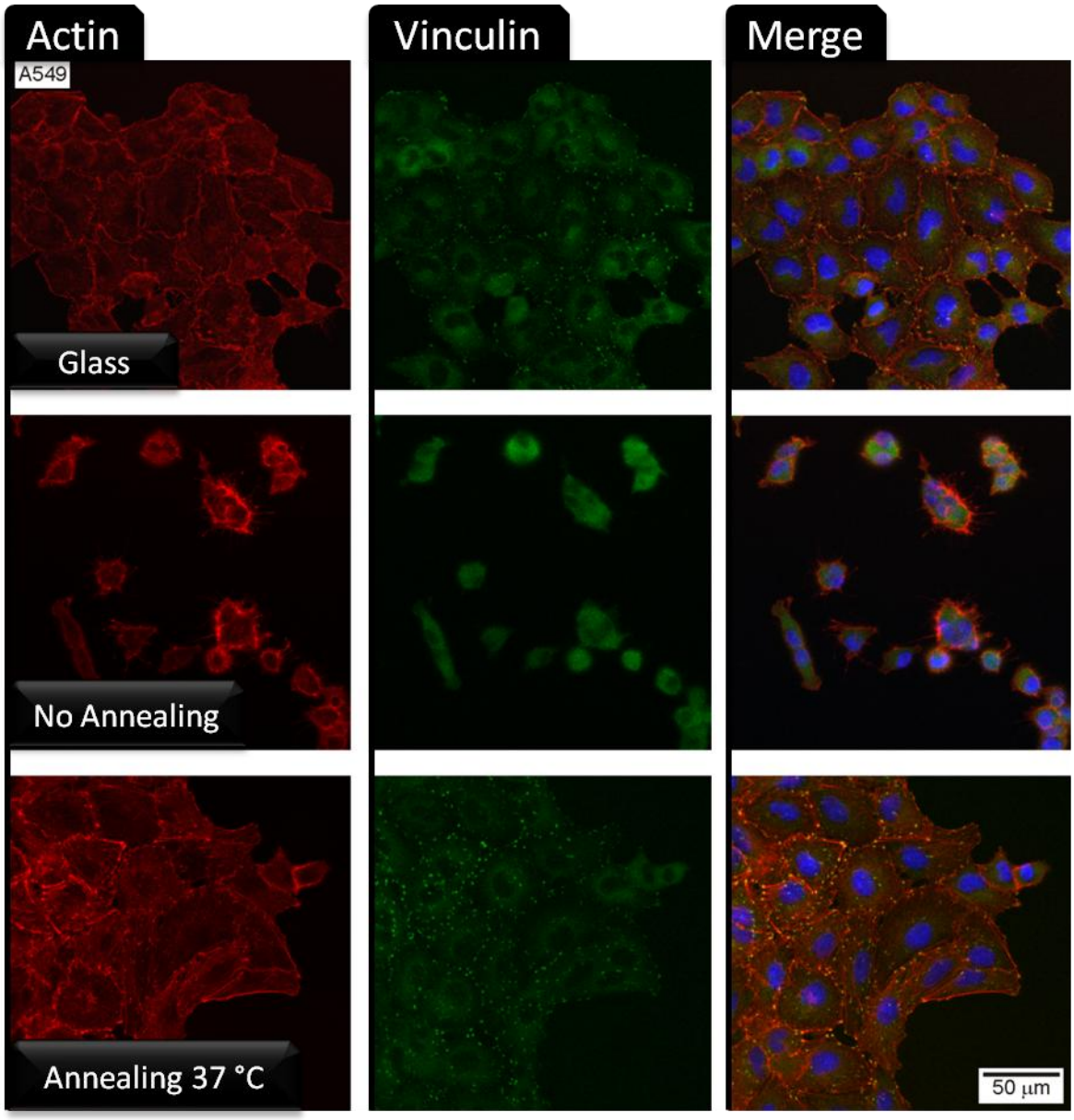

Figure 1.11 Typical CLSM images of stained A549 cells seeded on glass, non-annealed and annealed $(PLL/Alg)_{7.5}$ PEMs.

On the other hand, for C2C12 cells, the average area of vinculin-stained focal contact per cell resulted in 39.7 ± 0.1 μm^2 for cells adhered on glass, 12.1 ± 0.1 μm^2 for the non-annealed PEM and 37.9 ± 0.1 μm^2 for the annealed PEM. For both cell lines an improved adhesion after annealing was observed.

The cell lines employed in these experiments are very different in nature: tumor epithelial cell from human lung and myoblasts from a hamster. The latter is fibroblastic in shape, with high polarization, whereas the former tends to be more rounded. Morphological parameters were in agreement with these characteristics, and for both cell lines the same tendency to an enhancement of cell adhesion was observed. The average spreading area and morphological parameters for both cell lines on annealed PEMs were similar to those obtained from cells on glass. Furthermore, immunostaining reveals that focal contact area per cell, assessed by vinculin staining, was more than 3 times larger for annealed substrates than for non-annealed ones. Cells adhered on annealed PEMs show very well-defined stress fibres and display a much higher level of organization with a tendency to form compact colonies. This hints that the steps after the adhesion, i.e., spreading, migration, proliferation, are also enhanced on the annealed PEMs.

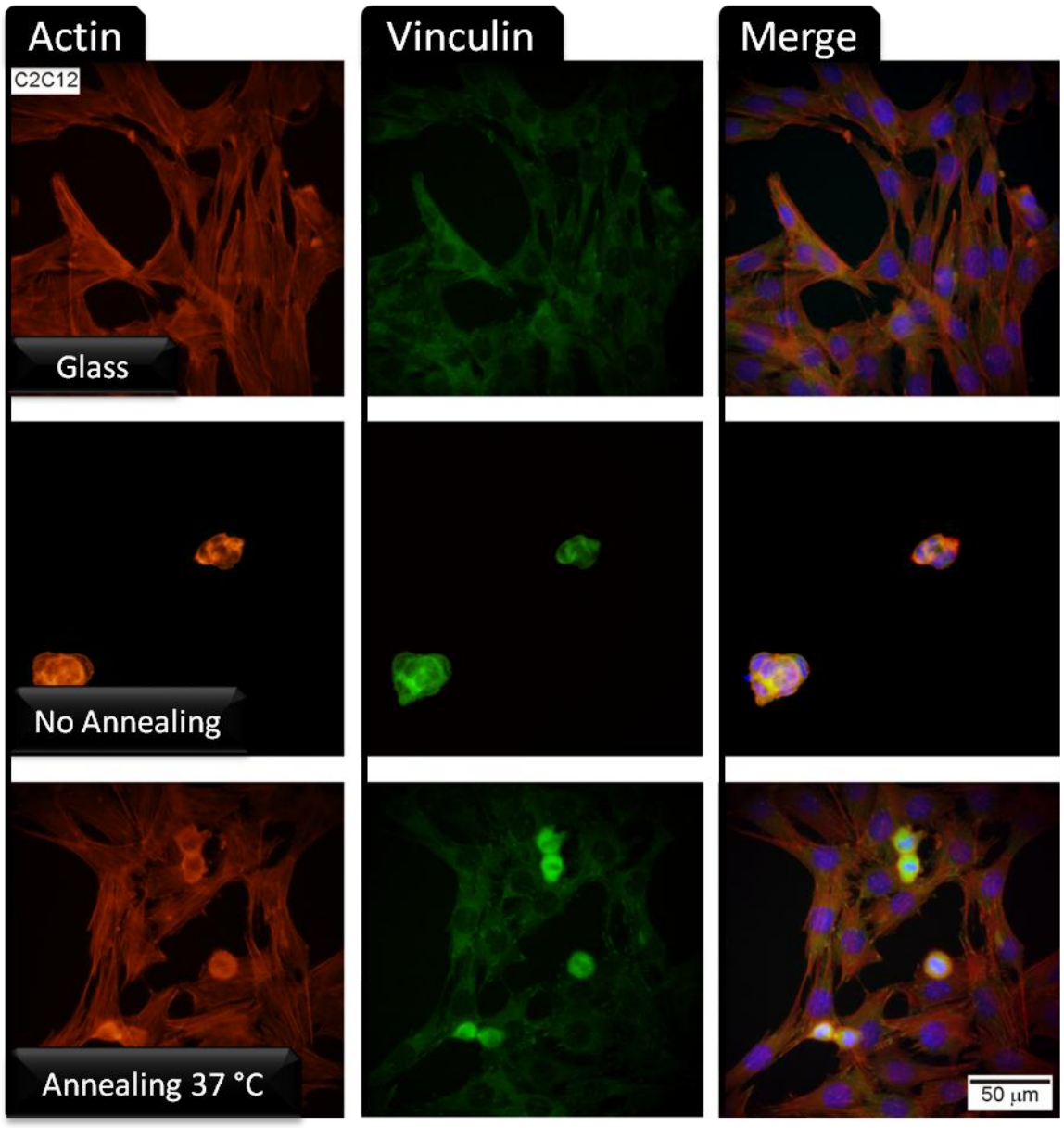

Figure 1.12 Typical CLSM images of C2C12 cells seeded on glass, non-annealed and annealed $(PLL/Alg)_{7.5}$ PEMs.

1.4 Conclusions

In this chapter we have shown that annealing of PLL/Alg PEMs at temperatures between 37 and 80 °C results in the film reorganization that could be interpreted as a change from stratified polyelectrolyte layers to the formation of complexes between the oppositely charged polyelectrolytes. Surface topography and charge change after annealing. Most interesting is that annealing has a clear impact on the wetting properties of PEMs, whose contact angle changes from 36° to values between 77° and 95°. Surface energy calculations show that the annealing affects the polar energy of the surface, hinting a large compensation of charges after annealing at 37 and 80 °C. Results in this chapter suggest that thermal annealing can be used as a simple way to change the wetting properties of surfaces from hydrophilic to hydrophobic without further chemical modifications. Annealed PEMs at 37 °C exhibited enhanced cell adhesion displaying well-defined stress fibres towards C2C12 and A549 cell lines in comparison to non-annealed films. Spreading, migration and proliferation enhanced on annealed PEMs which was most likely related to the increase in stiffness in the PEMs and in contact angle. Additionally results also revealed that annealing decreases protein deposition on the films.

In conclusion, this chapter shows a simple way of tuning the wetting and antifouling character of biocompatible films that can be applied to modulate cell adhesion in a simple and friendly manner, maintaining the chemical composition of the film unchanged with potential applications in tissue engineering and regenerative medicine.

References

(1) Ventre, M.; Netti, P. A. Engineering Cell Instructive Materials To Control Cell Fate and Functions through Material Cues and Surface Patterning. *ACS Appl. Mater. Interfaces* **2016**, acsami.5b08658.

(2) Biela, S. A.; Su, Y.; Spatz, J. P.; Kemkemer, R. Different Sensitivity of Human Endothelial Cells, Smooth Muscle Cells and Fibroblasts to Topography in the Nano-Micro Range. *Acta Biomater.* **2009**, *5* (7), 2460–2466.

(3) Bačáková, L.; Filová, E.; Rypáček, F.; Švorčík, V.; Starý, V. Cell Adhesion on Artificial Materials for Tissue Engineering. *Physiol. Res.* **2004**, *53* (SUPPL. 1).

(4) Engler, A. J.; Richert, L.; Wong, J. Y.; Picart, C.; Discher, D. E. Surface Probe Measurements of the Elasticity of Sectioned Tissue, Thin Gels and Polyelectrolyte Multilayer Films: Correlations between Substrate Stiffness and Cell Adhesion. *Surf. Sci.* **2004**, *570* (1–2), 142–154.

(5) Kharkar, P. M.; Kiick, K. L.; Kloxin, A. M. Designing Degradable Hydrogels for Orthogonal Control of Cell Microenvironments. *Chem. Soc. Rev.* **2013**, *42* (17), 7335–7372.

(6) Saxena, S.; Spears, M. W.; Yoshida, H.; Gaulding, J. C.; García, A. J.; Lyon, L. A. Microgel Film Dynamics Modulate Cell Adhesion Behavior. *Soft Matter* **2014**, *10* (9), 1356–1364.

(7) Boudou, T.; Crouzier, T.; Ren, K.; Blin, G.; Picart, C. Multiple Functionalities of Polyelectrolyte Multilayer Films: New Biomedical Applications. *Adv. Mater.* **2010**, *22* (4), 441–467.

(8) Costa, R. R.; Mano, J. F. Polyelectrolyte Multilayered Assemblies in Biomedical Technologies. *Chem. Soc. Rev.* **2014**, *43* (10), 3453–3479.

(9) Elbert, D. L.; Herbert, C. B.; Hubbell, J. A. Thin Polymer Layers Formed by Polyelectrolyte Multilayer Techniques on Biological Surfaces. *Langmuir* **1999**, *15* (16), 5355–5362.

(10) Chluba, J.; Voegel, J. C.; Decher, G.; Erbacher, P.; Schaaf, P.; Ogier, J. Peptide Hormone Covalently Bound to Polyelectrolytes and Embedded into Multilayer Architectures Conserving Full Biological Activity. *Biomacromolecules* **2001**, *2* (3), 800–805.

(11) Schneider, A.; Richert, L.; Francius, G.; Voegel, J.-C.; Picart, C. Elasticity, Biodegradability and Cell Adhesive Properties of Chitosan/hyaluronan Multilayer Films. *Biomed. Mater.* **2007**, *2* (1), S45-51.

(12) Picart, C.; Senger, B.; Sengupta, K.; Dubreuil, F.; Fery, A. Measuring Mechanical

Properties of Polyelectrolyte Multilayer Thin Films: Novel Methods Based on AFM and Optical Techniques. *Colloids Surfaces A Physicochem. Eng. Asp.* **2007**, *303* (1–2), 30–36.

(13) Boudou, T.; Crouzier, T.; Auzély-Velty, R.; Glinel, K.; Picart, C. Internal Composition versus the Mechanical Properties of Polyelectrolyte Multilayer Films: The Influence of Chemical Cross-Linking. *Langmuir* **2009**, *25* (24), 13809–13819.

(14) Köhler, K.; Shchukin, D. G.; Möhwald, H.; Sukhorukov, G. B. Thermal Behavior of Polyelectrolyte Multilayer Microcapsules. 1. The Effect of Odd and Even Layer Number. *J. Phys. Chem. B* **2005**, *109* (39), 18250–18259.

(15) Gao, C.; Leporatti, S.; Moya, S.; Donath, E.; Möhwald, H. Swelling and Shrinking of Polyelectrolyte Microcapsules in Response to Changes in Temperature and Ionic Strength. *Chem. - A Eur. J.* **2003**, *9* (4), 915–920.

(16) Köhler, K.; Shchukin, D. G.; Sukhorukov, G. B.; Möhwald, H. Drastic Morphological Modification of Polyelectrolyte Microcapsules Induced by High Temperature. *Macromolecules* **2004**, *37* (25), 9546–9550.

(17) Leporatti, S.; Gao, C.; Voigt, a; Donath, E.; Möhwald, H. Shrinking of Ultrathin Polyelectrolyte Multilayer Capsules upon Annealing: A Confocal Laser Scanning Microscopy and Scanning Force Microscopy Study. *Eur. Phys. J. E* **2001**, *5* (1), 13–20.

(18) Glinel, K.; Déjugnat, C.; Prevot, M.; Schöler, B.; Schönhoff, M.; Klitzing, R. V. Responsive Polyelectrolyte Multilayers. *Colloids Surfaces A Physicochem. Eng. Asp.* **2007**, *303* (1–2), 3–13.

(19) Picart, C.; Mutterer, J.; Richert, L.; Luo, Y.; Prestwich, G. D.; Schaaf, P.; Voegel, J.-C.; Lavalle, P. Molecular Basis for the Explanation of the Exponential Growth of Polyelectrolyte Multilayers. *Proc. Natl. Acad. Sci. U. S. A.* **2002**, *99* (20), 12531–12535.

(20) Caridade, S. G.; Monge, C.; Gilde, F.; Boudou, T.; Mano, J. F.; Picart, C. Free-Standing Polyelectrolyte Membranes Made of Chitosan and Alginate. *Biomacromolecules* **2013**, *14* (5), 1653–1660.

(21) Krikorian, V.; Kurian, M.; Galvin, M. E.; Nowak, A. P.; Deming, T. J.; Pochan, D. J. Polypeptide-Based Nanocomposite: Structure and Properties of poly(L-lysine)/Na+-Montmorillonite. *J. Polym. Sci. Part B Polym. Phys.* **2002**, *40* (22), 2579–2586.

(22) Aston, R.; Wimalaratne, M.; Brock, A.; Lawrie, G.; Grøndahl, L. Interactions between Chitosan and Alginate Dialdehyde Biopolymers and Their Layer-by-Layer Assemblies. *Biomacromolecules* **2015**, *16* (6), 1807–1817.

(23) Zhou, J.; Romero, G.; Rojas, E.; Ma, L.; Moya, S.; Gao, C. Layer by Layer

Chitosan/alginate Coatings on Poly(lactide-Co-Glycolide) Nanoparticles for Antifouling Protection and Folic Acid Binding to Achieve Selective Cell Targeting. *J. Colloid Interface Sci.* **2010**, *345* (2), 241–247.

(24) Mu, M.; Rieser, T.; Lunkwitz, K.; Meier-haack, J. Polyelectrolyte Complex Layers : A Promising Concept for Anti- Fouling Coatings Verified by in-Situ ATR-FTIR Spectroscopy. *Macromol. Rapid Commun.* **1999**, *20*, 607–611.

(25) Henke, L.; Nagy, N.; Krull, U. J. An AFM Determination of the Effects on Surface Roughness Caused by Cleaning of Fused Silica and Glass Substrates in the Process of Optical Biosensor Preparation. *Biosens. Bioelectron.* **2002**, *17* (6–7), 547–555.

(26) Andrade, J. D.; Smith, L. M.; Gregonis, D. E. The Contact Angle and Interface Energetics. In *Surface and Interfacial Aspects of Biomedical Polymers*; 1985; pp 249–292.

(27) Owens, D. K.; Wendt, R. C. Estimation of the Surface Free Energy of Polymers. *J. Appl. Polym. Sci.* **1969**, *13* (8), 1741–1747.

(28) van Oss, C. J. *Interfacial Forces in Aqueous Media, Second Edition*; 1994.

(29) Beamson, G.; Briggs, D. High Resolution XPS of Organic Polymers: The Scienta ESCA3000 Database. *J. Chem. Educ.* **1993**, *70* (1), A25.

(30) Decher, G.; Hong, J. D.; Schmitt, J. Buildup of Ultrathin Multilayer Films by a Self-Assembly Process: III. Consecutively Alternating Adsorption of Anionic and Cationic Polyelectrolytes on Charged Surfaces. *Thin Solid Films* **1992**, *210–211*, 831–835.

(31) Zhao, K.; Zhang, X.; Wei, J.; Li, J.; Zhou, X.; Liu, D.; Liu, Z.; Li, J. Calcium Alginate Hydrogel Filtration Membrane with Excellent Anti-Fouling Property and Controlled Separation Performance. *J. Memb. Sci.* **2015**, *492*, 536–546.

Chapter 2

The Role of Top-Layer Chemistry, Polyanions, Vesicle Composition and Phosphate Salts in the Formation of Lipid Bilayers on Top of Polyelectrolyte Multilayers

2.1 Motivation

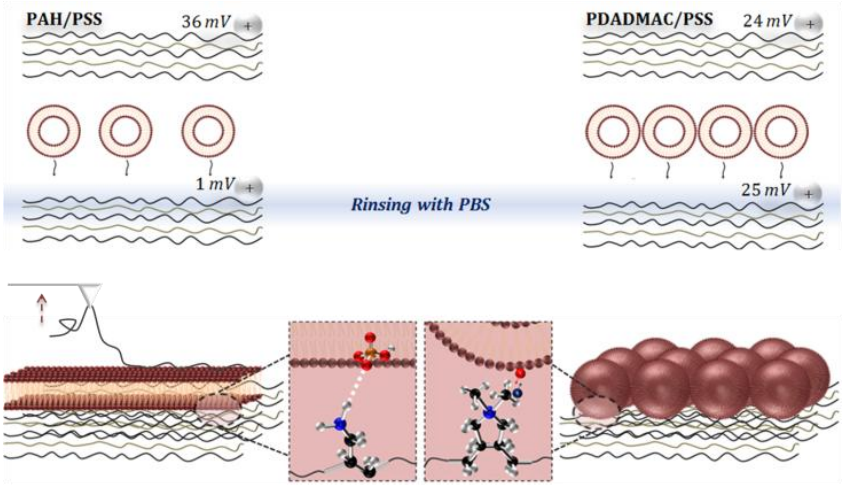

Supported lipid bilayers have been extensively studied as model membranes in biophysical studies or as part of sensors, and in biotechnology research[1–7]. Lipid bilayers have been supported on a diversity of solid supports such as silica, titania, mica etc[3,8–10]. The self-assembly of SLBs is usually performed via deposition of unilamellar lipid vesicles in aqueous media on a solid surface[3,11,12]. The conditions for the lipids to assemble into a bilayer must be properly adjusted for each type of surface by tuning precisely the buffer conditions, the ionic strength, the presence of specific ions like Ca^{+2}, temperature, etc.[11,13,14] While the mechanisms leading to the formation of lipid bilayers onto solid hard supports, i.e., TiO_2 or SiO_2, are well investigated with

experimental conditions and protocols for bilayer formation established[15–17] and easy to reproduce, the assembly of lipids on top of soft polymer films, like polyelectrolyte multilayers, in most cases, has not been successful. The assembly of lipid bilayers on polymer films is interesting from a fundamental point of view[18], as in their natural environment cell membranes are supported on a network of biopolymers, the glycocalyx or the cell wall. The assembly of lipids on top of polymer cushions has been performed with the aim of fabricating model membranes with characteristics that resemble the cell membrane; with the scope of fabricating biomimetic interfaces in devices and also for their use as templates in drug delivery systems[18–21]. PEMs are particularly interesting as supports due to their simple and stepforward assembly based on the alternating deposition of oppositely charged polyelectrolytes mainly due to electrostatic interactions (LbL technique) [22–25].

The mechanism of vesicle assembly on top of PEMs has been extensively studied by Fischlechner et al. for PAH/PSS multilayers[26]. This PE combination is one of the most commonly employed for PEM fabrication. Lipid vesicles form bilayers on top of PEMs of PAH/PSS when the vesicles are prepared upon a mixture of zwitterionic and charged lipids. Fischlechner et al. found that charged lipids are necessary for better interaction of the vesicles with the PEM but zwitterionic lipids are also necessary to trigger vesicles' fusion.

The interaction between the lipids and the PEMs has been assumed to be electrostatic, though the primary amines in PAH could form hydrogen bonds with the phosphate groups in the phospholipids. In the case of phosphatidylserine, employed for the bilayer formation, its carboxylate groups could also form hydrogen bonding with the primary

amines. In order to improve the conditions for the formation of lipid bilayers it is fundamental to understand the true nature of the interaction between the lipids and PAH. PAH displays primary amines and is a weak polyelectrolye, whose charge depends on the pH of the media. PDADMAC is also a commonly used polyelectrolyte for LbL assembly. Differently from PAH, PDADMAC displays quaternary amines and is a strong polyelectrolyte; its charge is not affected by the pH. The presence of primary (or secondary) amines is fundamental for hydrogen bonding while quaternary amines cannot form hydrogen bonding as the amines bear a permanent charge localized on the nitrogen, which is surrounded by an organic shell. In a quaternary amine, nitrogen is covalently bounded to four carbon chains.

Another aspect affecting bilayer formation, which has not been studied in detail, is the role of the polyanions when the lipid layers are assembled on top of a polycation. Polyelectrolyte multilayers are assembled from at least two polymers, a polycation and a polyanion. Despite the top layer of PAH, which is facing the lipid and is mainly responsible for the assembly, the layer underneath can also have an impact on the vesicle deposition as it is directly interacting with the PAH and together they define the properties of the film.

In addition, phosphate ions present in the solution of PBS used for the hydration of the lipid film may also play a fundamental role in the formation of lipid bilayers as they can also interact with the amines of the top layer of the PEM.

First, in order to study the influence of the lipid composition, SUVs of mixed lipids of the zwitterionic DOPC and the negatively charged DOPS were adsorbed on top of 11 layers

of PAH/PSS films. Their assembly into lipid bilayers was evaluated by means of QCM-D and CryoTEM.

Force vs distance curves measured by AFS using PAH modified cantilevers gave an insight into the lipid polymer interactions and unveil the role of electrostatic interactions and hydrogen bonding in the formation of a lipid bilayer. For further analysis of the role of hydrogen bonding, vesicles of 50:50 molar ratio of DOPC:DOPS were assembled on top of PDADMAC/PSS and characterized via QCM-D and FRAP measurements.

Besides the type of interaction of the lipids with the top PE layer other characteristics of the multilayer; their mechanical properties, a different degree of swelling and PE arrangement can also have influence on the bilayer formation. PAH/PSS multilayers have a modulus of elasticity of around 500 MPa[27] while PDADMAC/PSS close to 100 MPa[28]. We fabricated multilayers of PAH/PSS with a few layers of PDADMAC on top and studied the SUVs assembly with the scope to split the effect of the quaternary amines independently from other parameters as the mechanical properties of the PEM. Following a similar strategy, we coated multilayers of PDADMAC/PSS with a few PAH layers to study the impact of the primary amines on the interaction with phospholipids decoupled of other characteristics of the PAH/PSS multilayers.

A model for the interaction of the primary and quaternary amines with the phospholipids and the lipid assembly is presented in this chapter.

To understand how the properties of the multilayers with PAH as polycation change by varying the polyanion in the multilayer and the impact that this would have on the bilayer formation SUVs of 50:50 molar ratio DOPC:DOPS hydrated with PBS were assembled on top of PAH/Alg and PAH/PAA multilayers. QCM-D and FRAP measurements were

applied to evaluate the bilayer formation. XPS and ζ – potential measurements were applied to characterize the interaction of amine groups of PAH with phosphate ions of phosphate salts in PBS.

2.2 Experimental Section

2.2.1 Liposome Preparation and Characterization

The preparation of SUVs composed of mixtures of DOPC:DOPS and POPC:POPS was as follows. Briefly, lipid stock solutions in chloroform (10 mg mL^{-1}) were mixed together to a final concentration of 0.5 mg mL^{-1} at different molar ratios (100:0, 75:25, 60:40, 50:50, 30:70 and 20:80) of PC and PS respectively. The mixture was dehydrated with an argon stream forming a thin lipid film and incubated under vacuum afterwards for at least 1 hour to remove any remaining solvent. The lipid film was then rapidly hydrated with the respective aqueous solution forming multilamellar vesicles which resulted in SUVs of ~100 nm sizes after extrusion through a 50 nm polycarbonate membrane. The hydration solution varied to PBS 10 mM, Hepes 10 mM /NaCl 150 mM/ $CaCl_2$ 2 mM and NaCl 150 mM for the needs of the experiments. For FRAP experiments, 1 % of fluorescently labelled NBDPC:NBDPS lipids at 0.5:0.5 molar ratio was added to the initial lipid mixture.

^{1}H NMR measurements were conducted in order to reveal the exact molar ratio of PC to PS in the lipid mixture. Briefly, a concentration of 0.6 mg mL^{-1} was taken out from the initial mixture in chloroform for ^{1}H NMR measurements. All proton spectra were recorded at 298 K with a Bruker Avance 500 MHz spectrometer equipped with a 5 mm double resonance inverse probe. One pulse experiment was recorded with 15 seconds of recycled delay and 64 transients. A proton spectral width of 8000 Hz and a total of 64 k points were used with 90 deg. pulse of 7.5 us. The data was zero-filled to 128 k points after which it was Fourier transformed. All the spectra were processed with Bruker TOPSPIN software. The ratio of the two different lipids was calculated from the integrals

of the peaks from the terminal methyl groups in the hydrocarbon chains (0.9 ppm) of both PC and PS, and from the peak of the choline methyl groups (3.4 ppm), which is only present in PC and not in PS. The spectrum was calibrated to $CDCl_3$ at 7.24 ppm.

2.2.2 DLS and ζ – Potential Measurements

For SUVs characterization, vesicles of different compositions of PC:PS, were diluted in PBS to a final concentration of 0.2 mg mL^{-1} and characterised by dynamic light scattering (DLS) using a Zetasizer (Malvern, UK). ζ – potential and size measurements were conducted in a disposable folded capillary cell at 23 °C. ζ – potential measurements were performed at a cell drive voltage of 40 V, using a monomodal analysis model. Five repetitions were conducted for each sample. Size measurements were conducted at a detection angle of 173°. Three repetitions were performed for each sample.

For the evaluation of the interaction of phosphate ions with the PEMs ζ - potential measurements were conducted using in a disposable folded capillary cell at 23 °C and a cell drive voltage of 40 V. All parameters were set in automatic mode. PEMs of PAH/PSS and PDADMAC/PSS were assembled on top of 1 μm SiO_2 particles. SiO_2 particles were initially suspended in 0.5 M NaCl at 1 mg mL^{-1}. Then, the particles were incubated at the respective polyelectrolyte solution for 15 min. The procedure was repeated for every layer deposition for the assembly of 11 layers. In between polyelectrolyte depositions three washing steps with 0.5 M NaCl were performed via centrifugation. After the last washing step, samples were dispersed in different

solutions; H_2O, NaCl 10 mM, NaCl 150 mM and PBS 10 mM, Na_2HPO_4 10 mM or KH_2PO_4 10 mM and were kept shaking for 5 min. Finally, each sample was washed 3 times with the same solutions and their surface charge was characterized. Standard deviation errors were taken out of 3 repetition measurements for each sample.

2.2.3 QCM-D Measurements

QCM-D measurements were conducted with an E4 QCM-D at 23 °C employing SiO_2 coated (50 nm) quartz crystals (5 MHz) from Q-Sense. Initially the crystal was exposed to milliQ water for 10 min, for another 10 min to 0.5 M NaCl and then 11 layers of PEs were assembled in 0.5 M NaCl or acetate buffer with 0.2 M NaCl at 1 mg mL^{-1} in the QCM-D chamber. For each layer deposition polyelectrolyte solutions were flown in the chamber for 10 – 20 min until stable values for the frequency were reached. Every deposited layer was then rinsed with NaCl 0.5 M. The last deposited layer was always a positively charged PE. When the PEM was completed, the chamber was rinsed with the solution used for lipids hydration. Then, the dispersion of SUVs (0.1 mg mL^{-1}) was injected into the chamber and flown through the chamber for 10 min, until a stable frequency value was reached. Surplus or non-adsorbed vesicles were removed by rinsing with the buffer solution for another 10 – 15 min.

2.2.4 CryoTEM Imaging

Lipid bilayer morphology was characterized by CryoTEM a JEOL JEM-2200FS field emission TEM with a digital camera and an in-column energy filter (Omega filter). SiO_2 particles were coated with 11 layers of PAH and PSS, with PAH always being the last deposited layer thus the SUVs were incubated with the PEM coated SiO_2 particles in PBS solution. SiO_2 particles were chosen as template as using nanoparticles yields to a better resolution of the bilayer than on a planar surface. Before vitrification the SUVs were incubated for half an hour with the polyelectrolyte coated SiO_2 particles in PBS. Afterwards, the specimen was deposited on quantifoil grids Holey Carbon Films (shape R2/2). The suspended sample in aqueous solution was then rapidly frozen in liquid ethane and cooled to liquid nitrogen temperature; the whole process was performed on a Vitrobot – FEI. Images were taken of the SiO_2 particles coated with PEMs and the SiO_2 particles with PEMs and PC:PS lipid vesicles.

2.2.5 AFM/Atomic Force Spectroscopy Measurements

Both PEMs with PAH as the outer layer and PEMs coated with lipid vesicles were mounted on the scanner of a Molecular Force Probe 3D AFM (Santa Barbara CA, USA). An aliquot of 0.5 mL of 0.1 M NaCl was deposited as a single drop between the cantilever and the multilayer/lipid coated multilayer. The rate of approach was set to 300 nm s^{-1}. The maximum loading force was limited to 500 pN. Calibration of the cantilever was performed after functionalisation by measuring the sensitivity of the optical level detection system by indenting on a glass substrate. This also allowed verification of the

effectiveness of the functionalisation method by recording characteristic force s distance curves of the PAH desorbing from the glass surface.

The spring constant of the cantilever was determined by the thermal noise method[29]. The spring constants of the used cantilevers ranged between 0.05 – 0.1 Nm^{-1}. Roughness was evaluated with the Software Igor Pro (wavemetrics 5.03). This software determines the root mean square roughness (R_q) being more sensitive to hills and valleys in the surface than the average roughness ($R_{a)}$

AFM tips were functionalised following the protocol described by Gaub et al.[30]. In brief, gold coated AFM tips (NPG-10 Bruker) were cleaned by immersion of the cantilevers in an aqueous solution of ammonia (30%) and hydrogen peroxide (30%) at 70 °C for no longer than 5 min and finally rinsed with Millipore water. Then, a self-assembled thiol monolayer was formed on gold by incubating the cantilevers for 24 h in 10 mL ultrapure ethanol containing 1.0 mg 11-mercapto-1-undecanol and 1.44 mg 16-mercaptohexadecanoic acid, respectively. Afterwards the cantilevers were washed repeatedly with ethanol and finally dried. A stock solution containing 1 mg of N-Hydroxysuccinimide (NHS) and 5 mg of N-(3-Dimethylaminopropyl)-N´-ethylcarbodiimide hydro-chloride (EDC) in 333 µL MES (pH 6) buffer was prepared. 50 µL of this stock solution were added to 4950 µL MES and the cantilevers were incubated in this solution for no longer than 20 min immediately after the cantilevers were transferred into a 40% PAH solution and incubated for 3 h. Finally, the cantilevers were repeatedly rinsed with Millipore water before force measurements were performed.

2.2.6 FRAP Measurements

FRAP measurements were performed with a Zeiss LSM 510 confocal laser scanning microscope. For FRAP measurements, PEMs and SUVs were assembled on top of glass (SiO_2) substrates of a diameter of 24 mm by dipping, employing the same number of layers and experimental conditions as for the QCM-D experiments. Experiments were performed as described in Materials and Methods.

2.2.7 XPS Measurements

XPS experiments were performed in a SPECS Sage HR 100 spectrometer with a non-monochromatic X-ray source (Aluminum Kα line of 1486.6 eV energy and 300 W), placed perpendicular to the analyzer axis and calibrated using the 3d5/2 line of Ag with a full width at half maximum (FWHM) of 1.1 eV.

The selected resolution for the spectra was 10 eV of Pass Energy and 0.15 eV/step. All Measurements were made in an ultrahigh vacuum (UHV) chamber at a pressure of about 5·10-8 mbar. An electron flood gun was used to neutralize for charging.

For the fitting of the P 2p spectra, Gaussian-Lorentzian functions were used (after a Shirley background correction) where the FWHM of all the peaks were constrained while the peak positions and areas were set free.

2.3 Results & Discussion

Figure 2.1 shows a scheme of the formation of lipid bilayers on top of a PEM from lipid vesicles via the adsorption of the vesicles, their deformation until rupture, and finally lipid bilayer formation upon fusion.

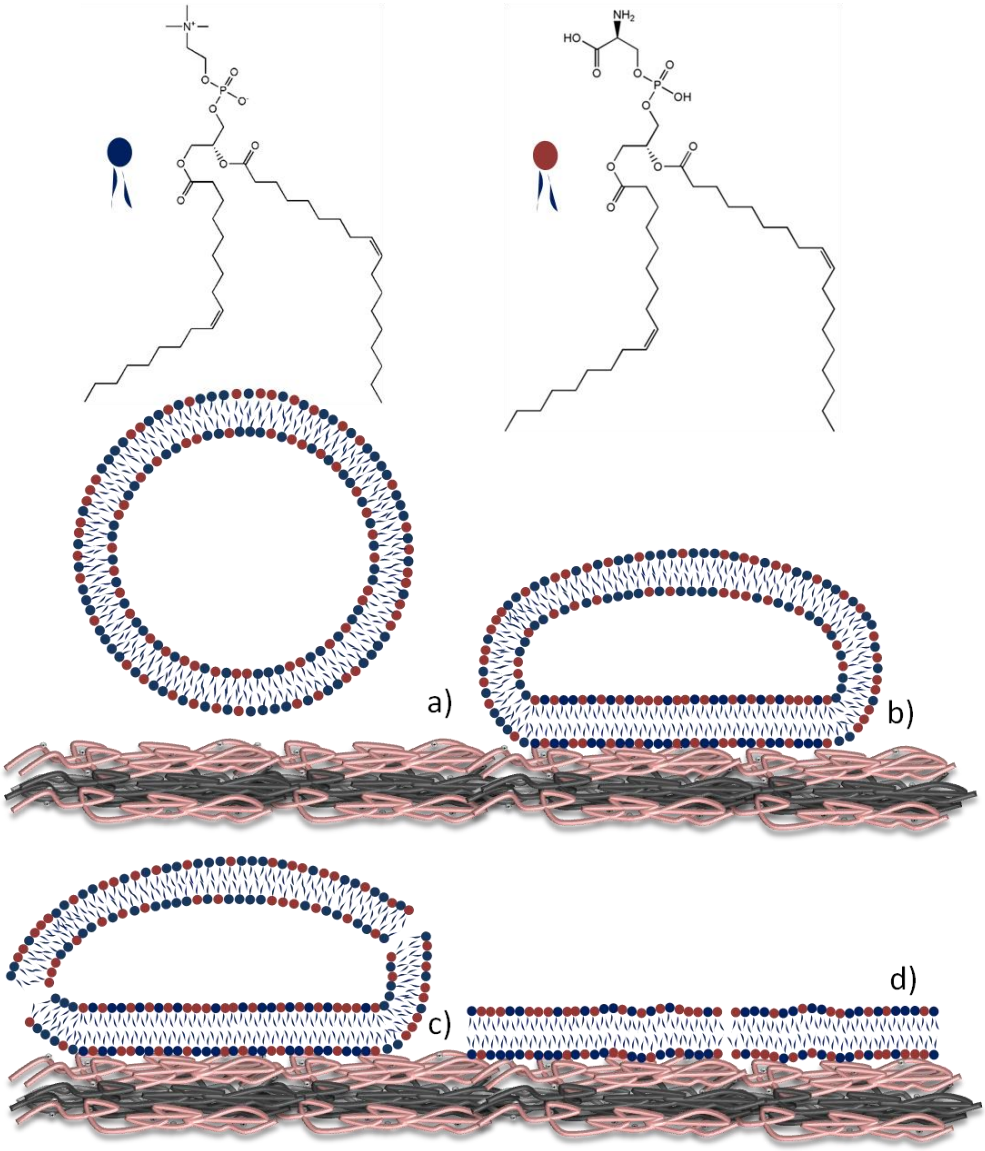

Figure 2.1 Chemical structures for DOPC and DOPS and schematic illustration of the mechanism of lipid bilayer formation on top of polyelectrolyte multilayers. a) Vesicle attraction to the surface, b) vesicle adsorption and deformation, c) vesicle rupture to areas of maximum curvature and d) fusion of neighbouring bilayer patches and final bilayer formation.

Vesicles adsorb to the surface, deform and rupture in areas of maximum curvature, losing their water content; then the lipids rearrange on the PEM and fuse to form a bilayer. This mechanism has been extensively proposed for lipid bilayer formation on solid surfaces[8,9,31], also showed in Richter et al.[16]

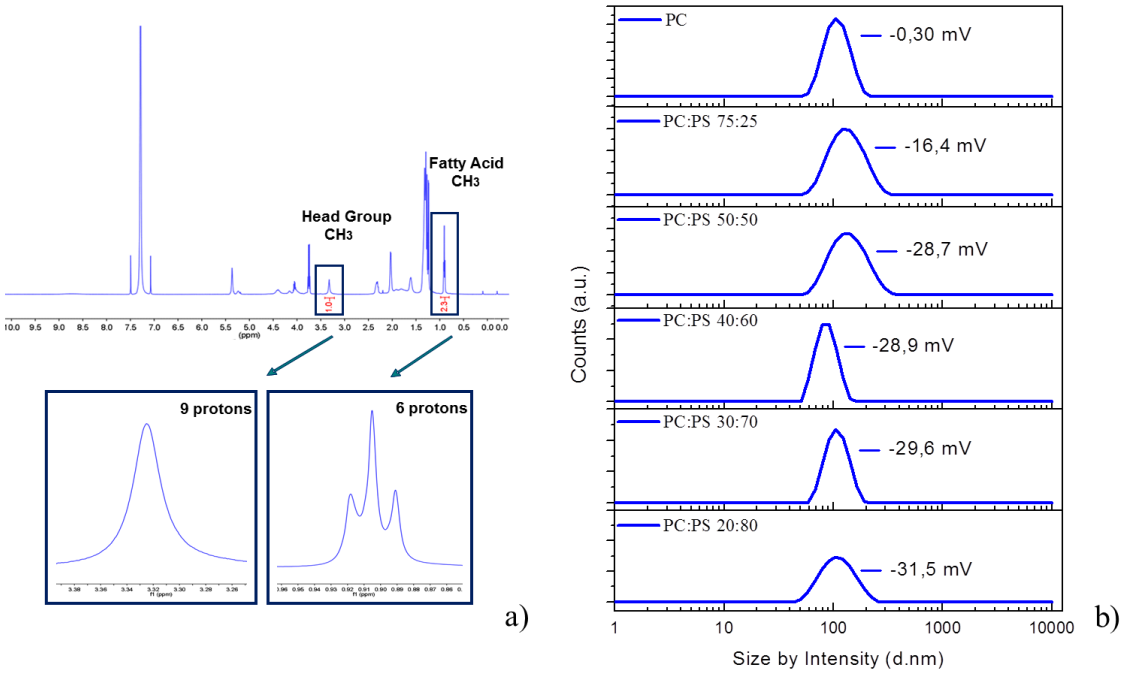

Figure 2.2 a) Typical ^{1}H NMR spectra of a DOPC:DOPS lipid mixture in $CDCl_3$, the spectral signal used to quantify the ratio of two lipids have been marked. The lower part of the figure is a magnification of the same peaks. The proton chemical shift at 3.3 ppm comes from the choline methyl head group, only present for DOPC. The proton chemical shift at 0.99 ppm corresponds to the terminal methyl groups of fatty acids, which are present in both, DOPC and DOPS respectively. b) DLS curves from the vesicles with different lipid composition including their ζ – potential values.

Initially, the conditions for obtaining a bilayer on top of PAH/PSS PEMs were determined. It has already been shown that the composition of lipid vesicles, i.e. the balance between charged and zwitterionic lipids is fundamental for forming bilayers on

top of PAH/PSS films. Vesicles of zwitterionic and charged lipids are prepared by mixing the two lipid components dissolved in chloroform to a desired molar ratio. Since the concentration of lipids in the chloroform solutions may differ from the given values, ^{1}H NMR studies were conducted to determine the exact molar ratio of the lipid mixtures in chloroform (**Figure 2.2a**). Vesicles were prepared from pure DOPC and with increasing values of DOPS.

2.3.1 Liposomes Characterisation

ζ – potential and size distribution measurements were performed for each composition of the extruded unilamellar vesicles. The presence of the negatively charged DOPS resulted in negative potential values for the vesicles of all compositions and increased in absolute values as the percentage of charged lipids increased, revealing an increasing surface charge (**Figure 2.2b**). Pure DOPC vesicles showed a potential of -0.30 mV very close to 0 mV. The potential decreased to -16.4 mV after addition of 25 % of DOPS. For DOPS molar ratios of 50%, 60%, 70% and 80 % the potential decreases only slightly with values of -28.7, -28.9, -29.6, and -31.5 mV, respectively. Size measurements revealed a size distribution of the extruded vesicles between ~100 and ~120 nm for all compositions.

2.3.2 Lipid Bilayer Assembly – QCM-D

The assembly of vesicles with different PC:PS ratios on PAH/PSS PEMs was studied by means of QCM-D. **Figure 2.3** displays the frequency and dissipation changes induced by the addition of vesicles to the PEM coated support for DOPC:DOPS of 100:0, 75:25, 50:50, 40:60, 30:70, and 20:80 molar ratios. Lipid vesicles were always assembled on 11 PAH/PSS layers, with PAH as the top layer. **Figure 2.3a** shows that the deposition of DOPC vesicles, lead to a frequency shift of 87 Hz. The deposition lasted over 2 h. We can distinguish two different trends in the lipid deposition as indicated by the decrease in frequency, which after ~30 min changed more abruptly. Dissipation followed a similar trend and increased continuously up to 9.3 - 10 × 10^{-6} dissipation units after which it remained constant for ~ 20 min. For the case of 75:25 DOPC:DOPS vesicles, the frequency shift after vesicle deposition was 70 Hz and the dissipation increased to 13.6 × 10^{-6} (**Figure 2.3b**). Despite the values of dissipation and frequency after lipid deposition being very similar to those observed for the pure DOPC, both dissipation and frequency change abruptly after the addition of the lipids to almost immediately reach their maximum values and remain constant thereafter indicating the presence of strong binding forces between the vesicles and the PEM surface. This difference in the kinetics of deposition between the pure DOPC vesicles and the vesicles with 25 % DOPS has to be due to the interaction of the PS with PAH. In both cases the frequency changes hint towards the adsorption of intact vesicles. Adsorbed vesicles and/or fragments of vesicles are soft structures that can bend during oscillations leading to pronounced dissipation.

For vesicles with an increasing percentage of PS in molar contribution to the composition, 50:50, 40:60 and 30:70 PC:PS, **Figures 2.3c**, **d** and **e** respectively, we can observe a different behaviour in the frequency and dissipation during lipid deposition on the PEM. Following the proposed rupture mechanism by Keller and Kasemo[32], after the adsorption and deformation, the vesicles form bilayer patches with autocatalytic edges allowing them to fuse and form a continuous bilayer covering the PEM surface. In QCM-D experiments, vesicle adsorption is observed as instant frequency decrease as SUVs are adsorbed on the surface. After fast adsorption kinetics the vesicles deform and rupture followed as a decrease in frequency due to liberation of the aqueous volume enclosed in the vesicles. Formation of a complete bilayer through fusion of bilayer patches is reflected by a frequency plateau. Dissipation is high when the vesicles are adsorbed on the PEM but when the vesicles rupture and a continuous membrane is formed liberating the internal solution the system becomes less dissipative or more solid like, which causes the dissipation decrease. The shift in frequency after the lipid deposition for the 3 lipid mixtures varied between 26 and 29 Hz. These changes in frequency are in agreement with that observed in literature for the formation of lipid bilayers on different supports[4,20,32]. When rinsing with PBS 10 mM and NaCl 0.5 M solution, the bilayer formed of 50:50 PC:PS SUVs did not display any change in frequency or dissipation. When NaCl 0.5 M was substituted for water, there was also no change observed in the frequency, indicating the formation of a complete and stable lipid bilayer[33]. A different behaviour was observed when the bilayer formed from 40:60 PC:PS SUVs was rinsed with PBS and NaCl solutions. The frequency decreased after rinsing with PBS and then after rinsing with NaCl increased reaching the values

obtained prior to PBS rinsing. Dissipation curves followed a similar trend. No further changes occurred when rinsing with water thus the observed changes when rinsing with PBS may be related to some screening of the overall attractive forces between the lipid head groups of the membrane and the interface. PC:PS SUVs with 30:70 molar ratio formed a less rigid and stable bilayer. Frequency and dissipation followed a similar trend to the bilayer formed from the 40:60 SUVs when rinsing with PBS and NaCl. The frequency was slightly decreased due to the presence of water and the dissipation was initially decreased and immediately increased to higher values. This behaviour would be interpreted as either a swelling of the bilayer, probably due to the presence of intact vesicles that grow osmotically with the change in ionic strength or as a deformation of the membrane produced by the 30:70 PC:PS SUVs.

A further increase in the ratio of DOPS to DOPC; 20:80 (**Figure 2.3f**) resulted in the adsorption of vesicles without bilayer formation (Δf = 90 Hz). Frequency and dissipation reached a small plateau after 20 min when the adsorption of the vesicles took place After rinsing with PBS and NaCl no significant changes took place for both frequency and dissipation until rinsing with water, where the frequency increased up to 27 Hz hinting a possible removal of non-adsorbed vesicles. At the same time the dissipation decreased to 9×10^{-6} units.

QCM-D experiments clearly show that the balance of zwitterionic and charged lipids in vesicles is crucial in determining the formation of a bilayer on top of the PAH/PSS multilayers. As highlighted in Fischlechner et al. the presence of PS lipids, which are negatively charged with a carboxylate group in addition to the phosphate group, is fundamental for the formation of a bilayer[34]. The chemistry of the PS group allows for

more attractive interactions with the amine groups of PAH than with PC phospholipids. In PC the quaternary amines should have repulsive interactions with the primary amines of PAH and only the phosphate groups can lead to attractive interactions. Pure PC vesicles adsorb slowly over the PEM and vesicles do not rupture as a consequence of the weak interaction of the lipids with the PAH. Increasing the percentage of charged lipids seemed to increase the kinetics of vesicle deposition as PS is involved in the interaction with PAH but the amount of PS was not enough to trigger vesicle rupture until 50 % of PS was present in the vesicles. We observed vesicle rupture together with bilayer formation when the charged lipids were present in molar ratios from 50 % to 70 %. When vesicles contained more than a 70 % or less than a 50 % of charged lipids no bilayer was obtained. This probably means that a certain percentage of PC is critical for the reorganisation of the lipids on the surface as probably the PS headgroups are frozen by their strong binding with PAH groups. Rosetti et al. [13] have shown, with similar techniques, among others via FRAP, the importance of the balance between DOPC and DOPS lipids in order to accomplish lateral mobility of the vesicles adsorbed on TiO_2 surfaces. Likewise, in the 20:80 PC:PS case there are strong attractive forces between the vesicles and the PEM surface and strong repulsive forces within the highly charged vesicles that restrict their ability to fuse and form a bilayer. The presence of higher concentration of PC is necessary to diminish this repulsion.

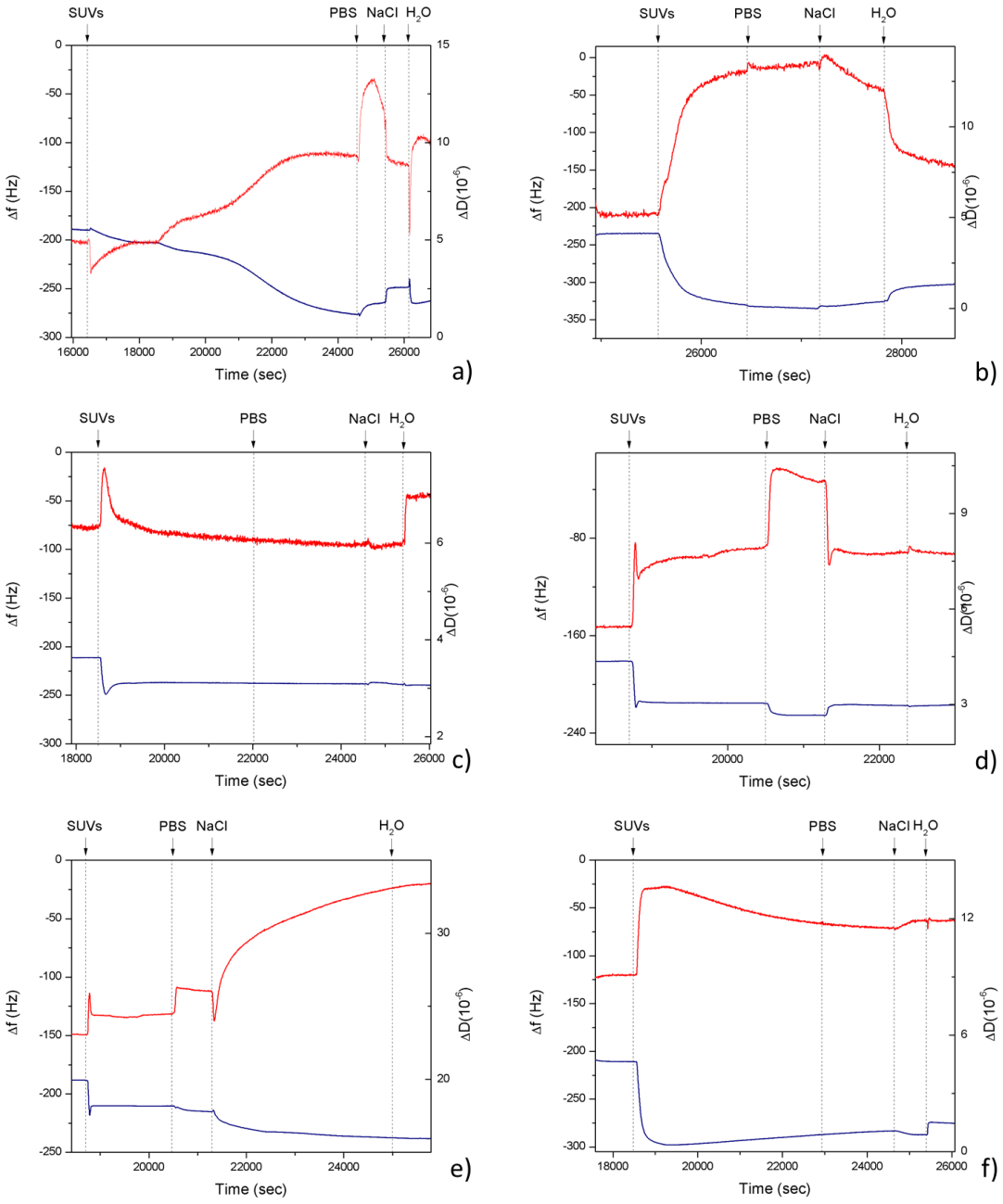

Figure 2.3 QCM-D curves of frequency (blue line) and dissipation (red line) obtained by the assembly of $(PAH/PSS)_{5.5}$ and vesicles of a) pure DOPC, b) DOPC:DOPS 75:25, c) DOPC:DOPS 50:50, d) DOPC:DOPS 40:60, e) DOPC:DOPS 30:70 and f) DOPC:DOPS 20:80. Experiments were conducted at 23 °C.

2.3.3 Lipid Bilayer Characterisation

CryoTEM was used as an additional mean to prove the presence of the lipid bilayer on PEMs coated on SiO_2 colloidal particles (**Figure 2.4**). A thin layer of 5 nm, characteristic of a lipid bilayer, can be distinguished on top of the SiO_2 particles, which was not present on the particles before the coating with SUVs (**Figure 2.4a**). In **Figure 2.4b** and **c** we observe the presence of the bilayer with vesicles of 30:70 and 50:50 DOPC:DOPS. Vesicles´ adsorption and deformation without rupture can be observed in **Figure 2.4c** for SUVs with 25:75 PC:PS composition.

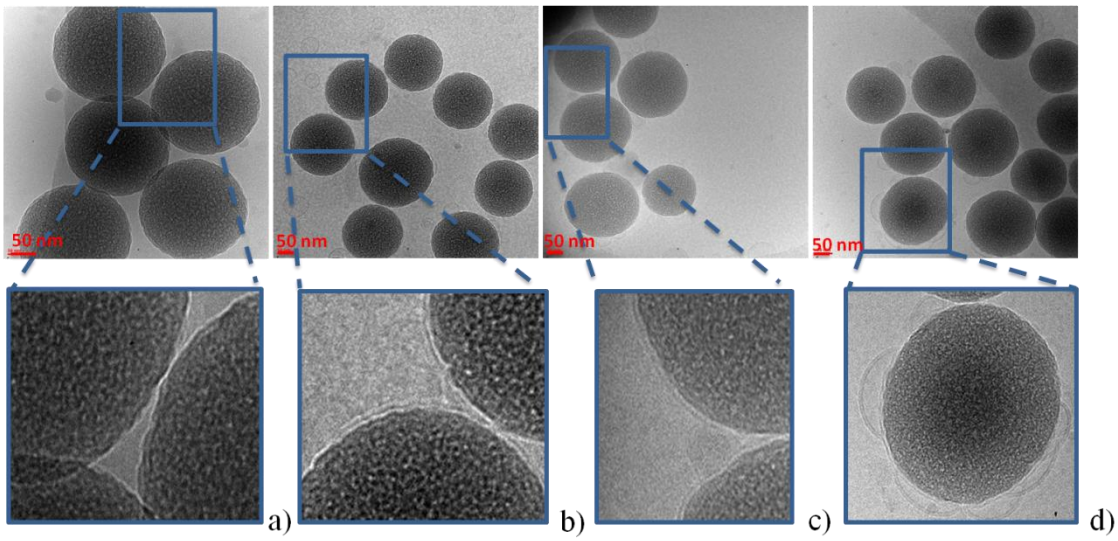

Figure 2.4 CryoTEM images of $(PAH/PSS)_{5.5}$ films, on top of SiO2 particles with a) no addition of SUVs and with addition of SUVs of DOPC:DOPS at b) 30:70, c) 50:50 and d) 25:75 molar ratios. The images at the bottom are a 5x magnification of the marked area in the corresponding upper image.

2.3.4 Understanding the Interaction and Binding Forces

In order to better understand the interactions between the vesicles and the surface of the PEMs AFS measurements were conducted[10]. First, AFM Imaging was used to image the changes in topology of the PEMs after the assembly of the lipid bilayer.

Measurements were performed in 0.1 M NaCl immediately after PEM fabrication and vesicle coating. **Figure 2.5a** displays the AFM image of the PEM surface, which shows a grainy morphology. Mostly flat grains of about 50 – 70 nm in diameter can be identified. A small number of white spots indicate the presence of larger grains on top of the multilayer surface.

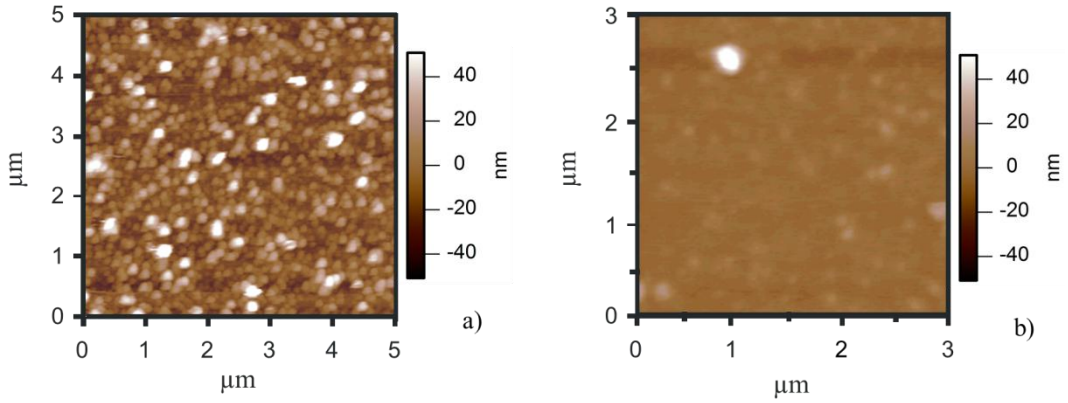

Figure 2.5 AFM height images in contact mode of 9 layers of PAH/PSS multilayer with PAH as the outermost layer. $(PAH/PSS)_{5.5}$, a) before and b) after incubation with PC:PS liposomes at 50:50 molar ratio.

The roughness of the PEM calculated by the variance in height over the scanned area was approximately 15.5 nm, in agreement with previous findings[35]. On the contrary, the roughness of the glass substrate was of the order of only 0.5 nm. Upon incubation with POPC:POPS vesicles the surface texture changed drastically (**Figure 2.5b**); the surface became much flatter and more homogeneous. The few elevations probably represent the locations of the pronounced spots, which have been detected on the surface of the multilayers. The roughness of the lipid coated surfaces was about 5 nm. Therefore AFM

imaging additionally proved the presence of a continuous lipid bilayer on the PEM support.

As the lipids form a continuous layer they do not cover the whole surface PE grains but the upper regions. For this reason the features displayed by the lipid bilayer are flatter in comparison with the multilayer support. Incubation with pure POPC as well as with pure POPS vesicles did not result in such a homogeneous and smooth coverage. In both cases the presence of non fused vesicles can be easily recognized (**Figure 2.6**)

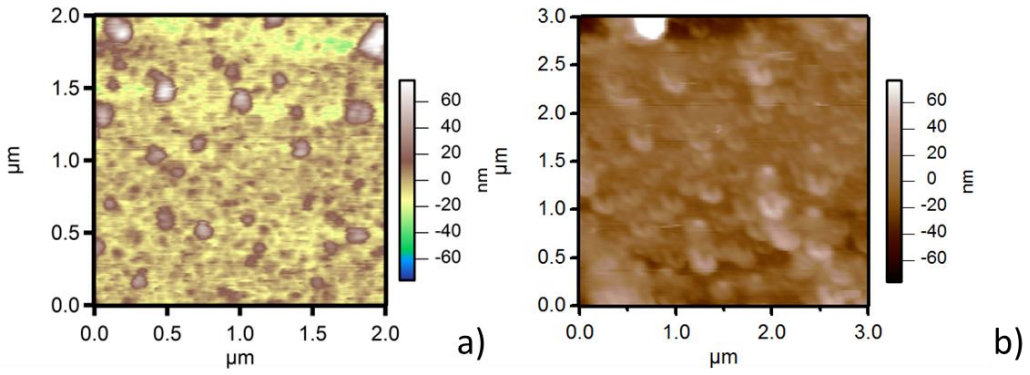

Figure 2.6 AFM height images in contact mode of $(PAH/PSS)_{5.5}$ after adsorption of a) pure POPC vesicles and b) pure POPS vesicles.

After covalent functionalization of AFM tips with PAH employing the primary amino groups of PAH, force spectroscopy measurements consisting of repetitive approach-retraction cycles of the tip against the surface under investigation were performed. The scheme in **Figure 2.7a** and **b** display the experimental approach.

Figure 2.7c, **d** and **f** displays a typical AFS curve describing the approach-retraction of a PAH modified cantilever against a PAH/PSS multilayer coated with vesicles formed with a mixture of POPC and POPS (50:50), only POPC and only POPS. In **Figure 2.7c**

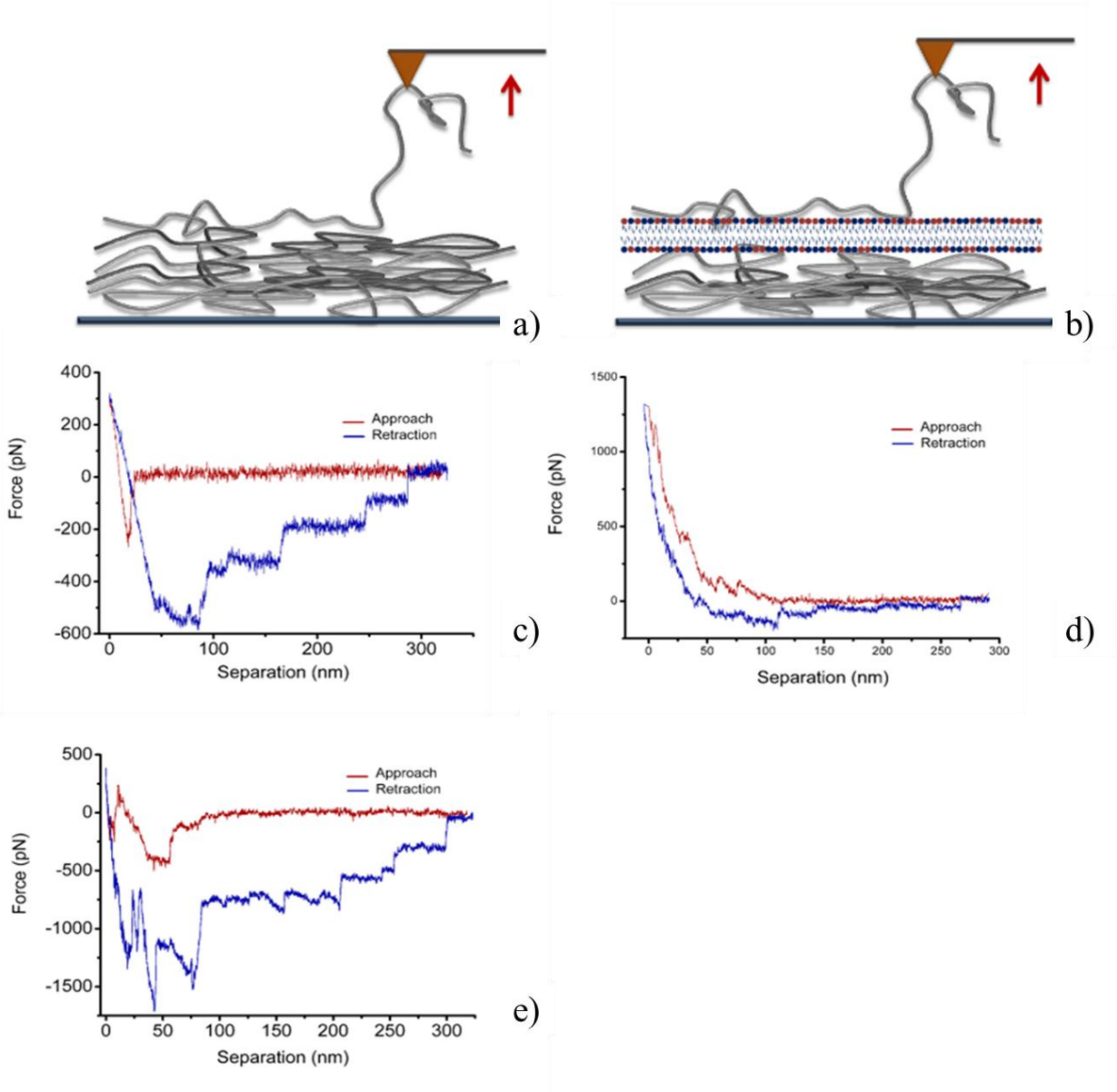

Figure 2.7 Schematic representation of the approach followed to measure PE-lipid interactions between PAH and the PE supported lipid membranes. Probing a PAH modified cantilever against a) PEM with PAH as the top layer and b) the lipids deposited onto the PEM. Typical approach-retraction curves of a PAH functionalised tip probed against lipid bilayers supported on a $(PAH/PSS)_{5.5}$ PEM. The approach (in red) – retraction (in blue) curves for c) POPC:POPS 50:50 molar ratio, d) pure POPC and e) pure POPS.

it can be appreciated the approach-retraction curve for the PEM coated with POPC and POPS (50:50), the approach-retraction cycle contained a number of characteristic

features; upon approach a jump can be observed at very short distances of the order of 50 - 100 nm in front of the lipid layer. This is evidence of an attractive interaction pulling the cantilever towards the surface. When the tip approached the surface it was observed that the attractive force changed to a repulsive one. The loading force was restricted to a maximum of about 500 pN in order to avoid perforation of the lipid layer.

Such forces are quite below the average normal forces required to perforate a lipid membrane with a regular AFM tip[36,37]. Withdrawing the tip from the surface lead to an initial pronounced adhesion force of about 1.7 nN with a broad desorption well of about 500 nm in width. Within this distance the shape was quite complex. For larger retraction distances, the single molecule behaviour of PAH appeared and a constant force plateaus with a final desorption step are recorded. The depth in the adhesion force observed at the start of the retraction curve indicated the total contribution of multiple chains desorbing simultaneously from the membrane surface. As shown in **Figure 2.7c** every desorption step brought the cantilever closer to the base line, which was finally approached after the last desorption step. On average the desorption force for a single chain from the PC:PS layer was of 114 ± 5 pN.

The interaction of PAH with a lipid coated surface formed after incubation with POPC vesicles showed a different response in the approach-retraction curves compared with the case of the mixture of POPC and POPS (**Figure 2.7d**). There was neither an attractive pulling force upon approach nor a strong adhesive interaction during withdrawal. Although force plateaus were also obtained, the height of the plateaus and its frequency decreased considerably. The repulsive behaviour upon approach together with the weaker desorption steps indicated a weaker interaction of PAH with this

zwitterionic lipid. The repulsive behaviour can be attributed to intramolecular electrostatic and steric repulsion of the PAH chain upon approach.

The interaction of PAH with the POPS lipids shown in **Figure 2.7f** resembles that of PAH with the lipid membrane consisting of pure POPS but the curves were significantly more noisy and the repulsion after approach was less pronounced. Nevertheless, small plateaus on adsorption can be identified.

From the AFS curves one can assume that the major contribution of binding can be attributed to short range forces, because long-range electrostatic forces become effectively screened in 0.1 M NaCl with a Debye length of about 1 nm[38]. The distances recorded during the force steps together with the magnitude of the measured forces, strongly suggest hydrogen bonding as the main molecular mechanism of interaction between PAH and lipids. Additionally, electrostatic interactions beyond the range of hydrogen bonds will contribute somewhat to the total binding energy.

The force corresponding to the last remaining plateau can be unambiguously related to desorption of a single PAH chain or to a loop. The same is consistent for the first plateau upon adsorption. It has to be kept in mind though that the longest chains are the last ones to desorb from the lipid layer upon retraction. Therefore, there is a diminished probability of loops to be recorded upon desorption.

The amino groups of PAH can interact with two specific binding sites in the POPS head group: the phosphate group PO_2^- and the carboxyl group COO^-. On the other hand for POPC, the only possibility for bond formation is with the phosphate group. The small strength of attractive interaction between PAH and POPC, agrees very well with earlier

experimental results where it has been found that the force between POPC vesicles and PAH coated surfaces is attractive enough to maintain the vesicles attached to the surface but not enough to induce rupture of the vesicles[26]. Furthermore, the presence of quaternary ammonium groups in POPC could introduce a repulsion term against the binding force between PAH and the lipid head group.

2.3.5 The Role of Top-Layer Chemistry; Primary versus Quaternary Amines

To have a better understanding of the role of hydrogen bonding on the formation of lipid bilayers on PEMs, we decided to compare the liposome adsorption and the transformations that these undergo on PAH/PSS with their behaviour on top of PEMs assembled from PDADMAC and PSS. The chemical structure of PAH, PSS, PDADMAC and phosphate salts in PBS are shown in **Figure 2.8**.

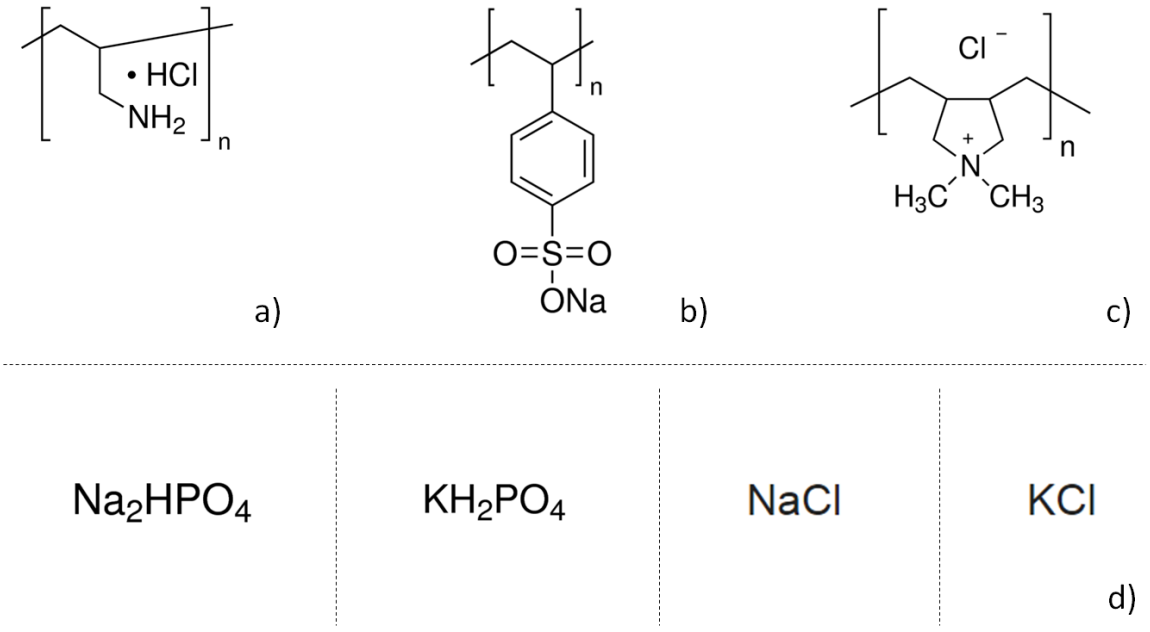

Figure 2.8 Representation of the chemical structures of a) PAH, b) PSS, c) PDADMAC and d) PBS salts; Na_2HPO_4, KH_2PO_4, NaCl and KCl.

As mentioned previously the interaction between DOPC:DOPS vesicles and PAH is based on hydrogen bonding mainly between the amine groups of PAH and the carboxylate and phosphate groups of DOPS together with some electrostatic interactions[39]. The assembly of DOPC:DOPS vesicles on $(PDADMAC/PSS)_{5.5}$ multilayers is shown in **Figure 2.9**. After the deposition of the SUVs the frequency decreased to Δf = 212 Hz, a value significantly higher than the observed for a lipid bilayer. The frequency decreased and reached a plateau immediately. Dissipation increased slightly to 4 x 10^{-6} dissipation units. These observations indicate that the vesicles are adsorbed without subsequent rupture retaining the water and forming a soft and dissipative structure. When the surface is washed with PBS, frequency and dissipation did not change.

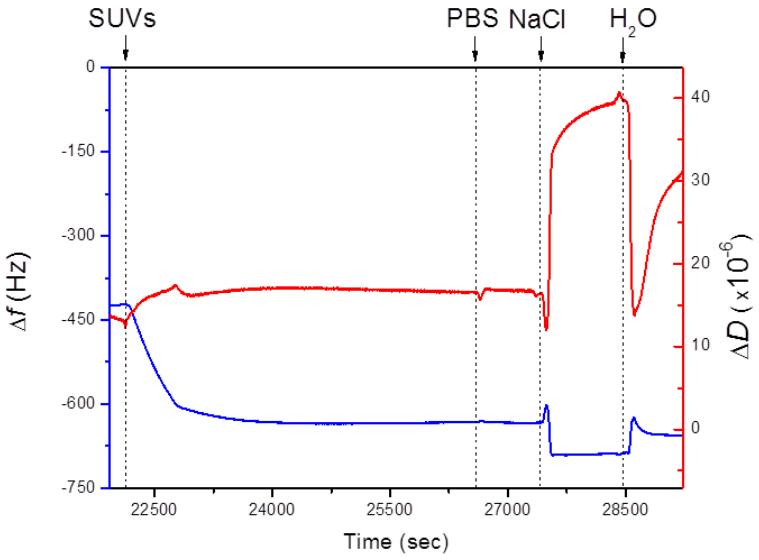

Figure 2.9 QCM-D curves of frequency (blue line) and dissipation (red line) obtained by the deposition of 50:50 molar ratio DOPC:DOPS SUVs on top of $(PDADMAC/PSS)_{5.5}$ multilayer cushions.

After rinsing with NaCl, the frequency decreased and increased again when rinsing with water. These changes in frequency are mainly associated with the change of ionic strength. Dissipation increased significantly after rinsing with NaCl ($\Delta D = 23 \times 10^{-6}$) and water ($\Delta D = 14 \times 10^{-6}$), which is hinting at a possible swelling of the deposited vesicles as there is a positive osmotic difference from the interior of the vesicles containing PBS and water in bulk. A conclusion that can be drawn is that the attraction forces, in the conditions employed, are not sufficient for vesicles´ rupture. Additionally the absence of rupture in the case of PDADMAC in comparison to the PAH confirmed that the hydrogen bonding between the primary amines of PAH and the DOPS is mainly responsible for the rupture of the vesicles. We can also conclude that even though the vesicles are adsorbed on the PEM, they are weakly interacting with the polymer. In addition, another possible explanation of the absence of rupture and formation of a bilayer on $(PDADMAC/PSS)_{5.5}$, is the stiffness of the film. Thus, it may be possible that the stiffness of the $(PDADMAC/PSS)_{5.5}$ film is not enough for vesicles` rupture and spreading remaining immerged within the PEM.

FRAP measurements were conducted on $(PAH/PSS)_{5.5}$ and $(PDADMAC/PSS)_{5.5}$ PEMs after lipids adsorption. In FRAP experiments bleaching, damages the fluorophore embedded in the lipids reducing or eliminating the fluorescence from the bleached area. If the SUVs have been fused into a lipid bilayer, lipids from the surrounding areas will diffuse into the bleached region and will be exchanged with bleached lipids causing a recovery of the fluorescence in the bleached area. When adsorbed SUVs are bleached, there will not be any recovery of fluorescence in the bleached area as the bleached lipids cannot be exchanged with non bleached lipids from nearby areas on the surface

since there is no connectivity among the membranes of different vesicles. From the diffusion coefficient values, conclusions can be drawn on the interaction of the lipids with the PEMs and on the homogeneity and connectivity among the deposited lipids.

FRAP experiments conducted on 50:50 DOPC:DOPS SUVs deposited on top of $(PAH/PSS)_{5.5}$ multilayers clearly show lipid bilayer formation.

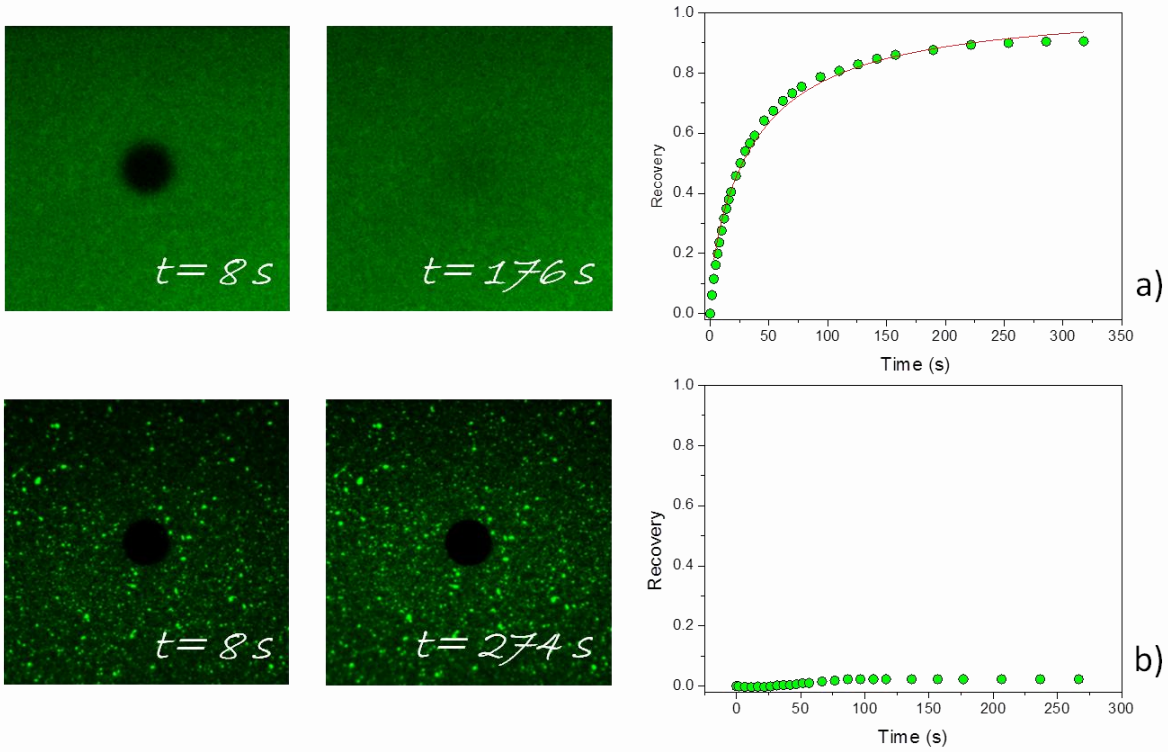

Figure 2.10 Fluorescence images after photobleaching and the respective fluorescence recovery curves obtained by the deposition of 50:50 molar ratio DOPC:DOPS labelled with 0.5:0.5 NBDPC:NBDPS fluorescent SUVs on top of a) $(PAH/PSS)_{5.5}$ and b) $(PDADMAC/PSS)_{5.5}$ multilayer cushions.

Fluorescent images in **Figure 2.10a** show nearly complete recovery of fluorescence in the bleached spot after 2.93 min which can be as well deduced from the typical fractional fluorescence recovery curve (**Figure 2.10a**). From the best fit of the experimental data to **Eq. 12,** the values of the mobile fraction of lipid assemblies are

derived. The diffusion coefficient calculated from the fitting to **Eq. 12** was D = 9.2 x 10^{-9} cm^2 s^{-1} which is in accordance with previews reported values for phospholipid bilayers[40,41]. Thus, the FRAP experiments confirm the formation of a continuous bilayer on PAH/PSS. However, FRAP experiments for lipid vesicles (50:50) deposited on PDADMAC/PSS films shown in **Figure 2.10b** have a different outcome. No recovery is observed in this case 5 min after bleaching, meaning that there is no interconnection between deposited vesicles.

To further explore if the surface characteristics of the PAH/PSS film are responsible for the rupture and fusion of the vesicles, a film of PDADMAC/PSS was prepared with 1, 3 or 4 layers of PAH deposited on top as finishing layers. PAH/PSS multilayers grow linearly with the number of deposition steps and have high elasticity modulus. PDADMAC/PSS grows supralinearly and can be considered as a film with intermediate properties between a glassy and a gel behaving material.

First, a film of 10 layers of PDADMAC/PSS was prepared with the addition of PAH as a last layer ((PDADMAC/PSS)$_5$PAH). The deposition of SUVs was recorded via QCM-D (**Figure 2.11a**). The frequency decreased upon deposition of the SUVs, increased after a few seconds and remained stable several minutes afterwards, even after rinsing with PBS. The behavior of the frequency could be indicative of the formation of a complete and stable bilayer; however, the total frequency shift was 46 Hz more than the expected value for a bilayer.

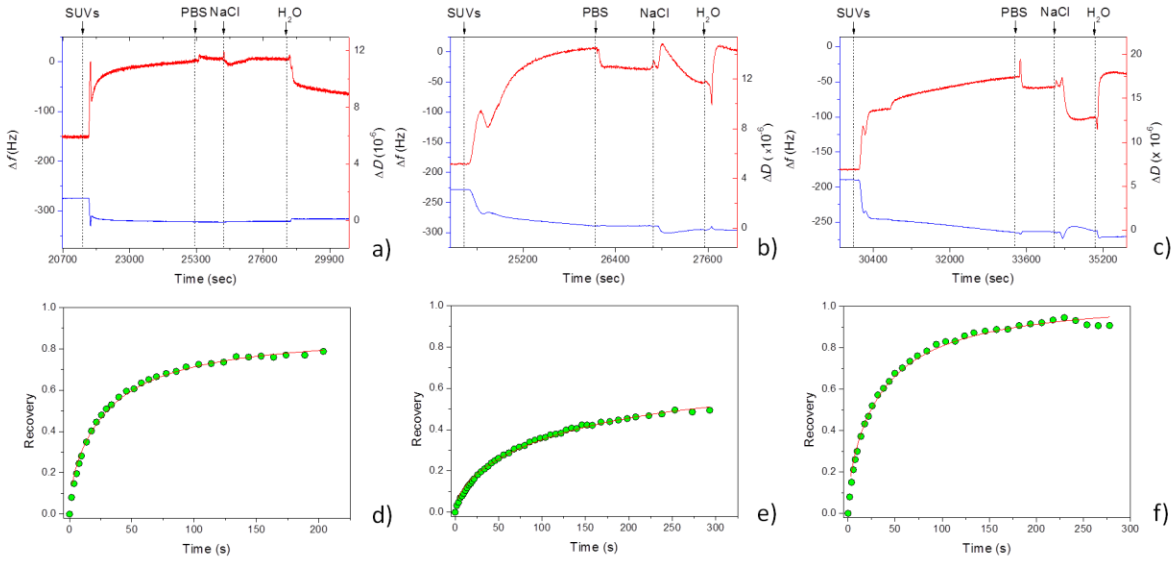

Figure 2.11 QCM-D curves of frequency (blue line) and dissipation (red line) obtained by the deposition of DOPC:DOPS SUVs on top of a) $(PDADMAC/PSS)_5PAH$, b) $(PDADMAC/PSS)_3(PAH/PSS)_{2.5}$ and c) $(PDADMAC/PSS)_2(PAH/PSS)_{3.5}$ PEMs. Fluorescence recovery curves after photobleaching obtained by the deposition of 50:50 molar ratio DOPC:DOPS labelled with 0.5:0.5 NBDPC:NBDPS fluorescent SUVs on top of PEMs of the cases of a), b) and c), respectively.

FRAP measurements on the same system revealed bilayer patches (**Figure 2.12a**). The diffusion coefficient after photobleaching was D = 12 x 10^{-9} cm^2 s^{-1}. When the SUVs were deposited on $(PDADMAC/PSS)_4(PAH/PSS)_{1.5}$, vesicles' rupture can be observed with a resulting Δf = 60 Hz. Fluorescence imaging showed bilayer patches (**Figure 2.12b**), which displayed diffusion coefficient values similar to those in $(PDADMAC/PSS)_5PAH$ (**Table 2.1**).

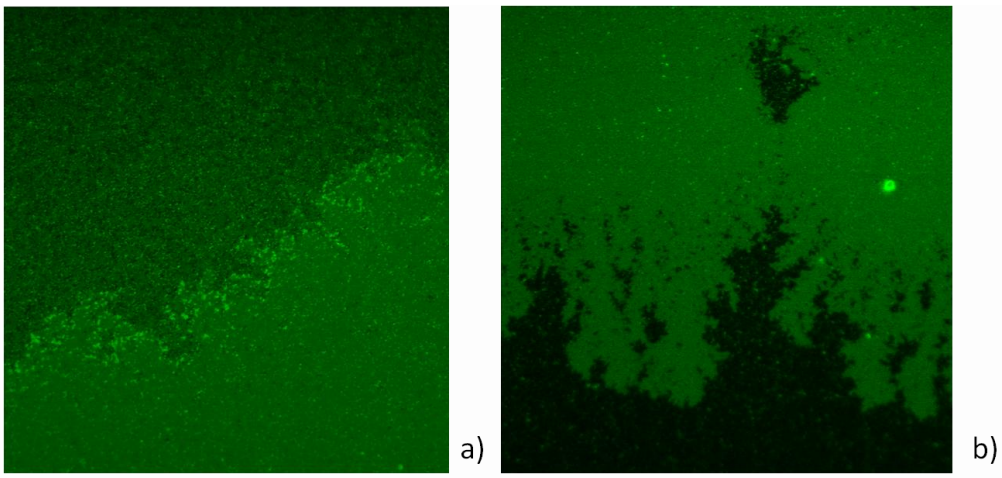

Figure 2.12 Fluorescence images obtained by deposition of 50:50 molar ratio DOPC:DOPS labelled with 0.5:0.5 NBDPC:NBDPS fluorescent SUVs on top of a) $(PDADMAC/PSS)_5PAH$ and b) $(PDADMAC /PSS)_4(PAH/PSS)_{1.5}$ PEM surfaces.

Table 2.1 Mobile fraction and diffusion coefficient obtained from the deposition of DOPC:DOPS SUVs on top of different PEM supports.

Sample	*M*	*D* ($10^{-9}cm^2\ s^{-1}$)
$(PAH/PSS)_{5.5}$	1.03 ± 0.019	9.2 ± 0.65
$(PDADMAC/PSS)_{5.5}$	No Recovery	
$(PDADMAC/PSS)_5PAH$	0.89 ± 0.011	12 ± 0.6
$(PDADMAC/PSS)_3(PAH/PSS)_{2.5}$	0.83 ± 0.079	10 ± 0.45
$(PDADMAC/PSS)_2(PAH/PSS)_{3.5}$	1.05 ± 0.012	9.8 ± 0.49
$(PAH/PSS)_5PDADMAC$	No Recovery	
$(PAH/PSS)_3(PDADMAC/PSS)_{2.5}$	No Recovery	

Additional PAH layers were deposited on top of PDADMAC/PSS multilayers to form PEMs with the following composition: $(PDADMAC/PSS)_3(PAH/PSS)_{2.5}$. In that case in QCM-D, when the SUVs were deposited, the frequency decreased, then increased a few Hz and then decreased again slowly for several minutes, resulting in Δf = 73 Hz after rinsing with PBS. Again in this case, fluorescence imaging showed the formation of bilayer patches, which after photobleaching revealed the same mobile fraction M = 1.05 and diffusion coefficient was $D = 9.8 \times 10^{-9}\ cm^2\ s^{-1}$ as in the case of $(PAH/PSS)_{5.5}$.

For PAH/PSS multilayers with either 1 or 3 layers of PDADMAC on top, SUVs deposition resulted in vesicle adsorption without rupture as can be observed in QCM-D graphs in **Figure 2.13a** and **b**. The frequency decreased after SUVs deposition, producing shifts in the total frequency of 155 Hz and 325 Hz, **Figure 2.13a** and **b** respectively. When rinsing with PBS almost no change in frequency or dissipation occurred in both the cases. In **Figure 2.13a**, it can be seen that after rinsing with NaCl solution and then with water, the frequency decreased to 142 Hz and 72 Hz, respectively, indicating removal of non-adsorbed vesicles.

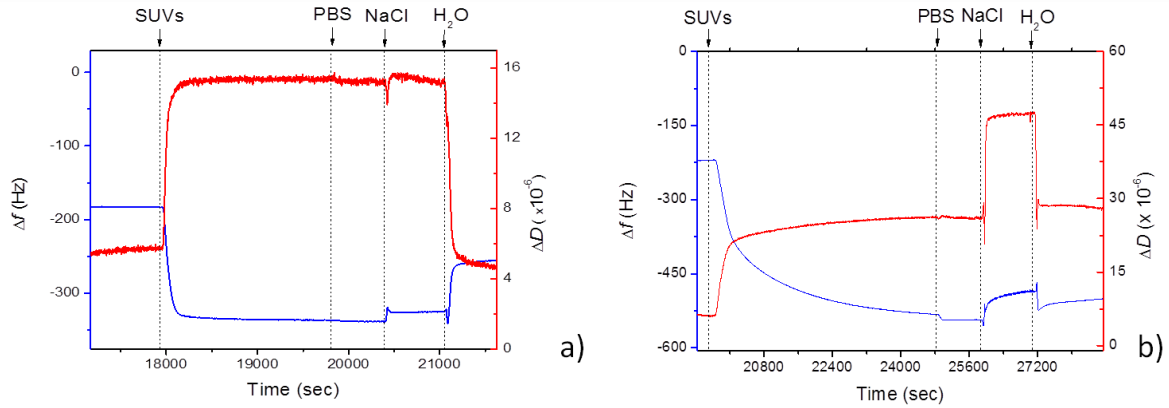

Figure 2.13 QCM-D curves of frequency (blue line) and dissipation (red line) obtained by the deposition of DOPC:DOPS SUVs on top of a) $(PAH/PSS)_5PDADMAC$ and b) $(PAH/PSS)_3(PDADMAC/PSS)_{2.5}$ PEMs.

Similarly, in **Figure 2.13b**, when rinsing with NaCl solution, the frequency increased resulting in a frequency difference of 268 Hz, but after rinsing with water, the frequency decreased again indicating that there was no removal of vesicles and thus the change in frequency when rinsing with NaCl is most likely due to swelling of the adsorbed vesicles. In FRAP measurements, no recovery of fluorescence was observed, proving

that the vesicles only adsorbed on the PEM and did not rupture, in agreement with QCM-D results (**Figure 2.14**).

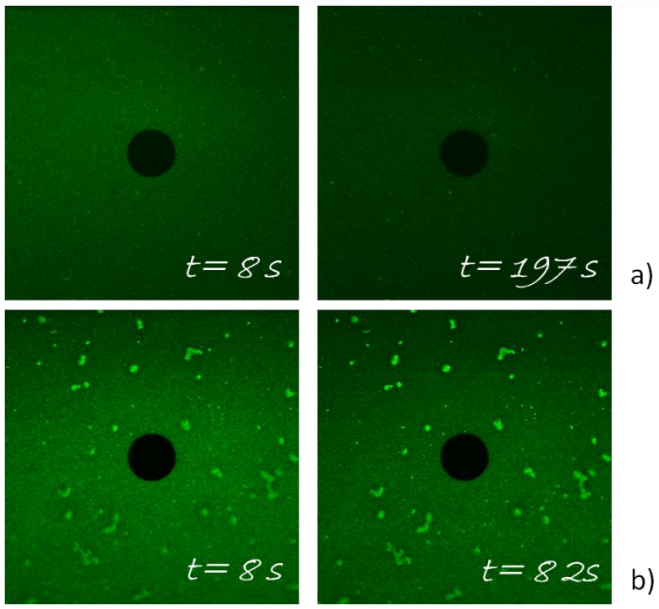

Figure 2.14 Fluorescence images after photobleaching obtained by deposition of 50:50 molar ratio DOPC:DOPS labelled with 0.5:0.5 NBDPC:NBDPS fluorescent SUVs on top of a) $(PAH/PSS)_5$PDADMAC and b) $(PAH/PSS)_3(PDADMAC/PSS)_{2.5}$ PEM surfaces.

In the case of one layer of PDADMAC on top we can assume that the stiffness of the PEMs is close to the PAH/PSS film thus an increase in stiffness of the PEM with the top layer of PDADMAC does not enhance the possibility for vesicles´ rupture . On the other hand just one layer of PAH on top of PDADMAC/PSS, increases lipids' fusion pointing out in this case that the surface chemistry is responsible for the rupture. However, fusion is not as favorable as for PAH/PSS PEMs, and the assembly of up to 2 additional PAH layers does not improve fusion conditions.

We cannot therefore be conclusive regarding surface characteristics vs other multilayer properties so far. Taking this into account the experiments may indicate that there is interdigitation between the layers. Usually, when a layer is deposited, this interdigitates

up to 4 layers below the rest of the deposited layers[42]. Then, both PDADMAC and PAH could be present on the surface of the PEM, even for the case of 3 PAH layers on top of the PDADMAC/PSS PEM.

2.3.6 Influence of Phosphate Ions

Another important aspect to take into account is the role of the phosphate buffer, used for the hydration of the vesicles, on the formation of a bilayer. When the assembly of SUVs was conducted in NaCl with the same ionic strength as PBS; 150 mM, there was no bilayer formation on top of the 11 layers of PAH/PSS. QCM-D experiments have been conducted depositing SUVs that have been prepared in PBS 10 mM, NaCl 150 mM, Hepes 10mM/NaCl 150 mM/$CaCl_2$ 2 mM, and Hepes 10 mM on top of $(PAH/PSS)_{5.5}$ PEMs. Results were interesting as only in the case of SUVs prepared with PBS 10 mM (**Figure 2.15c**) a lipid bilayer was obtained while in all other cases the changes in frequency are different from the expected for a bilayer and there is no vesicle rupture to be observed (**Figure 2.15a**, **b** and **c**).

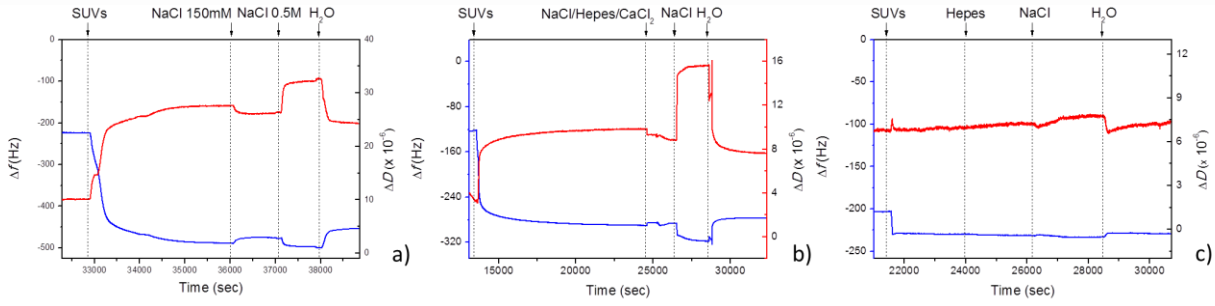

Figure 2.15 QCM-D curves of frequency (blue line) and dissipation (red line) obtained by the deposition of DOPC:DOPS SUVs in a) NaCl 150 mM, b) Hepes 100 mM/ NaCl 150 mM/$CaCl_2$ 2 mM and c) Hepes 100 mM on top of $(PAH/PSS)_{5.5}$ films.

In the last case of Hepes 10 mM, although the obtained Δ*f* = 28 Hz, is typical of a bilayer formation, no rupture of vesicles is taking place (**Figure 2.15c**). These experiments suggest that the PBS could be having an additional role in the interaction of the lipids with the multilayers.

XPS measurements were performed on PAH/PSS and PDADMAC/PSS multilayers exposed to PBS. Both samples were carefully washed in water before drying them. While the PAH/PSS sample displayed a strong phosphor signal, which is coming from phosphate ions, the PDADMAC/PSS multilayer showed no phosphor signal (**Figure 2.16**). In other words, the phosphate ions of PBS do not or they only interact weakly with the quaternary amines of PDADMAC while the interaction with the primary amines is so strong that it cannot be removed through washings with water. It is known that this interaction is mediated through hydrogen bonding between the primary amine groups of PAH and the phosphate ions. PAH is used as chelator for phosphate ions.

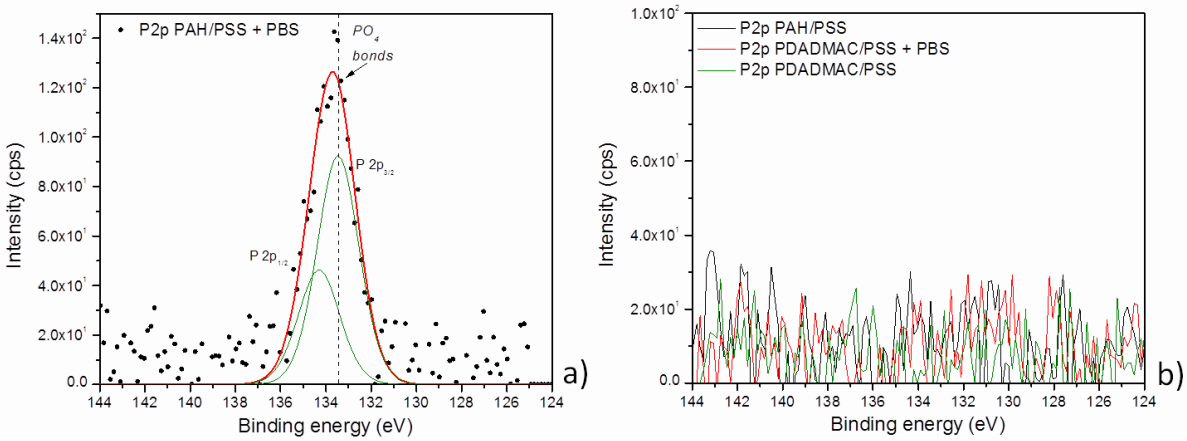

Figure 2.16 a) P 2p spectrum of the PAH/PSS + PBS sample. The P $2p_{3/2}$ peak position at around 134.4 eV can be assigned to the PO_4 bonds in the Na_2HPO_4 and KH_2PO_4 salts present in the PBS buffer solution. b) XPS region where the P 2p spectra are expected. None of the samples show a phosphorous signal.

Also, with the charges displayed from the quaternary amines in PDADMAC being shielded by an organic environment, the interaction with the highly hydrated phosphate is likely to be unfavorable as it would result in the dehydration of the phosphate by the chaotropic environment of the quaternary amines.

Since the interaction of PDADMAC with phosphate ions is weak, we studied the possible formation of a lipid bilayer on the PEMs by using vesicles consisting of only DOPC by QCM-D (**Figure 2.17**). Pure DOPC vesicles are adsorbed on the $(PAH/PSS)_{5.5}$ surface without rupturing (**Figure 2.1**). By addition of DOPC vesicles to the $(PDADMAC/PSS)_{5.5}$, PEM no change in frequency or dissipation could be observed (**Figure 2.17a**), meaning that the zwitterionic DOPC vesicles are not interacting with the positively charged PDADMAC surface. No change occurred even after rinsing with PBS.

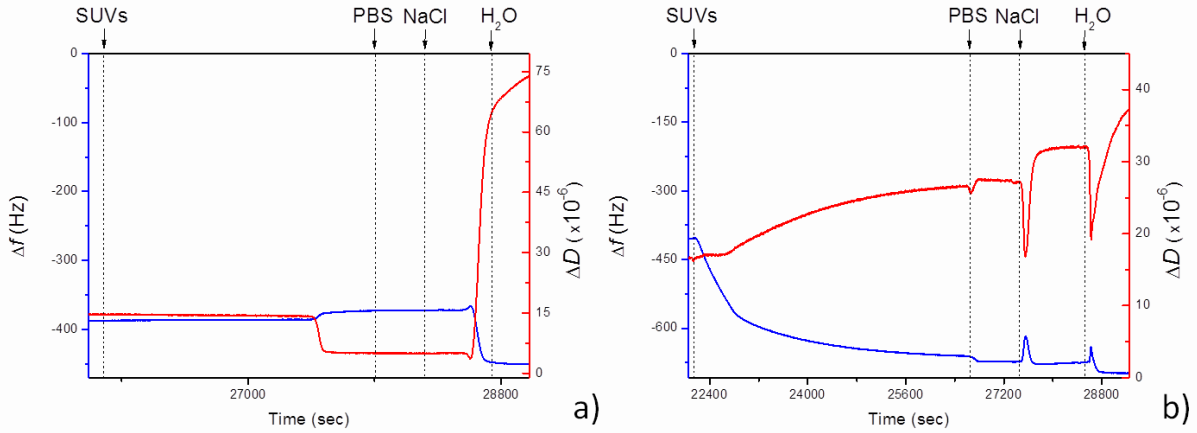

Figure 2.17 QCM-D curves of frequency (blue line) and dissipation (red line) obtained by the deposition of a) of pure DOPC and b) pure DOPS on top of $(PDADMAC/PSS)_{5.5}$ multilayer cushions.

The frequency increased by 20 Hz after NaCl and decreased by 78 Hz after rinsing with water. The decrease in frequency in the presence of water together with the enhanced increase in dissipation as observed in **Figure 2.17a**, is due to the swelling of

PDADMAC/PSS PEM, deposited in NaCl 0.5 M, which is known to form highly hydrated films when PDADMAC is deposited as the top layer[43]. However, the increase in dissipation was very high and it could mean that there are some vesicles on top of the film. In any case, the interaction of pure DOPC vesicles with PDADMAC is very week and we can assume that the deposition of DOPC:DOPS 50:50 vesicles is due to the interaction of PDADMAC with DOPS, through the negatively charged carboxylate groups at the polar heads of the lipids. The assembly of pure DOPS vesicles, as control, resulted in a frequency decrease of 270 Hz (**Figure 2.17b**). The frequency decrease lasted almost 1 hour until it reached a plateau, while no significant change in frequency and dissipation occurred after rinsing with PBS or NaCl. When water was flushed through the chamber, the frequency decreased around 26 Hz and dissipation increased by 10 x 10^{-6} dissipation units, which could be associated with a swelling effect of the deposited vesicles due to water absorption. We can conclude that the interaction of phosphate groups in lipids with PDADMAC is very weak.

Considering the strong interaction of the phosphate groups of phospholipids with primary amines, it is still surprising that the primary amines require the presence of PBS in order to form a lipid bilayer. The phosphate ions in PBS must play a role in the interaction of the amine with the phospholipid. Therefore, zeta potential measurements were performed on particles coated of PAH/PSS and PDADMAC/PSS with the same number of layers as for the planar surfaces, and with the polycations as top layer. Measurements were performed in PBS and NaCl with the same ionic strength as for the assembly, NaCl 150 mM or PBS 10 mM. The PDACMAC/PSS PEMs were not affected

by PBS and the potential was approximately the same as for the NaCl, around 35 mV (**Table 2.2**).

Table 2.2 ζ – potential values of the $(PAH/PSS)_{5.5}$ and $(PDADMAC/PSS)_{5.5}$ coated SiO_2 in different solutions, at 25 ºC.

Sample	Solution	ζ-Potential (mV)
$(PAH/PSS)_{5.5}$	H_2O	44.9 ± 1.5
	NaCl 10mM	45.8 ± 1.1
	NaCl 150mM	36.3 ± 0.9
	PBS 10mM	1.46 ± 0.1
$(PDADMAC/PSS)_{5.5}$	H_2O	34.6 ± 1.1
	NaCl 10mM	34.5 ± 0.6
	NaCl 150mM	24 ± 1.3
	PBS 10mM	25.4 ± 1.3

In the case of PAH/PSS there was a significant difference between the ζ – potential in NaCl, 40 mV, and the value in PBS, close to 0.mV. XPS and ζ – potential measurements show that the phosphate interacts strongly with the PAH and is screening the surface charge of the multilayers while their interaction with PDADMAC is weak or not existent. A potential close to 0 mV means that the electrostatic interaction between the PAH/PSS multilayers and the vesicles will be very weak as well. We can conclude that this is a key point in the formation of a lipid bilayer on top of PEMs.

When PDADMAC is the last layer of the PEM or the PAH/PSS film is not rinsed with PBS, the main interactions taking place are electrostatic. From the fast decrease of frequencies in both cases we can presume that strong electrostatic interactions cause a rapid coverage of the multilayer surface, which is that fast that does not allow for vesicles´ rupture and lipid rearrangement. However, even if rupture could take place the surface of the PEM is so saturated by vesicles that the space is restricted for rearranging and spreading. The screening of the charges of the primary amines of PAH

in presence of PBS decreases the electrostatic interactions and prevents the fast coverage of the surface. Then, when the vesicles are approaching the PEM, there is formation of hydrogen bonding between the amine groups of PAH and the phosphate groups of the lipids that leads to the rupture of the vesicles (**Figure 2.18**).

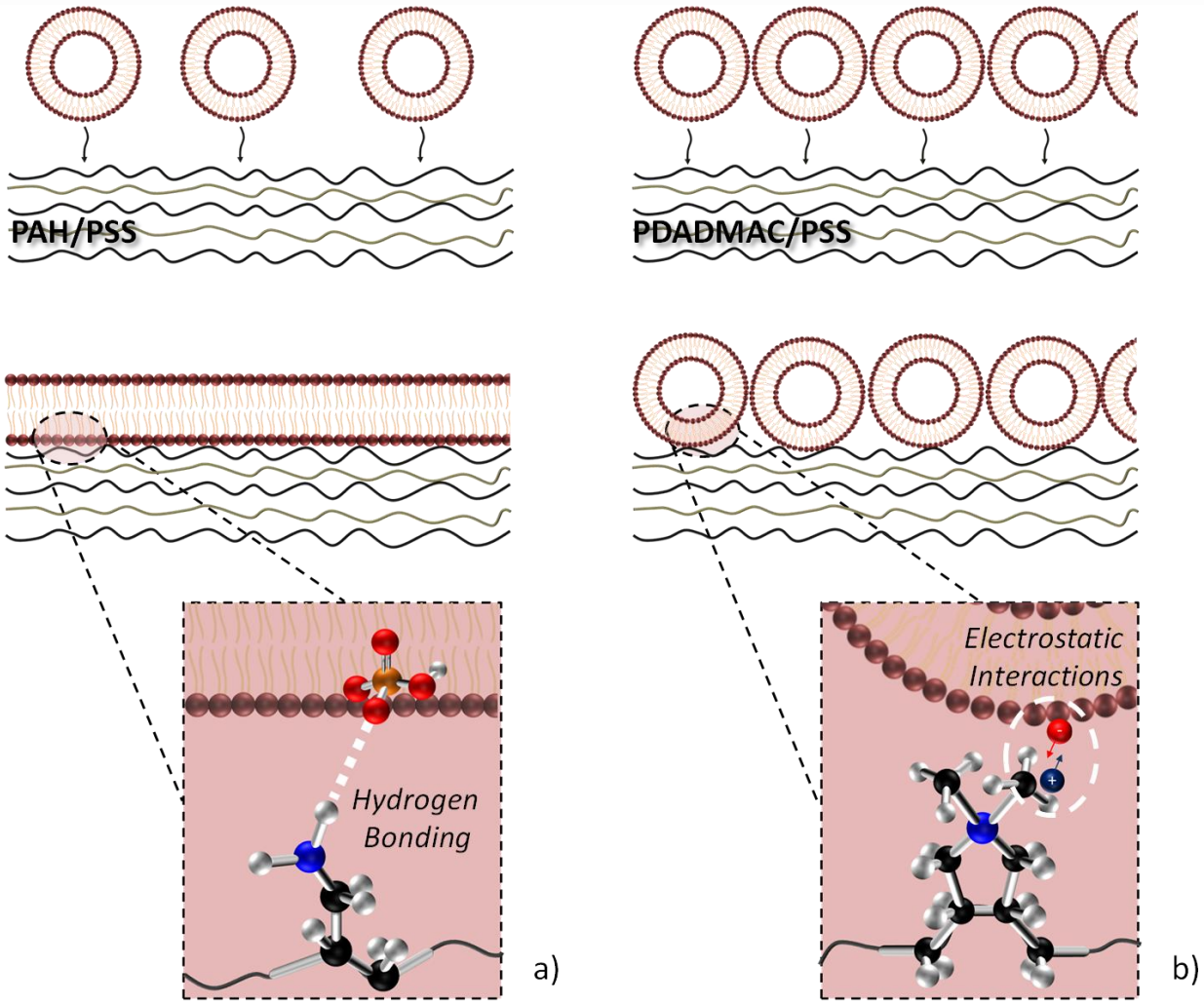

Figure 2.18 a) Schematic representation of the assembly of vesicles on top of PAH/PSS films and their adsorption and rupture to subsequently fuse into a bilayer due to hydrogen bonding between the primary amines of PAH and phosphate groups of DOPS. b) Schematic representation of the assembly of vesicles on top of PDADMAC/PSS films and their adsorption with no rupture due to electrostatic interactions between the quaternary amines of PDADMAC and phosphate groups of DOPS.

From XPS measurements it has been calculated the ratio of amines present in the last two layers of PAH to the phosphate groups, assuming that in a linear growth the amount of PE chains and consequently of amines is constant per layer. We assume as well that the amines from the two last PAH layers are mainly responsible for the interactions with the phosphate ions. The calculated ratio of phosphorous content to the amine content in the last two PAH layers was 0.26 at.% therefore only a quarter of the PAH/PSS surface was covered with phosphate ions while this value increased to 0.52 if we consider just the top PAH layer. Therefore, one can conclude that despite that in PBS the surface charge of PAH/PSS is neutral there are amine groups available to interact with the phosphate groups of the lipids when the vesicles come close enough to the PEM surface to form hydrogen bonding.

2.3.7 Impact of Polyanions

The properties of a PEM are a combination of the properties of both the polycation and polyanion that form the multilayers. Lipid vesicles interact with the top layer of PAH, but the characteristics of the multilayer, like hydrophilicity, wettability, mechanical properties, which could affect the assembly of the lipids are defined by the two components in the multilayers.

Keeping PAH as polycation, we fabricated PEMs varying the polyanions. We employed two different polyanions instead of PSS: Alg and PAA. Then, we assembled SUVs on top, at the same composition at which a bilayer is obtained on top of $(PAH/PSS)_{5.5}$. The adsorption of the SUVs was studied by QCM-D (**Figure 2.19**). Using Alg as polyanion, the adsorption and rupture of the vesicles takes place as for PAH assembled with PSS.

In **Figure 1.19a** frequency decreased in presence of the SUVs and then, immediately increased, hinting that the vesicles have been ruptured, liberating the enclosed solution. In parallel dissipation increased and then decreased. However, as we can observe, the changes in frequency and dissipation are higher than the expected for a bilayer. We can assume either the formation of bilayer patches or the adsorption of intact vesicles on top of the PEM.

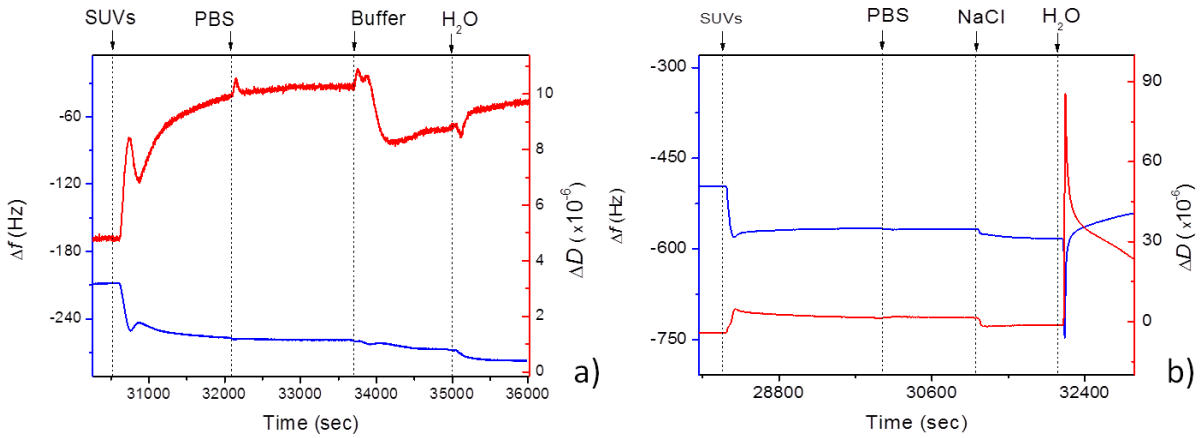

Figure 2.19 QCM-D curves of frequency (blue line) and dissipation (red line) obtained by the deposition of DOPC:DOPS SUVs on top of a) $(PAH/Alg)_{5.5}$ and b) $(PAH/PAA)_{5.5}$ multilayer cushions.

When the polyanion is PAA we observe a rapid decrease in frequency, followed by a jump to higher frequencies (**Figure 2.19b**) during the assembly in the QCM-D. The final frequency shift after the lipid deposition was 150 Hz, which is higher than the shift corresponding to a bilayer formation. Dissipation also displayed a jump following a similar trend with that of the frequency. We can conclude that the vesicles are only partially rupturing and there is a mixture of adsorbed vesicles and bilayers patches. Despite the fact that the interaction of the PAH with the vesicles is the main driving force behind the assembly of the vesicles on top of the PEM, the lipid assembly is also

affected by the underlying polyanion. This can be understood as a consequence of the type of interaction between the polyanion and polycation, which is very strong for PAH/PSS but weak for PAH/PAA. The different mechanical properties of the film could also affect the formation of the bilayer. PAH/PSS has an elastic modulus of over 700 MPa[44] while the elastic modulus of PAH/Alg must be in the order of kPa[25].

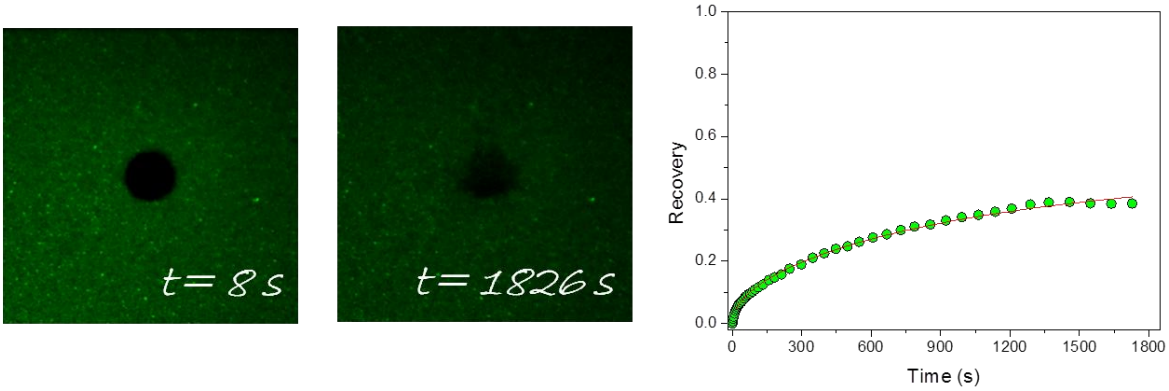

Figure 2.20 Fluorescence images after photobleaching and the respective fluorescence recovery curves obtained by the deposition of DOPC:DOPS labelled with 0.5:0.5 NBDPC:NBDPS fluorescent SUVs on top of $(PAH/Alg)_{5.5}$ multilayer cushions.

FRAP measurements in the case of $(PAH/Alg)_{5.5}$ for fluorescently labelled lipids showed that fluorescence recovery was not complete, as illustrated in **Figure 2.20**. The diffusion coefficient was low; $D = 0.36 \times 10^{-9}$ cm^2 s^{-1} corroborating the interpretation of the QCM-D data. FRAP experiments on SUVs deposited on $(PAH/PAA)_{5.5}$ (**Figure 2.21**) revealed the formation of bilayer patches with different fluorescence intensities. When lower fluorescence intensity regions were photobleached no recovery was observed. The lack of recovery can be explained as the result of intact SUVs adsorbed on the PEMs. When the higher fluorescence intensity region was photobleached fluorescence recovery was observed, however the recovery was not complete (M = ~ 0.89) and the diffusion

coefficient was, 7.7 x 10^{-9} cm^2 s^{-1}, lower than for the bilayer formed on $(PAH/PSS)_{5.5}$ hinting as well the adsorption of the SUVs without subsequent rupture. We can conclude from FRAP results that SUVs are only partially fused on PAH/PAA PEMs in agreement with QCM-D data.

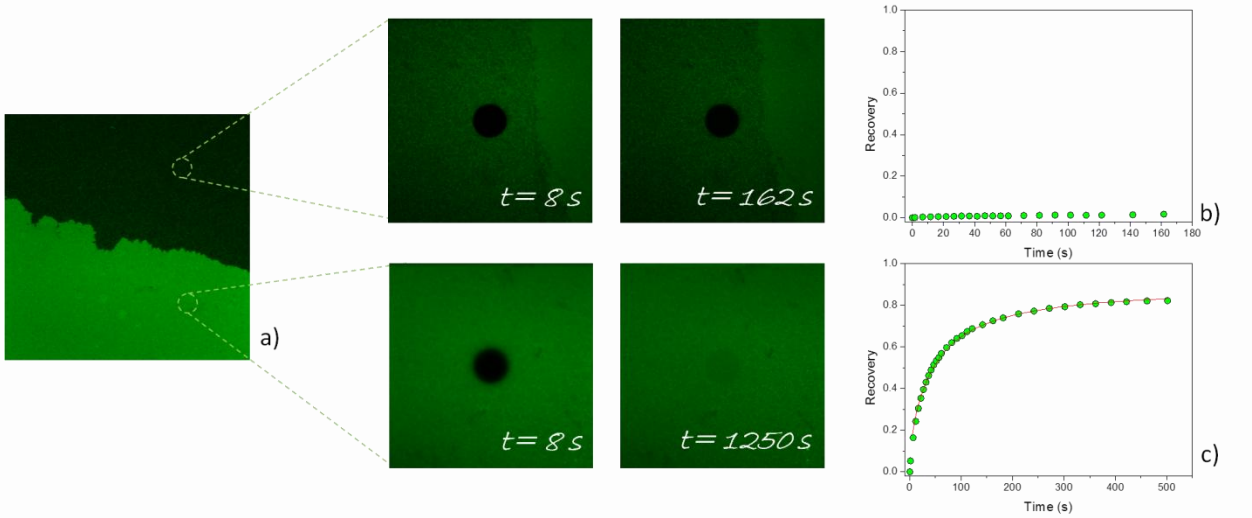

Figure 2.21 a) Fluorescence image obtained by the deposition of DOPC:DOPS labelled with 0.5:0.5 NBDPC:NBDPS fluorescent SUVs on top of $(PAH/PAA)_{5.5}$ PEMs where bilayer patches are present. Fluorescent images and the respective fluorescence recovery curves after photobleaching are obtained for b) the area with low fluorescence intensity and c) the area with higher fluorescence intensity.

2.4 Conclusions

We have shown that a lipid bilayer can be formed on top of PAH/PSS multilayers with PAH as the outermost layer from mixed vesicles of phospholipids with DOPC and DOPS headgroups. Bilayer formation takes place for percentages of PS lipids between 50 and 80 %. AFS showed that the main interaction between the amine groups of PAH and the lipids takes place through hydrogen bonding that can be present between the amines of PAH on one side and the carboxylate, and phosphate groups in DOPS on the other side, together with some electrostatic contribution. Lipid vesicles with pure or an excess of DOPC lipids do not rupture as the interaction with PAH is weak. The presence of DOPC is however important as it is necessary for the rearrangement of the lipids on the PEM and/or to decrease the repulsion among charged vesicles. When DOPC is below 20 % in the vesicles, lipid bilayer formation does not take place as either the vesicles are frozen by the interaction with the PAH layer or the repulsion among vesicles is too strong.

Additionally we have shown that vesicles with 50:50 DOPC:DOPS are adsorbed without subsequent rupture and fusion on top of PDADMAC/PSS PEMs in the conditions for a lipid bilayer formation on PAH/PSS multilayers. Quaternary amines in PDADMAC interact weakly with pure DOPC vesicles with apparently almost no adsorption of vesicles on the PEMs. Moreover, the phosphate ions present in PBS, the solution used for the hydration of the lipids, play also a fundamental role in the bilayer formation. PDADMAC does not interact with phosphate ions of PBS, while the phosphate complexes with the primary amines of PAH rendering the surface almost neutral decreasing the electrostatic

interactions with charged vesicles. Therefore we have proposed a model, showing that that as PDADMAC does not interact with PBS there is enhanced electrostatic interaction between the negatively charged SUVs and the positively charged surface resulting in a fast coverage of the $(PDADMAC/PSS)_{5.5}$ PEM with vesicles leaving no place for vesicles´ spread, rupture and fusion. On the contrary, in the case of $(PAH/PSS)_{5.5}$ PEMs, the phosphate ions form complexes with the PAH rendering the surface almost neutral and leading to weak electrostatic attractions. Thus the surface coverage with vesicles is now slow and hydrogen bonding can take place among the SUVs that are approaching the surface and the PAH to finally adsorb, spread, rupture and fuse, forming a bilayer.

Despite the resulted lipid bilayer on PAH/PSS PEMs is due to hydrogen bonding, between amine groups in the outermost PAH layer and the SUVs, the choice of other polyanions instead of PSS such as Alg or PAA did not result on bilayer formation but to bilayer patches. Results indicate that the nature (i.e. mechanical properties) of the resulting PEM affects as well the formation of the bilayer.

References

(1) McConnell, H. M.; Watts, T. H.; Weis, R. M.; Brian, A. A. Supported Planar Membranes in Studies of Cell-Cell Recognition in the Immune System. *BBA - Rev. Biomembr.* **1986**, *864* (1), 95–106.

(2) Hladky, S. B.; Haydon, D. A. Ion Transfer across Lipid Membranes in the Presence of Gramicidin A. I. Studies of the Unit Conductance Channel. *BBA - Biomembr.* **1972**, *274* (2), 294–312.

(3) Cremer, P. S.; Boxer, S. G. Formation and Spreading of Lipid Bilayers on Planar Glass Supports. *J. Phys. Chem. B* **1999**, *103*, 2554–2559.

(4) Keller, C. A.; Glasmästar, K.; Zhdanov, V. P.; Kasemo, B. Formation of Supported Membranes from Vesicles. *Phys. Rev. Lett.* **2000**, *84* (23), 5443–5446.

(5) Richter, R. P.; Him, J. L. K.; Brisson, A.; Lai, J.; Him, K.; Brisson, A. Supported Lipid Membranes http://www.sciencedirect.com/science/article/pii/S1369702103011295 (accessed May 26, 2015).

(6) Allen, T. M.; Cullis, P. R. Liposomal Drug Delivery Systems: From Concept to Clinical Applications. *Adv. Drug Deliv. Rev.* **2013**, *65* (1), 36–48.

(7) Ryu, H.; Lee, H.; Iwata, S.; Choi, S.; Kim, M. K.; Kim, Y.-R.; Maruta, S.; Kim, S. M.; Jeon, T.-J. Investigation of Ion Channel Activities of Gramicidin A in the Presence of Ionic Liquids Using Model Cell Membranes. *Sci. Rep.* **2015**, *5* (January), 11935.

(8) Jing, Y.; Trefna, H.; Persson, M.; Kasemo, B. Soft Matter Formation of Supported Lipid Bilayers on Silica : Liposome Size †. *Soft Matter* **2014**, *10*, 187–195.

(9) Rossetti, F. F.; Textor, M.; Reviakine, I. Asymmetric Distribution of Phosphatidyl Serine in Supported Phospholipid Bilayers on Titanium Dioxide. *Langmuir* **2006**, *22* (8), 3467–3473.

(10) Reviakine, I.; Brisson, A. Formation of Supported Phospholipid Bilayers from Unilamellar Vesicles Investigated by Atomic Force Microscopy. *Langmuir* **2000**, *16* (4), 1806–1815.

(11) Nollert, P.; Kiefer, H.; Jähnig, F. Lipid Vesicle Adsorption versus Formation of Planar Bilayers on Solid Surfaces. *Biophys. J.* **1995**, *69* (4), 1447–1455.

(12) Raedler, J.; Strey, H.; Sackmann, E. Phenomenology and Kinetics of Lipid Bilayer Spreading on Hydrophilic Surfaces. *Langmuir* **1995**, *11* (11), 4539–4548.

(13) Rossetti, F. F.; Bally, M.; Michel, R.; Textor, M.; Reviakine, I. Interactions between Titanium Dioxide and Phosphatidyl Serine-Containing Liposomes : Formation and Patterning of Supported Phospholipid Bilayers on the Surface of a Medically Relevant Material. *Langmuir* **2005**, *21*, 6443–6450.

(14) Lind, T. K.; Cárdenas, M.; Wacklin, H. P. Formation of Supported Lipid Bilayers by Vesicle Fusion: Effect of Deposition Temperature. *Langmuir* **2014**, *30* (25), 7259–7263.

(15) Reimhult, E.; Zäch, M.; Höök, F.; Kasemo, B. A Multitechnique Study of Liposome

Adsorption on Au and Lipid Bilayer Formation on SiO2. *Langmuir* **2006**, *22* (7), 3313–3319.

(16) Richter, R. P.; Escarpit, R. R.; Cedex, P. In V Ited Feature Article Formation of Solid-Supported Lipid Bilayers : An Integrated View. *Langmuir* **2006**, *22* (8), 3497–3505.

(17) Cho, N. J.; Frank, C. W.; Kasemo, B.; Hook, F. Quartz Crystal Microbalance with Dissipation Monitoring of Supported Lipid Bilayers on Various Substrates. *Nat. Protoc.* **2010**, *5* (6), 1096–1106.

(18) Lautscham, L. a; Lin, C. Y.; Auernheimer, V.; Naumann, C. a; Goldmann, W. H.; Fabry, B. Biomembrane-Mimicking Lipid Bilayer System as a Mechanically Tunable Cell Substrate. *Biomaterials* **2014**, *35* (10), 3198–3207.

(19) Merz, C.; Knoll, W.; Textor, M.; Reimhult, E. Formation of Supported Bacterial Lipid Membrane Mimics. *Biointerphases* **2008**.

(20) Kalb, E.; Frey, S.; Tamm, L. K. Formation of Supported Planar Bilayers by Fusion of Vesicles to Supported Phospholipid Monolayers. *Biochimica et Biophysica Acta (BBA) - Biomembranes*. January 1992, pp 307–316.

(21) Singh, S.; Junghans, A.; Tian, J.; Dubey, M.; Gnanakaran, S.; Chlistunoff, J.; Majewski, J. Polyelectrolyte Multilayers as a Platform for pH-Responsive Lipid Bilayers. *Soft Matter* **2013**, *9* (37), 8938.

(22) Boudou, T.; Crouzier, T.; Nicolas, C.; Ren, K.; Picart, C. Polyelectrolyte Multilayer Nanofilms Used as Thin Materials for Cell Mechano-Sensitivity Studies. *Macromol. Biosci.* **2011**, *11* (1), 77–89.

(23) Decher, G.; Hong, J. D.; Schmitt, J. Buildup of Ultrathin Multilayer Films by a Self-Assembly Process: III. Consecutively Alternating Adsorption of Anionic and Cationic Polyelectrolytes on Charged Surfaces. *Thin Solid Films* **1992**, *210–211*, 831–835.

(24) Decher, G.; Eckle, M.; Schmitt, J.; Struth, B. Layer-by-Layer Assembled Multicomposite Films. *Curr. Opin. Colloid Interface Sci.* **1998**, *3* (1), 32–39.

(25) Detzel, C. J.; Larkin, A. L.; Rajagopalan, P.; Detzel, C. J.; Larkin, A. L.; Rajagopalan, P. Multilayers in Tissue Engineering. *Tissue Eng. Part B. Rev.* **2011**, *17* (2), 101–113.

(26) Fischlechner, M.; Zaulig, M.; Meyer, S.; Estrela-Lopis, I.; Cuéllar, L.; Irigoyen, J.; Pescador, P.; Brumen, M.; Messner, P.; Moya, S.; et al. Lipid Layers on Polyelectrolyte Multilayer Supports. *Soft Matter* **2008**, *4* (11), 2245–2258.

(27) C. Gao, E. Donath, S.Moya, V. Dudnik, H. M.; Gao, C.; Donath, E.; Moya, S.; Dudnik, V.; Möhwald, H. Elasticity of Hollow Polyelectrolyte Capsules Prepared by the Layer-by-Layer Technique. *Eur. Phys. J. E* **2001**, *5* (1), 21–27.

(28) Mueller, R.; Köhler, K.; Weinkamer, R.; Sukhorukov, G.; Fery, A. Melting of PDADMAC/PSS Capsules Investigated with AFM Force Spectroscopy. *Macromolecules* **2005**, *38* (23), 9766–9771.

(29) Sader, J. E.; Chon, J. W. M.; Mulvaney, P. Calibration of Rectangular Atomic Force Microscope Cantilevers. *Rev. Sci. Instrum.* **1999**, *70* (10), 3967–3969.

(30) Friedsam, C.; Del Campo Bécares, A.; Jonas, U.; Gaub, H. E.; Seitz, M. Polymer Functionalized AFM Tips for Long-Term Measurements in Single-Molecule Force Spectroscopy. *ChemPhysChem* **2004**, *5* (3), 388–393.

(31) Wacklin, H. P.; Thomas, R. K. Spontaneous Formation of Asymmetric Lipid Bilayers by Adsorption of Vesicles. *Langmuir* **2007**, *23* (14), 7644–7651.

(32) Keller, C. A.; Kasemo, B. Surface Specific Kinetics of Lipid Vesicle Adsorption Measured with a Quartz Crystal Microbalance. *Biophys. J.* **1998**, *75* (September), 1397–1402.

(33) Richter, R.; Mukhopadhyay, A.; Brisson, A. Pathways of Lipid Vesicle Deposition on Solid Surfaces : A Combined QCM-D and AFM Study. *Biophys. J.* **2003**, *85* (November), 3035–3047.

(34) Moya, S. E.; Georgieva, R.; Bäumler, H.; Richter, W.; Donath, E. Composite Lipid Polyelectrolyte Capsules Templated on Red Blood Cells: Fabrication and Structural Characterisation. *Med. Biol. Eng. Comput.* **2003**, *41* (4), 504–508.

(35) Leporatti, S.; Voigt, A.; Mitlhner, R.; Sukhorukov, G.; Donath, E.; Mhwald, H.; Mitlo, R. Scanning Force Microscopy Investigation of Polyelectrolyte Nano- and Microcapsule Wall Texture Scanning Force Microscopy Investigation of Polyelectrolyte Nano- and Microcapsule Wall Texture. *Langmuir* **2000**, No. 8, 4059–4063.

(36) Li, J. K.; Sullan, R. M. A.; Zou, S. Atomic Force Microscopy Force Mapping in the Study of Supported Lipid Bilayers †. *Langmuir* **2011**, *27* (4), 1308–1313.

(37) Butt, H.-J.; Cappella, B.; Kappl, M. Force Measurements with the Atomic Force Microscope: Technique, Interpretation and Applications. *Surf. Sci. Rep.* **2005**, *59* (1–6), 1–152.

(38) Hugel, T.; Grosholz, M.; Clausen-Schaumann, H.; Pfau, A.; Gaub, H.; Seitz, M. Elasticity of Single Polyelectrolyte Chains and Their Desorption from Solid Supports Studied by AFM Based Single Molecule Force Spectroscopy. *Macromolecules* **2001**, *34* (4), 1039–1047.

(39) Diamanti, E.; Cuellar, L.; Gregurec, D.; Moya, S. E.; Donath, E. Role of Hydrogen Bonding and Polyanion Composition in the Formation of Lipid Bilayers on Top of Polyelectrolyte Multilayers. *Langmuir* **2015**, *31*, 8623–8632.

(40) Przybylo, M.; Sýkora, J.; Humpolíčková, J.; Benda, A.; Zan, A.; Hof, M. Lipid Diffusion in Giant Unilamellar Vesicles Is More than 2 Times Faster than in Supported Phospholipid Bilayers under Identical Conditions. *Langmuir* **2006**, *22* (22), 9096–9099.

(41) Zhu, L.; Gregurec, D.; Reviakine, I. Nanoscale Departures: Excess Lipid Leaving the Surface during Supported Lipid Bilayer Formation. *Langmuir* **2013**, *29* (49), 15283–15292.

(42) Donath, E.; Walther, D.; Shilov, V. N.; Knippel, E.; Budde, a.; Lowack, K.; Helm, C. a.; Möhwald, H. Nonlinear Hairy Layer Theory of Electrophoretic Fingerprinting Applied to Consecutive Layer by Layer Polyelectrolyte Adsorption onto Charged Polystyrene Latex Particles. *Langmuir* **1997**, *13* (13), 5294–5305.

(43) Iturri Ramos, J. J.; Stahl, S.; Richter, R. P.; Moya, S. E. Water Content and Buildup of

Poly(diallyldimethylammonium chloride)/Poly(sodium 4-Styrenesulfonate) and Poly(allylamine hydrochloride)/Poly(sodium 4-Styrenesulfonate) Polyelectrolyte Multilayers Studied by an in Situ Combination of a Quartz Crystal Microb. *Macromolecules* **2010**, *43* (21), 9063–9070.

(44) C. Gao, E. Donath, S.Moya, V. Dudnik, H. M. Elasticity of Hollow Polyelectrolyte Capsules Prepared by the Layer-by-Layer Technique. *Eur. Phys. J. E* **2001**, *5*, 21–27.

Chapter 3

High Resistivity Lipid Bilayers Assembled on Polyelectrolyte Multilayer Cushions: An Impedance Study

3.1 Motivation

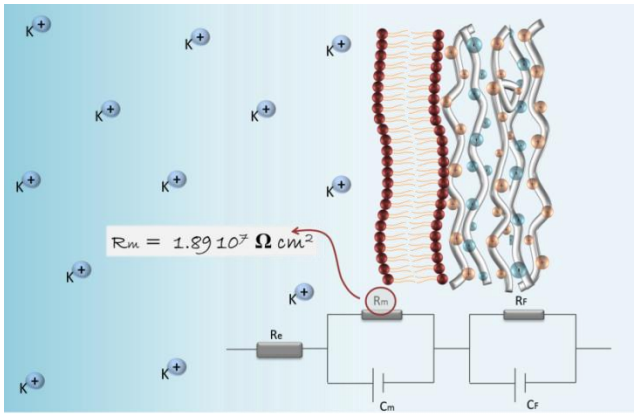

This chapter focusses on the characterization of the electrical properties of lipid bilayers supported on top of PEMs. As a model for cell membranes, lipid layers on a supporting interface have been very useful for the investigation of issues related to membrane transport, the spatial arrangement of lipids and biomolecules in the two lipid monolayers, the electrical properties of membranes, specific receptor ligand interaction, etc[1–3]. Supported membranes have been integrated in multiple devices, especially for sensing, where the membrane is used to provide a biological interface and a point of anchorage of enzymes or receptors, which will fulfil, for example, a sensing function[4,5]. Significant research has been conducted on membranes supported on planar and hard substrates such as TiO_2 or Au[6,7]. Comparatively less work has been dedicated to membranes supported on polymeric

surfaces, which are an interesting model system, as biological membranes are supported on top of a cushion of biopolymers, the glycocalix or the cell wall[2].

Of particular interest in this regard is the work of Möhwald et al. where they support lipid membranes on top of PEMs fabricated by the LbL technique[8]. The group of Möhwald applied the electrorotation technique to show that lipid membranes assembled on top of PE capsules display a capacity, which was not visible in the electrorotation spectra of pure capsules while the conductivity of bare polyelectrolyte capsules (1 S m^{-1}) decreased significantly after lipid assembly[9]. The characteristics of the assembled membrane varied significantly with the lipid composition. In these works the authors used lipid vesicles to coat the capsules which were based on dipalmitoyldiphosphatidylcholine and dipalmitoyldiphosphatidic acid (DPPA), with percentages of DPPA between 10 and 25 %. In those conditions the assembled lipid membranes will form several lipid bilayers or an assembly of lipid vesicles, as it has been proved on later studies[10]. The condition for assembly of lipid bilayers on top of polyelectrolyte multilayers requires a balance between zwitterionic and charged lipids, which is achieved when the proportion of charged lipids is more than 50 % mol. of the total lipid content as shown by Flischlechner et al.[10].

EIS studies have been conducted by Knoll et al. on lipid layers formed from negatively charged dimyristoyl-L-a-phosphatidylglycerole and the zwitterionc dimyristoyl-L-a-phosphatidylcholine SUVs assembled on PEM supports[11]. These studies showed the successful formation of a lipid bilayer on microcontact printed SAMs[12]. Electrical resistivity of lipid bilayers of anionic dioleoylphosphatidic acid and the zwitterionic dimyristoylphosphatidylcholine assembled on a PE multilayer support has been also

studied in the past by means of EIS in the frequency range of 0.1 Hz – 30 kHz[8]. The authors suggest that the polymer support participates in the formation of conducting defects.

Since the studies conducted so far with lipid layers deposited on polyelectrolyte cushions have only been performed with combinations of lipids and in conditions where the assembly does not lead to a bilayer but to non fully fused bilayers on the multilayers the electrochemical properties of a lipid bilayer interacting with PE multilayers remain a largely non studied issue. In this chapter we are willing to determine whether the assembled lipid bilayer on top of a PE cushion can display resistance and capacity values close to those of a black lipid membrane. When a bilayer supported on the PEMs shows a high resistance, in the order of 10^7 Ω cm^2 is indicative of a continuous, dense bilayer. Up to now works related with PEMs and lipids showed much lower resistivity and capacitance values[8,11,13] than the ones obtained for black membranes[14–16].

Another aspect studied in this chapter is the impact of the presence of cholesterol on the lipid membrane as well as the impact of PE layers deposited on top of the upper leaflet of a lipid bilayer in the electrical properties of the bilayers which has not been analysed so far. When the bilayer is coated with additional polyelectrolyte layers could generate defects on the membranes. The charged and zwitterionic lipids should reorganize themselves around the charged moieties of the polyelectrolyte generating regions of different density of lipids and this could be translated in the appearance of pores or defects. A sandwiched bilayer between polyelectrolytes could have interesting applications in the design of devices or sensors.

To address these issues we have conducted EIS studies on lipid bilayers supported on PEMs of PAH and PSS assembled by the LbL technique on planar substrates. Lipid vesicles formed by a mixture of DOPS and DOPC are assembled into a bilayer. The bilayer formation has been evaluated by means of the QCM-D and CryoTEM as shown in chapter 2. The assembly of PE layers on top of the lipid layers was also characterized by QCM-D and its impact on the electrical properties of the bilayer was evaluated by EIS.

3.2 Experimental Section

3.2.1 Polyelectrolyte Multilayer Supports

The multilayer film was deposited applying the LbL technique, as described in chapter 2 on top of quartz crystals with a fundamental frequency of 5 MHz coated with SiO_2 (Q-Sense) for the QCM-D measurements. Gold substrates coated with a self-assembled monolayer of MPS 0.1 M in ethanol were used for the EIS measurements and SiO_2 nanoparticles were assembled for CryoTEM measurements.

3.2.2 Liposome Preparation and Characterization

The procedure for the preparation of the vesicles composed of mixtures of DOPC, DOPS and cholesterol was as described in chapter 2 but here with the addition of cholesterol in the initial mixture. First lipid stock solutions in chloroform (10 mg mL^{-1}) were mixed together at a molar ratio 30:70 of DOPC, DOPS and 30 % of cholesterol. The chloroform was evaporated with an Argon stream and followed by overnight incubation under vacuum in order to remove any chloroform trace. The resulting lipid film was re-hydrated with PBS (10 mM) forming MLVs which were extruded through a 50 nm polycarbonate membrane forming SUVs.

The size and charge of the prepared vesicles were analyzed via DLS and ζ-potential measurements as shown in chapter 2. Likewise ^1H NMR measurements, revealed the exact composition of DOPC and DOPS, in the mixture as presented in chapter 2.

3.2.3 QCM-D Measurements

The assembly of PEMs of PAH and PSS as well as the assembly of the lipid bilayer on top of the PEM were followed by a Q-Sense E4, 4-channel QCM-D as described in chapter 2. In the case of cholesterol the concentration of SUVs including cholesterol in the formulation was the same as for the cholesterol free vesicles (0.1 mg mL^{-1}). Vesicles were flushed for 15 min through the chamber and followed by a rinse with PBS 10 mM and NaCl 0.5 M. For the additional deposition of PEs on top of the upper leaflet of the lipid bilayer PE solutions were injected as in the case of the assembly of the PEM.

3.2.4 EIS Measurements

A general purpose three-electrode electrochemical cell was used to perform the impedance characterization of the lipid membrane supported on top of the PEMs. A gold surface was used as the substrate of the working electrode. The multilayer cushion and the lipid bilayer were deposited on top of the gold surface, which had been previously modified with a self-assembled monolayer of MPS. For the assembly of the thiol monolayer the gold surface was left in MPS solution overnight resulting in a negatively charged surface. A platinum (Pt) plate served as the counter electrode. Potentials were measured with respect to a Silver/Silver chloride reference electrode (Ag/AgCl/Sat. KCl with a potential of 0.199 V vs. SHE (Standard Hydrogen Electrode)). Measurements were conducted in 0.1 M KCl electrolyte solution.

3.3 Results & Discussion

3.3.1 Lipid Vesicles Characterization

Results from DLS measurements for the vesicles with and without cholesterol are illustrated in **Figure 3.1**. Size distributions shown by intensity, revealed diameters of ~79 nm for the 30:70 DOPC:DOPS composition. The diameter of the vesicles increases to ~140 nm when 30 % of cholesterol is added to the same lipid composition. Cholesterol molecules orient themselves in the lipid vesicles with their hydroxylic groups close to the polar head groups of the phospholipid molecules, in this position, their rigid steroid ring interact and partly immobilize the hydrocarbon chain regions closest to the polar head groups, making the lipid vesicle and the bilayer less deformable.

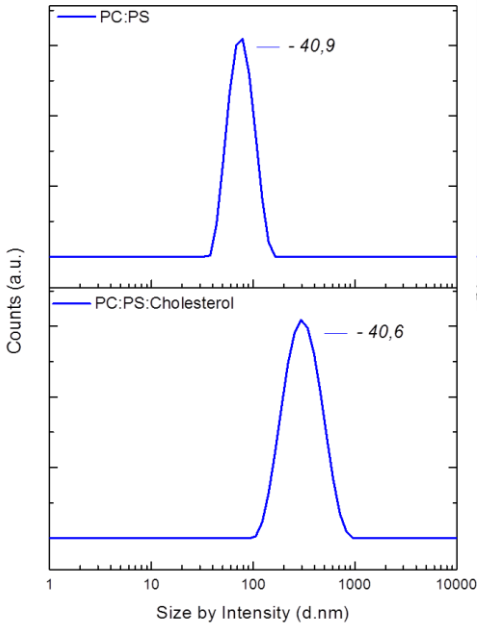

Figure 3.1 Dynamic light scattering results showing the size distribution by intensity for PC:PS, vesicles upper part, and PC:PS:Cholesterol, vesicles lower part. ζ – potential results are given at the right side of the curve.

ζ – potential measurements of the unilamellar vesicles had, as expected, negative potential values due to the presence of the negatively charged DOPS. ζ – potential values of -40,9 mV and -40,6 mV were measured for the PC:PS and PC:PS:Chol revealing similar charge values for the two different lipid compositions (**Figure 3.1**).

3.3.2 Evaluation of Lipid Bilayer Formation

The lipid bilayer formation using vesicles with a 30:70 ratio of PC:PS on top of 11 layers of PAH and PSS has been verified via QCM-D measurements, as shown in chapter 2. Typical frequency and dissipation shifts due to the formation of a lipid bilayer were observed[17] indicating that the experimental conditions used for the electrochemical studies were optimal for bilayer assembly.

By the addition of 30 % of cholesterol in the formulation of the vesicles (**Figure 3.2a**) the frequency decreases and remains constant, while no rapid increase is detected. The total shift was 130 Hz, a quite high value for the adsorption of vesicles. In similar experiments, when the same lipid and cholesterol compositions were deposited on top of 5 layers of PAH/PSS the resulting frequency shift was 53 Hz.

The frequency values, resulting from the assembly of vesicles with cholesterol, together with the absence of the jump in frequency and dissipation, hint that vesicles with cholesterol remain as such on the PEM, without fusing.

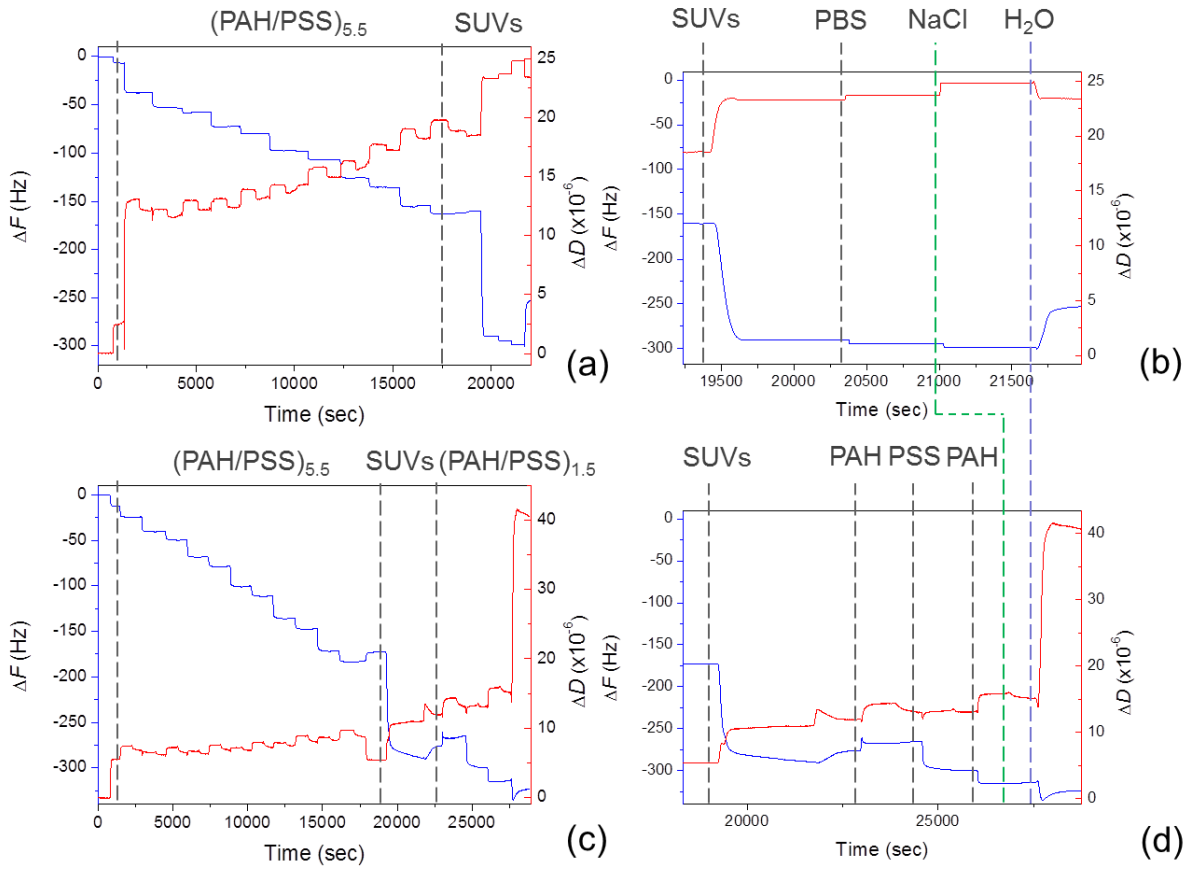

Figure 3.2 Changes in frequency (curve in blue) and dissipation (curve in red) of SiO_2 coated QCM-D crystals a) during the assembly of 11 layers of PAH/PSS and injection of 20:50:30 DOPC:DOPS:Chol. The area between the dashed lines corresponds to the PEM assembly until the moment of injection of the vesicles. b) Magnification of the area of the curve corresponds to the adsorption of the SUVs containing Chol. Dashed lines demonstrate the moments of injection of mentioned solutions. c) Assembly of 11 layers of PAH/PSS, injection of and addition of 3 layers of PAH/PSS. Dashed lines indicate the areas of PEM and assembly of SUVs containing Chol. d) Magnification of the area of the curve that corresponds to the SUVs containing Chol adsorption and the addition of 3 layers. Dashed lines correspond to the moments of injection of mentioned solutions.

However, when the same vesicles were fused on colloids coated with PEMs we observed by cryoTEM the presence of a bilayer (data not shown). The formation of a bilayer on top of PEMs is very much dependent in the proportion of charged and zwitterionic lipids. Charged lipids are fundamental for the interaction of the vesicles with the PEM and the vesicle rupture, while zwitterionic lipids seem to help in the

reorganization of the vesicle to rearrange on the surface and lead to the fusion of bilayer patches. The presence of cholesterol may make the vesicles too rigid to reorganize themselves and fuse or even restricts the vesicle rupture.

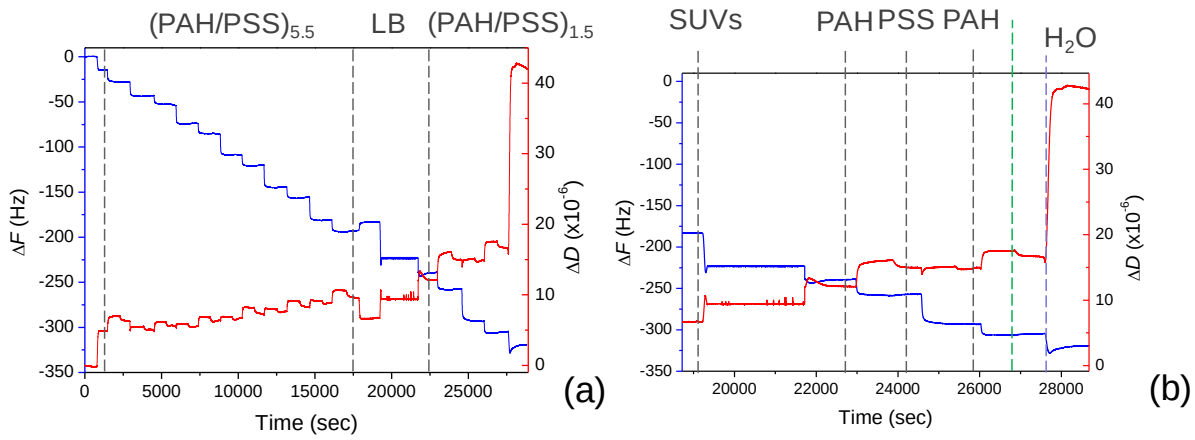

Figure 3.3 Changes in frequency (curve in blue) and dissipation (curve in red) of SiO_2 coated QCM-D crystals a) during the assembly of 11 layers of PAH/PSS, injection of 30:70 DOPC:DOPS vesicles and addition of 3 layers of PAH/PSS. Dashed lines indicate the areas of PEM and lipid bilayer assembly. b) Magnification of the area of the curve corresponds to the lipid bilayer formation and the addition of 3 layers. Dashed lines demonstrate the moments of injection of mentioned solutions.

Figure 3.3a shows the deposition of a PAH layer on top of the bilayer of DOPC:DOPS as described previously. Frequency decreases upon deposition of the positively charged polyelectrolyte and results to a total shift of 16 Hz similar to that of the previously deposited PAH layers. Another two polyelectrolyte layers where deposited on top afterwards. For these additional layers the frequency and dissipation shifts were as expected for the deposition of a polyelectrolyte layer.

3.3.3 Electrochemical Characterization

The experimental impedance of the gold substrates coated with polymer cushions in the form of 5 and 11 layers of the sequence PAH/PSS are shown as Bode plots in **Figure 3.4**. The measured impedance of the PEM films clearly exhibits a single capacitive relaxation behavior that can be fitted to the impedance of an equivalent circuit containing a series connection of the electrolyte resistance R_e and an impedance element resulting from the parallel connection of a capacitor and a large resistance. For the results shown in **Figure 3.4** the response at frequencies larger than 1 Hz resembles an ideally polarizable interface with a phase angle approaching −90°.

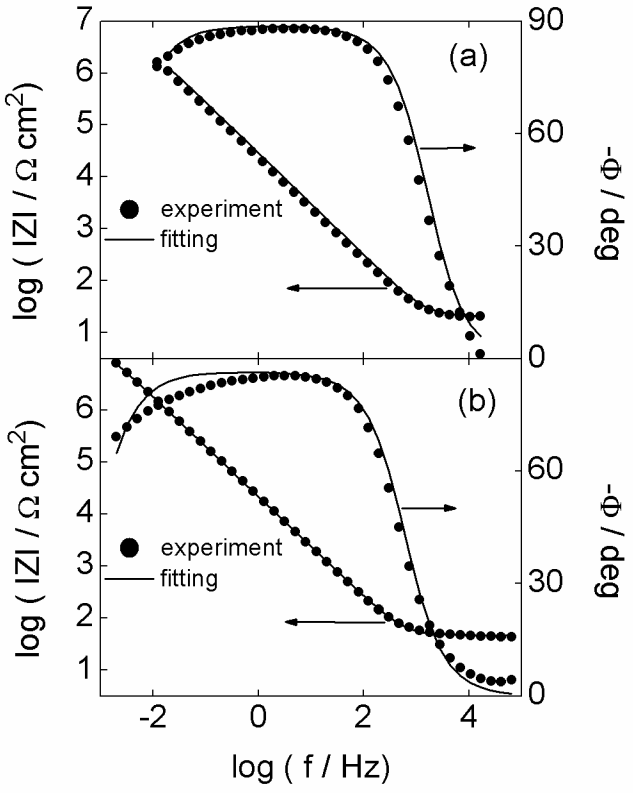

Figure 3.4 Bode plots for impedance spectra of multilayer cushions on gold electrodes: a) 5 layers cushion, b) 11 layers cushion. Experimental spectra were fitted to the impedance of the equivalent circuit in **Figure 3.5a**.

Table 3.1 Best-fit parameters derived from experimental impedance spectra in Figure 5 and theoretical impedance according to the equivalent circuit in **Figure 3.5a**.

PE cushion	$\mathbf{R_e}$ / Ω cm^2	$\mathbf{Y_O}$ / F cm^{-2} s^{n-1}	**n**	$\mathbf{R_f}$ / Ω cm^2
5 PAH/PSS layers	31.70	$6.23\ 10^{-6}$	0.97	$1.02\ 10^{7}$
11 PAH/PSS layers	49.40	$7.90\ 10^{-6}$	0.96	$2.06\ 10^{7}$

The capacitor has a slight frequency dispersion effect (that reflects a distribution of the interfacial capacitance due to surface inhomogeneity in the presence of the PE film) and consequently, it is represented here by a constant phase element Q_f (see circuit in **Figure 3.5a**). A resistance of the PE film R_f in parallel connection with Q_f is always considered here[18] but in the experiments shown in **Figure 3.4** R_f is apparently too large and it is detected for the measured frequency range f < 1 Hz. The exact origin of R_f as described in the literature, remains controversial. In fact, R_f was related to an electron charge transfer resistance at the substrate[19] or as described elsewhere "some electrochemistry" is expected to take place at defect sites in the film giving rise to a shunt resistance in the equivalent circuit[20]. In this work, however, there are no electroactive species present with a decomposition potential in the studied potential window. According to Guidelli and Becucci[18] a hydrophilic spacer, the polyelectrolyte multilayer in our experiments, on top of which the bilayer membrane is supported represents, from an impedance point of view, a dielectric slab contacting the substrate, across which there is a slight ionic flux or equivalently a resistance with a value that is high, though not infinitely high. Moreover, it has been shown that PAH/PSS films bear constant water content irrespective of their layer number and water is mainly located at

the film interface. Therefore, ion conductance is expected to take place through defects in the layers[21].

Best-fited results of impedance data in **Figure 3.4** are given in **Table 3.1**. The values of the exponent n are close to 1, i.e. a capacitance behavior, becoming slightly smaller the larger the number of layers in the hydrophilic spacer film.

Figure 3.5 shows the equivalent circuits used to interpret experimental impedance data for the different electrochemical interfaces. Circuit (a) is the electric analog of an electrode coated with a PE cushion and circuit (b) is used for determining the interfacial behavior of electrodes modified with PE layers and a lipid bilayer.

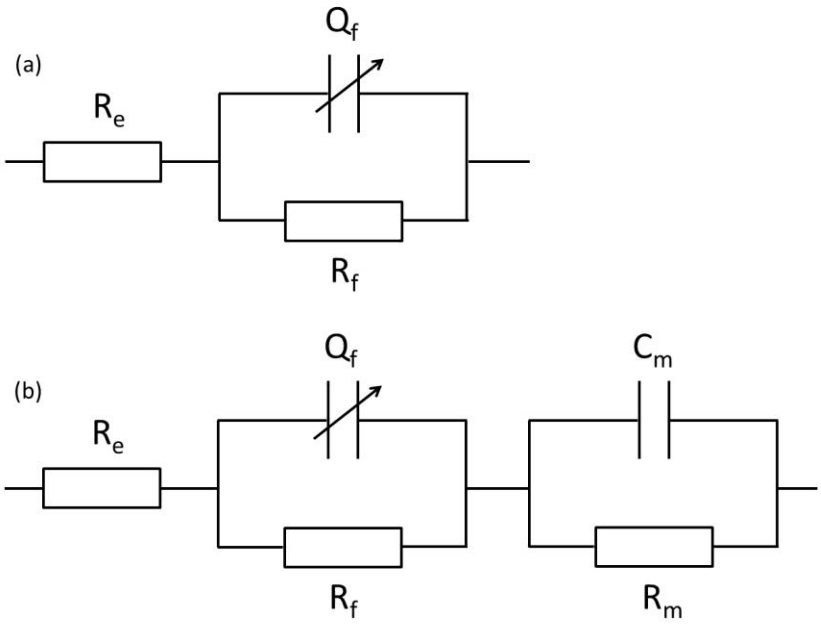

Figure 3.5 Equivalent circuits used to analyze experimental impedance data.

In the present study especially important parameters to derive by using EIS are the capacitance C_m and resistance R_m of the bilayer membrane. The expected values for

the membrane resistance of black lipid membranes that separate two aqueous electrolytes are larger than 10 MΩ cm^2 in the absence of species that promote the formation of conducting paths for ionic transport[14,22]. The typical range for R_m values of membranes on Au surfaces as measured by impedance spectroscopy is 10^5–10^7 Ω cm^2 [23]. For membranes supported on PE cushions low resistances of 2000 Ω cm^2 and capacitance values in the order of 10 μF cm^2 were reported[8].

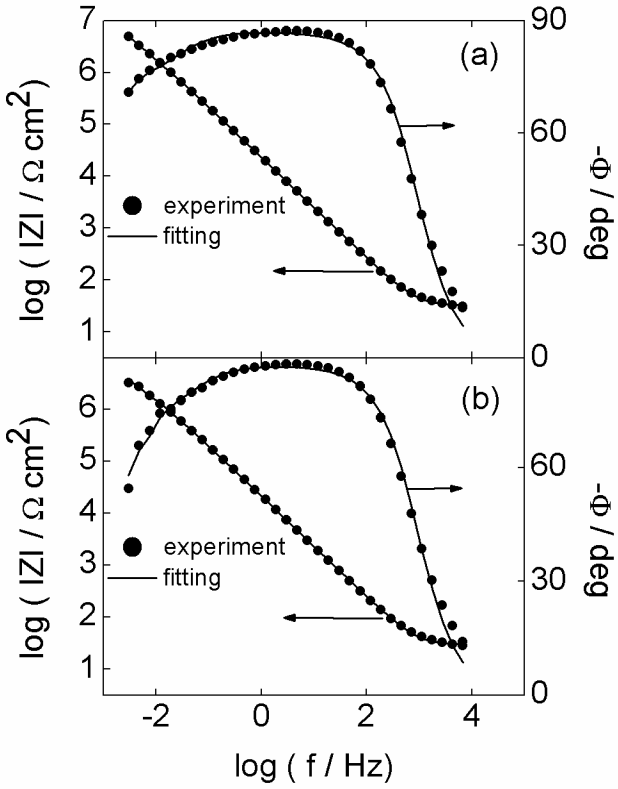

Figure 3.6 Bode plots for impedance spectra of lipid bilayers supported on an 11 layers PE cushion with compositions a) of 30:70 DOPC:DOPS and b) of 20:50:30 DOPC:DOPS:Chol. Experimental spectra were fitted to the impedance of the equivalent circuit in **Figure 3.5b**.

Figure 3.6a shows Bode plots of a lipid bilayer with a composition of 30:70 DOPC:DOPS and supported on a PE cushion in the form of 11 layers of PAH/PSS**.** **Figure 3.6b** displays Bode plots for the a bilayer with a composition of 20:50:30 DOPC:DOPS:Chol on top of 11 layers of PAH/PSS. Both spectra can be satisfactorily interpreted in terms of the equivalent circuit from **Figure 3.5b**.

The responses in the high-frequency region are dominated by the lipid membrane parameters R_m and C_m while the low-frequency portions of each spectrum are related to the relaxation phenomena in the PE films (Q_f-R_f)[19]. Best-fit results of impedance data in **Figure 3.6** are given in **Table3.2**.

Membrane resistances in **Table3.2** indicate the formation of coherent bilayers. SUVs of 30:70 DOPC:DOPS on top of PAH/PSS polyelectrolyte multilayer cushion display a resistance of 1.89 10^7 Ω cm^2. A value comparable with the resistance of black lipid membranes and a few orders of magnitude higher than the reported resistances shown for lipids assembled on PEMs. The presence of cholesterol in the vesicles leads in our case to lower resistances, 7.69 10^6 Ω cm^2. The lower resistance in presence of cholesterol can be a consequence of an incomplete bilayer as the QCM-D data suggested.

The membrane capacitance values measured are relatively high Membrane capacity will strongly depend on the lipid composition and conformational state (tilt angle, etc.) of the lipid chains through the resulting ratio dielectric constant/thickness[24]. The assembly of the lipids on the polyelectrolyte multilayers may induce significant changes in the dielectric environment of the lipid layer in contact with the polyelectrolyte as the

positively charged groups of PAH can compensate the opposite charges of DOPS and trigger reorganization of the lipids. The negatively charged lipid, DOPS, will tend to associate to the charged groups of PAH more strongly than DOPC and this will impact on the distribution of DOPC and DOPS in the membrane.

Table 3.2 Best-fit parameters derived from experimental impedance spectra in **Figure 3.6** and theoretical impedance according to the equivalent circuit in **Figure 3.5b**.

System	R_e	Y_o	n	R_f	C_m	R_m
	Ω cm^2	F cm^{-2} s^{n-1}		Ω cm^2	F cm^{-2}	Ω cm^2
11L cushion /membrane (30:70 DOPC:DOPS)	32.02	$2.27\ 10^{-5}$	0.91	$4.91\ 10^{5}$	$1.06\ 10^{-5}$	$1.89\ 10^{7}$
11L cushion /membrane (20:50:30 DOPC:DOPS:Chol)	29.27	$1.87\ 10^{-5}$	0.93	$4.90\ 10^{5}$	$1.38\ 10^{-5}$	$7.69\ 10^{6}$

We can also think that because of the interaction with PAH, the DOPS concentrated on the side of the membrane interacting with the polyelectrolyte may be higher generating an asymmetric lipid composition. All these issues could have an impact on the membrane capacitance and explain their elevated values.

The same qualitative results were obtained with lipid bilayers supported on 5-layers PE cushion (results not shown). From a quantitative point of view R_m still exhibits unusually large values ($0.5\ 10^7\ \Omega$ cm^2) that are somewhat smaller than those derived from the spectrum in **Figure 3.6a**.

We can assume that the resistance of the membrane is a result of the presence of pores spanning the bilayer thickness precisely, which are filled with the electrolyte solution. Making this assumption we can calculate the relative pore area fraction by the following equation:

$R_m/A_e = r_o\ L/A_p$ (**Eqn. 3.1**)

where, L is the length of the pore of the membrane (5 nm), A_p is the pore area, A_e is the area of the electrode and r_o is the resistivity of the electrolyte solution (16.67 Ω cm)[8].

Then,

$A_p/A_e = r_o\ L/\ R_m = 16.67\ \Omega\ cm \times 5\ 10^{-7}\ cm / 2\ 10^{7}\ \Omega\ cm^2 \approx 4\ 10^{-13}$ (**Eqn. 3.1**)

A pore area fraction of $4\ 10^{-13}$ of the total electrode area is indicative of a very dense membrane as one would expect from the calculated resistance. It is the first time that a dense lipid membrane, with resistance comparable with black membranes has been achieved on polyelectrolyte multilayers and to our knowledge none of the works on membrane supported on polymer cushions show so high resistances for the supported membranes.

The reason why such values for the resistance have not been achieved before is in our opinion, as outlined in the introduction, because previous works have used lipid mixtures and conditions for the assembly that do not lead to a lipid bilayer on polyelectrolyte multilayers but to the assembly of, at least partially, vesicles that do not fully fuse, restricting the continuity of the lipid assembly on the surface of the electrode and inducing pores or defects.

A logical step after achieving such dense membranes would be to incorporate channels or transmembrane proteins to increase selective passage of ions, which could have applications in the development of electrochemical sensors. A dense lipid membrane on top of a hydrophilic cushion as spacer from the electrode is of fundamental interest as it would allow the study of the electrochemical properties of ion channels and transmembrane proteins avoiding the direct contact of the molecules with the electrode, and reducing the impact of the electrode on the channels or the biomolecules.

Impedance spectra shown in **Figure 3.7** were measured with electrodes modified as described for **Figure 3.6a** with further assembly of 1 (**Figure 3.7a**) and 3 (**Figure 3.7b**) PE layers on top of the lipid layers. The experimental spectra can be successfully fitted to the impedance of the equivalent circuit in **Figure 3.5b** and resemble qualitatively those obtained with supported lipid bilayers doped with ionophores. The two time constants for the two RC networks (R_fQ_f and R_mC_m) result in an inflection point of the phase angle vs. log f plot that can be detected for a frequency range at which the transition between these two regimes takes place.

Best-fit results of impedance data in **Figure 3.7** are given in **Table 3.3**. A lipid bilayer confined in a sandwich structure between two PE films results in a decrease in R_m values and increase in C_m values, as compared with the system of **Figure 3.7a**. Moreover, R_f is also smaller in the presence of a film with 3 layers of PE on top of the bilayer, as compared with a capping film of only 1 layer of PE. Additionally, the capacitance (see Y_O values) of the PE film in the water subphase also decreases in the presence of 3 capping layers as compared with a 1 capping layer film. This is the reason why at each frequency the maximum of the phase shift for the relaxation

processes due to the underlying PE film exhibits lower values in the former case, although separation between the two maxima remains constant. Again, impedance data in **Figure 3.7** resembles the response measured for a lipid bilayer containing lipid-soluble ion transporters, or equivalently numerous ion channels. This suggests that the lipid-PE interaction in the present sandwich-like configuration enhances ion transport through the bilayer.

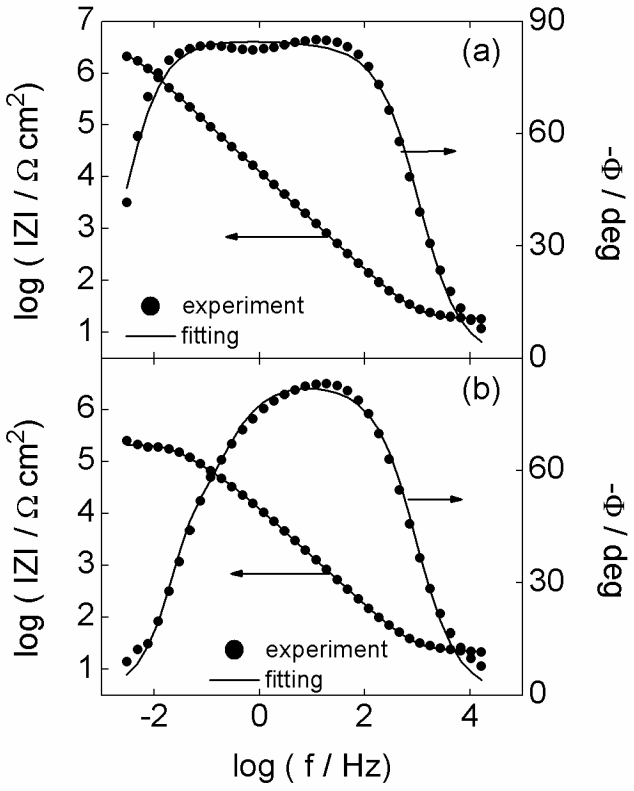

Figure 3.7 Bode plots for impedance spectra of lipid bilayers supported on an 11 layers PE cushion with a composition of a) 30:70 DOPC:DOPS with an extra assembled 1-layer and b) 3-layers PE array on top. Experimental spectra were fitted to the impedance of the equivalent circuit in **Figure 3.5b**.

Table 3.3 Best-fit parameters derived from experimental impedance spectra in **Figure 3.7** and the theoretical impedance according to the equivalent circuit in **Figure 3.5b**.

System	R_e	Y_o	n	R_f	C_m	R_m
	$\Omega\ cm^2$	$F\ cm^{-2}\ s^{n-1}$		$\Omega\ cm^2$	$F\ cm^{-2}$	$\Omega\ cm^2$
11L PE film /membrane (30:70 DOPC:DOPS)/1L PE film	18.36	$2.52\ 10^{-5}$	0.9	$1.87\ 10^{6}$	$3.17\ 10^{-5}$	$1.62\ 10^{6}$
11L PE film /membrane (30:70 DOPC:DOPS)/3L PE film	22.1	$2.32\ 10^{-5}$	0.89	$4.82\ 10^{4}$	$3.65\ 10^{-5}$	$1.64\ 10^{5}$

Charge imbalance across the bilayer[25], lateral tension for the lipid mobility[26] and mechanical stress[27] may cause the presence of pores in protein-free phospholipid membranes. The polyelectrolyte depositing on top of the lipid layers can induce rearrangement of the lipids underneath. DOPS lipids will tend to complex the charged amine groups of PAH inducing a redistribution of the lipids and probably generating some free space in the lipid layers as the negative charged lipids will accumulate in the areas where PAH is assembled. The assembly of PSS can also alter the lipid distribution repulsing the charged lipids but interacting with the quaternary amines of DOPC[28]. For three polyelectrolyte layers there is large interdigitation and it is likely that the third layer of PAH alters again the lipid distribution pattern. Our results show that three layers on top of the bilayer are more effective in increasing layer conductance, which can be interpreted as a consequence of the formation of a layer with more defects or pores. In conclusion, the PE-lipid membrane interactions enable pore-

mediated transport of ionic species across a lipid membrane. Capacitance is however only slightly affected by the assembly of the PEMs. The values of capacitance increase approximately 3 times after the polyelectrolyte assembly. The polyelectrolyte assembly on top of the bilayer seems to favor the high capacitance values probably due to the electrostatic interaction between the lipids and the polyelectrolytes or because there is more interdigitation between lipids when both lipid monolayers are facing polyelectrolyte. In any case, the high capacitance indicate that despite more defects are formed in the bilayer increasing conductivity the bilayer is not losing connectivity and continues acting as a capacitor. This would mean that the polyelectrolyte deposition only induce small defects in the bilayer in agreement with Pilbat et al[29] that observe that polyelectrolytes assembled on lipid layers deposited on PEMs do not get in contact with the supporting PEM and they do not cross the lipid layers.

3.4 Conclusions

EIS measurements show for the first time that a lipid bilayer deposited on top of a polyelectrolyte multilayer cushion can have a resistance such as 1.89 10^7 Ω cm^2. This high resistance is a consequence of a dense lipid bilayer with limited defects or pores. A pore or defects area of the order of 10^{-11} % of the total area could be calculated. Previous works on lipid bilayers on top of poyelectrolyte multilayes did not show such dense membranes hence the resistance for the lipid bilayer was significantly lower. The lipid composition of the vesicles used for lipid assembly with an excess of DOPS, 7:5, ensures the formation of a continuous bilayer on top of multilayers of PAH/PSS. Previous works on lipid bilayers on PEMs used other lipid compositions for the vesicles, which did not lead to complete fusion of the lipids into a bilayer resulting most likely in the assembly of bilayer patches. A continuous bilayer has less pores or defects than assembled bilayer patches explaining the high resistance values observed in this work.

The capacitance of the lipid bilayer is however larger than for other dense supported membranes. This is most likely a result of the lipid composition and the interaction of the lipids with the polyelectrolytes causing changes in the dielectric constant on the lipid side in contact with the polyelectrolyte and a redistribution of the charged lipids towards the lipid bilayer in contact with the PE.

The assembly of PE on top of the lipids results in the formation of pores or defects in the lipid layer with a subsequent decrease in the resistance of up to 2 orders of magnitude. Experiments in this chapter show the influence of the polyelectrolytes on the lipid arrangement in the bilayers, generating regions of different density of charged and zwitterionic lipids.

Results in this chapter open new perspectives on the use of lipid bilayers on supported polyelectrolyte cushions. The high resistance obtained here, envisage the combination of lipid layers with channels or trans-membrane proteins for selective transport in devices or as model for biological processes, profiting of the polyelectrolyte multilayer as hydrophilic spacer.

References

(1) Wiegand, G.; Arribas-Layton, N.; Hillebrandt, H.; Sackmann, E.; Wagner, P. Electrical Properties of Supported Lipid Bilayer Membranes. *J. Phys. Chem. B* **2002**, *106* (16), 4245–4254.

(2) Tanaka, M.; Sackmann, E. Polymer-Supported Membranes as Models of the Cell Surface. *Nature* **2005**, *437* (7059), 656–663.

(3) Chanana, M.; Gliozzi, A.; Diaspro, A.; Chodnevskaja, I.; Huewel, S.; Moskalenko, V.; Ulrichs, K.; Galla, H.-J.; Krol, S. Interaction of Polyelectrolytes and Their Composites with Living Cells. *Nano Lett.* **2005**, *5* (12), 2605–2612.

(4) Reimhult, E.; Kasemo, B.; Höök, F. Rupture Pathway of Phosphatidylcholine Liposomes on Silicon Dioxide. *Int. J. Mol. Sci.* **2009**, *10* (4), 1683–1696.

(5) Edvardsson, M.; Svedhem, S.; Wang, G.; Richter, R.; Rodahl, M.; Kasemo, B. QCM-D and Reflectometry Instrument: Applications to Supported Lipid Structures and Their Biomolecular Interactions. *Anal. Chem.* **2009**, *81* (1), 349–361.

(6) Rossetti, F. F.; Textor, M.; Reviakine, I. Asymmetric Distribution of Phosphatidyl Serine in Supported Phospholipid Bilayers on Titanium Dioxide. *Langmuir* **2006**, *22* (8), 3467–3473.

(7) Naumann, R.; Schiller, S. M.; Giess, F.; Grohe, B.; Hartman, K. B.; Kärcher, I.; Köper, I.; Lübben, J.; Vasilev, K.; Knoll, W. Tethered Lipid Bilayers on Ultraflat Gold Surfaces. *Langmuir* **2003**, *19* (13), 5435–5443.

(8) Cassier, T.; Sinner, A.; Offenhäuser, A.; Möhwald, H. Homogeneity, Electrical Resistivity and Lateral Diffusion of Lipid Bilayers Coupled to Polyelectrolyte Multilayers. *Colloids Surfaces B Biointerfaces* **1999**, *15* (3-4), 215–225.

(9) Georgieva, R.; Moya, S.; Leporatti, S.; Neu, B.; Ba, H.; Reichle, C.; Donath, E.; Mo, H. Conductance and Capacitance of Polyelectrolyte and Lipid-Polyelectrolyte Composite Capsules As Measured by Electrorotation. *Langmuir* **2000**, *16* (17), 7075–7081.

(10) Fischlechner, M.; Zaulig, M.; Meyer, S.; Estrela-Lopis, I.; Cuéllar, L.; Irigoyen, J.; Pescador, P.; Brumen, M.; Messner, P.; Moya, S.; et al. Lipid Layers on Polyelectrolyte Multilayer Supports. *Soft Matter* **2008**, *4* (11), 2245–2258.

(11) Kügler, R.; Knoll, W. Polyelectrolyte-Supported Lipid Membranes. *Bioelectrochemistry* **2002**, *56* (1-2), 175–178.

(12) Jenkins, A. T. A.; Bushby, R. J.; Boden, N.; Evans, S. D.; Knowles, P. F.; Liu, Q.; Miles, R. E.; Ogier, S. D. Ion-Selective Lipid Bilayers Tethered to Microcontact Derivatives.

1998, *14* (17), 1996–1999.

(13) Singh, S.; Junghans, A.; Tian, J.; Dubey, M.; Gnanakaran, S.; Chlistunoff, J.; Majewski, J. Polyelectrolyte Multilayers as a Platform for pH-Responsive Lipid Bilayers. *Soft Matter* **2013**, *9* (37), 8938.

(14) Benz, R.; Janko, K. Voltage-Induced Capacitance Relaxation of Lipid Bilayer Membranes Effects of Membrane Composition. *BBA - Biomembr.* **1976**, *455* (3), 721–738.

(15) Alonso-Romanowski, S.; Gassa, L. M.; Vilche, J. R. An Investigation by EIS of Gramicidin Channels in Bilayer Lipid Membranes. *Electrochim. Acta* **1995**, *40* (10), 1561–1567.

(16) Ries, R. S.; Choi, H.; Blunck, R.; Bezanilla, F.; Heath, J. R. Black Lipid Membranes: Visualizing the Structure, Dynamics, and Substrate Dependence of Membranes. *J. Phys. Chem. B* **2004**, *108* (41), 16040–16049.

(17) Keller, C. A.; Kasemo, B. Surface Specific Kinetics of Lipid Vesicle Adsorption Measured with a Quartz Crystal Microbalance. *Biophys. J.* **1998**, *75* (September), 1397–1402.

(18) Guidelli, R.; Becucci, L. Electrochemistry of Biomimetic Membranes. In *Modern Aspects of Electrochemistry*; **2012**; Vol. 53, pp 147–266.

(19) Lin, J.; Hristova, K.; Searson, P. Electrically Addressable, Biologically Relevant Surface-Supported Bilayers. In *Handbook of Biofunctional Surfaces*; Pan Stanford Publishing, **2013**; pp 769–820.

(20) Stelzle, M.; Weissmuller, G.; Sackmann, E. On the Application of Supported Bilayers as Receptive Layers for Biosensors with Electrical Detection. *J. Phys. Chem.* **1993**, *97* (12), 2974–2981.

(21) Iturri Ramos, J. J.; Stahl, S.; Richter, R. P.; Moya, S. E. Water Content and Buildup of Poly(diallyldimethylammonium chloride)/Poly(sodium 4-Styrenesulfonate) and Poly(allylamine hydrochloride)/Poly(sodium 4-Styrenesulfonate) Polyelectrolyte Multilayers Studied by an in Situ Combination of a Quartz Crystal Microb. *Macromolecules* **2010**, *43* (21), 9063–9070.

(22) Läuger, P.; Lesslauer, W.; Marti, E.; Richter, J. Electrical Properties of Biomolecular Phospholipid Membranes. *Biochim. Biophys. Acta* **1967**, *135*, 20–32.

(23) Janshoff, A.; Steinem, C. Supported Lipid Bilayers: Intelligent Surfaces for Ion Channel Recordings. In *Intelligent Surfaces in Biotechnology*; John Wiley & Sons, Inc.: Hoboken, NJ, USA, 2012; pp 141–182.

(24) Plant, A. L. Self-Assembled Phospholipid Alkanethiol Biomimetic Bilayers on Gold. *Langmuir* **1993**, *9* (11), 2764–2767.

(25) Gurtovenko, A. A.; Vattulainen, I. Pore Formation Coupled to Ion Transport through Lipid

Membranes as Induced by Transmembrane Ionic Charge Imbalance: Atomistic Molecular Dynamics Study. *J. Am. Chem. Soc.* **2005**, *127* (50), 17570–17571.

(26) Lin, J.; Szymanski, J.; Searson, P. C.; Hristova, K.; Chsearson, P.; Hristova, K. Effect of a Polymer Cushion on the Electrical Properties and Stability of Surface-Supported Lipid Bilayers. *Langmuir* **2009**, *26* (5), 3544–3548.

(27) Leontiadou, H.; Mark, A. E.; Marrink, S. J. Molecular Dynamics Simulations of Hydrophilic Pores in Lipid Bilayers. *Biophys. J.* **2004**, *86* (4), 2156–2164.

(28) Diamanti, E.; Cuellar, L.; Gregurec, D.; Moya, S. E.; Donath, E. Role of Hydrogen Bonding and Polyanion Composition in the Formation of Lipid Bilayers on Top of Polyelectrolyte Multilayers. *Langmuir* **2015**, *31*, 8623–8632.

(29) Pilbat, A. M.; Szegletes, Z.; Kóta, Z.; Ball, V.; Schaaf, P.; Voegel, J. C.; Szalontai, B. Phospholipid Bilayers as Biomembrane-like Barriers in Layer-by-Layer Polyelectrolyte Films. *Langmuir* **2007**, *23* (15), 8236–8242.

Chapter 4

Virosomes Engineering of Colloidal Particles and Surfaces: Bioinspired Fusion to Supported Lipid Membranes

4.1 Motivation

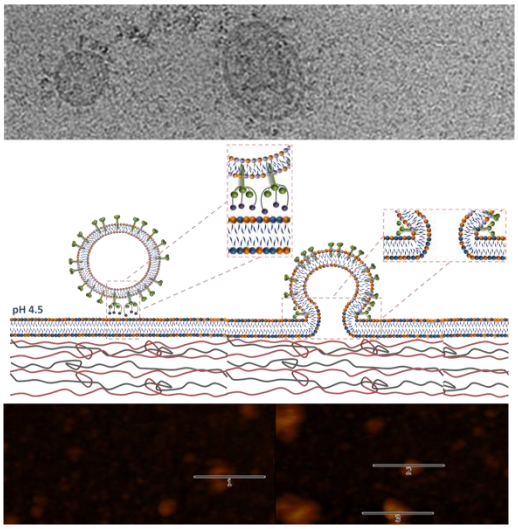

The focus of this chapter is the study of the fusion of IRIVs to artificial supported lipid membranes assembled on PEMs on both colloidal particles and planar substrates.

IRIVs are virus like nanoparticles similar to influenza virus envelopes but lacking any viral genetic material[1]. IRIVs fuse to cells and liposomes through the viral glycoprotein HA which is intercalated in the phospholipid bilayer of the vesicles of the IRIVs. Virosomes have been mainly developed as prospective adjuvants to potentiate an immune response, since antigens alone are often poor immunogens[1]. An unexplored domain where virosomes can be applied is their use to engineer colloids and surfaces in a way that liposomes have been often applied for the development of biocompatible surfaces, biosensors or drug delivery systems. Since virosomes retain fusion properties of the virus they could also be fused on artificial lipid

membranes bringing the functionalities carried on their membranes to the supported lipid bilayers[2–4]. Besides the potential use of IRIVs as drug carriers their functionalities are not limited as they can also serve as templates for the attachment or anchoring of antibodies or ligands. Modified IRIVs can be then fused to the supported bilayer membranes bringing functionalities to the membrane that otherwise would not be so easy to develop once the lipid bilayer is formed. By this way they can act as transfer agents of biological molecules to supported membranes through fusion mechanism without jeopardizing membrane formation and reducing particle aggregation in case of colloids. This chapter focuses on the proposed approach which up until now has not been studied in detail as in the case of fusion of virosomes in cell cultures[5–7].

The aim of this work is to show the fusion of the virosomes to supported membranes and to study the mechanism of fusion of the virosomes: the dependence of pH, temperature and HA content.

Supported membranes were fabricated on self-assembled PEMs, which were chosen as a model support and can be assembled on both planar and colloidal surfaces. The supported membranes were assembled from mixed vesicles of DOPS and DOPC, in conditions that ensure the formation of a lipid bilayer[8].

IRIVs fusion has been studied via flow cytometry, CLSM, fluorescence spectroscopy, QCM-D, AFM and Cryo-TEM.

4.2 Experimental Section

4.2.1 Polyelectrolyte Multilayer Assembly

PEMs based on PAH and PSS were assembled either on silica colloids (3 µm) or on plane surfaces by means of the LbL technique. PEMs were formed upon 11 polyelectrolyte layers; $(PAH/PSS)_{5.5}$ while the outermost layer was always the positively charged PAH. Polyelectrolytes were assembled in acetate buffer containing 0.2 M NaCl (pH 5.6) in a 1 mg mL^{-1} concentration. After each layer assembly surplus PE was removed by washing three times with the buffer.

4.2.2 Lipid Bilayer Assembly on Planar and Colloidal Supports

For the fusion of IRIVs on supported membranes LbL engineered colloids and planar surfaces were initially equipped with a continuous fluid lipid bilayer as described in chapter 2.

SUVS were composed of mixtures of DOPC and DOPS at a molar ratio of 40:60 following the procedure described in chapter 2.

SUVs and IRIVs were characterized regarding size and zeta-potential. The size was determined after 1:100 dilution (v/v) in buffer (50 mM phosphate, 83 mM NaCl; pH 7.4) by DLS using a Malvern ZetaSizer 3000HS. The ζ – potential was measured in 1 mM Tris (pH 7.0) with the Malvern ZetaSizer 3000HS.

4.2.3 CryoTEM Imaging

IRIVs morphology was characterized by CryoTEM as described in chapter 2. Imaging was conducted for IRIVs diluted in PBS at a concentration of 0.35 mg mL^{-1}. The specimen was deposited on quantifoil grids Holey Carbon Films (shape R2/2). The sample suspended in aqueous solution was then rapidly frozen in liquid ethane and cooled to liquid nitrogen temperature; as described in chapter 2.

4.2.4 R18 Labelling of Virosomes

The fusion of IRIVs with liposomes or lipid bilayer coated PEM-colloids was studied via the R18 fusion assay. The assay is based on the incorporation of the lipophilic Rhodamin B-octadecylester-perchlorate (R18) to lipid membranes taking advantage of the alkyl chain of the dye conjugate. IRIVs were labelled by adding a R18 solution in ethanol to the IRIVs suspension in such concentration that the R18 fluorescence is self-quenched as a result of dye-dye interaction. The R18 quenching was about 50 – 70 %. IRIVs were labelled with octadecyl rhodamine B (R18) by incubating them at a concentration 0.1 mg mL^{-1} in PBS from an ethanolic R18 stock solution (3 mg mL^{-1} in water containing 20 % (v/v) ethanol) at room temperature for 1 h under gentle shaking. Due to the excess of R18 (5 mol % R18 of total lipid) and the resulting dye-dye interaction in the supported lipid membrane, the fluorescence of the probe is self-quenched[9,10]. Surplus R18 was removed by Sephadex G-50 chromatography. When virosome fusion takes place into an unlabelled lipid bilayer the probe will be diluted and the fluorescence increases accordingly[10]. The fluorescence increase after fusion was

measured by fluorescence spectroscopy and flow cytometry. Fusion % was calculated with

$$(F - F_0)/F_{max} * 100 \qquad \textbf{(Eqn 4.1)}$$

F is the fluorescence intensity after addition of IRIVs or protein free IRIVs or PBS (control). F_0 is the fluorescence intensity before addition of IRIVs and F_{max} is the maximum fluorescence intensity after lysis with Triton X-100.

4.2.5 R18 Assay via Flow Cytometry and Fluorescence Spectroscopy

Silica colloids coated with $(PAH/PSS)_{5.5}$ and a DOPC:DOPS bilayer were incubated with R18 labelled IRIVs in citric acid/phosphate buffer (CIP) (pH 4.5 or pH 7.4). The fluorescence of the colloids was recorded using a CyFlow Space, Sysmex Partec flow cytometer. The mean particle fluorescence intensity was measured at a rate of 50 – 100 colloids per second in the fluorescence channel 4 (*λex*: 532 nm, *λem*: 590 $\pm$ 25 nm) at different time points: 0, 1, 2, 5, 10, 15, 20 min. The data were analysed using flowing software (version 2.5.1.; P. Terhu).

IRIVs – liposome fusion: R18 labelled IRIVs (0.5 mg mL^{-1}) were diluted in CIP buffer (pH 4.5 or pH 7.4). The fluorescence of the R18 probe was monitored immediately after IRIVs mixing with liposomes for 10 min using a Varian Cary50 spectrofluorimeter (*λex*: 532 nm, *λem*: 584 nm). After 1 min unlabelled SUVs (0.5 mg mL^{-1}) were added to the IRIVs dispersion. Finally Triton X-100 (1 % (v/v)) was added to derive the maximum R18 fluorescence value. Due to a small self-fluorescence of Triton X-100, control

measurements in the absence of virosomes were performed in buffer and subtracted from the Triton value of the sample.

IRIVs fusion with lipid bilayer coated PEM-colloids: Bilayer coated PEM-colloids (5 wt %) were diluted 1:500 in CIP buffer (pH 4.5 or pH 7.4). Control measurements without virosomes were performed. After addition of R18-labeled IRIVs the sample was incubated at 37 °C in a water bath for different set point times. The fluorescence of the sample was recorded using a Varian Cary50 Eclipse spectrofluorometer (*λex*: 532 nm, *λem*: 584 nm). Triton X-100 (1 % (v/v)) was added, mixed and measured to obtain the maximum value of R18 fluorescence.

4.2.6 CLSM Measurements

The distribution of the R18 fluorescence on the particle surface was analyzed by confocal fluorescence microscopy (Leica TCS Sp1). Free IRIVs were removed by three washing steps in PBS. Fluorescence was measured after excitation with a 532 nm laser in the emission range of 570 to 600 nm.

4.2.7 QCM-D Measurements

PEM assembly for PAH and PSS and the assembly of the lipid bilayer of SUVs of 40:60 DOPC:DOPS on top of the PEMs were monitored with an E4 QCM-D at 25°C as described in chapter 2. PEMs deposition was conducted from 1 mg mL^{-1} polyelectrolyte solutions in acetate buffer containing 0.2 M NaCl (pH 5.6). Once the lipid bilayer was

assembled the chamber was pre-equilibrated with milliQ water and then filled with CIP buffer (pH 4.5) or PBS (pH 7.4) before injection of the virosomes. IRIVs were added in a concentration of 0.014 mg mL^{-1} and left in the chamber for at least 1 h. Finally, the chamber was rinsed with PBS and milli-Q water in order to remove non-fused virosomes from the membrane.

4.2.8 AFM Measurements

AFM measurements were performed in liquid state using a Multimode AFM with a Nanoscope V controller (Bruker AXS, Santa Barbara, CA), equipped with a J-scanner. Oxide-sharpened silicon nitride cantilevers with a nominal spring constant of 0.06 N/m (Bruker) were used. The QCM-D sensors with the supported membranes and fused virosomes were attached to Teflon-coated metal disks using double-sided tape and placed on the AFM scanner. Images were acquired with minimal force. Tapping mode images were analyzed using the Gwyddion software (gwyddion.net).

4.3 Results and discussion

4.3.1 Lipid Bilayer Assembly

SUVs characterization and the successful assembly of the lipid bilayer were evaluated via DLS, ζ – potential, QCM-D and cryoTEM as shown in chapter 2.

4.3.2 IRIVs Fusion on Lipid Coated PEM Assembled Particles

In previous works it has been shown that the fusion of influenza virus in cells[11] or liposomes is triggered by acidic pH[12,13]. The membrane fusion protein of influenza virus, HA, is activated by low pH[11,14–16]. Upon exposure to low pH in endosomes, conformational changes of the HA protein result in the exposure of the fusion peptide (the hydrophobic N-terminus of the HA2 polypeptide subunit)[17,18]. The hydrophobic peptide is inserted into the hydrocarbon part of the cell membrane[11,18,19]. At pH 7.4 virosomes remain attached to the surface of the membrane, since HA is not activated to initiate fusion with the lipid bilayer. Since the pH is important for the influenza virus for its fusion with lipid membranes, the fusion activity of the IRIVs was tested on supported lipid membranes at acidic and neutral pH. The best conditions for virosome fusion in this study were established by evaluating temperature and virosome concentration.

Initially, IRIVs and *protein free* IRIVs (without HA), were characterized in liquid solution regarding size and zeta potential (**Figure 4.1**). The PDI of 0.096 obtained for IRIVs demonstrates that no aggregation or degradation takes place.

	IRIVs	*Protein free* IRIVs
Z average (nm)	127.2 ± 2.3	93.5 ± 1
Polydispersity Index - PDI	0.096 ± 0.02	0.11 ± 0.02
Zeta potential (mV)	-23.7 ± 7.5	- 8.9 ± 1.2
CryoTEM of IRIVs	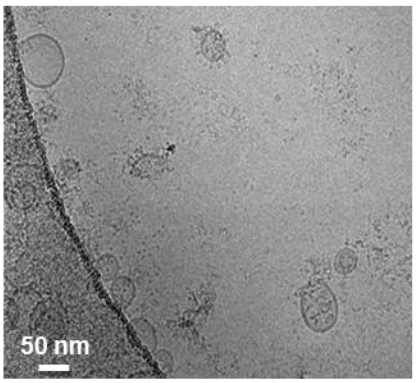	

Figure 4.1 Particle size, ζ – potential and cryoTEM imaging of IRIVs and protein free IRIVs.

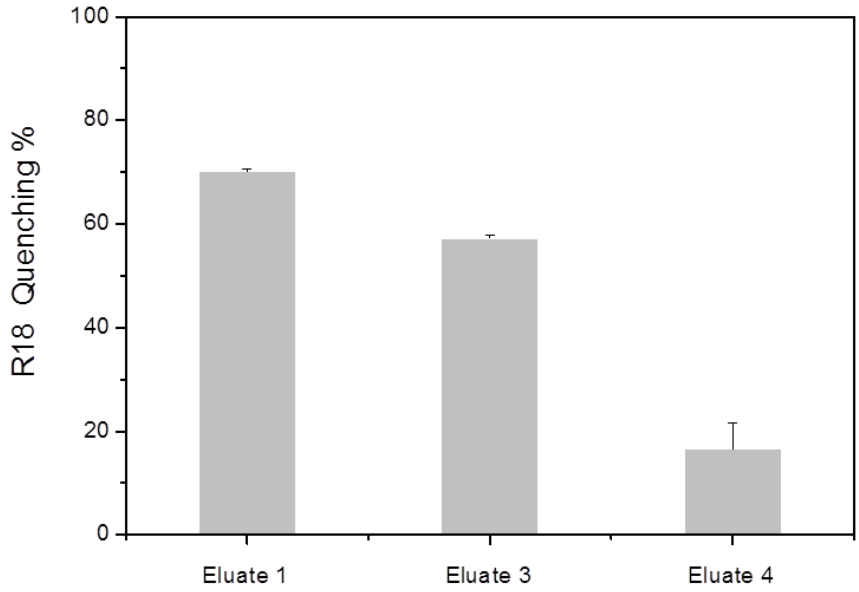

Figure 4.2 Self-quenching of R18-labeled virosomes. The quenching % was calculated with (F-F_0)/F *100. F_0 is the fluorescence intensity before lysis and F of the fluorescence intensity after lysis (addition of Triton X-100).

The fusion of the IRIVs was studied by means of the fluorescence self-quenching R18 assay (**Figure 4.2**). The fusion of R18-labelled IRIVs with liposomes was monitored by fluorescence spectroscopy measurements. **Figure 4.3** shows that the IRIVs – liposomes fusion was pH dependent. At pH 4.5 the fluorescence intensity increased after addition of liposomes reaching a plateau after approximately 3 min. At pH 7.4 the fluorescence intensity did not increase after addition of IRIVs, which indicates that at neutral pH IRIVs – liposomes fusion did not occur. Control studies with *protein free* IRIVs with identical lipid composition and concentration as IRIVs but without HA, showed no increase of fluorescence with time after the addition of the *protein free* IRIVs to the liposomes suspension at both pH 4.5 and 7.4.

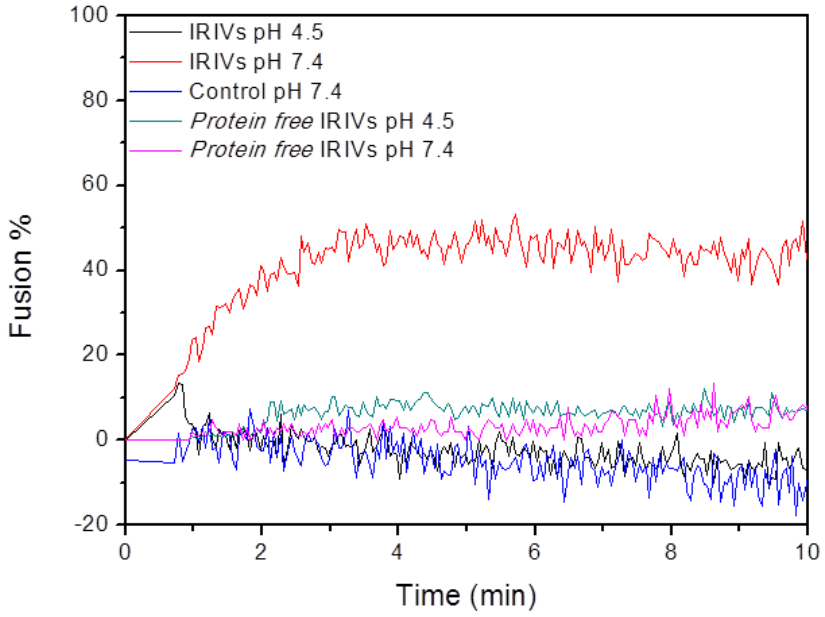

Figure 4.3 Kinetic analysis, via R18 assay, of the IRIVs – liposomes, *protein free* IRIVs – liposomes fusion at pH 4.5 and 7.4. IRIVs were also suspended in PBS (pH 7.4) and fluorescence was recorded as a control.

The fusion of R18-labelled IRIVs with lipid bilayer assembled on PEM-colloids was studied by flow cytometry. **Figure 4.4** shows that fusion was strongly dependent on pH. The mean fluorescence intensity was measured as a function of time and pH. At pH 4.5 the R18 fluorescence intensity increased over 20 min by more than a factor of two, while at pH 7.4 the fluorescence remained almost constant over this period of time. Further experiments showed that the fusion of IRIVs with lipid bilayer coated PEM-colloids, was completed within around 30 min at pH 4.5. The fusion of IRIVs with the supported bilayer on PEM-colloids proceeded much slower than in the case of the IRIVs – liposomes fusion. We attribute this difference to the restricted mobility and flexibility of the supported membrane compared with the free membrane of the liposomes.

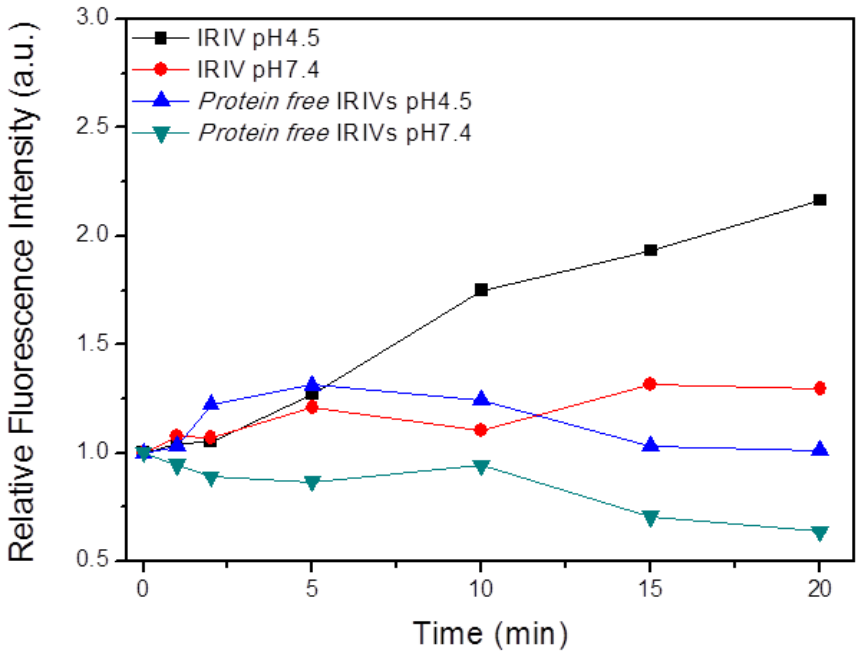

Figure 4.4 Kinetic analysis, via R18 assay, of the IRIVs fusion with lipid bilayer coated PEM-colloids at pH 4.5 and 7.4.

The different lipid surface ratios of liposomes and bilayer coated PEM-colloids may also play a role. Control measurements with *protein free* IRIVs at both pH values showed

also no increase of fluorescence with time, confirming that the presence of HA is responsible for the IRIVs fusion.

IRIVs fusion with bilayer coated PEM-colloids was also studied as a function of temperature. **Figure 4.5** shows that after 10 min the fluorescence intensity at 37 °C was only slightly increased than at 21 °C. The fluorescence intensity increases from 0 min (IRIVs addition) to 10 min, by 2 times for 21°C and 1.7 times for 37 °C. However, after lysis with Triton X-100 the R18 fluorescence intensity was much larger at 21 °C than at 37 °C. This indicates that an amount of IRIVs were still adsorbed on the lipid coated particles at 21 °C rather than fused within the lipid bilayer. This finding demonstrates that temperature increase facilitates fusion as demonstrated by Haywood et al. for the fusion of influenza virus with liposomes[20].

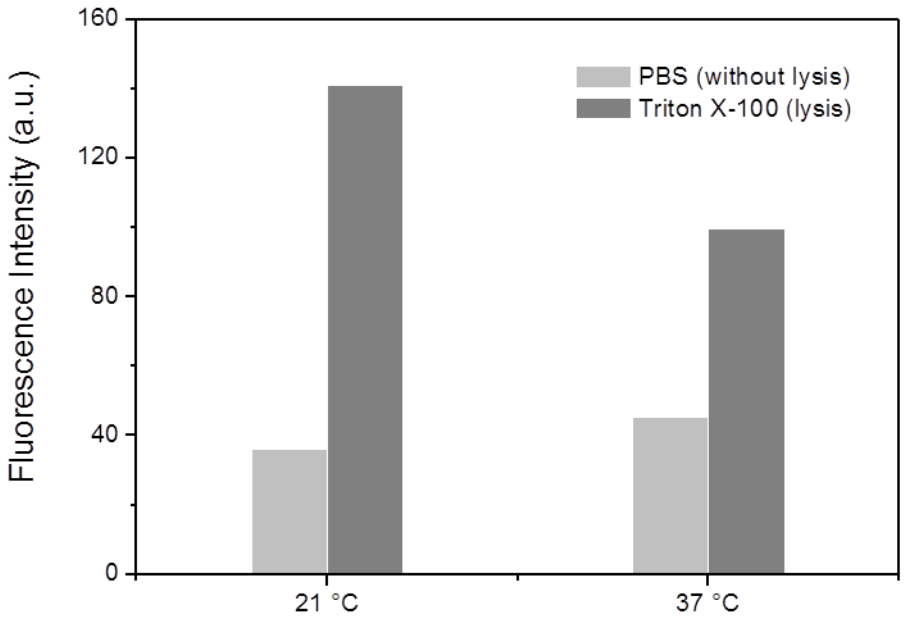

Figure 4.5 Fusion of IRIVs with bilayer coated PEM-colloids in dependence of temperature measured as the R18 fluorescence intensity. Measurements were conducted at CIP buffer (pH 4.5) at 21°C and 37°C for 10 min. Fluorescence intensity before and after lysis by addition of Triton X-100 was measured.

The effect of IRIVs concentration, and subsequently HA content, on the membrane fusion was also studied. In **Figure 4.6** two different IRIV concentrations are compared. The IRIVs concentration, given in the final amount of HA per mL, was 0.5 µg and 2 µg HA. At pH 4.5 the fluorescence increased two times for 0.5 µg HA and one time for 2 µg HA after 10 min of incubation of IRIVs.

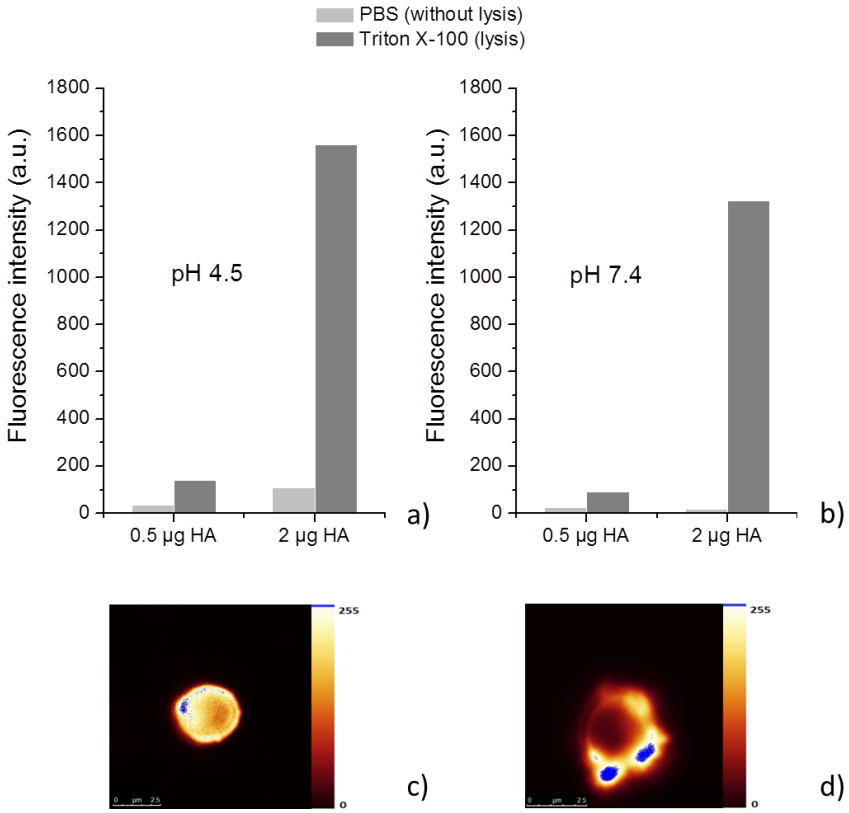

Figure 4.6 Fusion of IRIVs with lipid bilayer coated PEM-colloids in dependence of HA concentration. R18 fluorescence intensity was measured before and after lysis with Triton X-100 for 0.5 and 2 µg HA at a) pH 4.5 and b) pH 7.4. Confocal images c) and d) corresponding to a) and b) respectively. The colour bar indicates the R18-fluorescence intensity from 0 values (black) to 255 (blue).

This represents a more efficient fusion for the lower IRIVs concentration to lipid bilayer coated PEM-colloids. At pH 4.5, after lysis with Triton X-100 the R18-fluorescence intensity increased 14 times for 2 μg HA while for 0.5 μg HA the increase was less; about 4 times (**Figure 4.6a** and **b**). The pronounced difference in the fusion efficiency between 0.5 and 2 μg HA suggests that in the latter case a large amount of IRIVs remained attached to the supported membrane instead of fusing. It may also be related with the fact that as the concentration of R18 is significantly higher for the case with the larger concentration of virosomes their fusion does not cause a complete dequenching of the R18. However, the confocal fluorescence microscopy image (**Figure 4.6d**) shows a rather inhomogeneous fluorescence distribution confirming the adsorption of IRIVs to the supported membrane. Probably the lipid membrane is densely covered with IRIVs and fusion is inhibited as a consequence of topological constraints. In contrast for 0.5 μg HA the fluorescence distribution is homogenous indicating the IRIVs fusion to the supported membrane (**Figure 4.6c**).

4.3.3 IRIVs Fusion on Planar Supported Membranes

IRIVs adsorption and fusion was also studied by means of QCM-D on planar supported membranes. **Figure 4.7** shows the results from the real time monitoring of fusion of the IRIVs for the two different pH values; 4.5 and 7.4. As referred in the experimental part, a lipid bilayer was deposited on top of the 11 layer of PAH/PSS cushion prior to IRIVs deposition. **Figure 4.7a** shows the frequency and dissipation changes occurring upon interaction of the IRIVs suspended in CIP buffer with the supported membrane at pH 4.5

as a function of time. The frequency followed a steadily decreasing tendency for more than two hours reaching a total frequency shift of Δ*f* = 99 Hz. This comparatively large frequency shift demonstrates an ongoing adsorption of IRIVs on the membrane indicating that at this pH the HA protein in the IRIVs is able to recognize the lipid membrane. The strong parallel increase in dissipation confirms adsorption. The increase in dissipation is also indicative of the increase of the surface roughness during the virosome attachment to the membrane leading to an enhanced friction of the soft IRIVs. At this stage the QCM-D data do not allow to separate fusion and adsorption. However, after rinsing with PBS non-fused IRIVs were removed as seen by the decrease in dissipation and the increase in frequency reaching a Δ*f* = 46 Hz. The frequency increased even further to Δ*f* = 21 Hz when rinsing with water. So finally the total frequency shift for the fused IRIVs in the supported membrane at acidic pH was Δ*f* = 32 Hz. We attribute the frequency change after rinsing with PBS and water to the net mass increase caused by virosomes membrane fusion. At neutral pH the QCM-D data demonstrate a completely different behaviour as shown in **Figure 4.7b**. The frequency changes only slightly upon the deposition of the IRIVs. The small increase in dissipation, note the different scale in **Figures 4.7a** and **4.7b**, is consistent with adsorption of a small amount of IRIVs, which do not subsequently fuse with the lipid membrane. This was followed by the low total change in frequency of Δ*f* = 8 Hz after rinsing. *Protein free* IRIVs, did not fuse at pH 4.5 on the supported membranes (**Figure 4.7c**) confirming again that the effect of the pH is only related to the presence of the HA protein.

AFM imaging was conducted to have a visual proof of the IRIVs fusion to the lipid membrane. In **Figure 4.8a** the fused IRIVs at pH 4.5 can be recognized as they form features of a varying size of 190 – 270 nm, which is about twice as much as the diameter of the IRIVs.

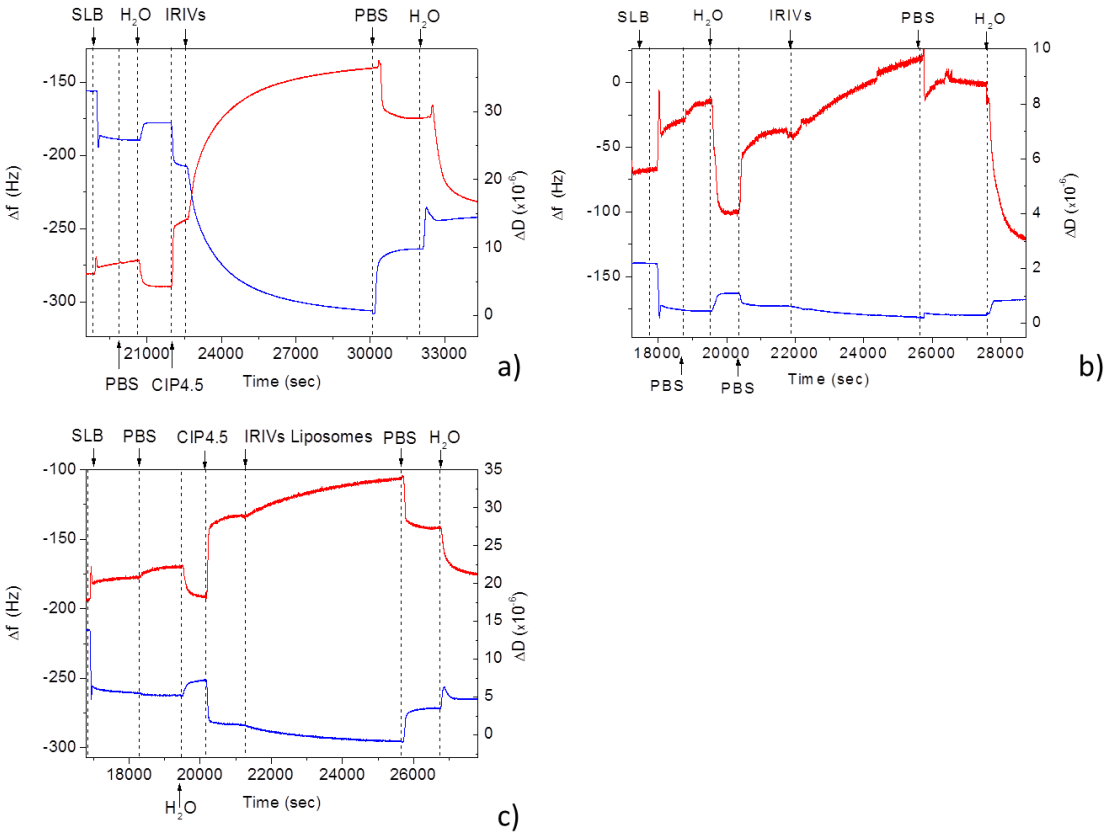

Figure 4.7 Frequency (blue line) and dissipation (red line) curves measured by QCM-D for the formation of phospholipid bilayer deposited on a PEM of 11 layers of PAH/PSS and later exposed to a) IRIVs in pH 4.5, b) IRIVs in pH 7.4 and c) *protein free* IRIVs with the same lipid composition and content as IRIVs in pH CIP 4.5.

These features were not present in the supported membrane before the exposure to the virosomes. The observed features have a height of 50 – 70 nm. These values are consistent with the measured size of the IRIVs of about 125 nm. From geometrical considerations it is obvious that after fusion of the IRIVs with the lipid membrane the

latter has to be lifted off in the regions of the fusion events, as fusion goes along with a net increase of the total membrane surface. By this is followed that the virosomes were embedded in the supported membrane. The fused virosomes appear to be aggregated and randomly distributed on the surface. The control at neutral pH is more revealing. **Figure 4.8b** shows features of a height of ~ 100 nm and lateral dimensions of 150 – 350 nm, which correspond to non-fused IRIVs displaying a size comparable to the one obtained by DLS and CryoTEM measurements for the IRIVs in bulk. The IRIVs at this pH appear as if they remained attached on the supported membrane without fusing.

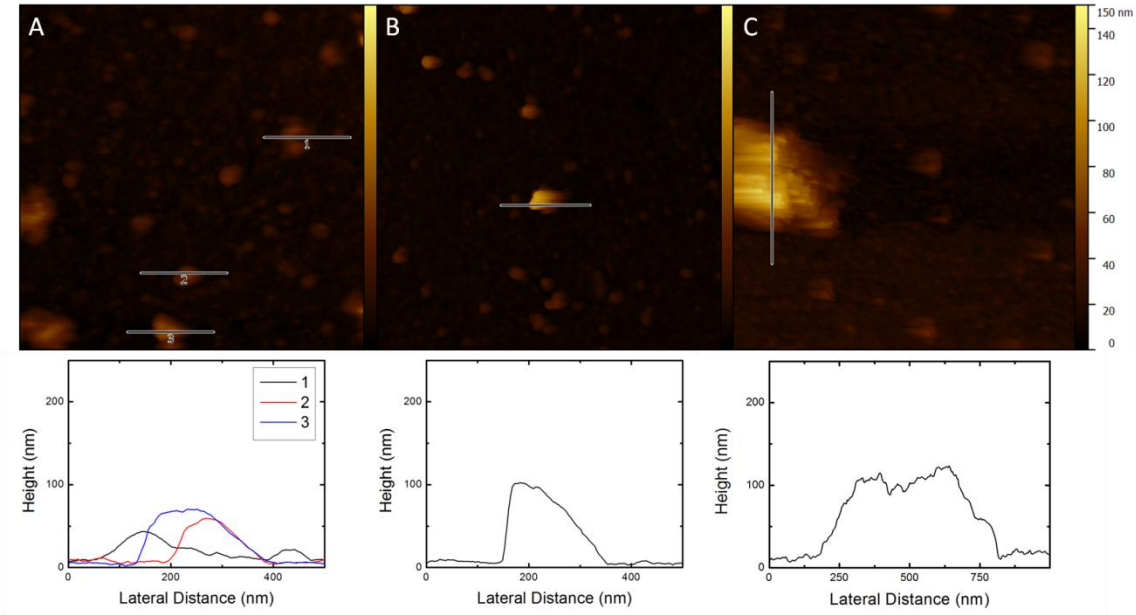

Figure 4.8 AFM images (2 x 2 µm) acquired in 150 mM NaCl (liquid mode) of $(PAH/PSS)_{5.5}$ DOPC:DOPS lipid bilayer membrane after addition of a) IRIVs in pH 4.5 or b) IRIVs in pH 7.4 and c) *protein free* IRIVs in pH 4.5. Bottom panels display roughness profiles taken as cross sections of above images.

AFM was also conducted for supported membranes exposed to *protein free* IRIVs, at pH 4.5. In this case the lipid surface displays the same features as the supported

membranes but with a few large aggregates with a height of 120 – 130 nm and width of ~500 nm (**Figure 4.8c**). The extended aggregation of the liposomes could be due to the lack of proteins.

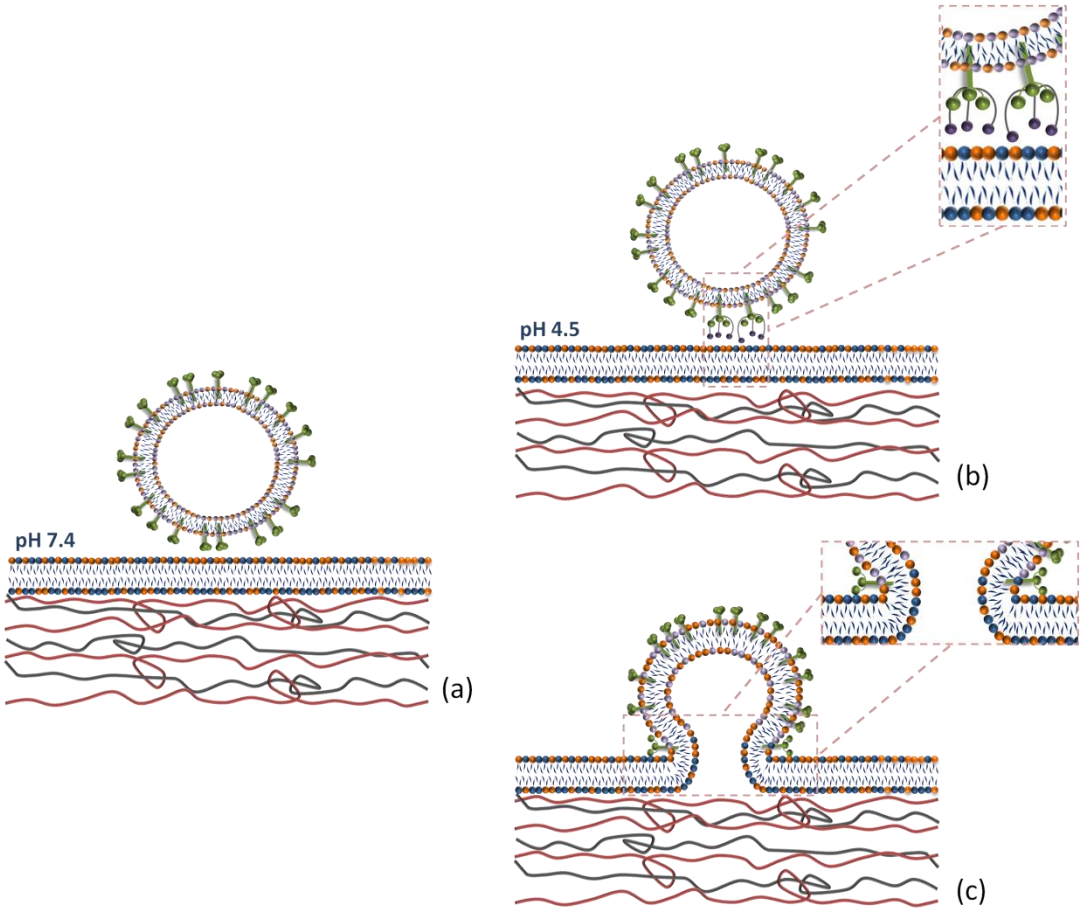

Figure 4.9 Schematic illustration of the a) virosome attached to a supported membrane at neutral pH without fusing; b) and c) fusion of the virosomes at low pH on the supported membrane. The virosome approaches the lipid membrane and there is rearrangement of the hemagglutinin protein at pH 4.5 b), the zoom out shows in more detail the rearrangement of the hemagglutinin protein. The virosome is fused to the lipid bilayer membrane c), the zoom out shows how the proteins are arranged at the area where the fusion occurs.

The virosome fusion is based on their interaction to the lipid membrane driven by the HA protein present on the surface of the IRIVs, which is responsible for the pH dependent fusion. **Figure 4.9a** displays a scheme of the behaviour of the IRIVs at

neutral pH where they remain on the membrane without fusing, while at low pH they fuse (**Figure 4.9b** and **c**). In the figure the change in the conformation of the HA with the hydrophobic peptide penetrating in the hydrocarbon part of the cell membrane have been sketched (**Figure 9b**)[11,18,19]. In **Figure 9c** the possible arrangement of the lipids and proteins after the fusion is shown. It is remarkable that the fusion of virosomes is taking place without the presence of a sialoglycan or any other receptor on the membrane that promotes the interaction of the virosome to the membrane. The fact that our supported membranes are formed by lipids only lacking additional components of cell membranes like the glycocalyx or proteins could explain that the virosomes can fuse directly on the membranes being the lipid layers easily accessible for the virosomes to fuse, triggered by the low pH when they get in close vicinity with the membrane.

4.4 Conclusions

We have shown that influenza virosomes carrying hemagglutinin can fuse on supported membranes on polyelectrolyte multilayers assembled on colloids as well as on planar surfaces. The mechanism of fusion is pH dependent as has been confirmed independently by the R18 assay, QCM-D and AFM. IRIVs fuse at low pH 4.5, but not at neutral pH 7.4. AFM imaging proves that the virosomes are integrated in the supported membrane at low pH as they can be recognized in the membrane as flattered features and have a reduced vertical thickness. Virosome fusion on supported membranes offers a novel strategy for the functionalization of supported membranes that can be used for the design of complex colloidal systems which can have applications in drug delivery or sensing devices.

References

(1) Kammer, A. R.; Amacker, M.; Rasi, S.; Westerfeld, N.; Gremion, C.; Neuhaus, D.; Zurbriggen, R. A New and Versatile Virosomal Antigen Delivery System to Induce Cellular and Humoral Immune Responses. *Vaccine* **2007**, *25* (41), 7065–7074.

(2) de Bruijn, I. A.; Nauta, J.; Gerez, L.; Palache, A. M. The Virosomal Influenza Vaccine Invivac: Immunogenicity and Tolerability Compared to an Adjuvanted Influenza Vaccine (Fluad in Elderly Subjects. *Vaccine* **2006**, *24* (44–46), 6629–6631.

(3) Douglas, T. Viruses: Making Friends with Old Foes. *Science (80-.).* **2006**, *312* (5775), 873–875.

(4) Moser, C.; Amacker, M.; Zurbriggen, R. Influenza Virosomes as a Vaccine Adjuvant and Carrier System. *Expert Rev. Vaccines* **2011**, *10* (7), 437–446.

(5) Bungener, L.; Serre, K.; Bijl, L.; Leserman, L.; Wilschut, J.; Daemen, T.; Machy, P. Virosome-Mediated Delivery of Protein Antigens to Dendritic Cells. *Vaccine* **2002**, *20* (17–18), 2287–2295.

(6) Kim, H. S.; Park, Y. S. Effect of Lipid Compositions on Gene Transfer into 293 Cells Using Sendai F/HN-Virosomes. *J. Biochem. Mol. Biol.* **2002**, *35* (5), 459–464.

(7) Johnson, D. C.; Wittels, M.; Spear, P. G. Binding to Cells of Virosomes Containing Herpes Simplex Virus Type 1 Glycoproteins and Evidence for Fusion. *J. Virol.* **1984**, *52* (1), 238–247.

(8) Diamanti, E.; Cuellar, L.; Gregurec, D.; Moya, S. E.; Donath, E. Role of Hydrogen Bonding and Polyanion Composition in the Formation of Lipid Bilayers on Top of Polyelectrolyte Multilayers. *Langmuir* **2015**, *31*, 8623–8632.

(9) Domecq, A.; Disalvo, E. A.; Bernik, D. L.; Florenzano, F.; Politi, M. J. A Stability Test of Liposome Preparations Using Steady-State Fluorescent Measurements. *Drug Deliv.* **2001**, *8* (3), 155–160.

(10) Buranda, T.; Yang, W.; Perez, D.; Chigaev, A.; Sklar, L. A. Real Time Partitioning of Octadecyl Rhodamine B into Bead Supported Lipid Bilayer Membranes Reveals Quantitative Differences in Saturable Binding Sites in DOPC and 1:1:1 DOPC/SM/Cholesterol Membranes. *J. Phys. Chem. B* **2010**, *114* (3), 1336–13449.

(11) Harrison, S. C. Viral Membrane Fusion. *Nat. Struct. Mol. Biol.* **2008**, *15* (7), 690–698.

(12) White, J. M.; Wilson, I. Anti-Peptide Antibodies Detect Steps in a Protien Conformation Changes: Low-pH Activation of the Influenza Virus Hemagglutinin. *J. Cell Biol.* **1987**, *105* (6), 2887–2896.

(13) Korte, T.; Herrmann, A. pH-Dependent Binding of the Fluorophore Bis-ANS to Influenza Virus Reflects the Conformational Change of Hemagglutinin. *Eur. Biophys. J.* **1994**, *23* (2), 105–113.

(14) Glück, R.; Metcalfe, I. C. Novel Approaches in the Development of Immunopotentiating Reconstituted Influenza Virosomes as Efficient Antigen Carrier Systems. *Vaccine* **2003**, *21* (7–8), 611–615.

(15) Amacker, M.; Engler, O.; Kammer, A. R.; Vadrucci, S.; Oberholzer, D.; Cerny, A.; Zurbriggen, R. Peptide-Loaded Chimeric Influenza Virosomes for Efficient in Vivo Induction of Cytotoxic T Cells. *Int. Immunol.* **2005**, *17* (6), 695–704.

(16) White, J. M.; Delos, S. E.; Brecher, M.; Schornberg, K. Structures and Mechanisms of Viral Membrane Fusion Proteins: Multiple Variations on a Common Theme. *Crit. Rev. Biochem. Mol. Biol.* **2008**, *43* (3), 189–219.

(17) Kielian, M. Mechanisms of Virus Membrane Fusion Proteins. *Annu. Rev. Virol.* **2014**, *1* (1), 171–189.

(18) Hamilton, B. S.; Whittaker, G. R.; Daniel, S. Influenza Virus-Mediated Membrane Fusion: Determinants of Hemagglutinin Fusogenic Activity and Experimental Approaches for Assessing Virus Fusion. *Viruses* **2012**, *4* (7), 1144–1168.

(19) Han, X.; Bushweller, J. H.; Cafiso, D. S.; Tamm, L. K. Membrane Structure and Fusion-Triggering Conformational Change of the Fusion Domain from Influenza Hemagglutinin. *Nat. Struct. Biol.* **2001**, *8* (8), 715–720.

(20) Haywood, A. M.; Boyer, B. P. Time and Temperature Dependence of Influenza Virus Membrane Fusion at Neutral pH. *J. Gen. Virol.* **1986**, *67* (12), 2813–2817.

General Conclusions

Overall the research conducted in this thesis has focused on the engineering of surfaces with polyelectrolyte multilayers alone or combined with lipid bilayers and virosomes, with potential applications in biomedicine and sensing: i.e in tissue engineering, as antifouling coatings, targeting drug delivery or as multifunctional sensor devices. The work developed has been mainly concerned with the fabrication and characterization of the polyelectrolyte lipid assemblies. Summing up the results from each chapter, the following conclusions can be drawn:

In **Chapter 1** it has been shown that thermal annealing can be used as a simple way to tune the wetting and antifouling character of biocompatible films based on PLL and Alg. The changes in properties of the films resulted in an enhanced cell adhesion on the annealed surfaces. Annealing of PLL/Alg PEMs at temperatures between 37 and 80 °C changed the wetting properties of the film from hydrophilic, 36° to highly hydrophobic, around 95°. The change in hydrophilicity is mainly related to the changes in topography of the film after annealing, as shown by AFM imaging, as well as to the compensation of the charges of PLL and Alg due to their reorganization in an energetically more favourable arrangement. Furthermore surface energy analysis showed that thermal annealing affects the polar energy of the surface, hinting a larger compensation of charges after annealing where the interaction between positive and negative charges of the PEs is maximized. Annealed PEMs at 37 °C exhibited enhanced adhesion, spreading and migration for the C2C12 and A549 cell lines in comparison to non-

annealed films, which was most likely related to the increase in stiffness in the PEMs and in contact angle. Results showed, as well, that annealing decreases protein deposition on the films hinting potential antifouling applications.

In **Chapter 2**, it has been shown that a lipid bilayer can only be formed on top of PAH and PSS multilayers, with PAH as the outermost layer from lipid vesicles composed of mixtures of the zwitterionic, DOPC and the negatively charged, DOPS, when DOPS is at least 50 %, in molar contribution to the composition, and no more than 80 %. Revealing that charged lipids are necessary, in order to enhance the interactions between lipids and PEs for vesicles' rupture. While the presence of more than 20 % of zwitterionic lipids, is also necessary to provide fluidity to the deposited lipids to rearrange and fuse to form a continuous bilayer. It has also been shown that the main interaction between the lipids and PAH is through hydrogen bonding between the amine groups of PAH and the carboxyl and phosphate groups of DOPS in addition to electrostatic interactions. Additionally, SUVs of 50:50 DOPC:DOPS were adsorbed without forming a bilayer on PDADMAC/PSS, with PDADMAC as top layer. Since the charged groups in PDADMAC are quaternary amines is not possible to form hydrogen bonding between the amines and the lipids.

Results also suggested that phosphate ions of PBS, used for the hydration of the lipids, interact with the primary amines of PAH forming complexes and rendering the surface of the PEM almost neutral. If vesicles are prepared in presence of other salts like NaCl or buffers of Hepes/NaCl/$CaCl_2$, or just Hepes no lipid bilayer is obtained after assembly of the vesicles on the PAH/PSS PEM. Taking into account that the interaction of phosphates with PAH renders the surface practically with no charge we propose the following model. For PAH/PSS PEMs, the electrostatic attraction with the vesicles in presence of phosphate is weak, the coating of the

surfaces with vesicles is slow, as they do not feel strong attraction to the surface. When vesicles approach the surface of the PEMs they can interact through hydrogen bonding with the PAH in order to spread, rupture and fuse, forming a bilayer. In cases of other salts instead of PBS the ζ – potential remains positive and the vesicles must face a stronger electrostatic interaction than in presence of PBS that causes the fast coverage of the PEMs with vesicles, which do not have place to rearrange and fuse. A similar situation can be observed for the case of PEMs that display PEs with quaternary amines like PDADMAC, where the interaction of the vesicles with the PEM is electrostatic and in presence of phosphates the surface remains positively charged with a potential of around 25 mV. In these conditions there is a fast coverage of the multilayers with vesicles leaving no place for vesicles´ spreading, rupture and fusion.

Additionally in **Chapter 2** it has been shown that besides the surface chemistry of the multilayer the composition of the PEM; the nature of the underlying polyanion, thus the interactions between polyanions and polycations also affect the formation of the lipid bilayer. When Alg or PAA is used, instead of PSS, the adsorption of the SUVs resulted in bilayer patches that do not fuse, to form a complete bilayer. This is attributed to the fine tuning of the interaction of the PEMs with phosphate ions and phospholipids.

In **Chapter 3**, electrochemical impedance spectroscopy measurements showed for the first time the formation of a dense lipid bilayer with limited defects or pores when SUVs of 30:70 molar ratio of DOPC:DOPS are adsorbed on top of a PEM cushion of 11 layers of PAH/PSS. The bilayer displays a high resistance; 1.89×10^7 Ω cm^2. Such resistance is comparable with the resistance of black lipid membranes. The obtained resistance, envisage the combination of lipid layers with channels or trans-membrane proteins for selective transport in sensor devices or as model for biological processes, profiting of the PEM as hydrophilic spacer. The assembly of

three additional PE layers of PAH and PSS on top of the lipid bilayer resulted in the formation of pores or defects in the lipid layer with a subsequent decrease in the resistance of up to 2 orders of magnitude.

In **Chapter 4** it has been demonstrated that influenza virosomes with HA protein on their membrane can fuse on supported lipid bilayers of SUVs of 50:50 PC:PS on 11 layers of PAH/PSS assembled either on colloids or on planar substrates. It has been confirmed that the mechanism of fusion of IRIVs is pH dependent as virosomes fuse at low pH 4.5, but not at neutral pH 7.4. Virosome fusion was studied as a function of HA concentration and the temperature. It was found that IRIVs fusion to the PEMs supported lipid bilayer was more favourable when their concentration thus the HA content was 0.5 μg mL^{-1} in comparison to 2 μg mL^{-1}. Better fusion was also succeeded at acidic pH when the temperature was set at 37 °C instead at 23 °C. Their fusion on supported membranes offers a novel strategy for the functionalization of supported membranes that can be used for the design of complex colloidal systems which can have applications in drug delivery or sensing devices.

List of Publications

1. **Eleftheria Diamanti**, Luis Cuellar, Danijela Gregurec, Sergio Enrique Moya, Edwin Donath; Role of Hydrogen Bonding and Polyanion Composition in the Formation of Lipid Bilayers on Top of Polyelectrolyte Multilayers, *Langmuir* (2015), 31, 8623-8632.

2. Nicolas Muzzio, Miquel Pasquale, Danijela Gregurec, **Eleftheria Diamanti**, Omar Azzaroni, Sergio Moya; Polyelectrolytes multilayers to modulate cell adhesion: the influence of film composition and polyelectrolyte interdigitation, *Macromolecular Bioscience* (2015), 16, 482-495.

3. Joseba Irigoyen, Nikolaos Politakos, **Eleftheria Diamanti**, Marco Marradi, Raquel Ledezma, Layza Arizmendi, J. Alberto Rodríguez Ronald F. Ziolo, Sergio E. Moya; Fabrication of Hybrid Graphene Oxide/Polyelectrolyte Capsules by means of Layer by Layer Assembly on Erythrocite Cell Templates, *Beilstein Journal of Nanotechnology* (2015), 6, 2310-2318.

4. Jana Fleddermann**, Eleftheria Diamanti**, Stavros Azinas, Marija Kosutic, Lars Dähne, Irina Estrela-Lopis, Martin Amacker, Edwin Donath, and Sergio Enrique Moya; Virosome Engineering of Colloidal Particles and Surfaces: Bioinspired Fusion to Supported Lipid Layers, *Nanoscale* (2016), 8, 7933-7941.

5. **Eleftheria Diamanti**, Nicolas Muzzio, Danijela Gregurec, Joseba Irigoyen, Miquel Pasquale, Omar Azzaroni, Sergio Enrique Moya; Impact of Thermal Annealing Triggers Changes on Wettability and Antifouling Characteristics of Alginate Poly - L - lysine Polyelectrolyte Multilayer Films, *Colloids and Surfaces B: Biointerfaces* (2016), 145, 328-337.

6. **Eleftheria Diamanti**, Danijela Gregurec, Gabriela Romero, Luis Cuellar, Edwin Donath, Sergio Enrique Moya; Lipid Layers on Polyelectrolyte Multilayers: Understanding Lipid – Polyelectrolyte Interactions and Applications on the Surface Engineering of Nanomaterials, Accepted, *Journal of Nanoscience and Nanotechnology* (2016), 16, 5696-5700.

7. **Eleftheria Diamanti**, Danijela Gregurec, María José Rodríguez-Presa, Claudio Gervasi, Omar Azzaroni, Sergio E. Moya, High Resistivity Lipid Bilayers Assembled on Polyelectrolyte Multilayer Cushions: An Impedance Study, *Langmuir* (2016), 32, 6263-6271.

8. Nicolas Muzzio, Danijela Gregurec, **Eleftheria Diamanti**, Joseba Irigoyen, Miguel Pasquale, Omar Azzaroni, Sergio E. Moya; Thermal Annealing of Polyelectrolyte Multilayers: a New Approach for the Enhancement of Cell Adhesion, *ACS Advanced Materials and Interfaces* (2016), DOI: 10.1002/admi.201600126.

9. **Eleftheria Diamanti**, Patrizia. Andreozzi, Ramiro Anguiano, Luis Yate, Danijela Gregurec, Nikolaos Politakos, Ron. F. Ziolo, Edwin Donath, Sergio. E. Moya,' The Role of Top-Layer Chemistry on the Formation of Supported Lipid Bilayers on Polyelectrolyte Multilayers: Primary versus Quaternary Amines, *Physical Chemistry Chemical Physics* (2016), published online DOI: 10.1039/C6CP06258J.

10. Maria Nerantzaki, Iro Koliakou, Martha G. Kaloyianni, Ioanna Koumentakou, Evangelia Siska, **Eleftheria Diamanti**, Michalis Karakassides, Aldo R. Boccaccini, Dimitrios N. Bikiaris, A biomimetic approach for enhancing adhesion and osteogenic differentiation of adipose-derived stem cells on poly(butylene succinate) bioactive composites, *submitted in European Polymer Journal* (2016).

11. Nicolas Muzzio, Miguel Pasquale, **Eleftheria Diamanti**, Marta Martinez, Omar Azzaroni, Sergio E. Moya, Enhanced antifouling properties of thermal annealed chitosan/hyaluronic acid polyelectrolyte multilayer: low adherence for mammalian cells and selective decrease in

biofilm formation for Gram-positive bacteria, *submitted in Materials Science & Engineering C* (2016).

12. **Eleftheria Diamanti**, Patrizia Andreozzi, Christopher Kirby, Ramiro Anguiano, Luis Yate, Hendrik Heinz, Ronald F. Ziolo, Edwin Donath, Sergio E. Moya, A Study of the Impact of Polyanions on the Formation of Lipid Bilayers on Top of Polyelectrolyte Multilayers with Polyallylamine Hydrochloride as Top Layer, *manuscript in preparation.*

13. Patrizia Andreozzi, Karen R. Py-Daniel, **Eleftheria Diamanti**, Nikolaos Politakos, Ricardo B. de Azebedo, Sergio E. Moya, Supramolecular Assembled Polyamine Nanoparticles (PANs) for Encapsulation of Anticancer Drugs, *manuscript in preparation.*

This thesis presents different approaches for surface engineering by means of polyelectrolyte multilayers (PEMs) alone or in combination with lipid bilayers and influenza virosomes, for potential biomedical applications. The work developed has been focused on fabrication and characterization aspects:

Biopolymer PEM films based on alginate and poly-L-lysine are thermally annealed as an alternative method to cross-linking in order to enhance cellular adhesion for applications in tissue engineering or for their use in antifouling applications.

The conditions for the assembly of lipid bilayer membranes on top of PEM cushions and the interactions between lipids and polyelectrolytes are studied. The conditions for the formation of the bilayer are studied in detail as a function of vesicles´ composition, top-layer chemistry, the presence of phosphate ions and polyanions. Electrochemical impedance spectroscopy is applied to measure the electrical properties of a supported lipid bilayer, showing resistance values similar to that of a black lipid membrane, 1.89 10^7 Ω cm^2.

The fusion of immunostimulating reconstituted influenza virosomes, lacking the virus genome, is studied in terms of pH, temperature and hemagglutinin content.